AFRL-RD-PS-
TR-2009-1066

MAGNETIZED TARGET FUSION – FIELD REVERSED CONFIGURATION FORMATION AND INJECTION (MTF-FRC)

Chris Grabowski
Wayne Sommars

Science Applications International Corporation
Applied Sciences Operation
2109 Air Park Rd SE
Albuquerque, NM 87106

06 November 2009

Final Report

APPROVED FOR PUBLIC RELEASE: DISTRIBUTION IS UNLIMITED

P/A Case # : 377ABW-2009-1541



AIR FORCE RESEARCH LABORATORY
Directed Energy Directorate
3550 Aberdeen Ave SE
AIR FORCE MATERIEL COMMAND
KIRTLAND AIR FORCE BASE, NM 87117-5776

NOTICE AND SIGNATURE PAGE

Using Government drawings, specifications, or other data included in this document for any purpose other than Government procurement does not in any way obligate the U.S. Government. The fact that the Government formulated or supplied the drawings, specifications, or other data does not license the holder or any other person or corporation; or convey any rights or permission to manufacture, use, or sell any patented invention that may relate to them.

This report was cleared for public release by the Air Force Research Laboratory [insert TD site] Public Affairs Office and is available to the general public, including foreign nationals. Copies may be obtained from the Defense Technical Information Center (DTIC) (http://www.dtic.mil).

AFRL-RD-PS-TR-2009-1066 HAS BEEN REVIEWED AND IS APPROVED FOR PUBLICATION IN ACCORDANCE WITH ASSIGNED DISTRIBUTION STATEMENT.

Wesley D. Tucker, DR-III
Chief, HPM Technologies Branch

Dr. Wallace T. Clark III, DR-IV
Chief, High Power Microwave Division

This report is published in the interest of scientific and technical information exchange, and it's publication does not constitute the Government's approval or disapproval of its ideas or finding

REPORT DOCUMENTATION PAGE

Form Approved
OMB No. 0704-0188

Public reporting burden for this collection of information is estimated to average 1 hour per response, including the time for reviewing instructions, searching existing data sources, gathering and maintaining the data needed, and completing and reviewing this collection of information. Send comments regarding this burden estimate or any other aspect of this collection of information, including suggestions for reducing this burden to Department of Defense, Washington Headquarters Services, Directorate for Information Operations and Reports (0704-0188), 1215 Jefferson Davis Highway, Suite 1204, Arlington, VA 22202-4302. Respondents should be aware that notwithstanding any other provision of law, no person shall be subject to any penalty for failing to comply with a collection of information if it does not display a currently valid OMB control number. **PLEASE DO NOT RETURN YOUR FORM TO THE ABOVE ADDRESS.**

1. REPORT DATE *(DD-MM-YYYY)* 06 November 2009	**2. REPORT TYPE** Final Report	**3. DATES COVERED** *(From - To)* 05 Jul 2006 to 31 Jul 2009
4. TITLE AND SUBTITLE Magnetized Target Fusion – Field Reversed Configuration Formation and Injection (MTF-FRC)		**5a. CONTRACT NUMBER** FA9451-05-D-0004/0016
		5b. GRANT NUMBER
		5c. PROGRAM ELEMENT NUMBER 61920F
6. AUTHOR(S) Chris Grabowski and Wayne Sommars		**5d. PROJECT NUMBER** D0E5
		5e. TASK NUMBER HB
		5f. WORK UNIT NUMBER AB
7. PERFORMING ORGANIZATION NAME(S) AND ADDRESS(ES)AND ADDRESS(ES) Science Applications International Corporation (SAIC) 2109 Air Park Road SE Albuquerque, NM 87106		**8. PERFORMING ORGANIZATION REPORT NUMBER**
9. SPONSORING / MONITORING AGENCY NAME(S) AND ADDRESS(ES) Air Force Research Laboratory 3550 Aberdeen Ave SE Kirtland AFB, NM 87117-5776		**10. SPONSOR/MONITOR'S ACRONYM(S)**
		11. SPONSOR/MONITOR'S REPORT NUMBER(S) AFRL-RD-PS-TR-2009-1066

12. DISTRIBUTION / AVAILABILITY STATEMENT
APPROVED FOR PUBLIC RELEASE; DISTRIBUTION IS UNLIMITED.

13. SUPPLEMENTARY NOTES
377 ABW Case Number: 377ABW-2009-1541

14. ABSTRACT

DETAR Task 0rder 0016 supports the Air Force Research Laboratory's ongoing effort to demonstrate magnetized target fusion in a laboratory environment. The experimental premise involves forming a plasma in a field-reversed configuration (FRC), translating it a short distance from where it was formed into a cylindrical flux-conserving shell (solid liner), and then adiabatically compressing it to fusion-relevant densities and temperatures by imploding the liner around it. The name "FRCHX," for "FRC Compression Heating eXperiment" has been given to this effort. SAIC and its subcontractors perform this work in collaboration with AFRL personnel, as well as with scientists from Los Alamos National Laboratory, the University of New Mexico, and the University of Nevada, Reno.

15. SUBJECT TERMS: Magnetized Target Fusion, Field-Reversed Configuration, MTF-FRC, Fusion Energy, Magneto-Inertial Fusion, FRCHX

16. SECURITY CLASSIFICATION OF:			**17. LIMITATION OF ABSTRACT**	**18. NUMBER OF PAGES**	**19a. NAME OF RESPONSIBLE PERSON**
			Unclassified	198	Dr. James Degnan
a. REPORT Unclassified	**b. ABSTRACT** Unclassified	**c. THIS PAGE** Unclassified			**19b. TELEPHONE NUMBER** *(include area code)* 505-846-1235

Standard Form 298 (Rev. 8-98)
Prescribed by ANSI Std. 239.18

THIS PAGE INTENTIONALLY LEFT BLANK

TABLE OF CONTENTS

Section **Page**

1.0 SUMMARY **1**

2.0 INTRODUCTION **1**

3.0 FRCHX PHASE I DEVELOPMENT EFFORT **3**

3.1 ASSEMBLY OF PULSED POWER SYSTEMS FOR BIAS, PI, AND MAIN BANKS 5

3.1.1 Bias Bank Systems *5*
3.1.2 PI Bank Systems *9*
3.1.3 Main Bank and Crowbar Switch Systems *11*
3.1.3.1 Initial System Tests 11
3.1.3.2 Changes Implemented on the FRX-L Main Bank and Crowbar Switch 14

3.2 HORIZONTAL VACUUM AND FIELD-COIL STAND 16

3.2.1 Wide-Segment Theta Coil with Passive Mirrors *17*
3.2.2 Support Stand and Vacuum System Description *17*

3.3 PLASMA DIAGNOSTICS 18

3.3.1 Magnetic Probes *18*
3.3.2 Fiber-optic Cable Light Monitor *20*
3.3.3 Micro-Channel Plate Camera *21*
3.3.4 Interferometry *22*
3.3.4.1 Four-Chord System 22
3.3.4.2 Single-Chord System 24

3.4 MANUAL CONTROL SYSTEM 25

3.5 EXPERIMENTAL RESULTS 26

3.5.1 Campaign to Improve Crowbar Switch Performance *27*
3.5.2 Early Bias Bank Modifications To Increase Current *35*
3.5.3 Phase I Vacuum and Plasma Tests with FRCHX *40*

4.0 FRCHX PHASE II DEVELOPMENT EFFORT **46**

4.1 FURTHER PULSED POWER SYSTEM DESIGN, ASSEMBLY, AND MODIFICATIONS 47

4.1.1 Upper and Lower Cusp Coil Bank Systems *47*
4.1.2 Modifications and Maintenance for the Bias Bank *51*

4.2 VERTICAL VACUUM AND FIELD-COIL STAND 54

4.2.1 Support Stands for the Field Coils, Vacuum System, and Theta Coil Cable Header *54*
4.2.2 Vacuum System *56*
4.2.3 Theta and Cusp Coil Configuration for Static FRC Formation *57*
4.2.4 Plenum Pre-Fill and Venting System *60*

4.3 DIAGNOSTICS 62

4.3.1 Flux Loops and B-dot Probes *62*
4.3.2 The Four-Chord Interferometer *63*
4.3.3 Side-On Fiber-Optic Translation and Continuum Array *65*
4.3.4 UNR Gated End-On Photography and Fiber Probe Diagnostic Package *67*
4.3.5 Receiver Box for Trigger Sync-Out Signals *69*

4.4 DATA ACQUISITION AND REMOTE SHIELDED ENCLOSURE 69

4.4.1 Plans for the FRCHX Data Acquisition System *69*
4.4.2 Setting Up the Remote Data Acquisition Enclosure *71*
4.4.3 Data Acquisition and Diagnostic Systems Placed Within the Enclosure *74*

4.4.4 Relocation of FRCHX Trigger-Timing Systems into the Enclosure *75*
4.4.5 Computer Link and Data Acquisition, Processing, and Archival Software *76*
4.5 COMPUTER-BASED CONTROL SYSTEM 78
4.5.1 Compact Field Point Controller and User Interface Computer *79*
4.5.2 Pneumatic Control and Fiber-Optic Status Lines for Pulsed Power *82*
4.5.3 Vacuum-System Controls *88*
4.5.4 Emergency Abort Link to the Compact Field Point Controller *91*
4.5.5 The LabVIEW Control Program *93*
4.6 EXPERIMENTAL RESULTS 95
4.6.1 Excluded Flux Diagnostic Calibration *95*
4.6.2 Overview of Pulsed Power System Performance *97*
4.6.3 Data from FRC Formation Tests *102*
4.6.3.1 Flux Loop and B-Dot Probe Excluded Flux Radius Measurements 103
4.6.3.2 Plasma Densities Measured with the Four-Chord Interferometer 106
4.6.3.3 Plasma Profile and Behavior Observed with the Side-On Fiber-optic Array 107
4.6.3.4 Results Obtained with the UNR End-On Photography and Fiber-Probe Package 110
4.6.4 Problems with Theta Coil Current Joints *111*
5.0 PREPARATIONS FOR TRANSLATION-ONLY AND FOLLOW-ON COMPRESSION HEATING TESTS 113
5.1 NEW SYSTEMS FOR FRC TRANSLATION TESTS 115
5.1.1 Guide/Mirror Bank *116*
5.1.2 Guide and Mirror Coil Design *120*
5.2 MODIFICATIONS AND ADDITIONS TO EXISTING FRCHX SYSTEMS 123
5.2.1 Improved Current Joints for Conical Theta Coil *123*
5.2.2 Higher-Voltage Power Supply for the PI Bank *127*
5.2.3 Further Diagnostic Development *128*
5.3 INTEGRATED FRC FORMATION, TRANSLATION, AND COMPRESSION SYSTEMS 129
6.0 PRESENTATIONS 131
7.0 CONCLUSIONS 132
8.0 RECOMMENDATIONS 135
9.0 REFERENCES 136
APPENDICES:
APPENDIX A 137
APPENDIX B 143
APPENDIX C 163
APPENDIX D 171

LIST OF FIGURES

Figure **Page**

FIGURE 1. VIEW FROM SHIVA C-ARM OF EARLY FRCHX EXPERIMENTAL SETUP 4

FIGURE 2. BIAS BANK JUST AFTER ITS ASSEMBLY WAS COMPLETED 6

FIGURE 3. BASIC CHARGING AND DUMPING CIRCUIT FOR BOTH PI AND BIAS BANKS 7

FIGURE 4. (A) PI AND BIAS BANK RESISTOR STANDS; (B) JENNINGS SWITCHES AND DIODE STACK ON BIAS BANK RESISTOR STAND 8

FIGURE 5. BIAS BANK CURRENT WAVEFORMS RECORDED WITH BIAS PEARSON MONITOR 9

FIGURE 6. PI BANK SF6 ENCLOSURE BEING TEST-FITTED 10

FIGURE 7. JENNINGS SWITCHES AND DIODE STACK ON PI BANK RESISTOR STAND 10

FIGURE 8. (A) NEW HOFFMAN BOX WITH 40168 INSIDE; (B) FEEDTHROUGHS THAT WERE ADDED 12

FIGURE 9. CURRENT WAVEFORMS OBTAINED FROM ROGOWSKI COILS ON MAIN BANK AND ON CURRENT FEED TO THETA COIL 13

FIGURE 10. MAXWELL 40151-B TRIGGER GENERATOR WITH ADDITIONAL 100 KV, 0.099 μF CAPACITOR 16

FIGURE 11. TEMPORARY THETA COIL, SUPPORT STAND, AND VACUUM SYSTEM 17

FIGURE 12. PLACEMENT OF B-DOT PROBES AND FLUX LOOP ALONG THETA COIL 19

FIGURE 13. FIRST LIGHT FIBER MONITOR (A) MOUNT ON THETA COIL; (B) PMT DETECTOR IN SCREEN ROOM 20

FIGURE 14. MCP CAMERA SETUP AT NORTH END OF QUARTZ TUBE 21

FIGURE 15. PLACEMENT OF FOUR-CHORD INTERFEROMETER AROUND FRCHX COILS 22

FIGURE 16. FOUR-CHORD INTERFEROMETER OPTICS TABLE AND ITS DUST COVER 23

FIGURE 17. (A) MOUNTING OF OPTO-MECHANICAL COMPONENTS ON OPTICS TABLE; (B) INTERFEROMETER DETECTORS AND RF COMPONENTS 24

FIGURE 18. SINGLE-CHORD INTERFEROMETER IN POSITION IN FRONT OF FRCHX THETA COIL 25

FIGURE 19. MANUAL CONTROL SYSTEM (A) TWO USER-INTERFACE CONTROLLERS; (B) TWO SYSTEM-INTERFACE BOXES 26

FIGURE 20. COMPLETED CROWBAR AUXILIARY BANK IN PLACE BEHIND MAIN AND PI BANKS 29

FIGURE 21. DISCHARGE-CURRENT WAVEFORM FOR CROWBAR AUXILIARY BANK 30

FIGURE 22. (A) ORIGINAL CROWBAR TRIGGER BOARD SETUP; (B) NEW SETUP WITH ADDITIONAL BLOCKING CAPS 31

FIGURE 23. BANK-CURRENT WAVEFORMS, SHOT IN WHICH AUXILIARY BANK PRE-FIRED 32

FIGURE 24. TRIGGER-BOARD-CIRCUIT SETUP FOR END-RAIL-GAP-ONLY TESTS 34

FIGURE 25. AUXILIARY BANK TO BE USED TO AUGMENT TRIGGER PULSE DELIVERED TO EACH CROWBAR RAIL GAP 35

FIGURE 26. COPPER BUS STRAPS, DAMPING RESISTOR, AND IGNITRON (UPPER RIGHT) FOR SECOND BIAS BANK MODULE 36

FIGURE 27. NEW 1:1, DUAL-SECONDARY ISOLATION TRANSFORMER FOR BIAS BANK IGNITRON TRIGGER UNIT 37

FIGURE 28. THREE TRIGGER PULSES FROM EACH SECONDARY OF IGNITRON TRIGGER TRANSFORMER 38
FIGURE 29. THETA COIL CURRENT (AVERAGED) FOR A BIAS-ONLY SHOT, TWO-MODULE BIAS BANK 38
FIGURE 30. NEW BIAS BANK ISOLATION INDUCTORS 39
FIGURE 31. THETA COIL CURRENT ALONG WITH THREE MCP CAMERA IMAGES 41
FIGURE 32. THETA COIL CURRENT, ALONG WITH FIVE MCP CAMERA IMAGES 42
FIGURE 33. FIRST LIGHT FIBER-MONITOR SIGNAL WITH THETA COIL CURRENT OVERLAID 44
FIGURE 34. (A) TWO 1.5 MF CUSP BANK MODULES STACKED ON TOP OF EACH OTHER; (B) IGNITRON TRIGGER UNITS 48
FIGURE 35. UPPER AND LOWER CUSP BANK POWER-SUPPLY STAND 49
FIGURE 36. RESISTOR STANDS FOR UPPER AND LOWER CUSP BANKS, BETWEEN POWER-SUPPLY STAND AND CUSP BANKS 49
FIGURE 37. (A) AND (B) CUSP COIL BUS PLATES 50
FIGURE 38. CUSP COIL TRANSMISSION-LINE CABLES AND HEADERS (CENTER) 51
FIGURE 39. INDUCTOR HOUSINGS ON BIAS BANK STAND 52
FIGURE 40. PEARSON MODEL 1423S INSTALLED ON EACH BANK MODULE 53
FIGURE 41. BIAS AND GUIDE/MIRROR POWER-SUPPLY STAND 54
FIGURE 42. (A) FRCHX VERTICAL SUPPORT STAND; (B) STAND AFTER ASSEMBLY 55
FIGURE 43. COMPLETED THETA COIL CABLE HEADER SUPPORT TABLE 55
FIGURE 44. VERTICAL STAND AND CABLE HEADER SUPPORT TABLE 56
FIGURE 45. CRYOPUMP, GATE VALVE, AND LOWER VACUUM HARDWARE 56
FIGURE 46. ROUGHING PUMP AND VACUUM-GAUGE CONTROLLERS BENEATH THETA COIL CABLE HEADER 57
FIGURE 47. CYLINDRICAL THETA COIL, WITH SIX-SEGMENT UNIFORM REGION IN THE MIDDLE BOUNDED BY TWO-SEGMENT MIRRORS TOP AND BOTTOM 59
FIGURE 48. (A) CUSP COIL AND INSULATORS; (B) CLOSE-UP OF TOP HAT AND CURRENT-FEED INSULATORS 59
FIGURE 49. COMPLETED THETA AND CUSP COIL ASSEMBLY ON VERTICAL STAND 60
FIGURE 50. D2 PRE-FILL AND N2 VENTING SYSTEMS FOR FRCHX VACUUM VESSEL 61
FIGURE 51. (A) D2 PRE-FILL; (B) N2 BACKFILLING AND VENTING SYSTEM COMPONENTS 61
FIGURE 52. FLUX-LOOP VOLTAGE DIVIDERS IN FIBERGLASS FRAME 62
FIGURE 53. FOUR B-DOT PROBES IN THETA COIL, SEGMENTS B, D, G, AND I 63
FIGURE 54. FOUR-CHORD INTERFEROMETER IN PLACE AROUND VACUUM AND FIELD-COIL STAND 64
FIGURE 55. DETECTORS AND RF DEMODULATOR CIRCUITS FOR FOUR-CHORD INTERFEROMETER 64
FIGURE 56. BLUE FIBERS USED FOR SIDE-ON FIBER-OPTIC ARRAY 65
FIGURE 57. UNR END-ON PHOTOGRAPHY AND FIBER-PROBE DIAGNOSTICS 68
FIGURE 58. TRIGGER SYNC-OUT RECEIVER BOX POSITIONED AMONG PXI DIGITIZER CRATES 69
FIGURE 59. (A) ENCLOSURE IN POSITION; (B) SPACE INSIDE ENCLOSURE 71

FIGURE 60. TEST AREA SHOWING PLACEMENT OF SHIELDED ENCLOSURE AND DATA-CABLE CONDUITS 72
FIGURE 61. CONDUIT ATTACHED TO ENDS OF RIGID CONDUIT EXITING CABLE TRAYS 73
FIGURE 62. DATA-CABLE CONDUITS AND HOFFMAN BOX COVERING PATCH PANEL 74
FIGURE 63. 18-SLOT PXI CRATE (RIGHT) AND TWO 8-SLOT CRATES (LEFT) 75
FIGURE 64. (A) NEW CABLE TRAY AND FIBER-OPTIC FEEDTHROUGHS; (B) DG-535S 76
FIGURE 65. DATA ACQUISITION COMPUTER, PXI CONFIGURATION PANEL DISPLAYED 77
FIGURE 66. CONTROLLER COMPONENTS IN HAMMOND ENCLOSURE 81
FIGURE 67. CFP CONTROLLER, NEXT TO MAIN BANK POWER SUPPLY 82
FIGURE 68. NORTHEAST PERSONNEL DOOR-INTERLOCK BOX 83
FIGURE 69. (A) AND (B) V-TO-F CONVERTER CIRCUITS ON EACH OF THE BANK RESISTOR AND/OR SWITCH STANDS 84
FIGURE 70. CLIPPARD PNEUMATICALLY-ACTUATED SWITCHES 85
FIGURE 71. (A) PI BANK CCS POWER SUPPLY; (B) INTERFACE BOX 85
FIGURE 72. REMOTELY OPERATED CONTROLLER (UPPER LEFT) FABRICATED FOR CROWBAR SWITCH'S UV POWER SUPPLY 86
FIGURE 73. IFS 8-CHANNEL CONTACT TRANSMITTER IN HAMMOND ENCLOSURE 87
FIGURE 74. PNEUMATIC CONTROL VALVES AND THEIR MANUAL TOGGLE SWITCHES 89
FIGURE 75. V-TO-F CONVERTERS TRANSMIT PRESSURE MEASUREMENTS TO CFP CONTROLLER FIBER OPTICALLY 89
FIGURE 76. PNEUMATICALLY ACTUATED SET OF CONTACTS 90
FIGURE 77. GAUGE CONTROLLER DISCONNECT BOX ON VACUUM AND FIELD-COIL STAND 91
FIGURE 78. (A) KEY SWITCH AND PANIC BUTTON; (B) FIBER-OPTIC RECEIVER AND CONTROL RELAYS 92
FIGURE 79. VACUUM-SYSTEM CONTROLS ON CONTROL PROGRAM'S FRONT PANEL 94
FIGURE 80. ALUMINUM PIPE INSERTED ALONG THE LENGTH OF QUARTZ TUBE 95
FIGURE 81. EXCLUDED FLUX RADIUS TO PIPE RADIUS FOR 12-CABLE SETUP USING (A) SHORT TIME-SCALE INTEGRATORS; (B) LONG TIME-SCALE INTEGRATORS 96
FIGURE 82. EXCLUDED FLUX RADIUS TO PIPE RADIUS FOR SINGLE-CABLE SETUP USING (A) SHORT TIME-SCALE INTEGRATORS; (B) LONG TIME-SCALE INTEGRATORS 97
FIGURE 83. BIAS CURRENT WAVEFORM FROM TEST #4, 3 MAR 2008 98
FIGURE 84. THETA COIL AND CROWBAR RAIL GAP CURRENT WAVEFORMS FROM TEST #9, 3 MAR 2008 99
FIGURE 85. UPPER AND LOWER CUSP CURRENT WAVEFORMS FROM TEST #7, 5 MAR 2008. 100
FIGURE 86. G-SEGMENT B-DOT PROBE WAVEFORMS FROM THREE SUCCESSIVE SHOTS, 7 MARCH 2008 101
FIGURE 87. THETA AND CUSP COIL CURRENT WAVEFORMS FROM TEST #7 IN FIGURE 86 101
FIGURE 88. G-SEGMENT (A) B-DOT PROBE AND (B) FLUX LOOP WAVEFORMS 104
FIGURE 89. FRC EXCLUDED FLUX RADIUS VS. TIME CALCULATED, (A) TEST #6; (B) TEST #7 104
FIGURE 90. INTERFEROMETER DATA: (A) PHASE SHIFT AS A FUNCTION OF TIME; (B) CORRESPONDING LINE-INTEGRATED DENSITY 107

FIGURE 91. SIDE-ON FIBER-OPTIC-ARRAY DATA: (A) SIGNAL INTENSITY VS. TIME; (B) SURFACE PLOT 108
FIGURE 92. EXCLUDED FLUX RADIUS VS. TIME CALCULATED AT (A) THETA COIL SEGMENT D; (B) THETA COIL SEGMENT G 109
FIGURE 93. SIDE-ON FIBER-OPTIC-ARRAY DATA: (A) SIGNAL INTENSITY VS. TIME; (B) SURFACE PLOT 110
FIGURE 94. (A) AND (B) IMAGES OF THE SPUTTERED ALUMINUM AND ARC MARKS ON QUARTZ TUBE 112
FIGURE 95. CURRENT JOINT ON TOPMOST (J) SEGMENT OF THETA COIL SHOWING EXTENSIVE ARCING 112
FIGURE 96. T2-MF GUIDE/MIRROR BANK MODULES, IN HIGH BAY 116
FIGURE 97. GUIDE/MIRROR BANK MODULES, STACKED TWO-HIGH 117
FIGURE 98. TWO GUIDE/MIRROR IGNITRON-TRIGGER GENERATORS, WITH 1:1 ISOLATION TRANSFORMERS 118
FIGURE 99. TWO RESISTOR STANDS FOR GUIDE/MIRROR BANK PLACED SIDE BY SIDE 118
FIGURE 100. GUIDE AND MIRROR COIL ASSEMBLY AROUND SOLID LINER 120
FIGURE 101. (A) FIRST MIRROR COIL; (B) SEVERAL COILS IN G-10 SPOOLS 121
FIGURE 102. GUIDE/MIRROR COIL ASSEMBLY AND CABLE HEADER AND OTHER BUS WORK DESIGNED FOR IT 122
FIGURE 103. GUIDE/MIRROR COIL CABLE HEADER ALONG WITH MYLAR PACK PREPARED FOR IT 123
FIGURE 104. COPPER GASKET, DESIGNED FOR IMPROVED CURRENT-JOINT CONTACT 124
FIGURE 105. THETA COIL SEGMENT, SHOWING LOCATION FOR ADDING A THIRD BOLT 125
FIGURE 106. NEW THETA COIL COPPER GASKETS SPREAD OUT SIDE BY SIDE 126
FIGURE 107. (A) MODIFIED CUSP AND THETA COIL SEGMENTS; (B) CLOSE-UP VIEW OF TAPPED HOLES ADDED TO SEVERAL COIL-SEGMENT HALVES 126
FIGURE 108. 100 KV, 60 MA, NEGATIVE POLARITY SPELLMAN POWER SUPPLY 128
FIGURE 109. LAYOUT FOR FRCHX FORMATION AND TRANSLATION SECTIONS WITH SOLID LINER 129
FIGURE 110. FRCHX FORMATION, TRANSLATION, AND LINER-COMPRESSION REGIONS 134

LIST OF TABLES

Table **Page**

TABLE 1. LIST OF MAJOR COMPONENTS NEEDED FOR CFP CONTROLLER 80
TABLE 2. GUIDE AND MIRROR COIL PARAMETERS 121

THIS PAGE INTENTIONALLY LEFT BLANK

1.0 SUMMARY

This task order was established to perform the Air Force Research Laboratory's (AFRL) ongoing effort to demonstrate Magnetized Target Fusion (MTF) in a laboratory environment. The experimental premise for this effort involves forming a plasma in a field-reversed configuration (FRC), translating this plasma a short distance from where it was formed into a cylindrical flux-conserving shell (solid liner), and then adiabatically compressing the plasma to fusion-relevant densities and temperatures by imploding the flux-conserving shell around it. The name FRCHX, for FRC Compression Heating eXperiment has been given to this effort. SAIC and its subcontractors performed this work under the guidance of AFRL personnel and in collaboration with scientists from Los Alamos National Laboratory (LANL), the University of New Mexico (UNM), and the University of Nevada, Reno (UNR).

2.0 INTRODUCTION

The concept of the FRC has been in existence for more than 40 years, but FRCs continue to be of considerable scientific interest, primarily because of several inherent features that FRCs have that make them attractive for use in a fusion-reactor scheme. Such features include a simple geometry with a high β and high power density, implying that a relatively efficient and compact reactor could be developed. In addition, their magnetic field configuration includes a natural diverter, which will assist in reducing the amount of impurities entering the plasma from vacuum vessel walls. They also have a demonstrated translatability, allowing them to be formed in a location that is isolated from the region where subsequent heating occurs (Tuszewski 1988).

Over the past nine years, the AFRL has been working in close collaboration with LANL on their FRC experiment, FRX-L (Field Reversed eXperiment-Liner). The focus of this experiment has been to study the formation of FRCs and to identify appropriate pulsed power and deuterium pre-fill parameter regimes in which high-density, long-lifetime FRCs can be reliably formed. Under Task Order 16 of the Directed Energy Technology, Applications, and Research (DETAR) contract, which began approximately three years ago, SAIC and our subcontractors, with guidance from AFRL, expanded these joint efforts to include the design, assembly, and testing of a second FRC experiment located at AFRL's Shiva Star facility at Kirtland Air Force Base. This new experiment, FRCHX, has the goal of not only forming a high-density, long-lifetime FRC plasma but of also translating it into an aluminum flux-conserving shell (solid liner), where it

will be subsequently heated through rapid compression of the liner. This experiment will serve as the first MTF demonstration experiment in a laboratory using FRCs.

The FRC formation section of FRCHX has been designed to match closely the electrical properties of FRX-L so that FRCs of similar parameters can be formed. Likewise, the translation region of FRCHX, which was designed and fabricated concurrently with the translation region of FRX-L, is also quite similar to FRX-L's, though with slower-rise-time magnetic fields to enable penetration of the field through the solid liner structure surrounding the capture region. The approach for compressively heating the FRC in the capture region of FRCHX has relied on the "deformable-contact" 10-cm diameter, 30-cm length solid liner design that was tested during two earlier vacuum liner experiments. These experiments were performed with the Shiva Star High Energy Capacitor Bank in December 2003 and January 2005, and unique to these experiments was the presence of 8-cm-diameter holes on the axes of the liner electrodes both to permit entry of the FRC into the liner and allow diagnostic access. Both of these vacuum-liner tests were found to be very successful in that the ends of the aluminum liner—approximately 6 cm at each end—stretched and maintained contact with the electrodes while the body of the liner—the remaining 18 cm—glided radially inward to implode uniformly.

This report concentrates primarily on outlining the design of the FRC formation region of FRCHX and its associated pulsed power systems and diagnostics, as the majority of the work under this Task Order was concentrated on this part of FRCHX. Section 3.0 discusses the build-up and integration of the Bias, Pre-Ionization (PI), and Main pulsed power systems and several of the key plasma diagnostics needed for FRC formation. This section describes the performance of these systems and diagnostics during a series of preliminary operational evaluation tests that used an early FRX-L-like (horizontal) vacuum and field coil configuration. A rudimentary manual control system was used to operate the charging supplies and then perform the dumping operations for each bank following these tests, and the Shiva Star data acquisition system was used to collect the data. This combined effort then comprises the first phase of the FRCHX formation region development.

Following the completion of tests with the horizontal vacuum and field-coil arrangement, the vacuum system and Theta coil were rebuilt in a vertical orientation, which was more consistent with the requirements for subsequent FRC translation and compression in a solid liner under the Shiva Star bank. Two additional pulsed power systems (for the Upper and Lower Cusp coils)

were brought on line at this time, as were some additional plasma diagnostics and a computer-based control system to automate many of the bank operations. Furthermore, a dedicated, well-shielded data acquisition system was set up for recording the data from the FRCHX diagnostics. Once these changes were completed, a series of static FRC formation tests were then performed to both verify that FRCHX was in fact forming FRC plasmas, as well as to identify the density, temperature, and lifetime baselines that could be expected for FRCHX FRCs. Section 4.0 covers this second phase of the FRHCX formation region buildup and testing with the vertical vacuum and field coil configuration.

Though the majority of the work under DETAR Task Order 16 concentrated on systems and diagnostics pertaining to the FRC formation region of FRCHX, the basic design of the translation and capture regions were also established under this Task Order, and fabrication and assembly of several of the key hardware components and systems for these regions were started. Section 5.0 briefly outlines the FRCHX translation and capture region design and their integration with the formation region. In addition, the sixth and final pulsed power system – the Guide/Mirror pulsed power system—to be brought on line for FRCHX is described here, as are the field coils that are driven by this bank, which are used to guide the FRC from the top of the Theta coil into the solid liner and to capture it within the liner.

During the course of this Task Order, SAIC personnel had the opportunity to travel to two conferences and give presentations on the work being performed on FRCHX. Section 6.0 presents a brief description of these two conference trips.

Section 7.0 summarizes the overall technical efforts carried out under Task Order 16 and presents a compilation of the principal conclusions drawn from the FRC formation tests described in Sections 3.0 and 4.0. Section 8.0 summarizes the present status of FRCHX, along with some recommendations for future work on this experiment.

3.0 FRCHX PHASE I DEVELOPMENT EFFORT

This section of the report describes the early stages of SAIC's and subcontractors' efforts toward building up and integrating the Bias, PI, and Main banks (including the Crowbar switch on the Main bank) into the FRCHX. These particular systems (and among them especially the Crowbar switch) were found to be the most problematic at FRX-L, partly because they all drive the same Theta coil load. The series of operational tests that were performed during this first phase of the

FRCHX effort thus provided a means through which personnel could begin checking for and mitigating problems early with these systems or, alternatively, verifying that their operation was acceptable. A quickly assembled, horizontally oriented vacuum and field-coil stand served as the test load for the three formation banks. The presence of the vacuum system also enabled personnel to start experimenting with the various FRC formation parameters during tests, as well as to begin developing and fielding some of the key FRC plasma diagnostics. As soon as it was felt that enough tests had been performed to characterize adequately and/or troubleshoot the pulsed power systems and the new diagnostics and to identify any changes that needed to be made to these systems, the Phase I effort was ended. Personnel resumed work that was directed toward completing the assembly of the remaining FRCHX systems and putting together the vacuum and field-coil stand in a configuration that was appropriate for the FRC compression-heating tests. Figure 1 shows the experimental setup, located in the northeast corner of the Building 322 high bay, just as the tests being conducted for this Phase I effort were beginning.

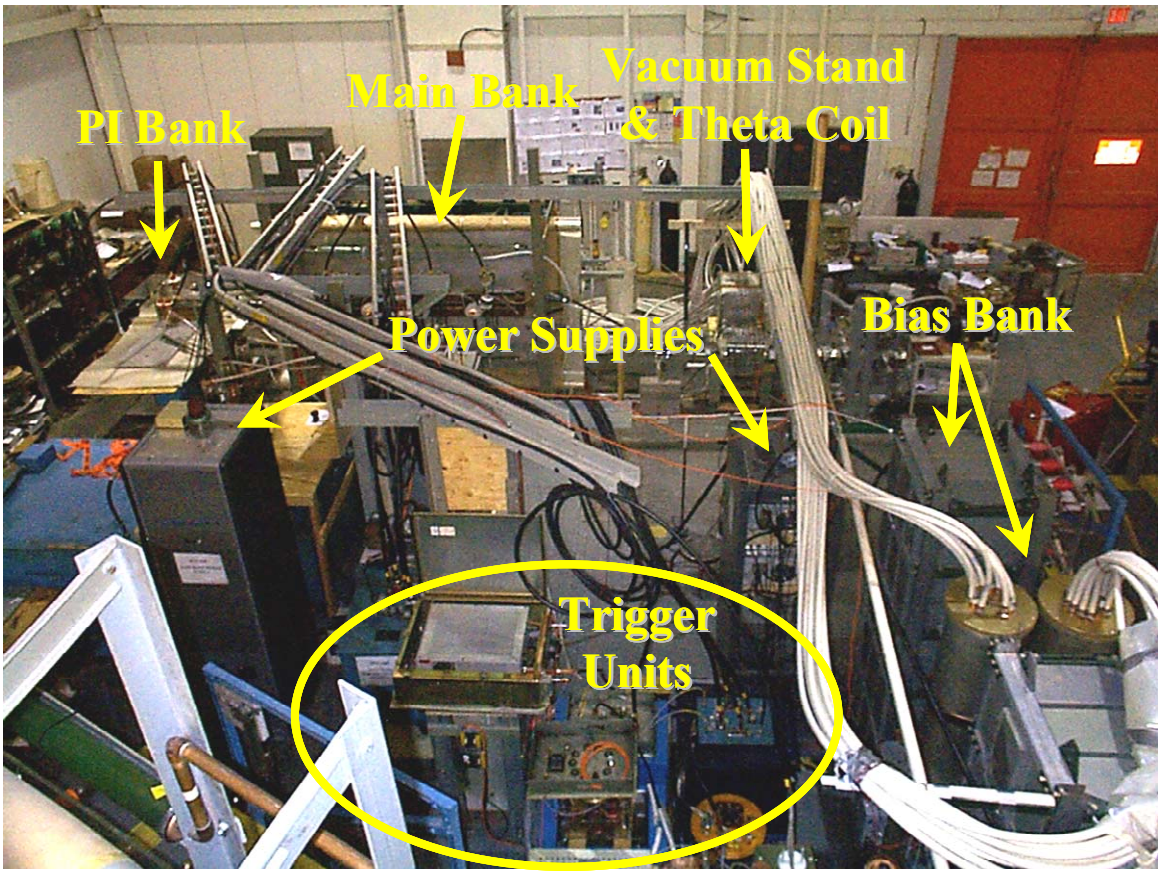


Figure 1. View from Shiva C-arm of early FRCHX experimental setup

We discuss the various pulsed power systems, the horizontal vacuum and field-coil stand set up to test these systems, and the first plasma diagnostics fielded at this time to diagnose FRC formation in Sections 3.1, 3.2, and 3.3. All diagnostic signals were routed to the Shiva Star screen room for these tests, where the established Shiva Star data acquisition system was used to record the data. The manual control system used to operate the charging supplies and to manage the dumping operations for each bank is presented in Section 3.4. Section 3.5 then concludes this presentation of the initial development of FRCHX with a brief analysis and discussion of the data recorded during the tests with the horizontal vacuum and field-coil test stand.

3.1 Assembly of Pulsed Power Systems for Bias, PI, and Main Banks

3.1.1 Bias Bank Systems

The FRCHX Bias bank is used to set up the initial bias magnetic field throughout the FRC formation region as the formation process is beginning. In its initial configuration, the principal components of the Bias bank circuit, aside from the Theta coil, consisted of a 2.55-mF, 10-kV capacitor module that had previously been a part of the “Slow Bank” in Building 322, one size-D ignitron switch, and two 7.05-μH isolation inductors that were borrowed from LANL, which served to protect the Bias bank from the higher voltages applied across the Theta coil by the other two banks. Though these items for the Bias bank were already in hand, it was necessary to fabricate a number of additional structural parts to integrate all the components and form the basic Bias bank system. In the process of doing so, provision for incorporating a second capacitor module and ignitron switch into the bank was added to enable the bank current to be increased later, should it be necessary; this increase indeed turned out to be the case.

We present a brief outline of the construction process for the Bias bank. First, an aluminum base plate for the bank was set up in position. This plate was placed on insulating feet to allow the bank to float when discharging, thereby enabling a single-point connection to ground to be maintained at the Theta coil. Next, the two Slow bank capacitor modules (though, again, the second was intended to only be spare initially) were hoisted onto the plate using the crane. Once the bank modules were bolted onto the plate, the inductor stand and two parallel inductors were set up between the modules. Before lowering the inductors completely into place in their respective return-conductor tubes, the RG 17/14 transmission-line cables that carry the bank current to the Theta coil were attached. A short span of G-10 cable tray was set up to support the RG 17/14 cables above ground as they were run from the bank and the inductors over to the

Theta coil cable header. Lastly, 3 in.-wide, 0.125-in.-thick copper straps were used to connect the working Bias bank module to the ignitron and to the base of the inductor-return conductors. A 6.8 mΩ resistor was placed in the circuit in series between the inductor returns and the capacitor case/ground to ensure that the maximum Coulomb transfer during a bank discharge (assuming the bank was charged to its maximum voltage of 10 kV) was kept below the rating for the ignitron. A Pearson current monitor was placed around this same ground-side copper strap to provide a measurement of the Bias bank current. Figure 2 shows the bank following the completion of its assembly. The module to be used is seen in the lower right, while the spare module is the one in the center left.

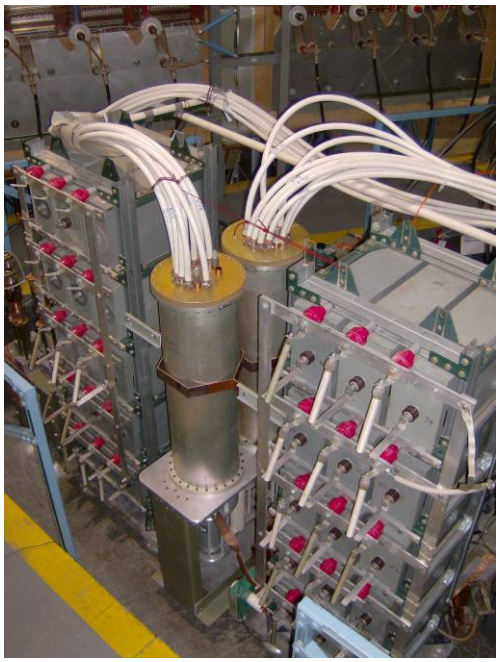


Figure 2. Bias bank just after its assembly was completed

A small 1.5 ~ 2.0 kV pulser, built in-house by SAIC personnel, was used to trigger the ignitron switch on the Bias bank. The trigger unit receives its input trigger through a fiber-optic line, and the output of the trigger unit is then connected to one of the igniter pins on the ignitron through a 1:1 isolation transformer. The trigger unit is small enough that it was possible to mount it near the ignitron on one of the G-10 legs of the inductor stand.

The last items required before charge tests could begin with the Bias bank were charge and dump resistors for the bank and a controller (manual) to allow personnel to operate remotely both the bank power supply and the various high-voltage switches. Temporary control units, which can be used again in later FRCHX tests perhaps to control some of the more complex diagnostic

systems, were assembled and set up to provide this remote control capability. (See Section 3.4 for descriptions of these control units.) As for the charge-and-dump resistors, Figure 3 shows a circuit diagram illustrating how the resistors are interconnected with the Bias bank and its power supply.

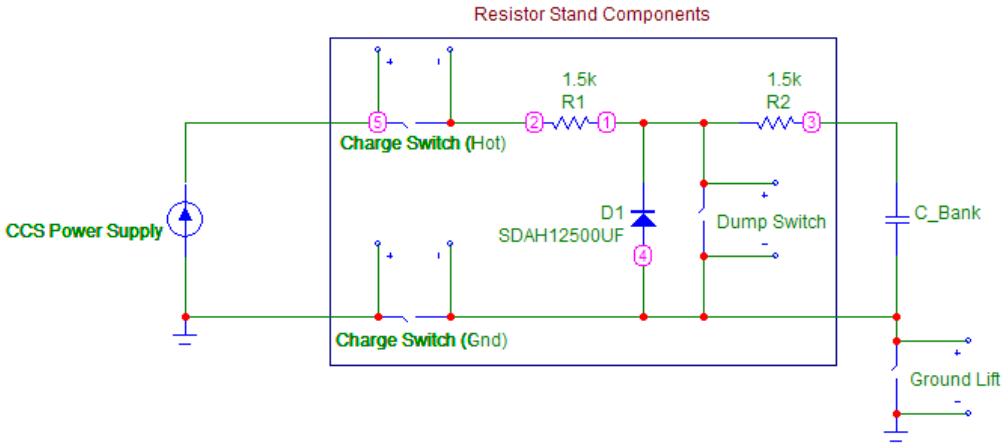
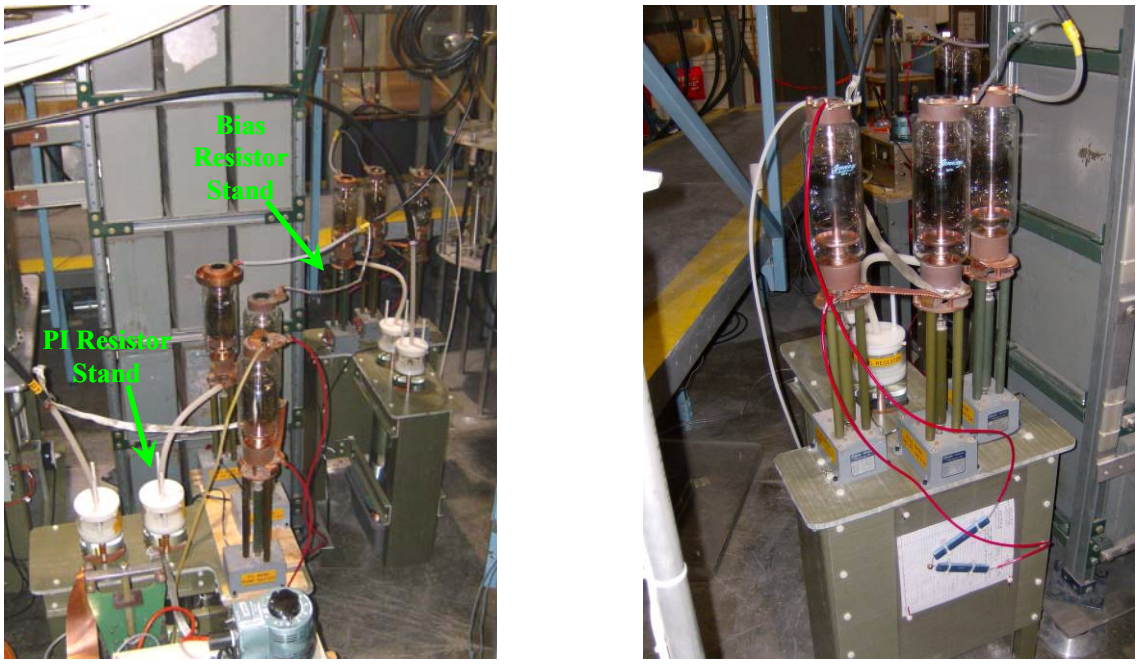


Figure 3. Basic charging and dumping circuit for both PI and Bias banks

As can be seen in the diagram, both of the resistors, R_1 and R_2, are intended to serve as charge resistors, while the second resistor, R_2, also serves as the dump resistor. Once the bank has reached its target charge voltage, the supply is turned off and the charging switches on both the high voltage and ground side of the power supply are opened to isolate the bank completely before it is triggered. The diode stack, which is comprised of several 12.5 kV SDAH12500UF diodes, is connected at the node between the two resistors and in parallel with the dump switch. The diode stack serves to protect the charging supply from voltage reversals should the bank pre-fire before the charging switches are opened. After triggering, the dump switch is close to discharge any remaining energy in the bank through R_2.

Parts for a total of five charge-and-dump resistor stands, which were designed based upon the $CuSO_4$ resistor stands currently in use at FRX-L, were fabricated at a local machine shop and then assembled in-house by Voss Scientific personnel. Each of the switches in the Figure 3 diagram is implemented on the resistor stand using a Jennings vacuum switch. Once assembled, the charge-and-dump resistor stand for the Bias bank was moved into place just west of the bank, and high-voltage cables were run between the resistors and the bank and its power supply to complete all the connections shown in Figure 3. Figure 4a shows the completed resistor stands for both the Bias bank and the PI bank in place adjacent to the Bias bank. Figure 4b shows a

close-up view of the protection diodes (two SDAH12500UFs so that the diode stack is rated at greater than two times the maximum charge voltage of the bank) and the three Jennings switches on the Bias bank resistor stand.



a b

Figure 4. (a) PI and Bias bank resistor stands; (b) Jennings switches and diode stack on Bias bank resistor stand

Figure 5 shows the first triggered tests with the Bias bank performed in the fall of 2006. Bias bank current waveforms from two of these early tests, the second of which included the Main bank, which had also been brought on-line by this time. The plot shows two recent tests of waveforms with (Shot 32) and without (Shot 30) the Main bank also being triggered.

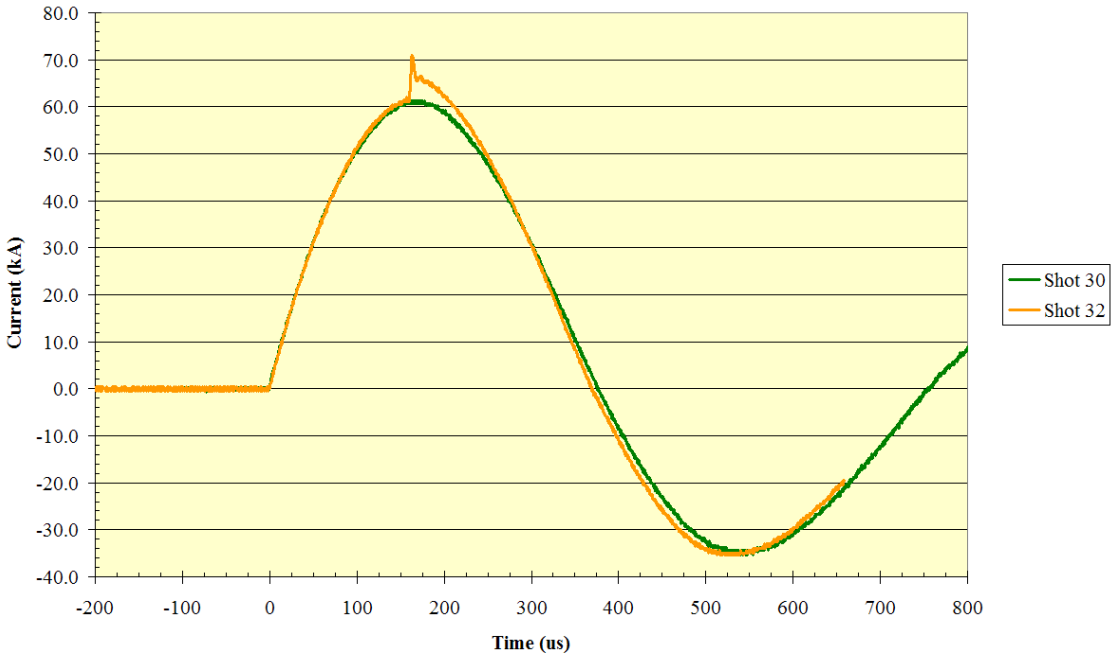


Figure 5. Bias bank current waveforms recorded with Bias Pearson monitor

In both tests, the Bias bank was charged to 4 kV, and a maximum current of ~60 kA was achieved. The abrupt increase in current at the maximum of the Shot 32 waveform is a result of the Main bank being triggered at this time.

3.1.2 PI Bank Systems

Assembly of the PI bank was largely carried out under the previous MTF-FRC task order, DEHPM Task Order 36 (Grabowski 2006c). Work remaining to be performed as Task Order 16 began included primarily the fabrication of an SF_6 enclosure for the bank's cable header, which was to allow the header to be backfilled with SF_6 to prevent flash-over during tests, as well as the setting up of the power supply, the charge-and-dump resistors for the bank, and a manual controller that would allow personnel to operate remotely the power supply and the high-voltage switches on the resistor stand.

Figure 6 shows the bank with the parts of the SF_6 enclosure being test-fitted.



Figure 6. PI bank SF_6 enclosure being test-fitted

Figure 3 and Figure 4a showed, respectively, the basic electrical layout for the charge-and-dump resistor stands and the stand for the PI bank being placed near the Bias bank at the same time that the Bias bank resistor stand was being set up. Because the maximum charge voltage of the PI bank was 50 kV instead of 10 kV, as was the case for the Bias bank, the number of protection diodes in the diode stack was increased to eight to maintain the same percentage voltage hold-off for the stack (Figure 7).



Figure 7. Jennings switches and diode stack on PI bank resistor stand

A temporary manual control unit, like that for the Bias bank, was set up to provide the remote control capability for the power supply and the resistor-stand switches. Section 3.4 discusses these control units.

A Maxwell 40168 trigger amplifier and 40151 trigger generator are being used to trigger the PI bank. These, like most of the bank-assembly work, had been set up as part of the effort carried out under DEHPM Task Order 36. Trigger tests with these units were performed for the first time in November 2006, however, and these tests showed that the PI bank rail-gap switch was multi-channeling quite well. Once the trigger tests had been performed and all interconnections between the PI bank, its charging supply, and its resistor stand had been made, charge tests with the bank were then able to commence. The first charge tests with the PI bank were performed in December 2006, and tests up to the full charge voltage of the bank (50 kV) were able to be successfully carried out at this time.

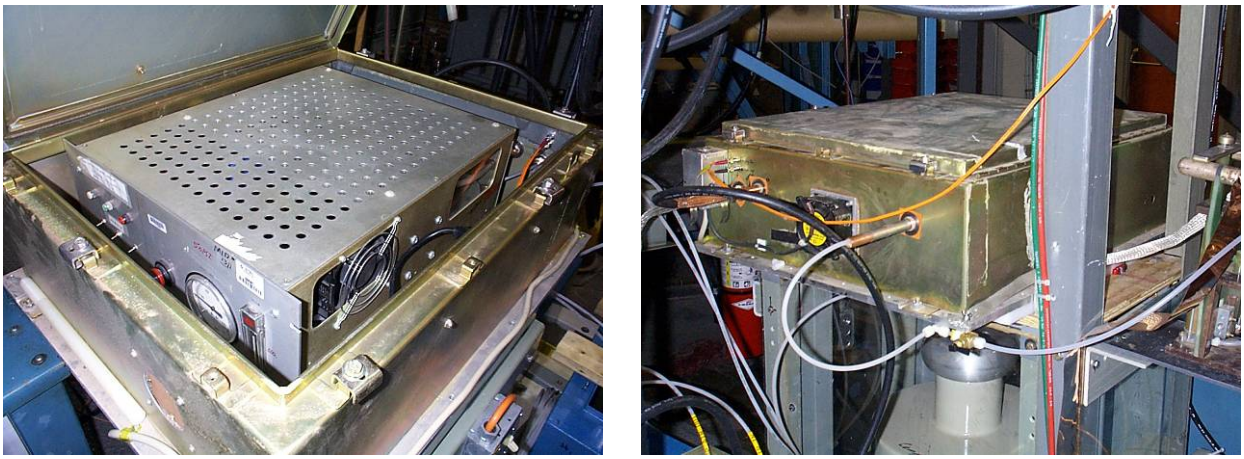
3.1.3 Main Bank and Crowbar Switch Systems

3.1.3.1 Initial System Tests

As with the PI bank, the design and assembly of the Main bank, together with its Crowbar switch, were carried out under the DEHPM Task Order 36 (Grabowski 2006c). By the time the new DETAR task order was put into place, triggering and charging tests with the Main bank and Crowbar switch were ready to commence.

These characterization tests began in the summer of 2006, and the test series started with "trigger-only" tests, followed by charge-and-dump tests and then "charge-and-trigger" tests. Only minor problems were encountered during the Main and Crowbar switch trigger-only tests, and these were easily corrected. No problems at all were encountered with the Main bank charging system during charge-and-dump tests that were performed up to ±20 kV. Upon reaching ±20 kV, the first charge-and-trigger tests were performed. At this point it became apparent that a shielded enclosure would be necessary for the Crowbar switch's 40168 trigger amplifier, as the triggering of the Main bank closing switch was causing the Crowbar 40168 to pre-trigger. A small Hoffman box almost perfectly suited for this application, in that it already contained a cooling fan and an AC power filter, was located in the Building 276 storage facility. After making only minor modifications to the box (e.g., adding appropriate feedthroughs for cables and gas lines), the Crowbar 40168 was able to be placed inside and connected again to all

the other Crowbar trigger system components (Figure 8). Subsequent tests then showed that the Hoffman box had indeed eliminated the pre-triggering problem.



a b

Figure 8. (a) New Hoffman box with 40168 inside; (b) feedthroughs that were added

With the pre-triggering problem eliminated, subsequent Main bank tests then showed, most unfortunately, that the FRCHX Crowbar switch was behaving very similarly to its counterpart at FRX-L; specifically, one or more of the Crowbar rail gaps were failing to conduct when the Crowbar switch was triggered. What made this problem particularly troublesome was that the number of conducting rail-gap switches varied from shot to shot, as did the rail gaps themselves that conducted, and it led to increased and varying amounts of modulation on the crowbarred Theta coil-current waveform, as well as increased wear on the rail-gap switches when only one or two of them were conducting. Furthermore, as with FRX-L's Crowbar switch, performance was found to worsen (that is, fewer Crowbar rail gaps would conduct) as the trigger time for the Crowbar switch was moved away from the time of the peak in the Main bank current. This behavior is opposite to that observed for the original Crowbar switch when the characterization tests for it were being performed during early 2001.

Testing had begun with the Main bank having a positive polarity, like the FRX-L Main bank, so personnel reconfigured the Main bank to operate with a negative polarity to match the bank configuration better used during the 2001 characterization tests of the original Crowbar switch. Such changes also included adding an insulated grounding connection between the Main bank frame and the Crowbar switch-triggering system to ensure that the triggering-system ground floated with the Main bank ground, but these efforts did not yield any improvement or changes.

A few shots were performed at this time with the Main bank in which the Crowbar switch was not triggered to evaluate the quarter-cycle time, the inductance, and the resistance of the overall Main bank circuit. Figure 9 shows a plot of the current waveforms that were recorded with the Rogowski coils around the Main bank cable header and at the Theta coil.

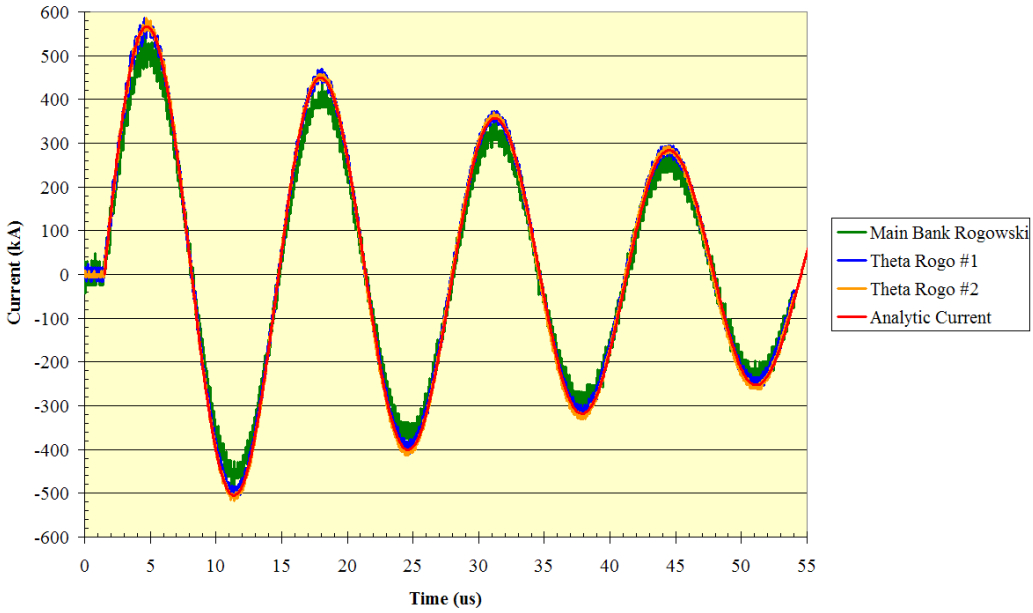


Figure 9. Current waveforms obtained from Rogowski coils on Main bank and on current feed to Theta coil

Examining the period of each of the three recorded current waveforms shows that the quarter-cycle rise time is ~3.26 μs. Using the analytic expression for current in an RLC circuit,

$$I = I_o e^{-\alpha t} \cos(\omega_n t), \tag{1}$$

where

$$\alpha = R/2L, \tag{2}$$

$$\omega_n = \left[\frac{1}{LC} - \frac{R^2}{4L^2}\right]^{1/2}, \tag{3}$$

I_o is the peak current, t is time, and R, L, and C are the circuit resistance, inductance and capacitance, respectively, an analytic current waveform was calculated and overlaid with the experimental waveforms in Figure 9. To obtain good agreement with the Theta Rogowski waveforms, values of 0.0043 Ω, 36 μF, 123.5 nH, and 600 kA were used for R, C, L, and I_o, respectively.

3.1.3.2 Changes Implemented on the FRX-L Main Bank and Crowbar Switch

Concurrently with our attempts to characterize (and improve) the new FRCHX Main bank and Crowbar switch, SAIC personnel were also continuing to assist LANL personnel in their efforts to improve the performance of the FRX-L Crowbar switch. Both these switches were experiencing identical problems, suggesting that the reason for these problems rested with something intrinsic in either the Main bank or Crowbar switch design. Motivation to experiment simultaneously with changes on both the FRCHX and FRX-L Crowbar switches was driven by the fact that more variations could be tested more rapidly utilizing the two systems rather than just one. We discuss here the two primary changes that were tested at FRX-L. Unfortunately, neither of these changes yielded any improvement in the FRX-L Crowbar switch, but we include them so that they may be archived along with the other changes to the switch that were explored under this task order. By building a database of all the changes and their corresponding results, it is hoped that a better understanding can be obtained of the Crowbar switch problem.

FRX-L Crowbar Test Results with Slotted Bus Work to Provide Rail Gap Isolation. The final two quarterly reports for DEHPM Task Order 36 (Grabowski 2006a, 2006b) describe the design work performed by SAIC personnel associated with modifications to the upper half of the bus work between the FRX-L Main bank and the Crowbar switch. Specific details of these modifications are described more fully in a memo (Grabowski 2006a), but, in short, the basic concept focused on introducing longitudinal slots in the bus work to provide a measure of inductive isolation between each of the rail-gap switches in the Crowbar switch. The inductive isolation was intended to offer a slightly greater time window in which the trigger pulse delivered to each rail gap could initiate breakdown before the voltage across the rail gap collapsed due to the closure of adjacent gaps.

Testing of the new slotted bus work configuration for the FRX-L Crowbar switch began as SAIC's work under the DETAR Task Order 16 began, but unfortunately it appeared that the level of inductive isolation provided by this new hardware was insufficient, with little change in Crowbar switch operation. SAIC personnel were present to observe and support the testing on several occasions, and the "standard" parameters such as switch pressure and time delay between Main bank and Crowbar triggering were varied with little sign of improvement. A key assumption for the slotted bus-work design was that the Crowbar rail-gap jitter was comparable to the jitter of the closing switch rail gaps, which is only a few ns or less (Grabowski 2006a). The

bus work was designed, therefore, to provide 2 ~ 3 ns of isolation, compared to the sub-ns isolation that was previously present. However, based upon the test results, the conclusion is that the Crowbar rail-gap jitter is somewhat poorer than expected, and the amount of inductive isolation that was added was too small to provide any significant benefit.

Higher Energy Trigger Unit. With the slotted bus work having turned out to be insufficient to improve the Crowbar switch triggering, FRX-L and SAIC personnel shifted their attention toward a second possible solution, that of enhancing the Crowbar switch-triggering system (Grabowski 2006a). Rather than attempting to increase the amplitude of the trigger pulse as discussed in the memo, however, which would require both running an additional trigger cable for each rail-gap switch and changing and adding some components on the trigger board to increase the voltage hold-off, an alternative scheme was suggested that involved increasing the energy of the trigger pulse instead.

To enable a higher-energy trigger pulse to be produced it was necessary to make some modifications to the Maxwell 40151-B Multiple Trigger Generator that was currently being used to trigger the FRX-L Crowbar switch. Specifically, the 40151-B was converted from a charged-cable arrangement back to one in which the capacitive energy store was located within the trigger tank. The amount of the capacitance in the trigger tank was then increased well beyond that which was provided by the four trigger cables and also beyond that which was originally incorporated into the unit by the manufacturer. Such an increase in capacitance was accomplished by inserting additional capacitors (according to what the available space in the tank would permit) in parallel with the original ones in the trigger circuit. With the triggering system no longer employing a charged-cable configuration, the blocking caps at the trigger board, which connect the RG-218 trigger cables to the peaking gaps and to the ground side of the switch, were then removed. The peaking switch was left in place to serve as a means of sharpening the rise time of the trigger pulse.

Figure 10 shows a Maxwell 40151-B Multiple Trigger Generator like the one being used at the FRX-L facility.



Figure 10. Maxwell 40151-B trigger generator with additional 100 kV, 0.099 μF capacitor

A 100 kV, 0.099 μF Maxwell capacitor was placed on one side of the trigger generator to show that it is sufficiently small to allow it to be connected in parallel with the orange "doorknob" capacitors above the spark-gap switch, which comprise the original capacitive store of the trigger unit.

When the modified 40151-B trigger generator was fielded at the FRX-L facility, it also failed to solve the Crowbar rail-gap-triggering problem, and it in fact appeared to introduce additional problems for the Crowbar switch. Some of these problems were mitigated when the blocking capacitors between the trigger-cable braid and the ground side of the Crowbar switch were put back in place. However, the switch still did not perform as well as with the charged-cable triggering system. In retrospect, it is believed that due to dispersion in the trigger cables the rise time of the more energetic trigger pulses was not as fast as the rise time of the pulses delivered by the charged-cable triggering arrangement. As a result, the trigger pulses, though more energetic, had greater difficulty in initiating breakdown in more than one Crowbar rail gap.

3.2 Horizontal Vacuum and Field-Coil Stand

As mentioned, a rudimentary, horizontally oriented vacuum and field-coil stand was put together to provide an appropriate load for the bank tests described in Section 3.1.3.2, as well as to enable personnel to start experimenting with the various FRC formation parameters during tests and to begin developing and fielding some of the key FRC plasma diagnostics. This section presents the

details of the field coil (Theta coil) load that was assembled for the bank tests and the vacuum system that was put together to go with it.

3.2.1 Wide-Segment Theta Coil with Passive Mirrors

The magnetic field coil driven by the banks was very similar to the original FRX-L Theta coil, consisting of four 3.25-in.-wide (8.26-cm-wide) parallel coil segments spaced 0.391 in. (1 cm) apart. The bore radii of the segments on each end, however, were 0.5 cm smaller than the radii of the two inner segments, which were the same as the radii of the FRX-L Theta coil segments. The intent of the smaller bore radii for these outer segments was to introduce a passive mirror on each side of the formation region that we expected would aid in the FRC formation, because the Cusp coils were not yet being set up.

Appendix A contains a series of magnetic field calculations performed with Quick Field® for this Theta coil geometry before any machining was started. These calculations were performed both to obtain an estimate of what the field profile should look like inside the Theta coil bore as well as to check for any obvious problem areas.

3.2.2 Support Stand and Vacuum System Description

Figure 11 shows the Theta coil just described, the cable header that had been designed for it, and the vacuum system and quartz tube that allowed simple FRC formation tests to be performed. The system was set up for both bank tests and preliminary FRC formation tests.

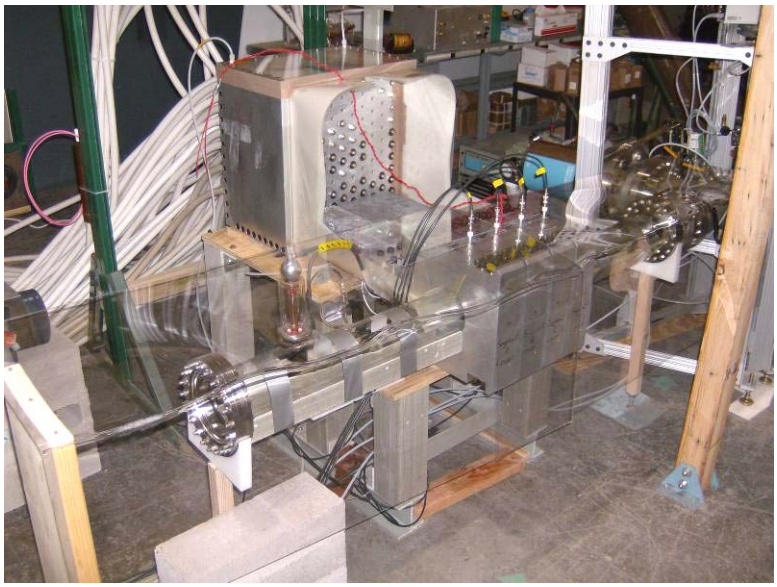


Figure 11. Temporary Theta coil, support stand, and vacuum system

The Theta coil and its cable header were placed on a G-10 and wood support stand, which can be seen in the center of the photo. With the Theta coil oriented horizontally, the primary stainless steel components of the system—two vacuum tees borrowed from the FRX-L facility—were able to be placed just to the south of the Theta coil on a separate stand. These tees each had three 8-in. (20.32-cm) main ports, and one also had three smaller 2.75-in. (6.99-cm) side ports. (Note that these are the diameters of the respective flanges of the ports.)

Once the tees had been set up on their stand, the quartz tube was placed within the bore of the Theta coil, and the tees were leveled to align their collinear 8-in. ports with the axis of the tube. Windows on the north end of the quartz tube (to the left) and on the south end of the vacuum tee assembly (to the far right) provide for both a vacuum seal on each end and allowed for axial photography of the FRC with a gated micro-channel plate (MCP) camera. A vacuum bellows between the vacuum tee assembly and the quartz tube provides some measure of shock isolation for the quartz tube. In addition, a thin Lexan shield has been placed around the top and west side of the quartz tube where most of the personnel work and traffic are located. This shield served to protect the tube from accidental breakage and personnel from injury in that event.

The pumps for the vacuum system included a Varian dry scroll pump that was purchased for this effort and a CTI Cryogenics cryopump that was available in-house. The dry scroll and cryopumps were attached to one of the 2.75-in. ports and to one of the 8-in. ports respectively, with appropriate gate valves in between. A Pfeiffer full-range vacuum gauge on one of the other 2.75-in. ports provided for a measurement of the vacuum pressure within the system. Two needle valves connected with a tee to a ¼-in. Swagelok® fitting on the last 2.75-in. port allow for backfilling of the vacuum system with dry nitrogen or pre-filling it with deuterium before a shot.

3.3 Plasma Diagnostics

3.3.1 Magnetic Probes

A minimal set of plasma diagnostics was fielded around the Theta coil for the preliminary FRC formation tests that were to be performed. Diagnostics that were deemed most essential for confirming the formation an FRC plasma were magnetic diagnostics such as B-dot probes and flux loops. As described by E. Um (Um 1994), the measurements from these two types of probes allowed obtaining an estimate of both the magnetic flux trapped by the FRC plasma as it is formed and its excluded flux (separatrix) radius.

A single voltage divider, like the ones used by E. Um, was available from the FRX-L facility for us to use, so it was possible to install one flux loop right away in the test setup. This loop was placed in the center of the formation region. Four single-turn B-dot probes, manufactured by Prodyn Technologies, were inserted into ports in the tops of the Theta coil segments, one probe per segment. Figure 12 shows the placement of these probes along the length of the Theta coil.

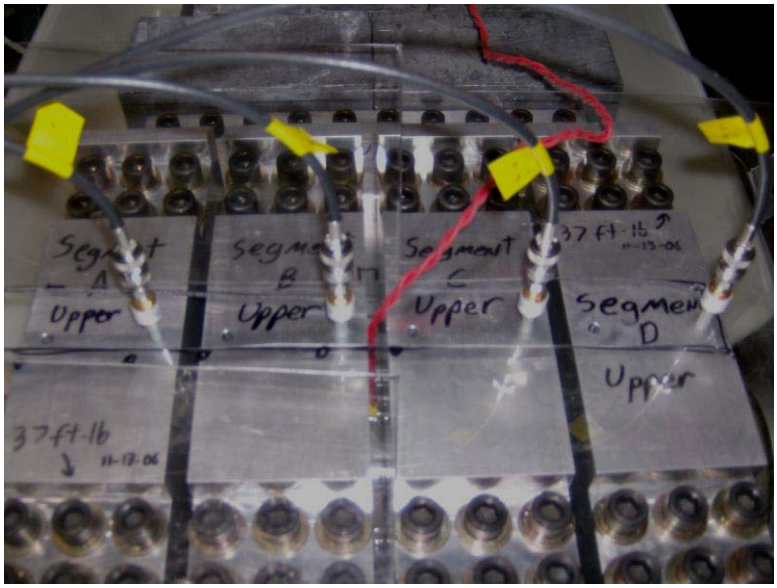


Figure 12. Placement of B-dot probes and flux loop along Theta coil

As it turned out, because the B-dot probe ports were located rather close to the edges of their respective Theta coil segments, it was often difficult to interpret the measurements of these probes.

Shortly after the initial FRC plasma formation tests had begun, several UNR researchers joined us for several weeks and during that time fabricated a simple analog circuit that would allow the resolution of the excluded flux measurements to be improved. It did this by "pre-processing" the flux loop and B-dot probe signals before they were recorded on digitizers; that is the analog circuit was simply an adder circuit that combined the flux loop signal and a nearby B-dot probe signal (the one from "B" segment) and then integrated that sum. Expressed mathematically and in a simplified form

$$\Phi_{\Delta\varphi} = -C_1 \int V_{ac}\, dt = -\int \left(C_2 V_\ell + C_3 \left(-V_p \right) \right) dt \,, \tag{4}$$

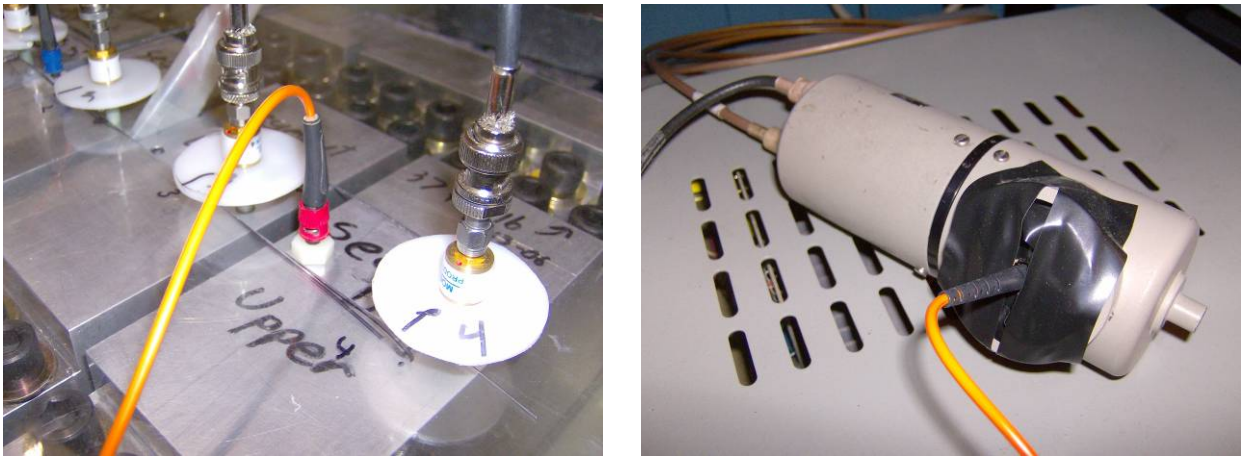
where $\Phi_{\Delta\varphi}$ is the excluded flux, V_{ac} is the analog circuit output, V_p and V_ℓ are the B-dot probe and flux loop signals, respectively, and C_1, C_2, and C_3 are constants. As suggested by the minus

sign in front of V_p, the determination of excluded flux actually requires one to take the difference between the B-dot probe and flux loop signals, which is accomplished with the analog adder circuit by fixing the orientations of these two diagnostics such that the signals have opposite polarity. To correct for errors in the probe measurements, the difference obtained during a vacuum shot is subtracted from the difference obtained during a plasma shot.

The advantage of performing this operation with an analog circuit instead of with a computer during post-processing is that the difference in these two signals may at times be very small while the individual signals themselves may have a very large amplitude. In such a case, the bit noise of the digitized large-amplitude signals may be of a similar magnitude as the difference, making it very difficult to resolve any differences. Digitizing the difference of the signals, though, as provided by the analog circuit, allows the sensitivity of the oscilloscope to be increased significantly, and small variations in the difference can then be resolved more readily.

3.3.2 Fiber-optic Cable Light Monitor

During their visit, the UNR researchers also facilitated the setting up of a "first light" fiber-optic monitor. As its name implies, the monitor's primary function was to indicate when the plasma first broke down and began to emit light. This first light fiber-optic monitor was much like the fiber-optic monitors that were being used on FRX-L to follow the motion of the plasma, except that the light from this monitor was not filtered with a mercury line filter before being injected into a photomultiplier tube (PMT). These monitors are now used on FRCHX, as well; see Section 4.3.3. Figure 13 shows the monitor setup that the UNR scientists helped to assemble.



a b

Figure 13. First light fiber monitor (a) mount on Theta coil; (b) PMT detector in screen room

As seen in Figure 13a, a nylon fitting was used to capture the end of the fiber (a standard ST-type fiber-optic connector) and to hold it in place in the port in the Theta coil segment. The porthole into which the fiber was looking also served to collimate the light that entered the fiber, which provided a spatial resolution for the fiber signal approximately equal to the diameter of the porthole, 0.125 in. or 0.318 cm. In the Shiva screen room the light signal was then converted into an electrical signal with the PMT (Figure 13b), the sensitivity of which was varied by adjusting the bias power-supply voltage.

3.3.3 Micro-Channel Plate Camera

As mentioned in Section 3.2.2, windows on the north end of the quartz tube and on the south end of the vacuum tee assembly allowed fast photography of the FRC plasma to be performed. For these first FRC formation tests a gated MCP camera, with gate widths as short as 100 ns, was set up at the north window to take visible light images of the FRC as it was forming. The camera was housed in a shielded box that was placed off-axis from the quartz tube and with its optical axis at 90° with respect to that of the quartz tube; a collimated mirror then allowed the camera to view down the tube and into the Theta coil bore where the FRCs were being formed. Figure 14 shows the MCP camera setup, somewhat obscured by the protective shielding around the evacuated quartz tube.

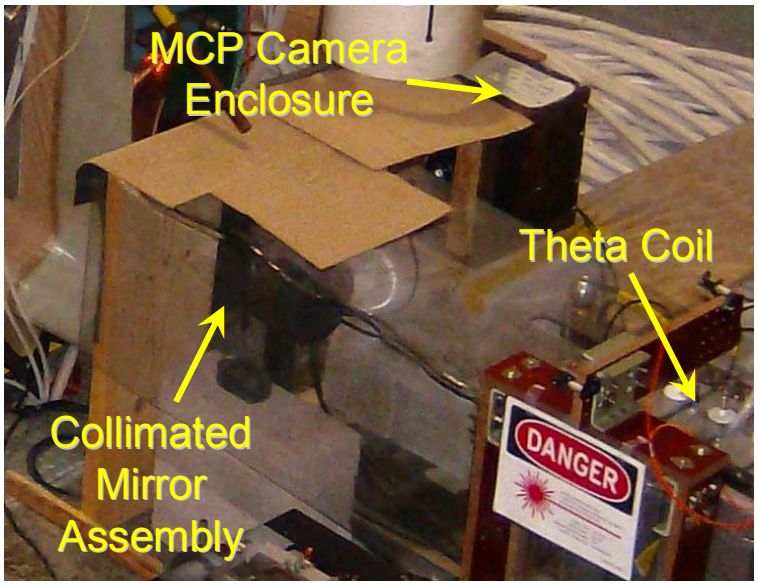


Figure 14. MCP camera setup at north end of quartz tube

3.3.4 Interferometry

Interferometery is a key diagnostic for not only measuring plasma density but also for confirming whether or not an FRC was formed in a given shot. This confirmation is made by examining the density along several chords through the plasma at a given axial location. In addition, an interferometer can supply information regarding instabilities that might develop in the FRC, for example the n = 2 instability. The FRX-L interferometer has, in fact, given evidence of the n = 2 instability developing in several of the FRCs formed there.

3.3.4.1 Four-Chord System

Because of its importance in plasma measurements, AFRL personnel put special emphasis at this time on the design of a four-chord interferometer for the FRCHX experiment. This interferometer is in many ways be similar to the eight-chord system also designed by AFRL personnel and fielded at FRX-L. However, its size has been kept relatively small—hence four chords instead of eight—to allow it to be placed under the Shiva Star bank when FRC translation experiments are performed in this location just before an integrated compression-heating experiment. Furthermore, because the vacuum and field-coil stand is to be oriented vertically when such tests are being performed, the four-chord interferometer system has been laid out on a horizontal optics table. Thus, the four-chord system was not intended to be fielded on the temporary horizontal vacuum and field coil stand being used at this time; it is described in this section because it was designed and constructed during this first phase of the FRCHX effort.

Figure 15 shows a top view illustration of how the interferometer optics table is intended to be put into place around the FRCHX formation (or translation) regions to probe the plasma.

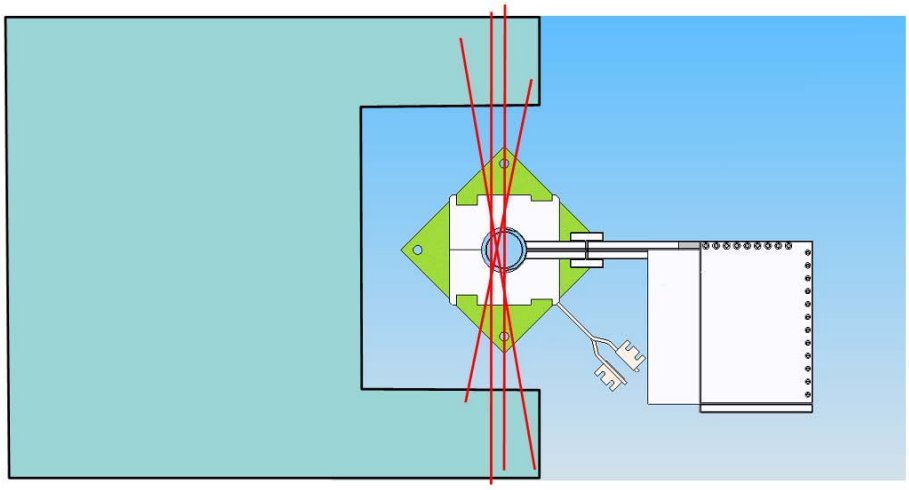


Figure 15. Placement of four-chord interferometer around FRCHX coils

As illustrated, careful placement of the mirrors on the table will allow four distinct chords to be directed across one half of the quartz tube. A density profile of the plasma can then be generated once the data from the interferometer is processed.

Along with the interferometer design, AFRL personnel also provided detailed lists of electronic and opto-mechanical parts that were needed to construct the interferometer. SAIC personnel then took care of ordering them, while NumerEx personnel oversaw their assembly and alignment on the optics table or on equipment-rack shelves. In addition, a special dust cover and ventilation system were designed for the table to keep all the components as clean as possible. SAIC personnel designed the dust cover, and an outside machine shop fabricated it. Figure 16 shows the optics table ordered for the interferometer with the special dust cover being test-fitted on it.

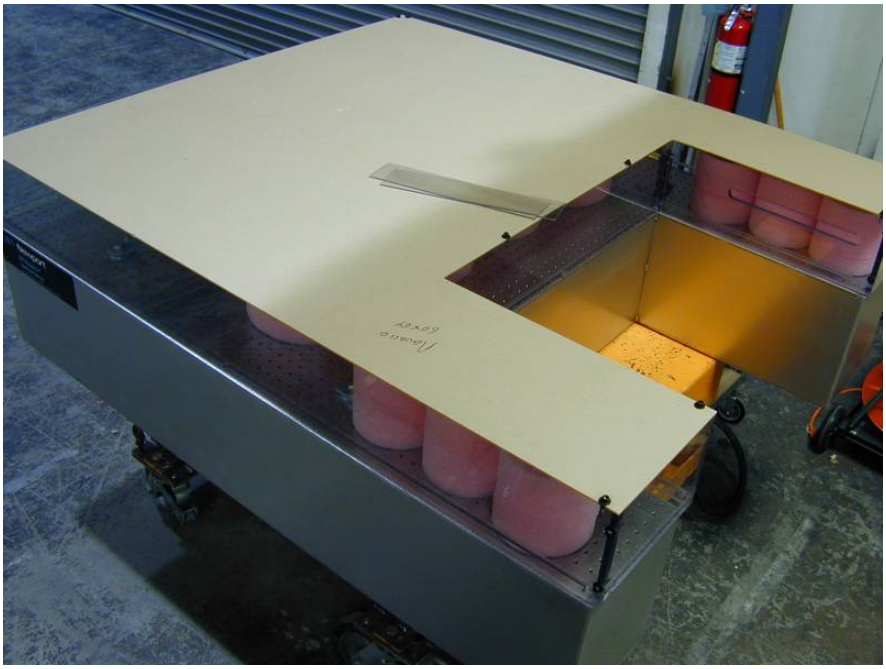


Figure 16. Four-chord interferometer optics table and its dust cover

Figure 17 shows the four-chord interferometer system midway through its assembly. Figure 17a shows the interferometer optics table as various optical components were being positioned on it. The detectors and the RF components for modulating and de-modulating the interferometer signals were mounted to two equipment-rack shelves (Figure 17b).



a b

Figure 17. (a) Mounting of opto-mechanical components on optics table; (b) interferometer detectors and RF components

3.3.4.2 Single-Chord System

While the four-chord interferometer was being designed for the later vertically oriented vacuum and field-coil stand, it was still of interest to gain some experience with interferometry during these preliminary FRC formation tests. As a result, FRX-L personnel offered us the use of a single-chord interferometer that was available at their facility. SAIC personnel transferred the components for this interferometer from the FRX-L facility to Building 322. A UNM postdoctoral student (now a research professor) who had been regularly supporting the efforts at the FRX-L facility then began working on setting up and aligning its optics to make it operational.

Figure 18 shows the single-chord interferometer after the assembly and alignment had been completed and its optics table had been moved into position in front of the FRCHX Theta coil. Because the flux-loop wires emerged from the Theta coil between the B and C segments, the interferometer chord was positioned to pass between the A and B segments.



Figure 18. Single-chord interferometer in position in front of FRCHX Theta coil

3.4 Manual Control System

Mr. Phillip Sanchez and Mr. Robert Aragonez of LANL took on the task of designing, ordering the components, and assembling a Compact Field Point-based (cFP) controller for operating all the systems associated with FRCHX. (This controller is described further in Section 4.5.) Like the four-chord interferometer, though, the design and assembly effort for the controller required a significant amount of time, and continued throughout the duration of the Phase 1 work for FRCHX. However, because some manner of control system was needed before beginning the bank and FRC formation tests primarily to manage the Bias and PI bank systems, a very basic manual system was assembled to fulfill this role during the interim.

This manual control system was designed by NumerEx personnel and assembled by SAIC personnel, and it consisted of two simple eight-channel controller-box pairs. One controller-box pair was used with the PI bank, and the other with the Bias bank. Within each pair was a user interface and transmitter box with toggle switches on the front panel and an International Fiber Systems IFS DT3010 optical multiplexer within (Figure 19a). This box was linked through fiber-optic cable to a system interface and receiver box with display LEDs on the front panel and an IFS DR3010 optical demultiplexer within (Figure 19b).



a b

Figure 19. Manual control system (a) two user-interface controllers; (b) two system-interface boxes

The controllers worked by allowing operators to use the toggle switches to send signals to the receiver boxes, which in turn activated the Maxwell Technologies CCS power supplies used to charge the banks or the various Ross or Jennings switches that were in the charging and triggering circuits. To monitor the real-time bank charge voltage, a TV camera was placed in front of the power supply front panels (Figure 19b), and the image was then displayed on a monitor that was placed next to the user interface and transmitter boxes.

Though the use of the TV monitor and the need to orchestrate all the manual controls in the correct order was slightly awkward, these temporary controllers otherwise allowed operators to perform all the necessary tasks to charge and fire both the PI and Bias banks, and thus it was possible to perform both pulsed power tests with the banks and the FRC plasma-formation tests. After the cFP controller was delivered by Mr. Sanchez and Mr. Aragonez and integrated into the FRCHX systems, these two eight-channel controllers became available for remotely controlling other systems or instruments on the experiment.

3.5 Experimental Results

As discussed, the primary goals of the tests that were performed during this first phase of the FRCHX development effort were (1) to characterize and troubleshoot any problems with the Bias, PI, and Main banks; (2) to experiment with the various FRC formation parameters during

tests so that personnel gain familiarity and experience with the new FRCHX systems; and (3) to begin developing and fielding some of the key FRC plasma diagnostics. In addition to troubleshooting problems early with these systems and diagnostics or, alternatively, verifying their proper operation, these tests also proved useful for identifying several changes that were needed simply to improve the performance of the experiment. This section presents an overview of the Phase I tests, which were performed December 2006–May 2007. The discussion focuses first on continuing efforts to make the operation of the Crowbar switch more reliable. (See Section 3.1.3.1 for a description of problems during initial tests.) This section also describes changes made to the Bias bank to increase the Bias current and field in the Theta coil, after which the results from the FRC formation tests are reviewed.

3.5.1 Campaign to Improve Crowbar Switch Performance

The behavior of the FRCHX Crowbar switch was very much like that of the FRX-L Crowbar switch in that one or more of the rail-gap switches were failing to conduct after the Crowbar switch was triggered. During the first Crowbar switch tests (2001), there were no such problems encountered with triggering the Crowbar rail gaps, so changes were made to the Main bank and Crowbar switch to make conditions more like those that were present at that time: the polarity of the Main bank was changed from positive to negative, and the same master trigger generator (MTG) with external power supply used during those first Crowbar switch tests was brought in and set up to be used again with the FRCHX Crowbar switch. These changes, however, appeared to provide no noticeable improvement or even any variation in performance.

After 26 test shots had been performed, SAIC prepared a memo summarizing the various changes and their results to document everything that had been attempted and observed thus far (Appendix B). It includes a discussion of a meeting held at AFRL about possible methods of correcting the Crowbar triggering problem. Additional approaches to correcting the Crowbar problem were later added to this list.

After further discussion and consideration three approaches viewed as being the most promising included (1) inserting a finite resistance between each rail-gap switch and the connection to the Main bank bus work that feeds the Crowbar switch, (2) converting the pressurized rail-gap switches into vacuum switches and using a trigatron-like triggering scheme to initiate conduction, and (3) setting up an external capacitor bank to apply a more significant voltage (10 ~ 20 kV) across the Crowbar switch either just before or just after it is triggered. Appendix C

contains a review of the various issues that were identified with implementing each of these approaches.

As stated at the end of the discussion in Appendix C, the integration of an additional external capacitor bank (or “Auxiliary bank”) into FRCHX was determined to be the simplest and most straightforward of the concepts to implement. This bank which would apply a voltage across the Crowbar switch when it is triggered and thereby help to drive each of the rail gaps to closure. Choosing this bank was largely because much of the required hardware was already available at AFRL and because none of the existing hardware on the experiment needed to be modified. The Auxiliary bank approach was suggested by DOE-OFES Program Manager, Dr. Francis Thio. With the resistive isolation approach significant changes to the Main bank and Crowbar bus work were required. With the vacuum-switch approach some modifications to the Crowbar rail electrodes were required, though these were less substantial than the modifications required by the resistive isolation approach. The conversion to and fielding of a rail-gap vacuum switch also had several uncertainties about it, because it had not been tried before, though it was still considered for a while as a backup approach should time and resources permit and should the Auxiliary bank fail to add any significant improvements in Crowbar switch performance.

With the path forward narrowed down to a single approach, circuit analyses were performed to investigate just how such a bank would interact with the rest of the FRCHX Theta coil circuit. Appendix D summarizes the results of these circuit analyses. For the 12 μF bank described in Appendix C, the circuit simulations in Appendix D show that the voltage across the Crowbar switch can be increased by as much as 12.5 kV when the Main bank is not in the process of discharging. If the Main bank has been triggered, though, the voltage increase goes down to a mere ~1 kV, because the capacitance of the Main bank is rather large compared to the capacitance of the Auxiliary bank, and the Auxiliary bank is then effectively trying to pulse-charge the Main bank. Nevertheless, it was felt that the net gain of just 1 kV applied quickly across each of the Crowbar rail gaps could possibly be sufficient to aid in driving each of them to closure when they were triggered. Because this approach was still the simplest and fastest to implement, it was decided after reviewing the circuit-simulation results to go ahead and proceed with preparing the Auxiliary bank for testing.

Refurbishing the 12 μF bank that was be used for the Auxiliary bank was accomplished over the course of two to three weeks. Figure 20 shows the bank after its integration into the FRCHX experiment was completed.

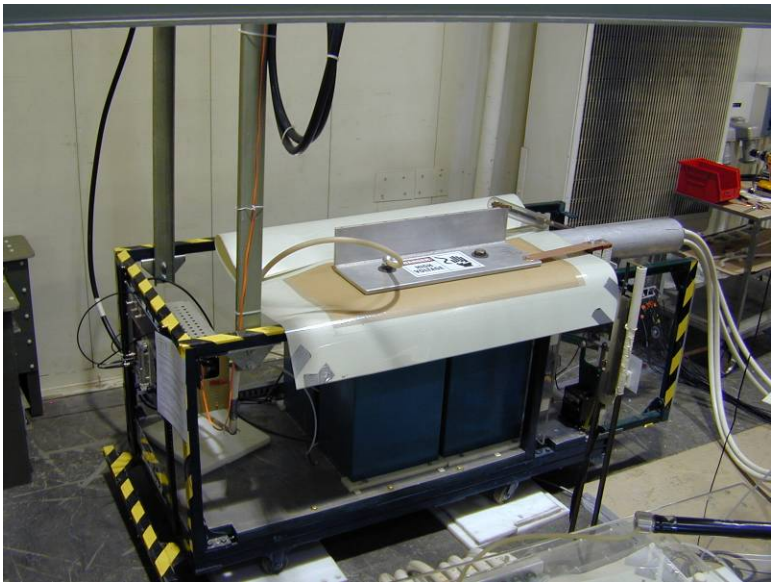


Figure 20. Completed Crowbar Auxiliary bank in place behind Main and PI banks

The four cables from the Auxiliary bank replaced cables 6, 16, 27, and 37 in the Crowbar switch cable header. These particular cables were located approximately adjacent to the centers of each of the Crowbar rail gaps. The Auxiliary bank was triggered using a Maxwell 40295 trigger generator. To keep the high-voltage portion of the unit from pre-triggering when other FRCHX banks were fired, it was powered through an isolation transformer. In addition, the low-voltage component of the trigger generator was placed in a shielded box to protect it from the noise radiated by the switches on the other banks, and it was powered by an uninterruptible power supply (UPS) also placed in the box.

Figure 21 shows a plot of the discharge current from the bank for a test shot involving only the PI and the Auxiliary banks.

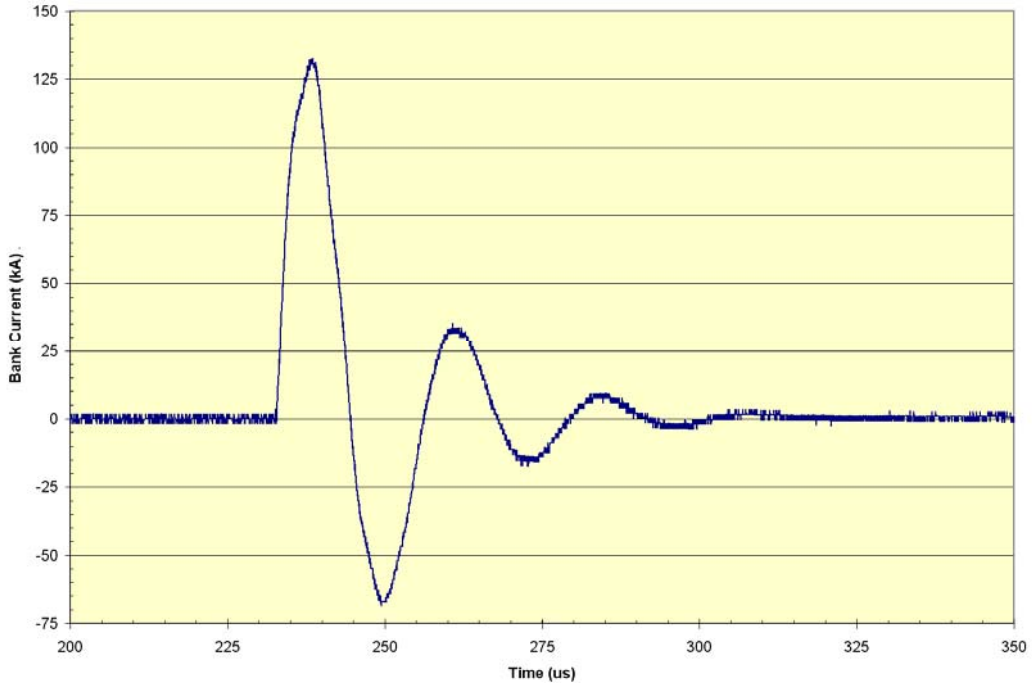
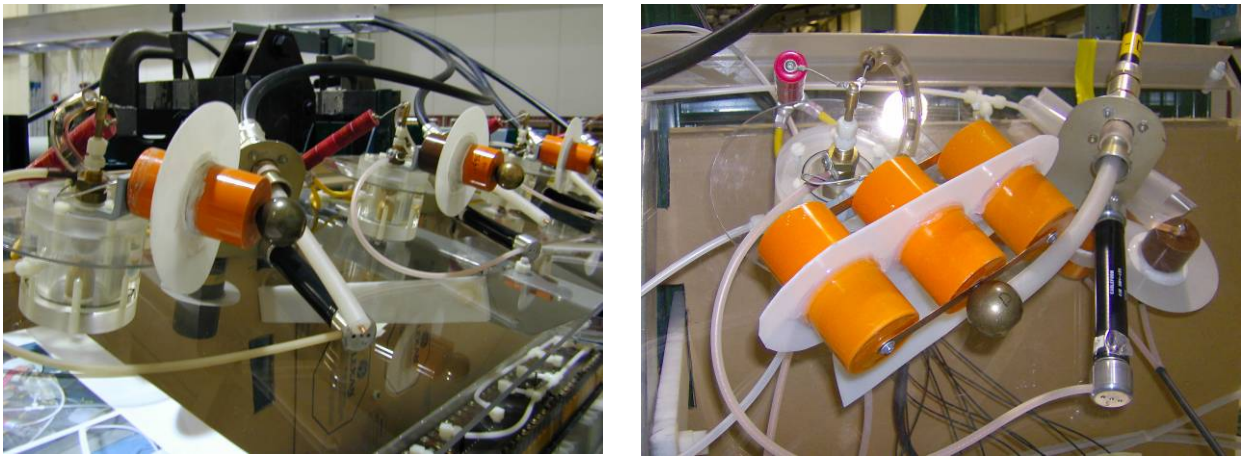


Figure 21. Discharge-current waveform for Crowbar Auxiliary bank

The charge voltage on both banks for this shot was -50 kV. A slight change in slope is seen as the current reaches ~110 kA—a result of the tip of the raw data waveform being clipped slightly when it was recorded. The important feature to note, however, is that the time scale of the Auxiliary bank current was shown to be fairly long compared to the PI and Main bank discharge currents. Thus, the injection of this current into the Main bank and Theta coil was not expected to influence dramatically the behavior of the plasma over the short time scales of FRC formation and translation out of the Theta coil.

Shortly after the Auxiliary bank setup was completed, several additional blocking caps were added at the ends of each of the Crowbar trigger cables to assist further the existing Crowbar triggering system. At 40 ft in length, the capacitance of each trigger cable (RG-218) is approximately 1.2 nF, whereas the total blocking capacitance for each trigger cable, from center conductor to ground braid, had been only 0.25 nF. (A capacitance of 0.5 nF was between the trigger cable center conductor and the peaking gap, and 0.5 nF was between the ground side of the Crowbar switch and the trigger cable ground braid, as is seen in Figure 22a).



a b

Figure 22. (a) Original Crowbar trigger board setup; (b) new setup with additional blocking caps

This capacitance suggests that not all the stored energy in the trigger cables was being delivered to the rail-gap switches during the trigger pulse. By increasing the blocking capacitance to 1.5 nF between the center conductor to the peaking gap and to 1 nF between the ground side of the Crowbar switch and the trigger cable ground braid, and by also adding 1 nF between the high-voltage side of the Crowbar switch and the trigger cable ground braid, the net blocking capacitance in the trigger circuit was increased by more than a factor of 3 to 0.86 nF (Figure 22b).

The results from the Auxiliary bank tests were mixed. Several time delays for triggering the bank had been examined, most in close proximity to the time at which the Crowbar switch was triggered. While some of the test data suggested that discharging the Auxiliary bank just before the Crowbar switch was triggered did help to ensure that multiple rail gaps conducted, there were no cases observed in which all four of the Crowbar rail gaps conducted, nor were there just two or just three of the Crowbar rail gaps consistently conducting; rather, the number of conducting rail gaps varied.

Interestingly, the only instances in which the Auxiliary bank did lead to all four Crowbar rail gaps conducting were also the instances in which the Auxiliary bank pre-fired just after the PI bank started its discharge. For these cases, the behavior was quite repeatable; that is, when personnel took steps to ensure that the Auxiliary bank pre-fired (e.g., by leaving the low-voltage portion of the trigger system plugged into the isolation transformer instead of powering it through the UPS), all four Crowbar rail gaps repeatably conducted, and they shared the current

quite uniformly between them. Figure 23 shows a graph of the current waveforms from such a shot.

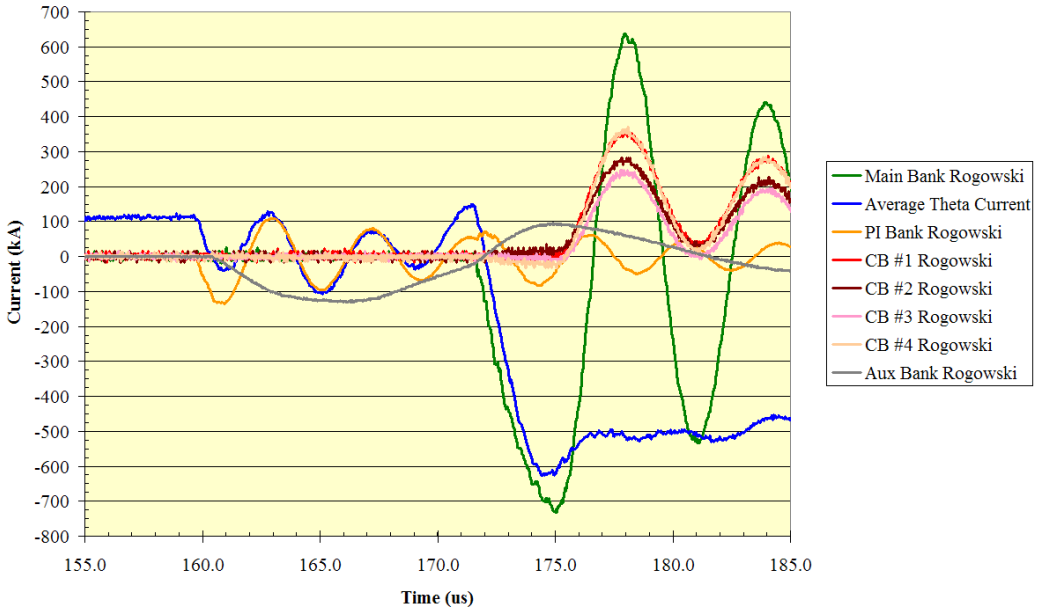


Figure 23. Bank-current waveforms, shot in which Auxiliary bank pre-fired

As can be seen from the graph, the Auxiliary bank had a half-period that was approximately equal to the 2 ¾ periods of the PI bank, so that the Auxiliary bank current was approaching zero again just as the Main bank discharge was starting. However, the introduction of the Auxiliary bank current into the Theta coil at this early time unfortunately altered the fields that were normally being set up as the plasma was being ionized. First, it appeared from the slow baseline shift of the blue trace in Figure 23 that the Bias field was essentially negated by the Auxiliary bank discharge; thus, the plasma formed with little, if any, embedded flux. Second, because of this slow variation in the baseline shift, the second PI bank oscillation actually had a much "harder" zero crossing than the first oscillation. Though a detailed study was not performed, such alterations in the fields led AFRL and SAIC personnel to conclude that plasmas that were generated in this manner would not be very satisfactory for forming an FRC and any consideration of triggering the Auxiliary bank at this early time should therefore be ruled out.

Comparing results from tests with and without the Auxiliary bank, it appeared at least that the additional blocking caps that were placed on the trigger board did provide some measurable improvement, though not of a degree that it resulted in all four rail gaps conducting during each shot. Rather, the improvement here was observed in the time delay between the arrival of the

trigger pulse to the Crowbar rail gaps and the start of current conduction in each rail gap (i.e., the rail-gap jitter). Previously, these delay times would vary from a few hundred ns to as much as several μs. After installing the additional blocking capacitors at the ends of the trigger cables and adding those to the high voltage side of the Crowbar switch, these delay times were reduced to almost exclusively within the range of 300 to 600 ns. It should be noted that all these recent tests had been performed with a Main bank-to-Crowbar switch trigger delay of 3.3 μs, the same delay that had been previously found to be optimal in the sense that the Crowbar performed best at this delay.

When a stopping point had been reached in the timing scans with Auxiliary bank, it was decided to shift briefly to an alternate triggering scheme that had been proposed by AFRL personnel. This scheme simply involved triggering only the outer two Crowbar rail gaps. The rationale for this approach was that the outer two gaps are separated by a considerably greater distance, and therefore have greater inductive isolation, than the adjacent rail gaps in the quad set. Thus, the outer two rail gaps would be more likely to conduct consistently from shot to shot, simplifying data analysis and decreasing the likelihood of the Crowbar switch incurring damage during a shot. The disadvantages, of course, were that the two-rail-gap Crowbar was somewhat more inductive than the three- or four-rail-gap Crowbar and that a greater amount of current must be consistently carried by these outer two rail gaps.

In preparing for these tests with the outer two rail gaps, the trigger cables going to the inner two gaps were simply moved over to the outer ones (Figure 24).

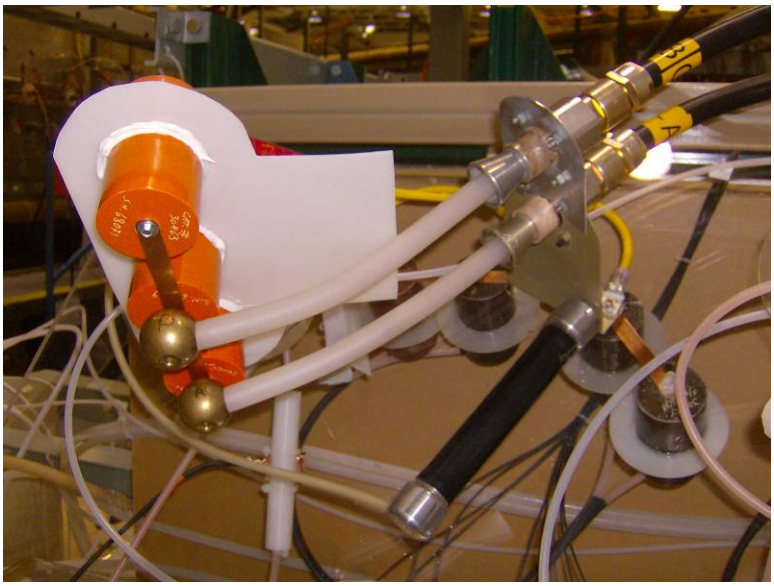


Figure 24. Trigger-board-circuit setup for end-rail-gap-only tests

Based upon the earlier discussion regarding trigger pulse energy and the blocking capacitors, it was known that placing the second cable on the outer rail gaps would not increase the total energy delivered to these rail gaps, but it would cut in half the time over which the energy was delivered to these rail gaps; that is, the current to these outer rail gaps would be doubled.

The results from these tests turned out to be quite promising. Only five test shots were performed, but these tests were carried out under both plasma and vacuum conditions. The Auxiliary bank was also included in some of these tests and was triggered just before the Crowbar trigger, as had previously been done; it was not included in the third and fifth shots, however. In all five test shots the outer two rail gaps conducted as intended, suggesting that the Auxiliary bank was not needed for this scheme. While not the most ideal solution, it appeared that at last a solution was found, as operating with only the outer rail gaps would at least provide the reliability and repeatability that was needed for the Crowbar switch.

Before the Phase 1 effort drew to a close, one final series of tests with the Auxiliary bank was planned. This series was to involve using the bank to augment directly the trigger pulse provided by the charged-cable triggering system. For these tests, the intent was to let the charged-cable trigger system provide a fast-rising pulse to break down the switch gaps in the typical fashion, while the Auxiliary bank followed shortly thereafter with a slower, higher energy pulse to increase the ionization in each of the switches. The setup for these tests entailed reducing the Auxiliary bank capacitance from 12 μF to 6 μF, and moving the bank's four transmission-line

cables from the cable header adjacent to the Crowbar to the top electrodes of each of the peaking gaps (Figure 25).

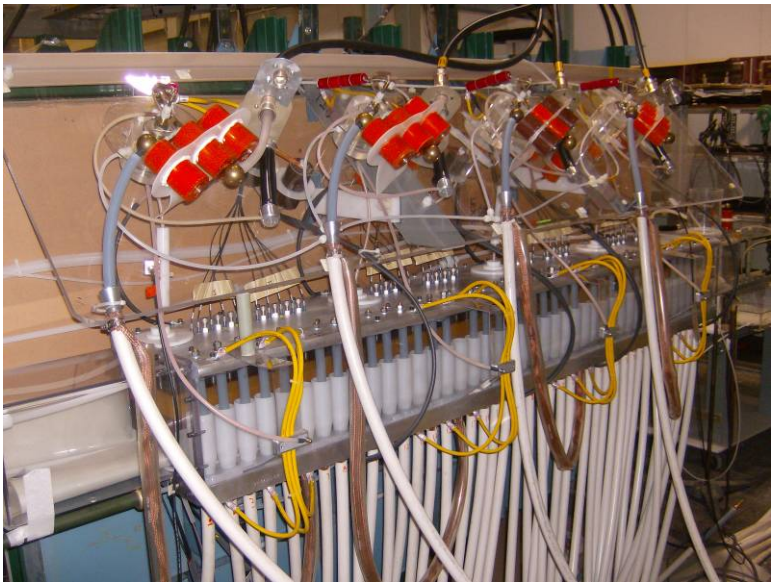


Figure 25. Auxiliary bank to be used to augment trigger pulse delivered to each Crowbar rail gap

It was decided later to abandon these tests in favor of doubling up the charged trigger cables on all four of the Crowbar rail gaps, a scheme that was tested during the Phase II effort for FRCHX and that, in fact, was finally successful in ensuring that all four Crowbar rail gaps conducted reliably during each shot. For further discussion of this scheme, see Section 4.6.2.

3.5.2 Early Bias Bank Modifications To Increase Current

As noted at the end of Section 3.1.1, when the Bias bank was charged to 4 kV, a current of only ~60 kA was achieved. The target current had been 200 kA; while it was possible to increase the Bias current by going to higher bank-charge voltages, it did not appear to be feasible to reach this final target Bias current with just the single slow-bank module that was active in the bank at that time. Furthermore, based upon test results that were being obtained at FRX-L at this time, the target Bias current needed to be raised to between 300 and 400 kA. In addition to these findings, during conversations with UNR's Dr. Richard Siemon, it was suggested that the present rise time for the Bias current (approximately 165 μs as seen in Figure 5) was too long. A quarter-cycle rise time that was closer to 80 μs was more desirable instead.

In light of these issues, SAIC personnel initiated efforts in the midst of the Crowbar switch tests and the FRC formation tests to bring the spare slow bank module quickly on-line in the Bias bank and also began considering a redesign of the Bias inductors to facilitate both a reduction in

the quarter-cycle rise time as well as a further increase in the peak current provided by the Bias bank. The new inductor design was finalized and the inductors fabricated towards the end of the Phase I effort for FRCHX, but as a result tests with these inductors were not performed until Phase II of the FRCHX tests were underway. As such, we discuss here the design and fabrication of the new inductors, and present their subsequent installation and the tests performed with them on the Bias bank in Section 4.0.

SAIC and Voss Scientific personnel were able to complete the refurbishment of the second 2.5 mF "Slow bank" module within a few weeks, because it had already been mounted onto the Bias bank base plate. To integrate the module with the rest of the Bias bank, personnel fabricated a similar set of copper bus straps to connect the module to the inductor stand and to the second ignitron that had been placed under the inductor stand (Figure 26).

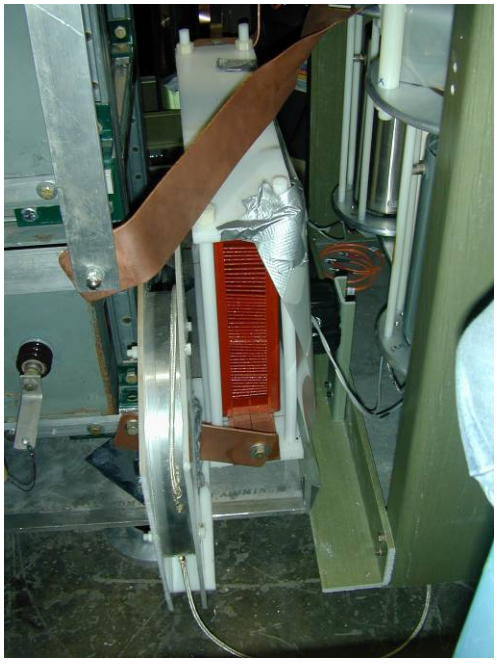


Figure 26. Copper bus straps, damping resistor, and ignitron (upper right) for second Bias bank module

A set of nine 60-mΩ Franklin resistors were bussed together in parallel and used to limit the module's current instead of the custom-built 6.8-mΩ resistor attached to the neighboring module, as a fair amount of time would have been required to fabricate a second 6.8-mΩ resistor. To monitor the discharge current directly from the second module, a pair of Rogowski coils (only one of which is currently used) that are housed in an aluminum electrostatic shield and that were already on hand were placed around the return conductor. A Pearson 1049 current transformer is

presently monitoring the current from the first bank module, but another such monitor for the second module was not on hand.

To avoid having to construct a second ignitron trigger unit and provide a command trigger for it, Voss Scientific personnel wound a new 1:1 isolation transformer similar to the first but with two secondary windings (Figure 27).



Figure 27. New 1:1, dual-secondary isolation transformer for Bias bank ignitron trigger unit

With this transformer, the original trigger unit was now able to trigger both ignitrons, and there were no issues with jitter. The pulses provided to both ignitrons were monitored a few times before the bank was actually charged and triggered, Figure 28 shows the observed waveforms.

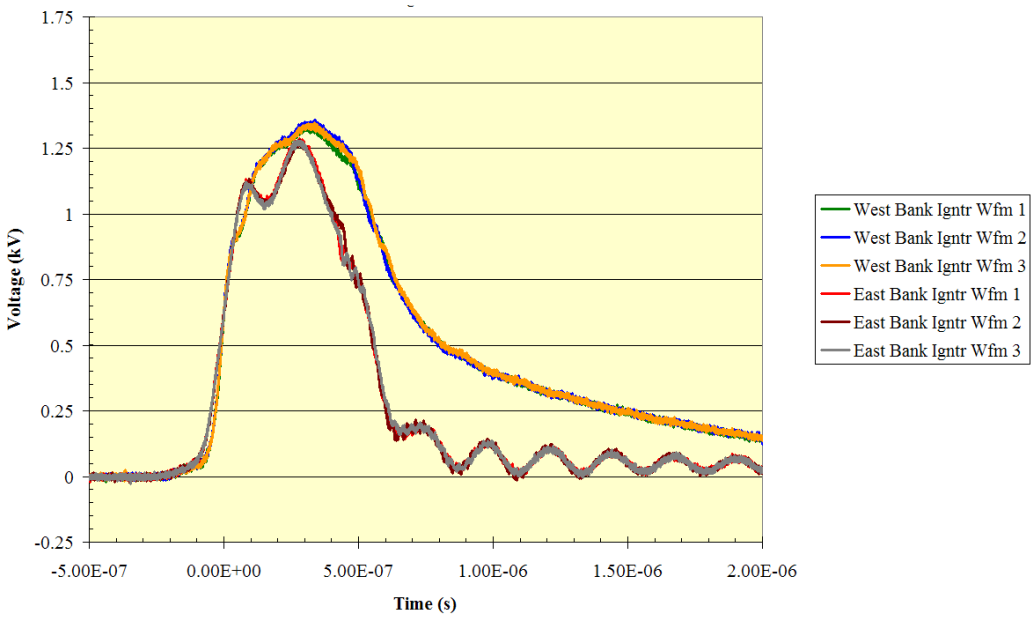


Figure 28. Three trigger pulses from each secondary of ignitron trigger transformer

The pulses are not identical in amplitude or in pulse width, but their rise times are virtually the same, so the igniters of both ignitrons should spark nearly simultaneously.

Figure 29 shows a Theta coil current waveform recorded for one of the first Bias bank-only shots performed with the new two-module Bias bank.

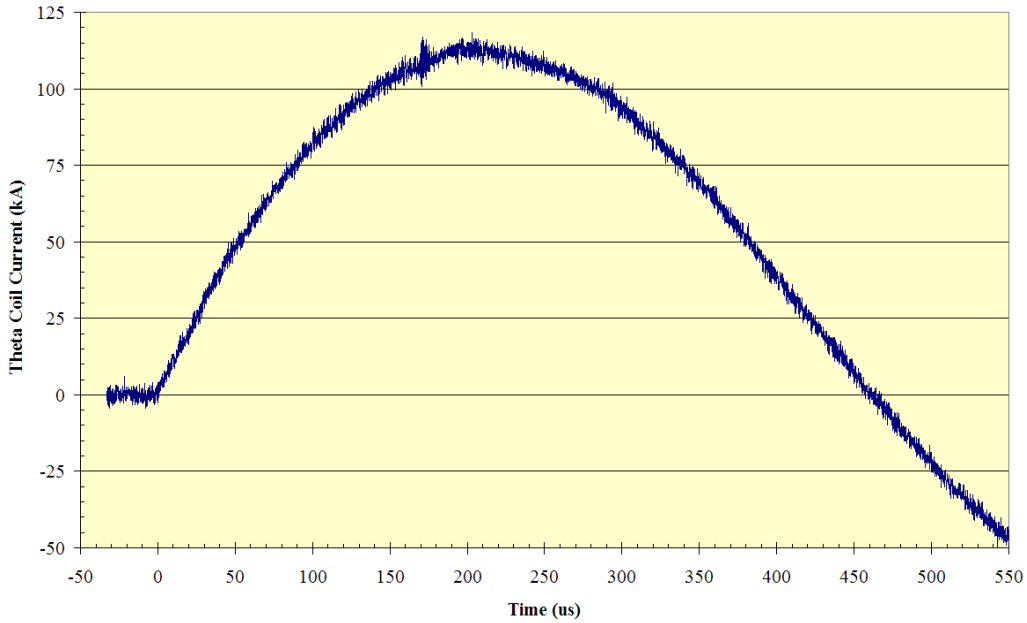


Figure 29. Theta coil current (averaged) for a Bias-only shot, two-module Bias bank

The charge voltage was ~4.3 kV for both modules, and it can be seen that the peak current is approximately 114 kA. This current is approximately the same as that previously obtained with the single module charged to 7 kV. Thus, the 200 kA goal was now easily reached with a 7 kV charge on both modules, and currents up to 300 kA were expected to be obtained with a 9 kV charge, though this voltage is approaching the 10 kV maximum for the capacitors.

Following the conversation with Dr. Siemon, SAIC personnel also began the task of designing and fabricating the parts necessary to wind two new lower-inductance isolation inductors for the Bias bank. These new inductors were to enable a faster Bias current-rise time to be achieved, according to Dr. Siemon's recommendation that a rise time closer to 80 μs for the Bias current would be more desirable for FRC formation. (Comparing the graphs in Figure 5 and Figure 29, the addition of a second module had actually increased the quarter-cycle rise time by ~43 μs.) Having the lower-inductance inductors would also serve to raise the peak Bias current even further, thereby lowering the required charge voltage to produce a 300 kA discharge.

Figure 30 shows the new inductors shortly after fabrication was completed.



Figure 30. New Bias bank isolation inductors

The inductors were fabricated in-house using eight parallel lengths of stranded 2 AWG copper wire for each inductor. The lengths of wire were wrapped five times around a polyethylene spool and secured to brass end plates using lugs appropriate for the 2 AWG wire. Once the windings were secured on the spools, they were wrapped with fiberglass and resin and allowed to cure overnight. Measured inductances for these two inductors ranged between 1.0 and 1.1 μH at the

oscillation frequencies of the Bias and Main banks. Using these inductance values MicroCap simulations suggest that the rise time for the bank current may be slightly above the target value at ~110 us, but this value should still be acceptable. It would be possible to obtain a 400 kA discharge into the Theta coil with a bank-charge voltage of ~9.25 kV.

As mentioned at the beginning of this section, by the time the new inductors were ready for installation in the Bias bank inductor housings, it was decided to conclude Phase I of the FRCHX tests. As a result the new inductors were installed when other Phase II preparations were going on and tested for the first time once the FRCHX Phase II tests got started. (See Sections 4.1.2 and 4.6.3.)

3.5.3 Phase I Vacuum and Plasma Tests with FRCHX

The PI bank was the last of the three formation banks to be brought on line, so once it was operational it was then possible to begin testing all three formation banks together. By itself this combination was a milestone for the experiment, but with the assembly of the vacuum system having been completed a few months before, it was then possible to begin plasma tests at this same time. The first plasma tests were thus performed in December 2006. Parameters for these initial FRC formation tests include charge voltages for the Bias, PI, and Main banks of 7 kV, -25 kV, and ±25 kV, respectively, and a deuterium pre-fill in the vacuum vessel of 50 mTorr according to the Pfieffer vacuum gauge. Note: When the correction factor for the gas species was applied to the gauge reading, the D_2 pressure was found to actually be ~25 mTorr.

Following these initial attempts at making an FRC in mid December, a more careful look was taken in January at the plasmas that were being formed with the 50 mTorr pre-fill. Several shots with only the PI and Bias banks were taken first (with the same -25 kV and 7 kV charge voltages), and with the MCP camera images of the plasma were recorded at various times during the PI bank discharge shortly after it had formed. (See Section 3.3.3.) Figure 31 shows several of these images that were collected along with a plot of the Theta coil current illustrating the times at which the images were taken.

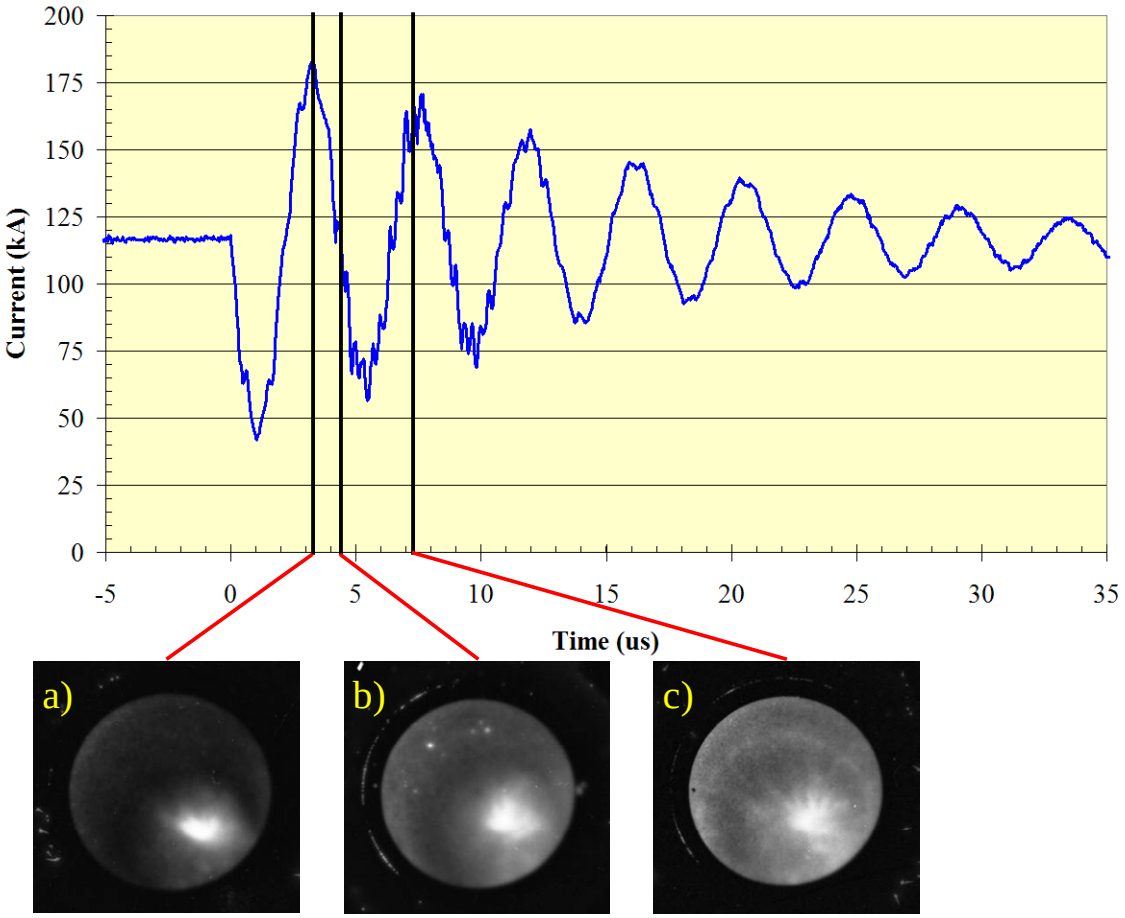


Figure 31. Theta coil current along with three MCP camera images

In Figure 31, images were taken at these times: a, 3/4 PI period; b, 1 PI period; and c, 1 PI period plus 2.9 μs. The gain and exposure time for the MCP camera was kept constant at 600 V and 500 ns, respectively.

The a image shows the plasma when the PI and Bias fields were additive, and thus the plasma was compressed the most; the b image then shows the plasma after one complete PI oscillation, when the net field had returned to a level provided by the Bias discharge alone and the plasma had expanded again somewhat; and the c image shows the plasma after it had undergone nearly a complete expansion and re-contraction cycle following the a image. Here, a filamentary structure is evident around the core plasma, which was not seen in the a image. Because the images are an axially integrated view of the plasma, it is possible that the filaments were located at either end of the formation region, where the field lines diverge outward from the Theta coil. These filaments could thus be the plasma that was streaming outward from the formation region along

these field lines. ICCD camera images taken at FRX-L have shown a very similar filamentary structure forming as the FRX-L PI bank discharge oscillates.

This series of PI and Bias shots was followed by a second shot series that then included the Main bank and attempted to form an FRC. The Main bank-charge voltage was kept constant at ±25 kV for these shots, and the PI and Bias bank voltages were kept at the same values that were used in the previous shot series. However, the MCP camera gain and exposure time were reduced to 300 V and 200 ns, respectively, because light emission from the plasma was considerably greater once the Main bank discharge started. We note that the utility of the visible light MCP camera images recorded during the FRC formation tests was that they made it possible to obtain a confirmation of the presence of plasma, and they were also a means for observing the general shape and radial extent of the plasma within the formation region. Other supporting diagnostics, such as the magnetic diagnostics or the interferometer would be required to confirm the presence of an FRC. Figure 32 shows a set of MCP images along with their corresponding Theta current waveforms.

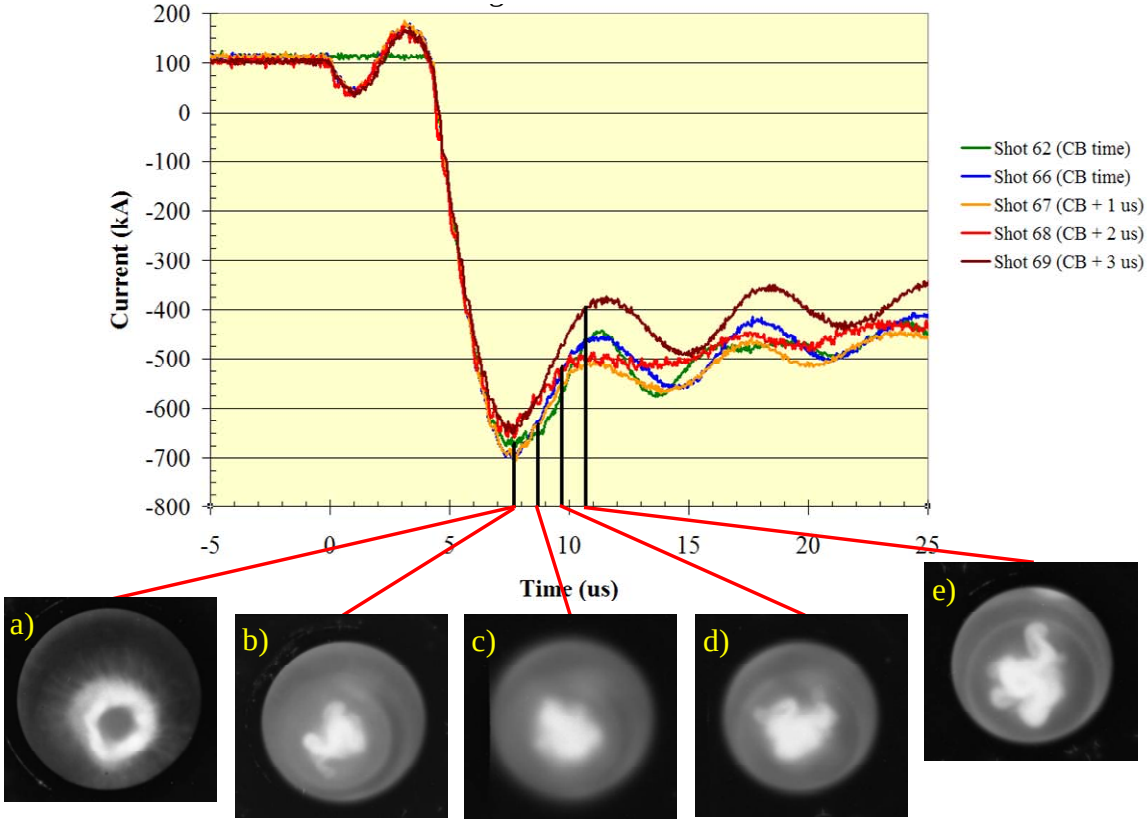


Figure 32. Theta coil current, along with five MCP camera images

In Figure 32, images were taken at these times: a and b, the Crowbar trigger time, t_{CB}; c, t_{CB} + 1 μs; d, t_{CB} + 2 μs; and e, t_{CB} + 3 μs. Each MCP image is shown with its corresponding Theta coil current waveform, because the waveforms all varied slightly depending on how many Crowbar rail gaps closed and conducted current.

The first two images, a and b, were taken at the same time, the Crowbar switch trigger time, but interestingly the PI bank failed to trigger at the right time for the shot with the a image. In this case, the PI bank trigger occurred slightly after the Crowbar switch trigger, yet, as can be seen in the image, the 50 mTorr D_2 pre-fill still broke down; the plasma that was formed was quite annular in profile. The c, d, and e images were collected with MCP camera trigger times at 1 μs, 2 μs, and 3 μs following the Crowbar switch-trigger time. These images, together with the b image, do not show the same annular structure as the one seen in the a image. However, the views here are axially integrated, as was mentioned before, and the plasma that was outside the formation region on the side closest to the camera was possibly masking the view of the plasma that was within the central formation region.

Another visible-light diagnostic that was fielded during these tests was the first light fiber-optic monitor (Section 3.3.2). As its name implies, the monitor's primary function in these tests was to indicate when the plasma first broke down and began to emit light. There was, however, some structure that appeared in the signal following the first indication of light that could possibly hold some interesting information. Figure 33 shows a plot of the fiber-monitor signal overlaid with the Theta coil current waveform, both of which were obtained during one of the early Phase I test shots.

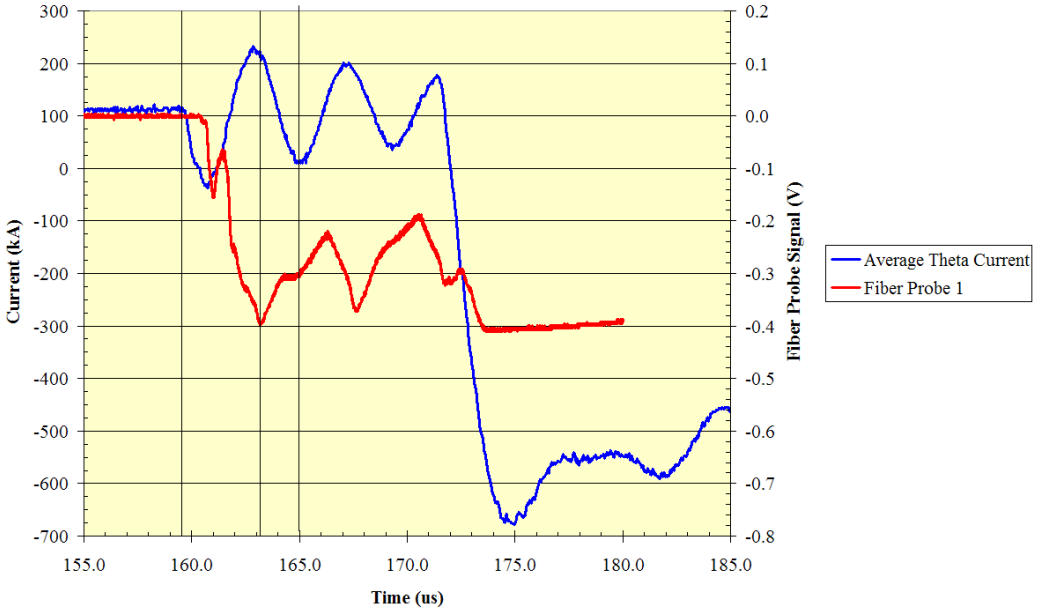


Figure 33. First light fiber-monitor signal with Theta coil current overlaid

As anticipated, the signal shows that the gas in the vacuum vessel does not break down until the first PI bank current zero crossing. After an initial spike in the signal, followed by its rise to 400 mV, the signal seems to show a somewhat periodic behavior with a period, not surprisingly, similar to that of the PI bank. Once the Main bank is triggered, the signal then appears to reach a saturation.

With regard to the magnetics diagnostics (Section 3.3.1), which again were key for confirming FRC formation, the principal parameters that were sought from their signals were the excluded flux and the separatrix radius. To obtain these values, the flux loop signal must be subtracted from signals recorded from B-dot probes located nearby during both vacuum and plasma shots. The vacuum difference is then subtracted from the difference obtained from a plasma shot, and the result is a time history of the flux excluded by the plasma. The separatrix radius can be calculated from the expression

$$r_e^2 = r_p^2 - \phi_p / \pi B_p \,, \tag{5}$$

where ϕ_p and B_p are the magnetic flux and flux density, respectively, measured at a given axial location, and r_p is the radius at which the B-dot probe is located (Tuszewski 1981). In trying to calculate both these quantities with the data obtained during the shots discussed in this section, there were problems encountered with obtaining a good zero-signal baseline from the subtraction of the vacuum-shot signals. That is, after subtracting, there was usually a non-zero signal

remaining. This effort was complicated further because the current and magnetic field time histories differed slightly from shot to shot as different numbers of Crowbar rail gaps conducted.

AFRL and SAIC personnel continued to process and analyze this data and the data obtained from these diagnostics during subsequent Phase I FRC formation tests. However, it did not appear from the excluded flux analyses that there was ever any conclusive evidence that FRCs had been formed. Subsequent Mach 2 simulations performed by NumerEx personnel showed that the absence of FRC formation was likely a result of the Cusp coils not being present on either side of the formation region. According to the simulation results, the passive mirrors on each end were not sufficient to encourage strong magnetic reconnection when the Main bank was fired, as the reconnection that occurred was within the plasma where diffusion slowed down the reconnection. When the Cusp coils were in place, the simulations indicated that reconnection would occur outside the quartz tube, between the Cusp coils and Theta coil, where it could occur in air and occur much more rapidly.

Of lesser importance, though it should also be noted, is that most of the Phase I FRCHX tests were at relatively low bank-discharge currents and had been primarily aimed at characterizing the pulsed power. It was anticipated that the currents from each of the banks needed to double approximately to improve the likelihood of forming FRCs that would be appropriate for the compression-heating experiments.

The final diagnostic that was fielded on the FRCHX vacuum and field-coil stand during the Phase I tests was the single-chord interferometer (Section 3.3.4). The data signals that were collected from the interferometer's two signal channels during the tests discussed here had a considerable amount of electrical noise on them. This noise is no doubt due to the detectors and other electrical components of the interferometer—though they were placed in a shielded enclosure—being located in such close proximity to the Theta coil and to some of the pulsed power banks. UNM and SAIC personnel examined several ways of reducing the noise on the signal channels, but an adequate solution had not been found by the time that the Phase I tests ended.

4.0 FRCHX PHASE II DEVELOPMENT EFFORT

As soon as it was felt that enough tests had been performed for the Phase I effort to characterize adequately and/or troubleshoot the FRCHX systems and the new diagnostics and to identify any changes that needed to be made to these systems, personnel quickly concluded these tests and directed their efforts toward assembling the remaining FRCHX systems. The vacuum and field-coil stand was completely rebuilt and reconfigured so that it could be placed in a vertical orientation, which was more consistent with the requirements for subsequent FRC translation and compression inside a solid liner under the Shiva Star bank. A new 10-segment Theta coil design, developed by LANL personnel following their experience with FRX-L, was also implemented on the stand, once the assembly of the stand was completed. With the help of FRX-L personnel, two more pulsed power systems (for the Upper and Lower Cusp coils) were also brought on line at this time, as were some additional plasma diagnostics and a computer-based control system to automate many of the bank operations. Furthermore, a dedicated, well-shielded data acquisition system that could be operated apart from wall power during tests was set up for recording all of the data from the FRCHX diagnostics. Once this new work was completed, a series of static FRC formation tests was again performed. Unlike the Phase I tests, however, it was assumed that any troubleshooting would be minimal. The goal of these tests was therefore both to verify that FRCHX was in fact forming FRC plasmas now, and to identify the density, temperature, and lifetime baselines that could be expected for FRCHX FRCs.

This section presents an overview of this second phase. The new pulsed power systems, and modifications to the existing ones, are outlined in Section 4.1. Sections 4.2 and 4.3 describe the vertical vacuum and field-coil stand and the additional plasma diagnostics fielded at this time. Instead of going to the Shiva Star screen room, all diagnostic signals were now sent to the dedicated data acquisition system; this system is described in Section 4.4. Section 4.5 presents the new computer-based control system, and Section 4.6 concludes the Phase II development work with another brief analysis and discussion of the data recorded during the static FRC formation tests performed at the end of this phase.

4.1 Further Pulsed Power System Design, Assembly, and Modifications

A significant portion of the pulsed power work for FRCHX was completed during the Phase I effort when the PI, Bias, and Main banks were made operational along with their charging and triggering systems, changes to the Bias bank were being implemented to increase its current, and tests to resolve the Crowbar switch triggering problem were performed. However, two additional banks were needed to drive the Upper and Lower Cusp coils; these and their charging and triggering systems were now set up at this time. As mentioned in Section 3.5.3, the Cusp fields on either side of the formation region were predicted by Mach 2 simulations to be essential for efficient FRC formation.

This section discusses SAIC's and our subcontractors' efforts to set up the Upper and Lower Cusp banks and their related systems. Modifications to the Bias bank, which included installation of the new isolation inductors and the setting up of higher-current charging supplies, are also described here. Efforts to set up the final FRCHX bank, the Guide/Mirror bank, also began at this same time, but because this bank is necessary for FRC translation and not formation, we address that work in Section 5.0.

4.1.1 Upper and Lower Cusp Coil Bank Systems

The Cusp bank modules were fabricated by LANL personnel at the FRX-L facility using capacitors, ignitrons, and support frames that had been in storage following the decommissioning of the FRX-C experiment a number of years earlier. The two Cusp bank modules were transported from the FRX-L facility to AFRL's Building 322 in August 2007, the first by SAIC personnel and the second a week later by FRX-L personnel. Figure 34a shows the two bank modules after they had been stacked in the position where they were to be placed in the FRCHX test area.



a b

Figure 34. (a) Two 1.5 mF Cusp bank modules stacked on top of each other; (b) ignitron trigger units

As can be seen, the modules each contain three capacitors, which have a capacitance of 500 µF and a voltage rating of 10 kV. Because each module is a separate bank and will be used to drive a separate Cusp coil, two separate ignitron trigger units have been set up on the modules (Figure 34b). Lower-cost, off-the-shelf units, which are able to drive only one ignitron each, were purchased for this application.

To charge the Cusp banks, two of the five new Peter Dahl power supplies were used, purchased by LANL personnel for FRCHX. These supplies could provide a charging current of 1 A at a voltage of 12 kV. A special stand was designed for the two supplies, which not only enabled the supplies to be moved more readily with either a forklift or the overhead crane throughout the high bay, but which also provided supports on which to mount their phase controllers, manual circuit breakers and contactors. Figure 35 shows the stand after it was positioned in the FRCHX test area just east of the vertical vacuum stand.



Figure 35. Upper and Lower Cusp bank power-supply stand

Resistor stands, like those assembled for the PI and Bias banks, were also assembled for the Upper and Lower Cusp banks to facilitate the charging and dumping of the banks (Figure 36).

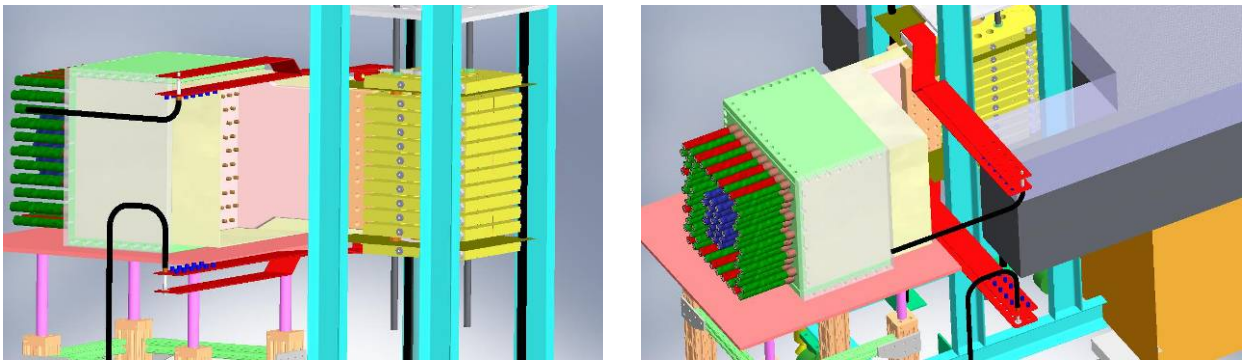


Figure 36. Resistor stands for Upper and Lower Cusp banks, between power-supply stand and Cusp banks

Once the power-supply stand was in place, the two bank-resistor stands were lined up between it and the Cusp banks, and then all the cabling was connected between the power supplies, the resistor stands, and the banks. Power cords for the ignitron-trigger units on the banks were run at this time, as well. Following the guidance of FRX-L's Bill Waganaar, the last steps to setting up the charging systems for both banks was to change a pair of jumper connections on both phase

controllers and to then set the phase-controller-current limit such that the power-supply-line current was within 80 ~ 90 % of the current rating for the breaker on the power supply. Setting the current limits in this manner allowed the charging times for the banks to be kept at a minimum without tripping the breakers for the supplies.

To enable transmission-line cables from each Cusp bank to be connected to their respective coil, two pairs of copper bus plates were designed with cable headers at one end and a mounting point for the Cusp coil on the other. The bus-plate pairs were of sufficient length that they could be mounted to the coils and project out far enough out from the vacuum and field-coil stand to allow the cables to be connected to the header portion. Figure 37 shows two Solid Works® renderings of the bus plate pairs (shown in red) mounted to each of the Cusp coils.



a b

Figure 37. (a) and (b) Cusp coil bus plates

Several sheets of 5-mil (127-μm) Mylar (not shown) were placed between the hot and ground plates in each pair to add high-voltage insulation between them. In addition, except for the current contacts at the coil end and around the cable header at the other end, the plates were also painted with a red electrically-insulating paint. This paint appears to have been very effective for insulating these plates, as no issues with arcing between the plates and other nearby hardware were observed during any of the subsequent tests.

SAIC machinists then fabricated the bus plates using 0.125-in. (3.18-mm) copper plate and 0.500-in. (12.7-mm) copper tube on which the cable braid could be clamped. Voss Scientific personnel measured and cut to length the cables needed for transmission lines between the banks and their respective coils. Afterwards they prepared the ends and soldered the brass lugs (1/4 – 20 cap screws) onto them. Though the banks were very close to the vacuum and field-coil stand at this time, the Upper and Lower Cusp cables were cut long enough to run to the center of the

Shiva bank. This length would allow the same cables to be used when the vacuum and field-coil stand was moved to this location for FRC compression-heating tests.

By the beginning of March 2008, all the transmission-line cables had been run between the coils and their respective banks, and the ends of the cables had been connected to the cable headers at each location. Figure 38 shows what the Cusp coil bus-plate assemblies looked like when in place on the vacuum and field-coil stand.

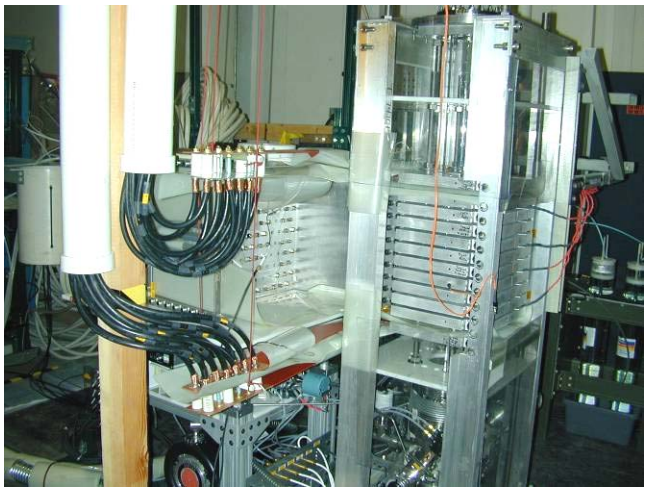


Figure 38. Cusp coil transmission-line cables and headers (center)

Once all the cable connections were completed, each bank was then successfully charged to its nominal operating voltage (4 kV) and then triggered, at which point it successfully discharged into its coil load.

4.1.2 Modifications and Maintenance for the Bias Bank

As discussed in Section 3.5.2, two lower-inductance isolation inductors were fabricated in-house for the Bias bank to allow the current-rise time for the bank to be reduced and its peak discharge current to be increased (Figure 30). The new rise time was estimated to be ~81 μs, and the peak discharge current for the bank with only a 4 kV charge voltage was expected to be as high as ~390 kA. Once the Phase II efforts for FRCHX were underway and disassembly of the horizontal vacuum and field coil stand began, personnel also took that time to remove the original isolation inductors from their housings (Figure 39) and install the new ones.



Figure 39. Inductor housings on Bias bank stand

The new inductors were designed to be identical in size to the original inductors so that the transition between the two would require no hardware modifications.

With the increased current expected from each bank module, perhaps up to 200 kA, there was some concern that the Pearson Model 1049 current transformer monitoring the current from the east Bias module could begin to saturate or even break down internally, because the unit's rated current is 200 kA. Two Pearson Model 1423 current transformers, which have a rated current of 500 kA, had recently become available in-house, so Voss Scientific personnel replaced the Model 1049 on the east Bias module with one of the Model 1423s. To standardize the diagnostic setup they also replaced the Rogowski coil monitoring the current from the west Bias module with the other Model 1423 current transformer (Figure 40).



Figure 40. Pearson Model 1423s installed on each bank module

During the Phase I experimental campaign, several capacitors had failed in the Bias modules—two in the west module and one in the east. The limited time between test days had not permitted replacing these capacitors at that time, but with the tests now halted, Voss Scientific personnel were able to carry out this task. Thus, both Bias bank modules were returned to their full complement of 15 170 μF capacitors.

With five new Peter Dahl power supplies purchased for use on FRCHX, power supply stand similar to the one built for the Upper and Lower Cusp banks was therefore put together for both the Bias bank and the Guide/Mirror bank. (See Section 5.1.1 for details.) For this stand, however, two 12 kV, 5 A power supplies were used, because the capacitances of the Bias bank and the Guide/Mirror bank were much larger than the capacitances of the Cusp banks. Like the Cusp bank power-supply stand, this stand was also designed to enable the supplies to be moved more readily with either a forklift or the overhead crane throughout the high bay, and there were again side supports on which the power-supply-phase controllers, manual circuit breakers, and contactors could be mounted. Figure 41 shows the stand after it was positioned adjacent to the Guide/Mirror bank.



Figure 41. Bias and Guide/Mirror power-supply stand

The Bias bank had been used recently during the Phase I FRCHX tests, and so it was only necessary to connect the power supply hot and ground to the rest of the Bias bank charging circuit—the rest of the components were already in place. The final steps needed to ready the new Bias bank power supply for operation were again to change a pair of jumper connections on its phase controller and to then set the phase-controller-current limit such that the line current was within 80 ~ 90 % of the current rating for the breaker on the power supply.

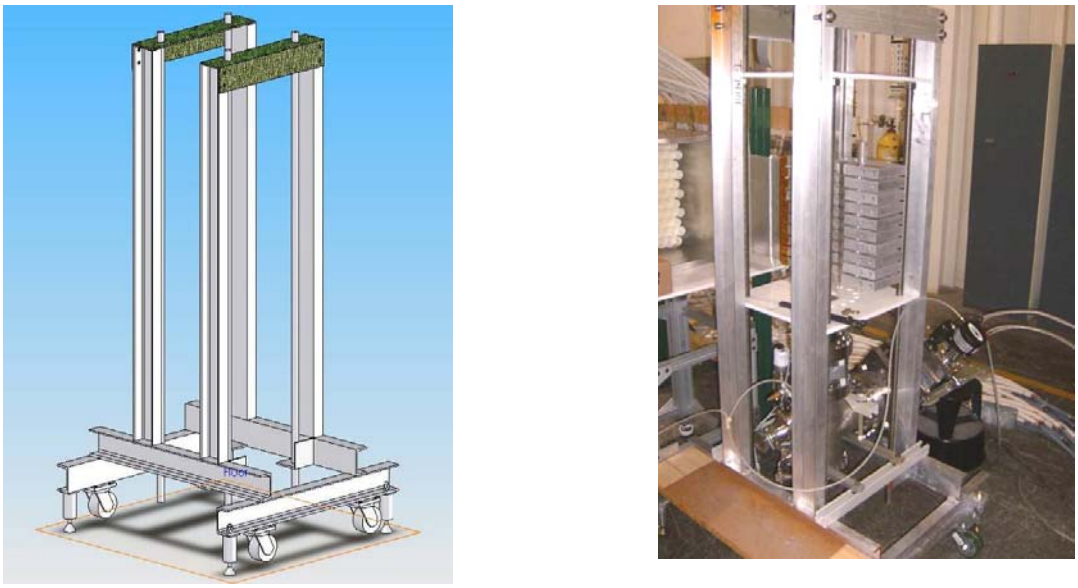
4.2 Vertical Vacuum and Field-Coil Stand

The design and assembly work performed on the vertical vacuum and field-coil stand can be divided into four categories: (1) focusing on the support structure for the stand, (2) pertaining to the setup of the vacuum pumps and other vacuum-system components, (3) related to the Theta coil and the Upper and Lower Cusp coils, and (4) dealing with the deuterium pre-fill and dry nitrogen venting and backfilling systems. With the introduction of the computer-based control system, the functions of many of the components in the second and last categories were now automated. This section discusses the specific tasks that were carried out for each of these four categories.

4.2.1 Support Stands for the Field Coils, Vacuum System, and Theta Coil Cable Header

The support structure for the vertical vacuum and field coil were designed for FRCHX largely by FRX-L's Paul Sieck. Materials for the stand were also ordered by FRX-L personnel, and as the summer of 2007 began these were ready to be picked up by SAIC personnel from the FRX-L

facility and brought to Building 322. Using the design drawings prepared by FRX-L personnel (Figure 42a), SAIC personnel were able to assemble the stand readily (Figure 42b).



a b

Figure 42. (a) FRCHX vertical support stand; (b) stand after assembly

While this work was in progress, SAIC personnel had also been working on the design of the support table needed for the Theta Coil cable header, ordering the materials needed to build it, and then shortly thereafter assembling it (Figure 43).

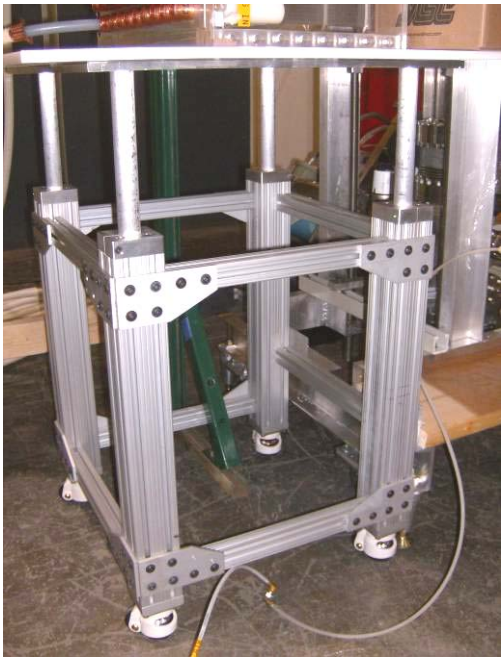


Figure 43. Completed Theta coil cable header support table

Once both the stand and table were ready, personnel began setting up the vacuum system, the Theta Coil cable header, and the Theta and Cusp coils.

4.2.2 Vacuum System

Figure 44 shows the vertical stand when assembly of the vacuum system (and the Theta coil) was just getting started.



Figure 44. Vertical stand and cable header support table

As can be seen, the vacuum hardware has been placed at the bottom of the stand, below the level of the Theta coil. Figure 45 shows a closer view of the cryopump, gate valve, and vacuum tee with 8-in. (20.32-cm) Conflat flanges, at the bottom of the vertical stand. The vacuum system produces base pressure ~10^{-7} Torr.

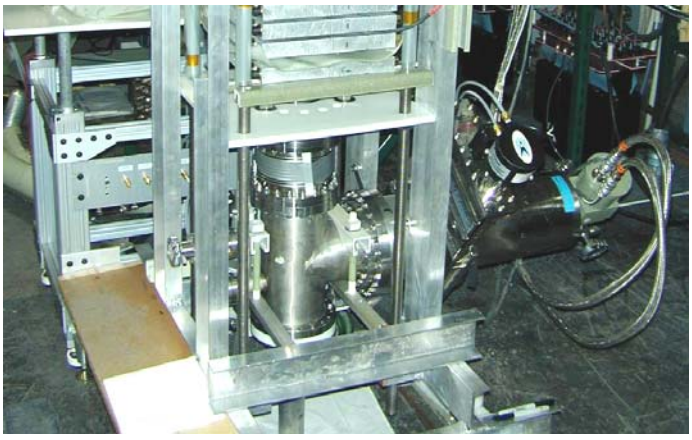


Figure 45. Cryopump, gate valve, and lower vacuum hardware

As was done for the horizontal vacuum system, a vacuum bellows was used to join the vacuum tee to the quartz tube, thereby making alignment of the quartz tube inside the Theta coil easier, and isolating the tube from vibrations occurring in the lower vacuum hardware (e.g., when the gate valve closes). Smaller 2.75-in. (6.99-cm) Conflat ports on the vacuum tee allow for connection of the mechanical roughing pump, the deuterium pre-fill system, and the dry nitrogen backfill and venting system. The mechanical vacuum pump was conveniently placed on a shelf at the bottom of the Theta coil cable header support table (Figure 46).



Figure 46. Roughing pump and vacuum-gauge controllers beneath Theta coil cable header

A second shelf was placed above the mechanical pump as a place to mount the vacuum gauge controllers and the various valves and components for the deuterium and dry nitrogen systems. (See Section 4.2.4.)

4.2.3 Theta and Cusp Coil Configuration for Static FRC Formation

The four-segment Theta coil was at this time being replaced by a new 10-segment Theta coil. The 10-segment Theta coil design was developed by LANL personnel based upon their experience at FRX-L, and was intended to allow for both greater diagnostic access as well as versatility in selecting the bore angle for conical Theta coil configurations. In addition to fabricating a set of Theta coil segments for FRX-L, LANL personnel also had a complete set of segments fabricated for FRCHX. Enough different segments were fabricated to allow Theta coils with bore angles ranging from 0º (i.e., a cylindrical Theta coil) to 6º, in 1º increments, to be assembled. Other fractional bore angles are also possible.

When preparing FRCHX for the Phase II tests, a cylindrical Theta coil with a passive mirror at each end was again set up. The Upper and Lower Cusp coils were placed immediately above and below the Theta coil, and these were simply two of the smaller-radius Theta coil segments that were driven independently by the Cusp banks.

A cylindrical configuration was chosen again in part because the Guide and Mirror coil set required for FRC translation and capture was not yet ready for placement on the vertical stand. Another reason for choosing a cylindrical Theta coil again was that it was a more "controlled" configuration. Because many changes were made to the overall FRCHX experiment (e.g., changing to a 10-segment coil, adding the Cusp coils, changing to a vertical orientation), it seemed reasonable to try to baseline the FRCs formed in this new setup using a static configuration before trying to diagnose FRCs that were translating as they were being formed. With the interferometer assembly nearing completion, density, temperature, and lifetime baselines could all be established for FRCHX FRCs in the static FRC formation tests.

During conversations with FRX-L personnel, a couple of different cylindrical geometries were considered. The variations involved mainly the choice of coil segments to be used for the passive mirrors on each end. A tapered mirror was considered initially, but per the recommendations of FRX-L's Tom Intrator a uniform mirror was implemented instead, made using the smallest-radius segments available. The radii of these mirror segments was 5.90 cm, and the radii of the six uniform segments in the middle of the Theta coil was 6.72 cm. Figure 47 shows this configuration after half of the coil had been assembled.

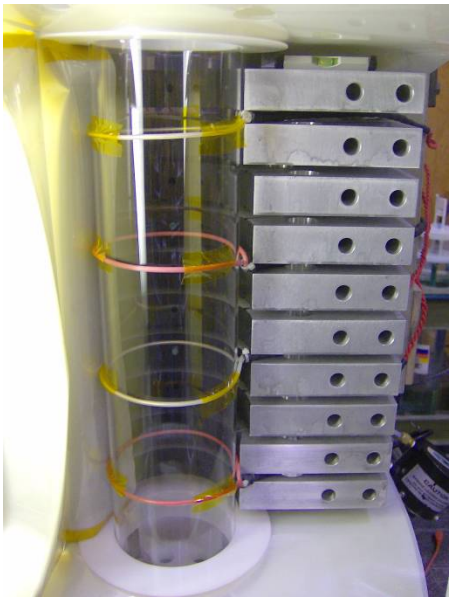
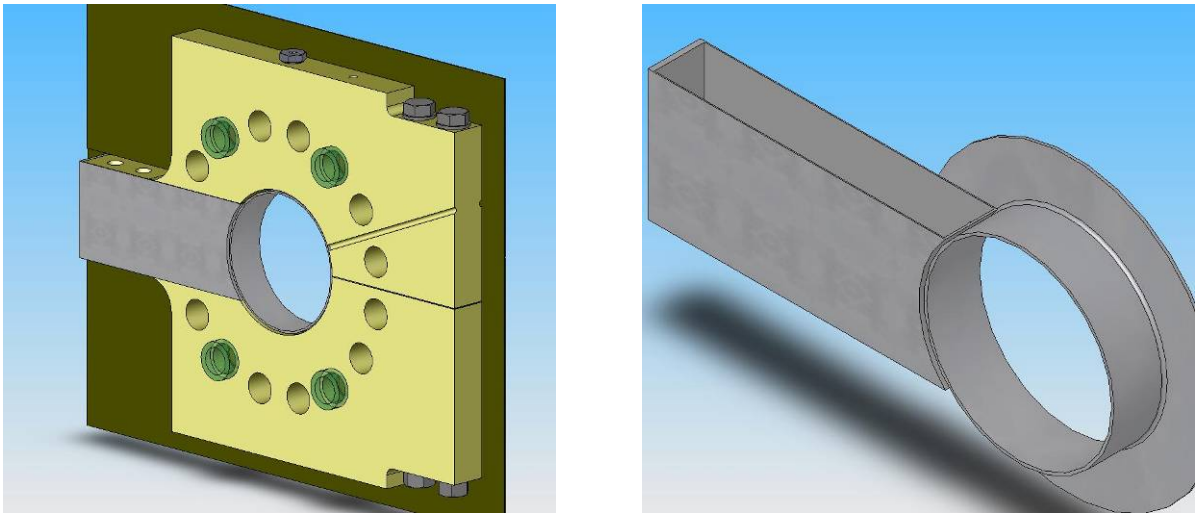


Figure 47. Cylindrical Theta coil, with six-segment uniform region in the middle bounded by two-segment mirrors top and bottom

Two segments having an inner radius of 6.17 cm were then used for Cusp coils. These coil segments were placed approximately 2 cm above and below the Theta coil. To insulate the Cusp coils from the Theta coil, eight sheets of 5-mil (127-μm) Mylar were placed on the sides of the Cusp coils that faced the Theta coil, and a "top hat" insulator, identical to that in use on the FRX-L Cusp coils, was slid into the bore of the Cusp coil sandwiching the Mylar between it and the coil (Figure 48a). To insulate the two current feeds on the Cusp coil segments from each other a second polyethylene insulator was designed (Figure 48b) that would envelop the current feeds.



a b

Figure 48. (a) Cusp coil and insulators; (b) close-up of top hat and current-feed insulators

Though fabrication of the insulators was challenging because of both the large block of stock material required initially as well as the thin walls that were left for the insulator after machining, this approach to insulation seemed more expedient for assembly because of the tight spaces around the Cusp coils. Furthermore, it seemed less likely to suffer problems with breakdown between the two sides of the current feeds than any approach using folded sheets of Mylar or polyethylene to insulate the coil current feeds. Figure 49 shows the Upper and Lower Cusp coils and the Theta coil after assembly was completed.

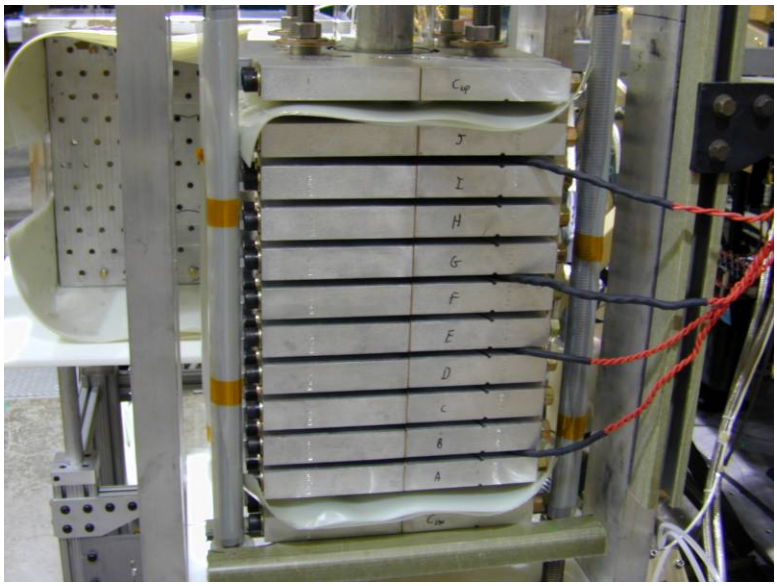


Figure 49. Completed Theta and Cusp coil assembly on vertical stand

4.2.4 Plenum Pre-Fill and Venting System

SAIC's Mark Kostora, who had worked for several years supporting the FRX-L team as a LANL contractor, began supporting the FRCHX work in the fall of 2007. One of his first FRCHX tasks was the design and layout of both a deuterium pre-fill system and a dry nitrogen backfilling and venting system for the FRCHX vacuum vessel. A basic block diagram layout for these two systems is shown in Figure 50.

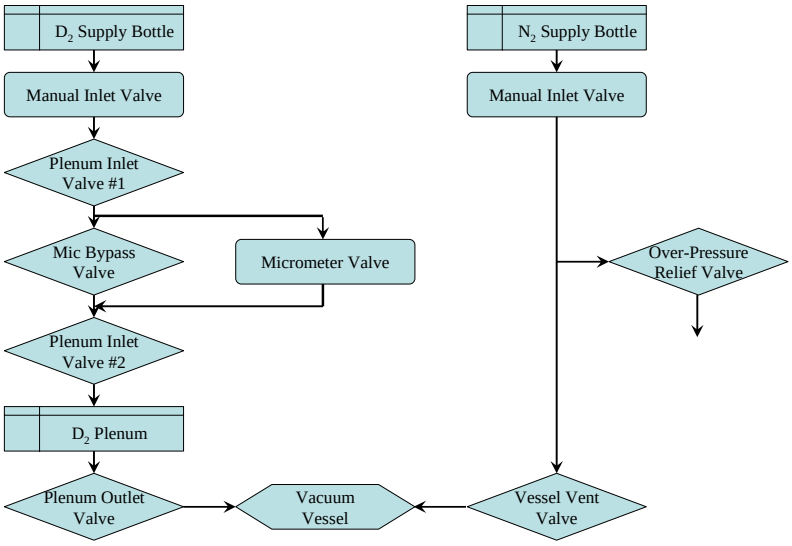
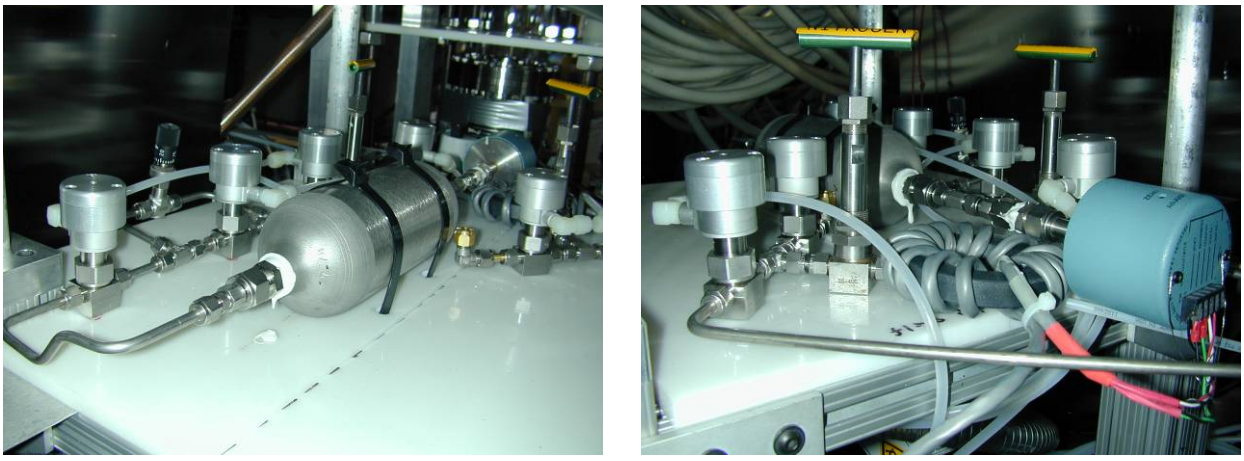


Figure 50. D2 pre-fill and N2 venting systems for FRCHX vacuum vessel

Except where indicated, the valves are pneumatically controlled, providing the ability for the cFP controller to operate these valves. Both systems are very similar to the corresponding FRX-L systems, so assembly and implementation was very straightforward.

Using the diagram in Figure 50, AFRL personnel assembled these systems on a bench top using components that were loaned to us from the FRX-L facility or were purchased. After the assembly was completed, the hardware was moved over to the upper shelf underneath the Theta coil cable header (Figure 46) and connected to the FRCHX vacuum vessel and to their respective gas cylinders. Figure 51 shows the pre-fill and venting systems after their setup was complete.



a b

Figure 51. (a) D_2 pre-fill; (b) N_2 backfilling and venting system components

A 10-Torr Baratron gauge, which is in view on the right in Figure 51b, is connected to the plenum to read the deuterium pressure in the plenum.

4.3 Diagnostics

4.3.1 Flux Loops and B-dot Probes

In Figure 47, the positions of the flux loops can also be seen. A total of four were placed within the bore of the Theta coil; going from bottom to top, the segments are labeled A through J, and flux loops were placed under segments B, D, G, and I. These positions allowed the flux to be measured in both mirror regions and at two locations within the uniform Theta coil region. The flux-loop wires were twisted tightly as they came out from the quartz tube, and the ends were taken out to four voltage dividers that were potted and housed in copper pipes. Figure 52 shows the dividers in the fiberglass support frame, east side of vertical stand.



Figure 52. Flux-loop voltage dividers in fiberglass frame

One of the four voltage dividers was the original divider borrowed from FRX-L for the previous series of FRC formation tests that had been performed. (See Section 3.3.1.) Because no others were available, it was necessary to fabricate the other three dividers in-house, along with the fiberglass frame on which they were mounted. The support frame was designed such that it kept the voltage dividers at least 24 in. (60 cm) away from the Theta coil.

Prodyn Technologies, which manufactured the single-turn B-dot probes used in the previous experimental setup, also was able to design and manufacture several 10-turn B-dot probes for us with a similar geometry. The probes were again inserted into ports in the Theta coil segments (Figure 53), and all were inserted far enough such that their ends rested against the quartz tube.



Figure 53. Four B-dot probes in Theta coil, segments B, D, G, and I

The increased number of turns was requested from the manufacturer to increase the signal-to-noise ratio from the probes and make the measurement of excluded flux somewhat easier. The probe stems were also longer than those of the earlier probes, eliminating the need to place insulator disks between the Theta coil and their connectors.

4.3.2 The Four-Chord Interferometer

The assembly of the four-chord interferometer and the subsequent alignment of all its opto-mechanical components on the optical table had been progressing in the "background" of other FRCHX efforts since the beginning of 2007, when the Phase I FRC formation tests were getting started. With the start of the Phase II, a concentrated effort was made to complete the steps necessary to bring the four-chord interferometer on-line so that plasma density could also be measured during these tests. It was particularly desired to begin interferometer measurements before starting any attempts to optimize the FRC parameters or any efforts to extend its lifetime.

By April 2008, the remaining tasks necessary to field the interferometer consisted primarily of completing the coarse alignment of all the optical components, moving the optics table into place around the vacuum and field-coil stand (Figure 54), moving the detector and demodulator components into the remote shielded enclosure where all the data acquisition components were housed (Figure 55), and then performing a final fine alignment of the optical components.

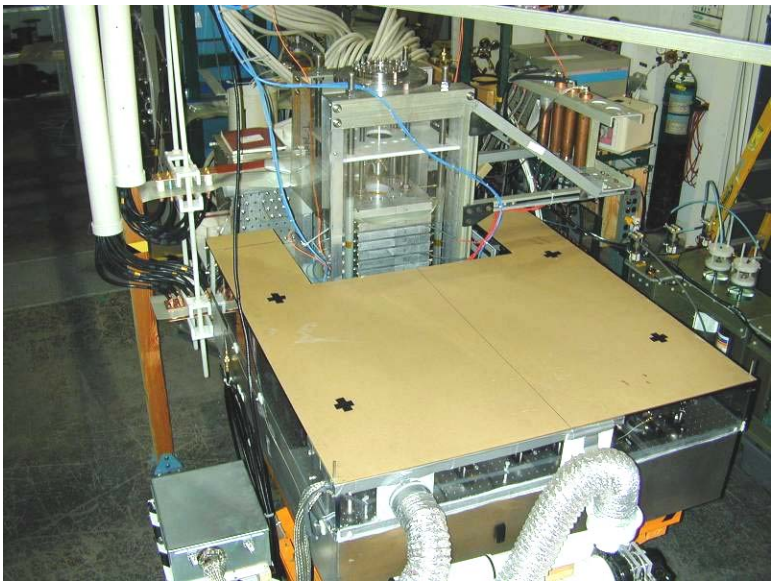


Figure 54. Four-chord interferometer in place around vacuum and field-coil stand

Figure 55 shows the interferometer detectors and circuits at the bottom of the remote data acquisition box.



Figure 55. Detectors and RF demodulator circuits for four-chord interferometer

Once the interferometer-optics table was in place, it was discovered that one of the all-thread rods running through the Cusp and Theta coil assembly was blocking the path of the fourth chord. The fourth chord is used primarily to correct for the heating in the quartz tube during a shot, but in order to serve this purpose its path must lie outside the plasma in the tube. (See

Section 4.6.3.2.) NumerEx and SAIC personnel were able to redirect the beam of the fourth chord sufficiently so that it was no longer blocked by the all-thread rod; however, the new beam path inadvertently intersected the periphery of the plasma. As a result, when analyzing the data it was not possible to correct accurately for the quartz-tube heating. Density measurements accurate to within an order of magnitude were still possible, however. Later, during the reconfiguration of the Theta coil from a cylindrical bore to a conical bore, the all-thread rod was repositioned through one of the adjacent axial holes in the coil segments such that it should no longer interfere with the path of the fourth chord.

4.3.3 Side-On Fiber-Optic Translation and Continuum Array

The motivation for developing and fielding the side-on fiber-optic translation and continuum array on FRCHX was primarily to have a diagnostic for monitoring plasma translation. However, this array can also have application in giving real-time evidence of both stability and symmetry of the FRC during formation and equilibrium, as well as in providing FRC axial profile information. Furthermore, information on pre-ionization uniformity can also be determined with this type of diagnostic. Similar continuum arrays have been used on other previous FRC experiments, i.e., TRX, LSX, and FRX-L.

The configuration of the FRCHX side-on fiber-optic array during the Phase II FRC formation tests was as follows. Eight 100/140 μm clad multimode fibers were placed at various locations along the west side of the Theta coil, as can be seen somewhat in Figure 56.

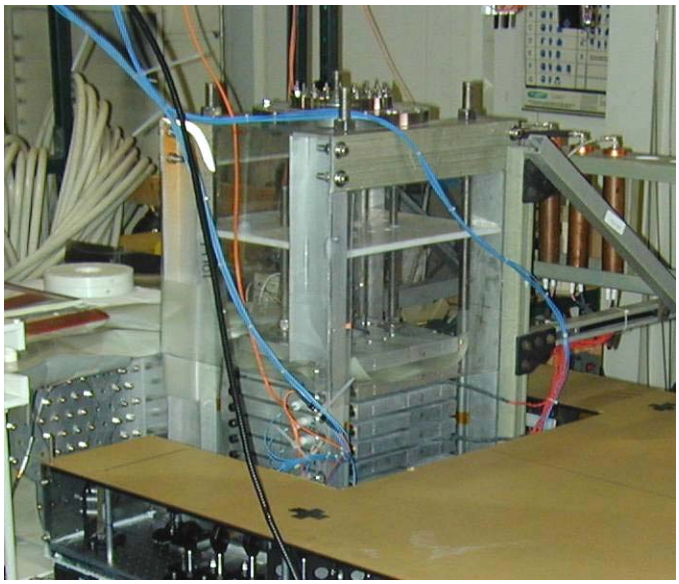


Figure 56. Blue fibers used for side-on fiber-optic array

The fiber ends were inserted into polyethylene holders, and these holders, in turn, were inserted into the radial access holes in the B, C, D, E, F, G, H, and I coil segments. In addition to holding the fibers in place, the holders also kept all the fibers inserted at a uniform depth, which was at this time approximately midway into the magnet structure. The partial insertion served to limit the viewing angles of the fibers and thereby provided a more precise determination of the time of passage of the plasma across the fiber's field of view during the initial formation and contraction.

The other ends of the fibers were run back to the remote data acquisition box and connected to eight receiver channels, which were comprised of x10-gain adjustable amplifiers driven by HFBR-24X6 820nm photodiodes. In Figure 55 the detectors for the side-on fiber-optic array are shown on a wooden shelf just above the interferometer components.

Eight additional receiver channels were also made available for future use. The electronics in each of the receiver circuits had a 14 MHz time resolution that was expected at least to meet the requirement of monitoring the plasma translation later on. Also, the sensitivity was expected to be sufficient to detect light variations during a PI-bank-only test with a 50 mT static fill of the vacuum chamber, however additional electronic amplification of the signals on each channel could be used to provide a better dynamic range in signal amplitude. End on imaging is often used in conjunction with side-on continuum array diagnostics such as these, and the UNR camera package, which will be discussed next, serves this purpose.

In addition to these eight photodiode channels, FRX-L personnel had provided a second optical continuum array diagnostic with 16 channels. The receivers in this diagnostic were comprised of PMTs, and eight of the 16 channels were set up with 546 nm mercury line filters installed between the fiber ends and the PMT receivers, while the other eight had neutral density filters at this location. Though the PMTs were much more sensitive than the photodiodes, their bandwidth was only 1 MHz, approximately. As a result, the optical PMT diagnostic was used only as a supplement to the fast optical photodiode array. Of the 16 channels available only four were utilized at this time, all of which had the 546 nm mercury line filters on them. The purpose of the mercury line filters was to let through only a fraction (~1%) of the wavelengths that passed through the fibers. Interestingly, the filtering effect at this particular wavelength produces a signal that (qualitatively) closely approximates the density profile of the plasma.

Fibers for the PMT detectors (four more 100/140 μm clad multimode fibers) were located in separate radial access holes in the B, D, F, and H Theta coil segments. The particular receiver to which a fiber was connected was distinguishable by the side on which the fiber was inserted into the Theta coil: the fibers inserted on the west side of the Theta coil were connected to the photodiode receivers, and those inserted on the east side were connected to the PMTs with the mercury line filters. The separate fiber bundles can be seen in Figure 56, where the view is directed toward the west side of the Theta coil.

4.3.4 UNR Gated End-On Photography and Fiber Probe Diagnostic Package

During the last week of March 2008 personnel from UNR visited Building 322 to install a gated end-on viewing camera package with which to capture images of the background plasma and the FRC during the formation process and throughout its lifetime. The principal components of the setup included one of the AFRL MCP cameras, to provide the temporal resolution (ranging from tens of nanoseconds to ~1 μs), and a CCD camera belonging to UNR that captured and temporarily stored the image.

Both cameras were housed in a small shielded enclosure. A laptop PC (also supplied by UNR) was set up in the Shiva control room to control the camera, and a fiber-optic USB extender was used to link the camera to the PC. Both the CCD and MCP cameras were able to be triggered fiber optically using the DG-535s in the remote data acquisition box and passive optical transmitters. The optical triggers were converted back to electrical signals using battery-powered trigger-receiver boxes that were placed inside the camera enclosure with the cameras. Such a receiver was already available for the MCP camera, but it was necessary to fabricate a second, special receiver for the CCD camera. The special requirements were that the trigger pulse had to be on the order of 5 ms in duration and be at Transistor-Transistor Logic (TTL) levels.

Figure 57 shows an overall view of the UNR end-on photography system after its setup was completed.

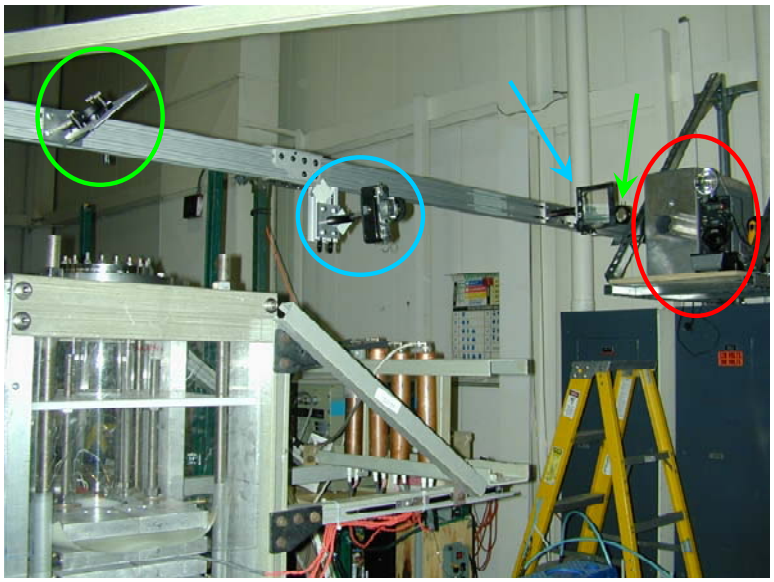


Figure 57. UNR end-on photography and fiber-probe diagnostics

The MCP and CCD camera enclosure (indicated by the red circle) was placed on a small platform attached to the east wall of the high bay, and a support arm was then set up between the platform and the cable tray holding the Upper and Lower Cusp bank transmission-line cables. Attached to the support arm was a mirror (green circle) that provided the end-on axial view of the quartz tube for the camera system, and a lens (green arrow) to focus the plasma light selectively onto the MCP camera from a particular axial location.

Also on the support arm was a small plate of glass (blue arrow) that served as a beam splitter for an elegant end-on fiber probe. The plate of glass reflected a small portion of the plasma light that was being directed to the MCP camera back to a Nikon camera body (blue circle) instead. The Nikon camera body retained its focusing lens, but instead of having film inside, it had a fiber-optic cable mounted to its back. The end of the fiber-optic cable was positioned in the focal plane of the lens, thereby allowing it to capture the light coming into the Nikon camera. The fiber-probe field of view was intended to be located off-center at a radial position that would normally be just outside the equilibrium radius of the FRC, but one at which it would begin to pick up plasma light if the FRC were to begin developing an n=2 instability. For the setup shown in Figure 57, the fiber was positioned to view along the axis at a radius of 2.5 cm. The other end of the fiber was run to the remote data acquisition box and connected to a ninth photodiode receiver, identical to those described in Section 4.3.3.

4.3.5 Receiver Box for Trigger Sync-Out Signals

One final diagnostic system that was added to the FRCHX was a 10-channel fiber-optic receiver box to convert optical sync-out signals generated by the various trigger generators into electrical signals that could then be recorded with the other data signals. Such signals are quite valuable for confirming the operation of the various trigger units, as well as the timing of their operation. The box was assembled by NumerEx personnel and consisted simply of five IFS VR1001 dual channel video-receiver units packaged into a single rack-mount box. Placing the units in a common box made the task of connecting fiber-optic cables to them and providing them with power much easier. Figure 58 shows the receiver box sandwiched between the PXI digitizer crates in the remote data acquisition box.

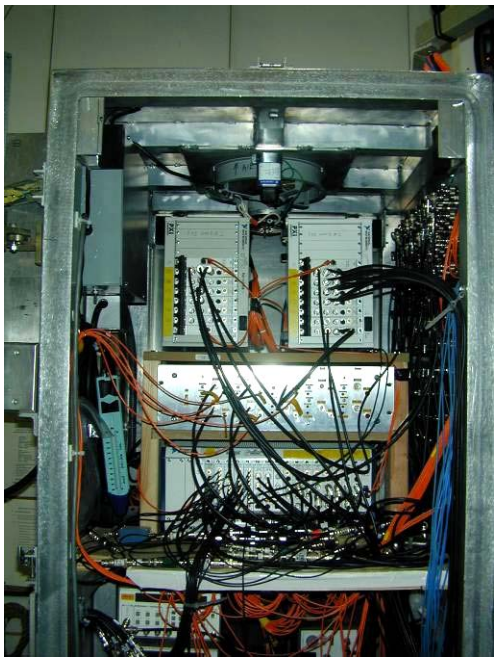


Figure 58. Trigger sync-out receiver box positioned among PXI digitizer crates

4.4 Data Acquisition and Remote Shielded Enclosure

4.4.1 Plans for the FRCHX Data Acquisition System

At the beginning of the FRCHX Phase II efforts, plans for a new shielded data acquisition enclosure that was separate from the Shiva screen room were developed with the goal of making it possible to continue FRCHX experiments uninterrupted while preparations for other Shiva experiments continued in the Shiva screen room. During the Phase I tests, the use of the Shiva Star screen room for other ongoing experiments often required that FRCHX tests be suspended for a week or more while the data cables, delay generators, and oscilloscopes in the screen room

were set up for these other tests and then afterwards returned again to the appropriate configuration for FRCHX. With there being a limited number of patch cables going to the Shiva screen room and a limited number of cable feedthroughs in the back wall of the screen room, a separate remote data acquisition enclosure would also make it considerably easier to increase the number of FRCHX data channels. By setting up the enclosure in the vicinity of the FRCHX experiment, the overall length of the diagnostic signal cables would be shortened, and by further setting up patch panels at several convenient points in the FRCHX test area with dedicated cable bundles running to the data acquisition box, fielding diagnostics on the experiment would be much more convenient. The initial cost and effort expended in setting up the remote data acquisition enclosure was expected to be recovered in the hours saved by not having to reconfigure the data acquisition system each time another Shiva test was being performed.

Plans were made to find a fairly large enclosure to use for this application, as the enclosure would need to contain all the FRCHX oscilloscopes and/or digitizer crates. In addition, power supplies for fiber-optic monitors and various other diagnostics and the detectors and RF components required for the four-chord interferometer would also need to be placed inside the enclosure. The electronic components for the single-chord interferometer potentially needed to be moved inside the enclosure, as well. Fortunately, there was an equipment-rack-sized shielded enclosure already in-house that could be adapted for use in this application.

To communicate with the oscilloscopes and/or digitizers in the enclosure, plans were also made to set up a dedicated computer in the Shiva Star screen room or control room, which would then be linked fiber optically to these devices. In this manner, personnel could remotely collect and review the data without having to go out to the remote enclosure.

Shortly after these plans were developed, an 18-slot National Instruments PXI crate (with appropriate fiber-optic MXI interface cards for the crate and a PC) and four 8-channel, 60-MS/s, 12-bit digitizer cards were purchased to address the need for digitizer channels in the remote enclosure. In addition, a considerable number of other PXI crates and data acquisition cards became available from another project a short time later. These other cards were largely 2-channel, 100-MS/s, 8-bit cards, but three 2-channel, 100-MS/s, 14-bit cards were also obtained. With the acquisition of this second set of crates and digitizer cards, the anticipated needs for digitizer channels in the enclosure (at least in the near term) were essentially met.

4.4.2 Setting Up the Remote Data Acquisition Enclosure

NumerEx personnel readily assumed responsibility for setting up the remote data acquisition enclosure. Under their direction, Voss Scientific personnel wired up AC power to it, and installed AC plugs and a ventilation fan inside. A small external junction box was mounted to the west side of the enclosure, and three relays were placed inside the box that when energized just before an FRCHX shot would break the enclosure's connection to the AC wall power. Figure 59 shows the remote shielded enclosure after it had been moved into its designated position along the north wall in the FRCHX test area.



a b

Figure 59. (a) Enclosure in position; (b) space inside enclosure

Figure 60 is a map of the northeast corner of the high bay indicating where the shielded data acquisition enclosure ("Data Acq Box") was placed relative to the rest of the FRCHX system components.

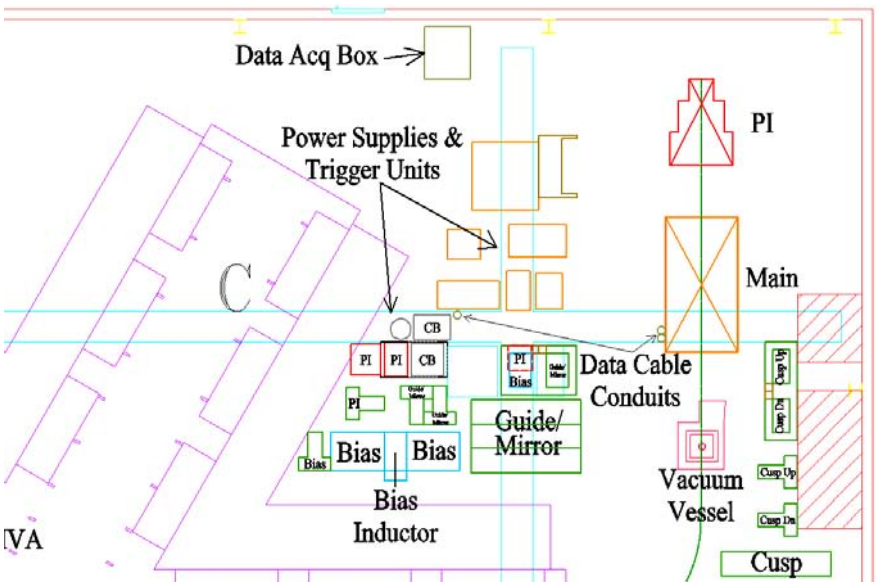


Figure 60. Test area showing placement of shielded enclosure and data-cable conduits

Also shown on this map are the locations to which three 3-in. (7.6-cm) conduits, each carrying a bundle of 25 to 27 diagnostic cables (RG-223 or RG214), were run from the shielded enclosure: two conduits were run to a point near the Main bank and the third to a location adjacent to the rail-gap-trigger units. A fourth conduit was run a few months later to the center of the Shiva bank in preparation for eventual FRCHX tests in this location. For such tests, which include both non-destructive FRC formation, translation, and capture tests as well as the FRC compression-heating tests, the vacuum and field-coil stand, the Main bank, and the PI bank were to be placed underneath the Shiva bank.) It was decided to use steel conduit for this task because of the magnetic shielding properties of steel.

Each of the conduits was run inside the cable trays in the floor as much as was possible, and as they were run, they were kept isolated from all other metal surfaces and from themselves. The reason for this constraint was that it was possible to use one of the conduits as a low-inductance, single-point ground connection for the shielded data acquisition enclosure. The conduit that passed the closest to the single point earth ground in the floor, which was located underneath the Bias and Guide/Mirror power supply stand, was simply tied to the grounding point with a 3-in. (7.6-cm) wide copper strap. This approach worked well for the Theta coil, as well, because the Theta coil is the only other component that also remains grounded during tests. A copper strap was simply run between the Theta coil and the conduit that had been grounded, because this conduit emerged from the cable tray a short distance from where the Theta coil was positioned.

Several additional feet of flexible conduit were added to the ends of the rigid conduit that stopped by the Main bank (Figure 61), because there was some concern about having the diagnostic signal cables run that close to the Main bank before entering the conduit. It was felt that it was better to have the diagnostic cabling and conduit routed to avoid high-field and high-fringe magnetic field regions around the Main bank. Using flexible conduit outside the cable tray has had the added advantage of allowing the positions of the two cable patch panels for these conduits to be adjusted slightly, as needed.

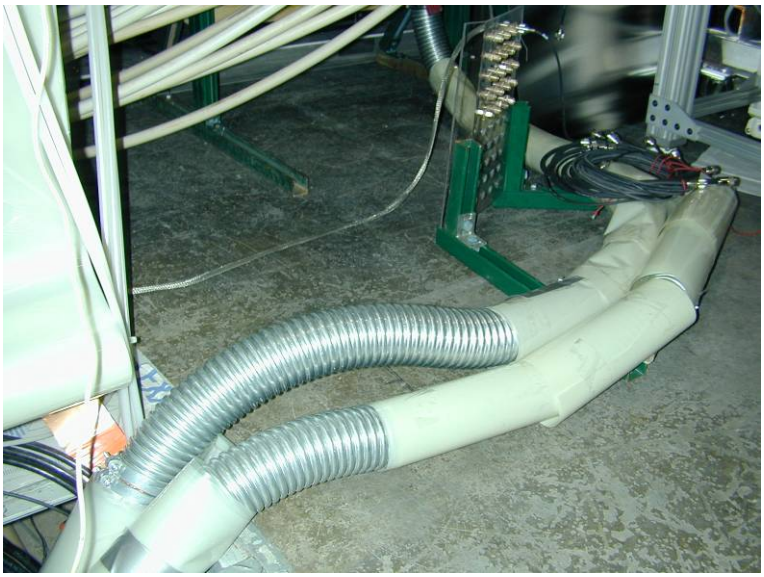


Figure 61. Conduit attached to ends of rigid conduit exiting cable trays

The patch panels were, again, placed at the ends of the conduits to simplify making connections between the various FRCHX diagnostics and the data cables. At the shielded enclosure, one large patch panel—an array of 100 N-type connector feedthroughs—for the cables from all four conduits was placed in the upper east wall of the enclosure. A Hoffman box with the back panel cut out was then placed over this array of connectors and sealed tightly around its edges to make a shielded covering around them. It was then possible to mount the data-cable conduits to the Hoffman box through portholes that had been placed in the bottom of the box. Figure 62 shows this assembly on the east side of the data acquisition enclosure.



Figure 62. Data-cable conduits and Hoffman box covering patch panel

Once inside the Hoffman box, the data cables were run through stacks of ferrite cores before being connected to the patch-panel connectors.

4.4.3 Data Acquisition and Diagnostic Systems Placed Within the Enclosure

Once all the external "assembly" work for the remote data acquisition enclosure was completed, NumerEx personnel began placing all the diagnostic elements for the FRCHX experiment inside it. These elements included initially the various PXI crates and their digitizer cards that were needed for recording data (Figure 63), 50 100-MHz data channels and 32 60-MHz data channels loaded into the crates here; the interferometer detectors and RF components (Figure 17b); the photomultiplier tube used as a first-light monitor and for other spectroscopic applications (Figure 13b); and the power supply required by the photomultiplier tube. Figure 63 shows crates just before installation in the remote enclosure.

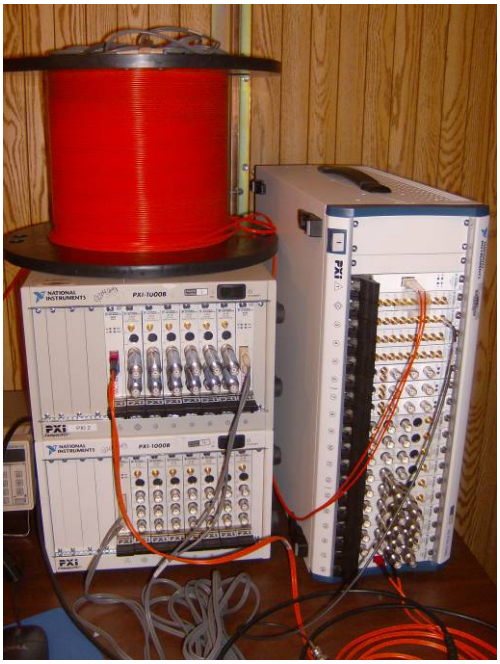


Figure 63. 18-slot PXI crate (right) and two 8-slot crates (left)

Other diagnostic items were, of course, added later, which include (among others) the photodiode and photomultiplier receivers for the side-on fiber-optic translation and continuum array (Section 4.3.3) and the trigger sync out receiver box (Section 4.3.5). Because wall power was to be lifted just before each FRCHX shot to remove any possible ground loops or sources of noise and interference, a UPS was placed within the shielded enclosure, as well, to maintain power for all the components inside.

4.4.4 Relocation of FRCHX Trigger-Timing Systems into the Enclosure

In keeping with the goal of not overlapping FRCHX activities with other activities in the Shiva screen room, it was eventually decided to move the DG-535 delay generators, which initiated all bank triggering following the command trigger, from the Shiva screen room out into the remote data acquisition enclosure. With this move, FRCHX operations were now totally independent of the Shiva screen room. To make this move, fiber-optic-trigger lines going to each of the bank-trigger units needed to be rerouted from the fiber-optic patch panel near the rail-gap-trigger units over to the shielded enclosure and then fed into the enclosure through “cut-off waveguide” pipes (Figure 64a).





a b

Figure 64. (a) New cable tray and fiber-optic feedthroughs; (b) DG-535s

Inside the shielded enclosure the fiber-optic lines were connected to optical transmitters. Each transmitter was then driven by an appropriately delayed output pulse coming from one of two DG-535 digital delay generators, shown in Figure 64b after setup. As before, the command trigger was being provided by the cFP controller, which was also brought into the remote box through a fiber-optic line.

4.4.5 Computer Link and Data Acquisition, Processing, and Archival Software

As mentioned, personnel had planned to set up a dedicated computer in either the Shiva Star screen room or control room to configure and arm the digitizers remotely in the data acquisition enclosure before each shot, and then to collect and review the data from them after the shot had occurred. Again in keeping with the goal of not overlapping FRCHX activities with other activities in the Shiva screen room, it was decided to place this computer in the Shiva control room. Once this decision was made, the fiber-optic cable purchased with the 18-slot PXI crate was run from the computer's position in the Shiva control room out to the PXI crates in the remote data acquisition enclosure so that the fiber-optic link between the two could be set up.

NumerEx and UNM personnel then began writing the software needed to carry out all the necessary data acquisition operations. Because of everyone's familiarity with LabVIEW®, it was chosen as the software in which to write the "upper level" part of the data acquisition program

that handled all communications with the PXI digitizer cards. NumerEx personnel set out to write the program such that it could be used to configure the various parameters, such as sensitivities and time bases, for each of the channels on each of the PXI cards as well as retrieve the data recorded by these digitizers. Because of the desire to establish an MDSPlus database, as well, in which all the experimental data was to be archived eventually, once the data from the PXI digitizers was retrieved, the LabVIEW program then stored the data in a format that MDSPlus could read. At that point, it was intended that MDSPlus would take over the management and post-processing of the data and store it in an organized database.

UNM personnel took on the work of writing the MDSPlus software to set up the database structure. In addition, several routines were also written to perform analysis operations that personnel had previously been doing manually. These analysis operations include the calculation of excluded flux radius using both plasma and vacuum magnetic probe data and determination of plasma density from the eight recorded interferometer detector waveforms. In addition, UNM personnel set up a number of virtual "scopes" to display related sets of waveforms together.

Because of differences between the PXI command syntaxes and GPIB command syntaxes (which personnel were most familiar with), the programming was somewhat arduous at times, but eventually a flexible and reliable joint LabVIEW and MDSPlus data acquisition program was developed that allows operators in the Shiva control room to set up the PXI digitizer cards remotely for shots, to collect the data from them after the shots, and then to plot the data for viewing and cursory analyses (Figure 65).



Figure 65. Data acquisition computer, PXI configuration panel displayed

Currently, up to four PXI crates have been successfully daisy-chained together with the computer being able to detect and set parameters for each digitizer channel, and more can easily be added. Figure 63 shows three PXI crates that have been linked together and contain a total of 82 digitizer channels. With the present number of FRCHX diagnostics these three crates are sufficient to handle all the data channels for the near term.

4.5 Computer-Based Control System

The FRCHX control-system architecture was based upon the architecture that had been established at FRX-L for both control of the experiment and control of vacuum-system operations. Namely, a central controller operated all system components either through switching on and off pneumatic control lines (for slower components or operations) or fiber-optic control lines (for faster components or operations). Binary status signals from various system components were read in fiber optically, as were analog signals such as charge voltages and pressures. In the case of the latter, the analog-voltage signal was converted into a fiber-optic signal using a voltage-to-frequency converter circuit placed near the analog signal's source, and it was then converted back into an analog signal again using a frequency-to-voltage converter at the controller. Inputs to the controller were thus digital (status) or analog (charge voltage, pressure) while outputs were primarily digital (a device was turned on or off). A LabVIEW-based program was run on a computer that was linked to the controller, and it provided the logic for the controller's operations. It enabled operators to activate or de-activate systems "manually" one at a time, or through programmed routines initiate a whole sequence of events on the experiment, such as the charging, firing, and subsequent safing and discharging of a capacitor bank.

This section describes the controller that was assembled for the FRCHX control system, the tasks of running control and signal lines to and from the various components on the experiment and the means of linking these lines to their respective components, and the methods and special hardware by which vacuum-system operations are handled by the control system. A separate emergency abort link that bypasses the computer and the control system's controller is described, and an overview of the LabVIEW control program presented.

4.5.1 Compact Field Point Controller and User Interface Computer

As mentioned in Section 3.4, Mr. Sanchez and Mr. Aragonez of LANL were asked to design and assemble the controller for FRCHX. Based upon what they had learned while setting up the FRX-L control system, placement of the controller in a large and spacious shielded box was important so that there would be plenty of room to run wires and fiber-optic and pneumatic control lines. A larger enclosure also made much easier the tasks of troubleshooting and of adding new components later to the controller. Furthermore, because of greater noise immunity and reduced cost, they also felt that a cFP controller would be a better choice than a PXI controller. (The FRX-L vacuum control system had a cFP controller, while the experiment itself was using a PXI controller.) Also, a goal that was motivated by SAIC personnel was that both experimental and vacuum system operations be integrated into one control system rather than two separate control systems.

After inventorying all the anticipated control (digital) output channels, status (digital) input channels, and voltage and pressure (analog) input channels for FRCHX, it was determined that five digital output cFP modules would be needed along with one digital input module and one analog input module. (All the cFP modules have 16 channels.) Mr. Sanchez prepared a list of these and the other major components that were needed from National Instruments, Clippard, and other vendors to assemble the controller so that all these items could be ordered (Table 1).

Table 1. List of Major Components Needed for cFP Controller

Amount	Description	Part Number
1	NI Compact FieldPoint Controller Module	cfp-2110
1	Backplane, 8 slot	CFP--BP-8
5	Digital Output Module	CFP-DO-401
1	Digital Input Module	CFP-DI-301
1	Analog Input Module	CFP-AI-112
7	Connector Block	CFP-CB-1
5	Clippard Valve Module	EMC4-12-24-70
1	Disconnect and Shoring Box	
1	Hammond Enclosure	1418N4S10
1	Fan it K	XF6115
2	Power Supply 24Volt	

Once all the hardware had arrived in-house, Mr. Sanchez and Mr. Aragonez began positioning the various components inside the shielded (Hammond) enclosure to establish a suitable layout for them. When the layout was decided upon, they began attaching the items to the mounting plate in the enclosure and then laying out the interconnecting wiring between them. Figure 66 shows the final layout of the components inside the Hammond enclosure.

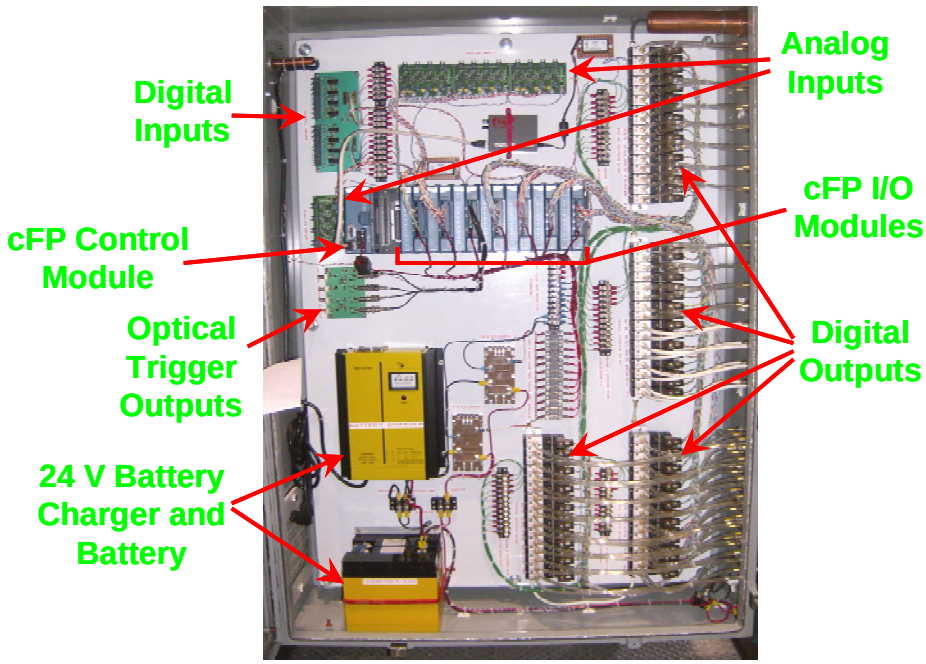


Figure 66. Controller components in Hammond enclosure

Once this work was underway, SAIC personnel purchased a Hewlett Packard laptop computer for use as the interface with the controller. A copy of LabVIEW 6i that was available was installed on the laptop, along with the LabVIEW control program for FRX-L and a number of the diagnostic routines used with the FRX-L control lines. It was envisioned that the cFP controller would be placed in the Building 322 high bay in the vicinity of the experiment, and a fiber-optic cable would be run between the controller and the Shiva control room to enable an Ethernet link to be set up between the laptop and the controller. This arrangement allowed operators to run the experiment from the Shiva control room.

In February 2007, when the assembly of the controller was nearly completed, SAIC personnel traveled to LANL to obtain some basic guidance from LANL personnel on setting up the link between the laptop and the cFP controller, as well as to conduct a series of preliminary trial tests with the hardware in the controller to see if there were any bugs that needed to be fixed. Only a few minor hardware problems were found that were easily corrected; however, it was also discovered then that LabVIEW 6i was not current enough to work with the cFP devices. When SAIC personnel returned to AFRL, steps were made to purchase an upgrade to version 8.2 for the LabVIEW software.

By the summer of 2007 the assembly work on the cFP controller had been completed, and LANL personnel then transported the controller to AFRL along with many of the materials needed to

begin interfacing the controller to the various FRCHX systems. Upon after arrival at AFRL, a Unistrut stand was fabricated to support the Hammond enclosure vertically. After attaching the enclosure to the stand, the controller was moved into place next to the Main bank power supply (Figure 67).



Figure 67. cFP controller, next to Main bank power supply

A final checkout of the cFP controller was then performed with Mr. Aragonez participating. The laptop computer was connected to the controller, and the LabVIEW diagnostic routine "Signal Line Test – 3 Button.vi" was used to send a command signal to every digital output and to check for digital and analog signals from every digital and analog input. A number of problems were encountered with the various banks of input and output channels, but these were all relatively minor, and Mr. Aragonez was able to correct them readily over the course of a week.

4.5.2 Pneumatic Control and Fiber-Optic Status Lines for Pulsed Power

Once the internal components of the controller were in proper working order, the efforts of SAIC and Voss Scientific personnel focused on connecting the controller channels to the various components of the experiment. Mr. Sanchez and Mr. Aragonez had fabricated five door-interlock boxes (Figure 68) for the FRCHX test area that would allow the controller to monitor these doors and shut down the experimental operations if there was any unauthorized entry.

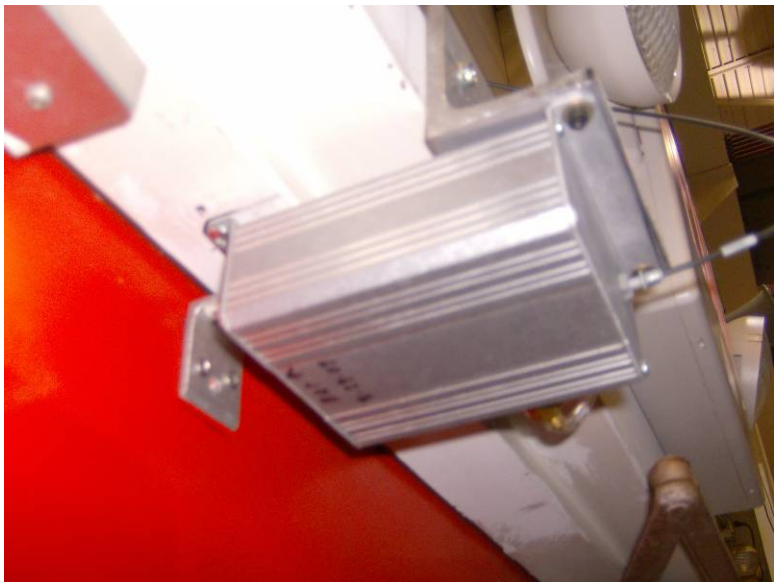


Figure 68. Northeast personnel door-interlock box

The boxes contain small fiber-optic-transmitter circuits that have magnetically actuated switches on their sides. The magnet for the switch was mounted on a small bracket attached to the door, and it turned on and off the transmitter circuit, as the door was closed and opened. These boxes were the first items to be installed in the test area. After their installation at each of the doors, pneumatic hoses and optical fibers were run between the boxes and the controller to allow the controller to turn on and off the battery power to the boxes and to receive the optical signals from the boxes, respectively.

Mr. Sanchez and Mr. Aragonez also fabricated 10 voltage-to-frequency (v-to-f) converter boxes for FRCHX that convert the output signals from the voltage monitors at each bank into optical signals that can be transmitted with high fidelity to the cFP controller. The v-to-f converter boxes were placed on the resistor stands for the PI, Bias, Upper Cusp, Lower Cusp, and Guide/Mirror banks, because the voltage probes for these banks were on or near these stands. Figure 69a shows these gray boxes, connected to high-voltage probes.



a b

Figure 69. (a) and (b) v-to-f converter circuits on each of the bank resistor and/or switch stands

Two converter boxes were used for the Main bank, since the Main bank is dual polarity; these were placed on the wooden table that also supported the Jennings charge switches and the bank's two voltage probes (Figure 69b). As with the door-interlock boxes, once the v-to-f boxes were all in place pneumatic hoses and optical fibers were run between them and the controller to allow the controller to turn on and off the battery power to the boxes and to receive the optical signals from the boxes, respectively. As described, once the optical signals were received back at the controller, they were converted into an analog voltage again that was then read in by the controller and interpreted by the LabVIEW control program.

In addition to the door-interlock boxes and v-to-f boxes, a large number of Clippard "ES-1" pneumatically actuated electrical switches were also provided to AFRL with the controller by Mr. Sanchez and Mr. Aragonez. SAIC personnel in turn purchased the appropriate pneumatic actuators to go on the switches. These switches were the primary item needed by the cFP controller to activate most of the relays and other system components on the experiment (Figure 70).



Figure 70. Clippard pneumatically-actuated switches

As each switch was connected to a particular item that was to be controlled, a pneumatic hose was then run from it back to the controller and plugged into the appropriate digital output channel.

A few of the FRCHX components, though, required more than just a simple Clippard “ES-1” switch to interface with the control system. These items included the PI bank CCS power supply, the Crowbar switch high voltage power supply, the Main bank power supply, and the vacuum gauge controllers. To control CCS power supplies remotely, external signals must be applied to inputs on the back of the supply to place it in remote mode, as well as to turn on and off the high voltage. Figure 71 shows remote control interfaces.





a b

Figure 71. (a) PI bank CCS power supply; (b) interface box

Once the supply is in remote mode, however, the front panel knob cannot be used anymore to provide the set point; rather, an analog voltage must be applied to the remote voltage-programming input on the supply.

The external control box shown in Figure 71b was fabricated so that it would be possible for the cFP controller to send the external signals that are needed at the supply's DB-25 connector and external interlock inputs to enable, operate, and disable the CCS supply. Presently, the cFP controller is not able to send out any analog signals—though if an analog output module were installed, it could. Thus, it could not apply an analog voltage to the remote voltage-programming input on the CCS supply, so a built-in potentiometer allowed the operator to dial it in manually before a shot.

Rather than trying to run pneumatic lines up to the Shiva control room to interface with the rack-mounted Crowbar trigger power-supply controller, a new controller was assembled and placed in the FRCHX test area next to the Crowbar's Universal Voltronics (UV) power supply. The new controller—the copper box shown in Figure 72—was modeled after the Main bank trigger-power-supply controller and requires only a single pneumatic line from the cFP controller, compared to at least two lines that would have been required to interface to the original controller in the Shiva control room.



Figure 72. Remotely operated controller (upper left) fabricated for Crowbar Switch's UV power supply

These same issues were faced when considering how best to interface the cFP controller to the Main bank power-supply controls in the Shiva control room. Because of its complexity, it was not entirely clear what all the processes were that the Main bank power-supply controller handled. Furthermore, building a simpler controller to place in the FRCHX test area and then attempting to shift the complexity of the power-supply operations to the software ran the risk of overlooking some important processes, which could possibly have catastrophic consequences. Instead of running pneumatic lines up to the control room, though, it was decided instead to use an IFS fiber-optic contact transmitter/receiver pair (model numbers DT1810 and DR1810) to transmit the control signals from the cFP controller up to the Shiva control room (Figure 73).

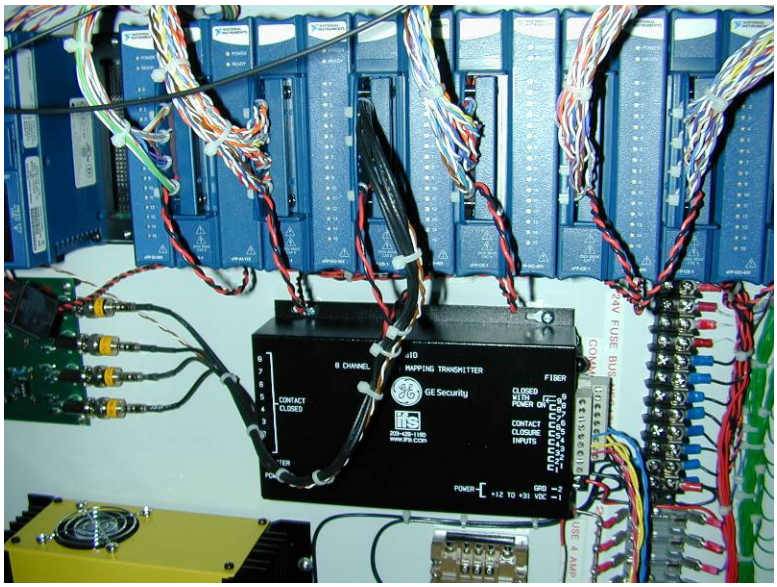


Figure 73. IFS 8-channel contact transmitter in Hammond enclosure

This approach was somewhat analogous to the manual control boxes used earlier to operate the PI and Bias power supplies and Jennings switches (Section 3.4), except that the transmitter was located in the cFP controller's Hammond enclosure, and it was to be operated by the cFP controller. The receiver, in turn, was embedded in the Main bank power supply controller in the Shiva control room. The contacts at the output of this IFS unit were simply wired in parallel to the front panel power-supply controls, essentially giving the cFP controller the ability to operate the Main bank power supply through the front panel buttons. Interestingly, interfacing the cFP controller to the Main bank power supply in this manner gave personnel the ability to continue to operate the Main bank manually at times, if desired.

Once all the pneumatic control lines and all the fiber-optic status and signal-input lines had been run, a second evaluation of the controller was performed. For this evaluation, the LabVIEW diagnostic routine “Signal Line Test – 3 Button.vi” was again run on the laptop computer, and command signals were again sent to every digital output, but now proper operation was checked of the appropriate control lines and pneumatic switches, and the FRCHX components to which they were attached. Similarly, remote status or other input signal devices were activated (e.g., the door interlock boxes or the v-to-f converter boxes), and the appropriate signal was checked for at the cFP controller using the Signal Line Test routine. As expected, minor problems were found, but these were all easily corrected. With the conclusion of these tests, the control-system hardware was therefore assured to be in working order.

4.5.3 Vacuum-System Controls

When the control and status lines were in place for the FRCHX pulsed power systems, Voss personnel began concentrating on the vacuum-system controls. A bundle of pneumatic control lines was run from the controller over to the vacuum and field-coil stand. At the base of the stand the pneumatic control lines were tied to three-way and four-way valves that in turn switched higher-pressure lines to drive the opening and closing of the roughing and gate valves for the vacuum system, as well as the various D2 and N2 valves. In the control path just before the three-way and four-way valves an improved set of manual switches was inserted to give personnel the ability to actuate the valves while standing beside the system, if desired. The manual switches have been set up to allow vacuum valves to be actuated if they are not already actuated by the control system, but they will not allow de-actuation if the cFP controller has already them actuated. Figure 74 shows the pneumatic and manual control valve setup at the base of the vertical stand.

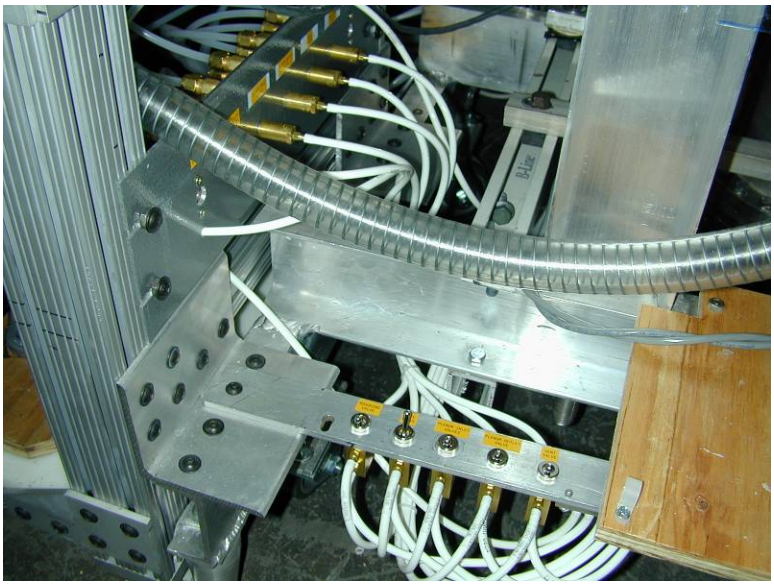


Figure 74. Pneumatic control valves and their manual toggle switches

Voss personnel also ran two fiber-optic lines from the cFP controller over to the vertical stand, after setting up two v-to-f converter boxes at the base of the stand on its east side (Figure 75).



Figure 75. V-to-f converters transmit pressure measurements to cFP controller fiber optically

The v-to-f boxes were identical to those in use with the bank-charge-voltage monitors, which provided charge-voltage information to the controller. In this case, however, the v-to-f boxes were connected to the Pfeiffer full-range gauge controller and to the two Baratron gauges, and they supplied pressure information to the cFP controller. While there were three gauges total, only two available analog input channels were in the cFP controller, so the two Baratron gauges

were connected to a common v-to-f box, and the cFP controller then activated a second ES-1 switch to select either the 10-Torr Baratron measuring the pressure in the plenum or the 1-Torr Baratron sensing the pressure in the vacuum vessel.

To isolate and protect the sensitive electronics in the vacuum-gauge controllers from EMI and other pulsed currents that may come through connections to the experiment or to wall power during a test shot, a set of contacts capable of providing a large air-gap separation are desired for all external electrical connections. FRX-L personnel have employed such a scheme to protect the gauge controllers in operation on their experiment. Using photos of the FRX-L setup as a guide, then, Voss Scientific personnel fabricated the contact apparatus shown in Figure 76.

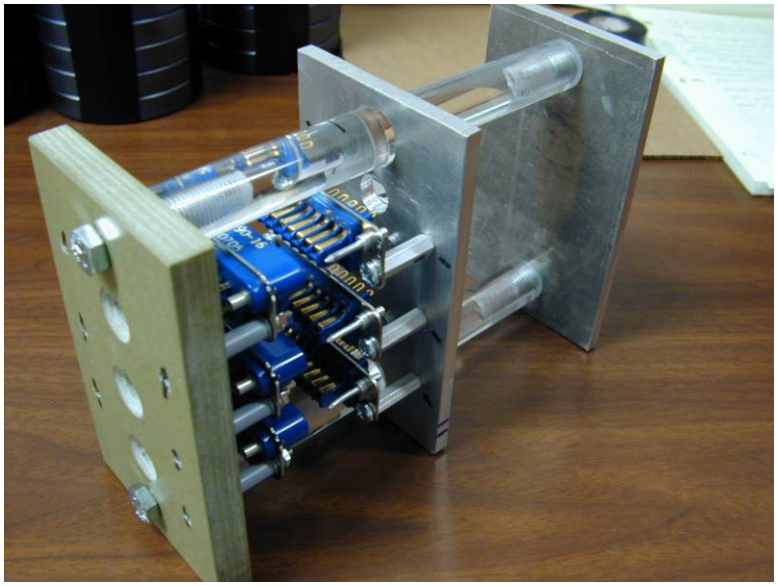


Figure 76. Pneumatically actuated set of contacts

The contacts were developed to isolate the vacuum gauge controllers electrically during shots. The contact assembly was designed to have a throw of 2.25 in. (5.7 cm) and to be opened and closed using an air solenoid driven by a single output channel from the cFP controller. All connections that the controllers have to their gauge heads and to wall power are run—and broken—through these contacts.

This pneumatically actuated breaker was mounted inside the shielded box shown in Figure 77, adjacent to the cryopump.

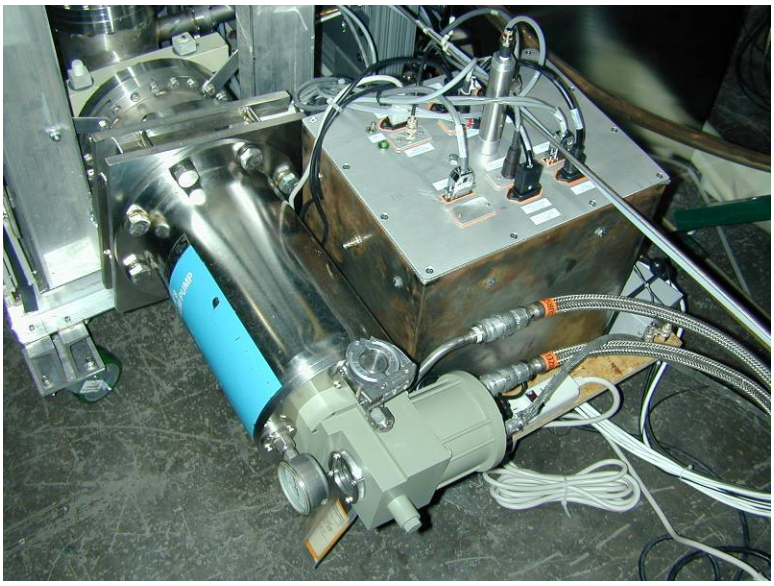


Figure 77. Gauge controller disconnect box on vacuum and field-coil stand

Bulkhead connections for signal and AC power lines were installed in the top of the box, allowing each of the cables coming from the gauge controllers and the cables coming from the gauge heads to be plugged into these connectors. Inside the box, the appropriate gauge controller wires were tied to the appropriate gauge-head wires through one of the pairs of contacts. AC power for the gauge controllers was handled in a similar manner. The 10-Torr Baratron did not actually have a controller, but it did require an external power supply. To ensure that this power supply was protected Voss personnel installed it directly inside the breaker box and included a toggle switch on top of the box to turn on and off the power supply.

4.5.4 Emergency Abort Link to the Compact Field Point Controller

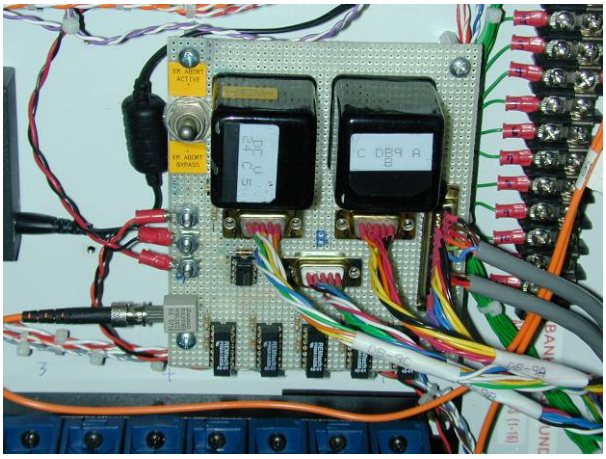
One final control-system component that was developed was an emergency abort link to the cFP controller's digital output control lines. The emergency abort was intended to be a means for the operator to bypass quickly the programmatic operations of the LabVIEW control program and shut down all critical components in the experiment (e.g., all power supplies and all dump switches) should there be an emergency. Having an alternate shutdown system that is non-computer controlled was of interest because the possibility always exists for the operator's computer or the cFP controller module in the Hammond enclosure to become locked up.

It was decided that a simple fiber-optic circuit that always transmits during normal operations would be an expedient way to set up such a system. A fiber-optic-receiver circuit in the cFP's Hammond enclosure was then designed to drive an amplifier/buffer that would in turn keep two

relays energized as long as the receiver was detecting the fiber-optic signal from the control room. The contacts of these relays would then be placed in series with the air solenoids that engage the power-supply contactors and the dump switches or in parallel with the pair of contacts on the IFS transmitter that would engage the Abort button for the Main bank power supply. Pressing the Emergency Abort button, therefore, would stop the transmitted fiber-optic signal, which would in turn de-energize the relays in the Hammond enclosure and open or close the appropriate FRCHX switches, regardless of what commands the cFP controller may be issuing. If the LabVIEW control program was operating under normal conditions when the Emergency Abort button was pressed, though, it would detect the premature fall in voltage on any banks that were changing and would itself begin to execute a dumping and safing sequence shortly thereafter.

Figure 78 shows the two components that make up the Emergency Abort link. Figure 78a shows the fiber-optic transmitter, which is placed next to the control computer; Figure 78b shows the fiber-optic receiver in the cFP controller's Hammond enclosure.





a b

Figure 78. (a) Key switch and panic button; (b) fiber-optic receiver and control relays

When constructing the transmitter box the red Abort button was wired in series with the internal batteries for the circuit and is normally closed; thus, pressing the button opens the circuit. A key switch has also been included—wired in series with the batteries, as well—to lock out the system when personnel enter the test area for any reason or when shutting the experiment down at the end of the day.

The fiber-optic receiver that detects the transmitter's signal was placed on an existing circuit board in the enclosure, one which held a set of relays used for controlling the Main bank power supply. The two large relays that the Emergency Abort circuit keeps energized were placed on this board, as well. DB9 connectors (shown just below the two relays) were a convenient means of connecting the relay contacts to the wires that run over to the pneumatic solenoids that actuate the power supply contactors and dump switches. In addition, a three-position toggle switch was placed beside the relays to (1) enable the emergency abort link, (2) disable the FRCHX experiment by preventing the relays from energizing, or (3) bypass the emergency abort link by keeping the relays energized at all times.

4.5.5 The LabVIEW Control Program

Because the FRCHX and FRX-L experiments are quite similar, not only could their control-system architectures be designed to be quite similar, but also their control programs could be written to operate in a similar manner. Knowing that the programs could be very similar was of considerable help when the time came to begin writing the FRCHX LabVIEW control program. For example, SAIC personnel had developed the FRX-L LabVIEW control program that operates the PXI controller and interfaces to the FRX-L pulsed power systems, and so already understood how the FRCHX program needed to function and what tasks it needed to do. Of even further help was that SAIC personnel could then use the FRX-L control program as a template for the FRCHX program, adapting it at various points so that it would meet the requirements specific to the FRCHX systems. The change from a PXI controller to a cFP controller presented very little difficulty, as the difference in controller hardware required only a software driver (or "vi") change at each of control signal statements.

Incorporating the vacuum-system control statements into the FRCHX LabVIEW control program was the only radical departure from the FRX-L program structure,; a separate controller and control program handles all the FRX-L vacuum operations. The FRCHX cFP controller was now able both to actuate the various valves on the vacuum stand and to read in the pressures in the plenum and in the vessel. (See Section 4.5.3.) However, it was necessary only to add some additional routines to perform simple operations like opening and closing the valves one at a time or even to perform more complex operations, such as pumping down the vacuum vessel, venting the vacuum vessel, and setting up a deuterium gas pre-fill in the vessel at a user-defined pressure (Figure 79). Being able to pump out the vessel remotely from the Shiva control room or

to set up a deuterium pre-fill at a prescribed pressure was expected to save considerable time when performing experiments, because personnel no longer had to go down to the vacuum stand after each shot and manually perform the processes.



Figure 79. Vacuum-system controls on control program's front panel

Once the task of writing the FRCHX control program was completed, SAIC personnel began the process of thoroughly validating its performance by stepping it through its various sequences to confirm proper operation of each system components at its proper time. The charging sequences for each of the banks were methodically checked in such a manner many times before the final tests with each bank, which involved actually charging and firing the bank, were performed. Less critical processes, such as turning on AC power for the rail-gap-trigger units, pumping down the vacuum vessel, and flushing the rail-gap switches, were also checked carefully to avoid any potential problems that software errors in these routines could cause. Once the program's operation through all its routines had been rigorously checked, personnel carried out the charge tests with each of the banks and then quickly transitioned into performing the static FRC formation tests.

4.6 Experimental Results

4.6.1 Excluded Flux Diagnostic Calibration

In December 2007, after completing the individual bank-charge tests with the PI bank and the new control system, the PI bank was used to perform an in situ calibration of the excluded flux diagnostic ensemble. This calibration procedure involved discharging the PI bank into the Theta coil with only the PI bank cables attached to the Theta coil cable header, so that there would be no ambiguities about the amplitude of the current.

For the first part of the calibration, several test shots were conducted with just air inside the quartz tube to obtain a baseline calibration for all the B-dot probes and flux loops without any plasma present. These test shots were followed by an equivalent number of test shots during which a 2.5-in. (6.35-cm) diameter aluminum pipe was now centered along the bore of the quartz tube (Figure 80).



Figure 80. Aluminum pipe inserted along the length of quartz tube

Polyethylene rings at the top and bottom of the vacuum stand ensured that the pipe stayed centered in the tube throughout the course of the tests. Having a high conductivity, the pipe acted as a surrogate plasma and had an excluded flux radius approximately equal to its physical radius. Because the diameter of the pipe could be easily measured, it was possible to derive a calibration factor from this analysis for each of the flux loop and B-dot probe pairs.

Two series of these calibration tests were performed. First, all 12 of the PI bank cables were connected in the Theta coil header to obtain excluded flux calibrations at the PI bank time scale. Afterwards, the 12 22-ft cables were replaced with one 42-ft cable, giving the PI bank an oscillation period that was approximately equivalent to that of the Main bank. In this manner calibrations at the Main bank time scale could then be obtained without actually performing the tests at the Main bank energy levels.

Figure 81 shows two plots of the ratio of the measured excluded flux radius to the pipe radius calculated from data acquired with the 12-cable PI bank setup.

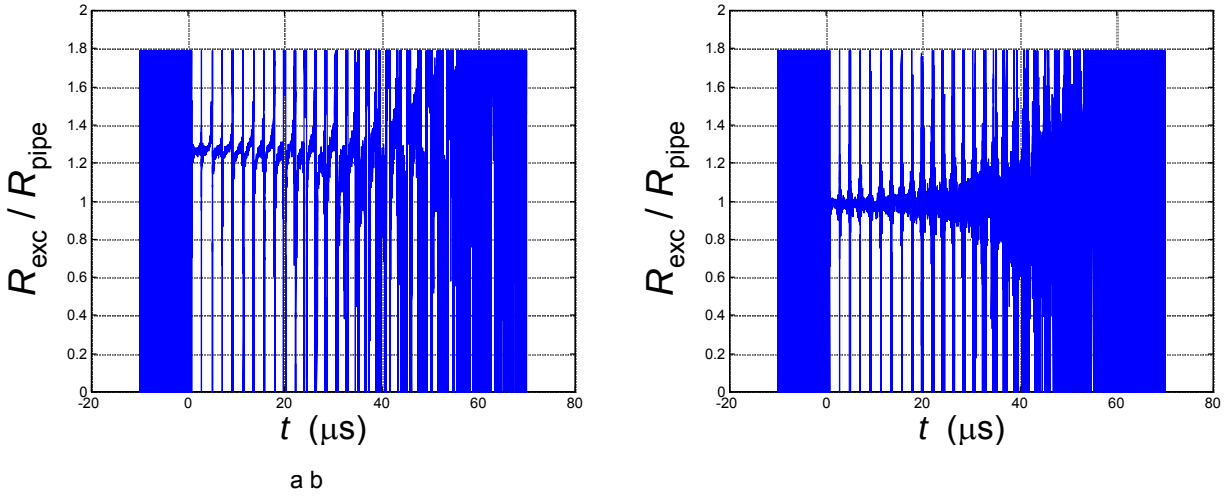


Figure 81. Excluded flux radius to pipe radius for 12-cable setup using (a) short time-scale integrators; (b) long time-scale integrators

Both short and long integration time constants for the B-dot probe and axial flux loop signals were used. (Here, short means between 6 and 25 μs, whereas long means ~100 μs.) The radius of the axial flux loop was taken to be 5.68 cm, which was approximately 1.8 times the pipe radius of 3.175 cm. The spikes seen approximately every 2 μs on both plots correspond to the zero crossings of the PI bank current, and hence zero crossings of the magnetic field and flux signals measured by the B-dot probe and axial flux loop, respectively. At these points, the expression for the excluded flux radius becomes singular.

The data taken using integrators with short time constants (Figure 81a) resulted in an excluded flux radius that was more than 20% larger that the radius of the pipe. It was unclear why this result was obtained. In contrast, the data taken using integrators with long time constants (Figure

81b) resulted in an average excluded flux radius that corresponded very closely to the pipe radius.

Figure 82 shows two plots of the ratio of the excluded flux radius to the pipe radius calculated from data acquired with the single-cable PI bank setup.

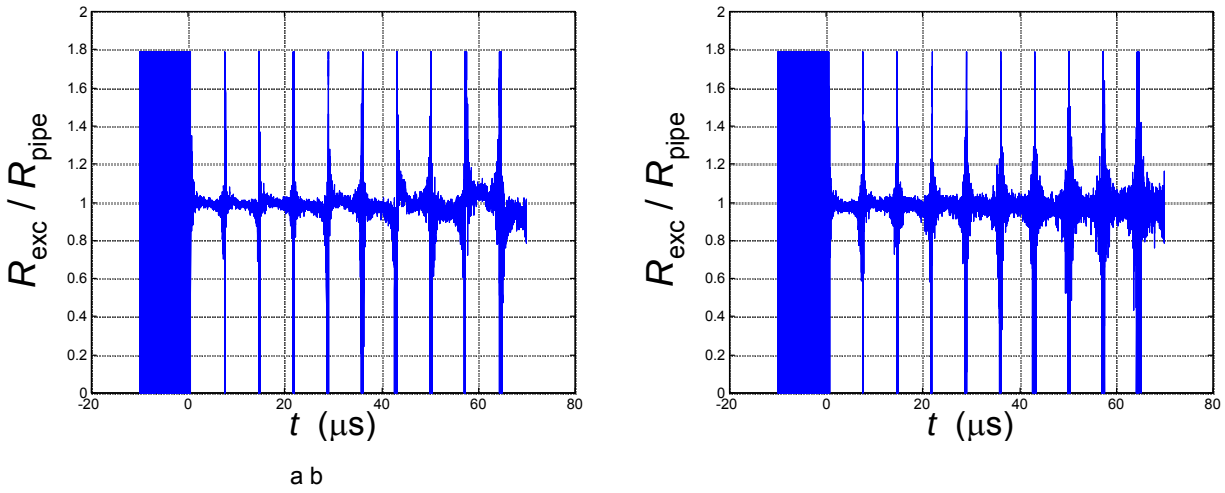


Figure 82. Excluded flux radius to pipe radius for single-cable setup using (a) short time-scale integrators; (b) long time-scale integrators

Again, both short and long integration time constants for the B-dot probe and axial flux loop signals were used. Likewise, the spikes on both plots, seen approximately every 7 μs this time, again correspond to the zero crossings of the PI Bank current, and hence zero crossings of the magnetic field and flux signals.

Unlike the case for Figure 81, however, the data recorded using *both* the short and long time constant integrators (a and b, respectively) resulted in an excluded flux radius that corresponded very closely to the pipe radius. The data from Figure 81 and Figure 82 was later used to scale (calibrate) the results that were obtained when performing FRC formation tests.

4.6.2 Overview of Pulsed Power System Performance

Following the excluded flux diagnostic calibration tests, personnel connected the Bias and Main bank cables to the Theta coil cable header and finished other final preparations that were needed before the remaining single-bank charge tests could begin. At the end of February and the beginning of March 2008, these tests were performed using the new control system. The Bias bank was tested first, followed by the Main bank, and then the Upper and Lower Cusp banks. The bank tests were started at low charge voltages, and as the tests progressed the charge voltage

was incrementally increased until the expected nominal charge voltage needed for FRC formation tests was achieved.

The Bias bank was tested at charge voltages ranging from 500 V to 4 kV. These were the first tests that were performed with the Bias bank since installing both the new isolation inductors and the Peter Dahl power supply. As expected, the bank charged much faster with the new power supply. Figure 83 shows a current waveform, measured by Theta Rogowski #2 during one of the 4 kV tests.

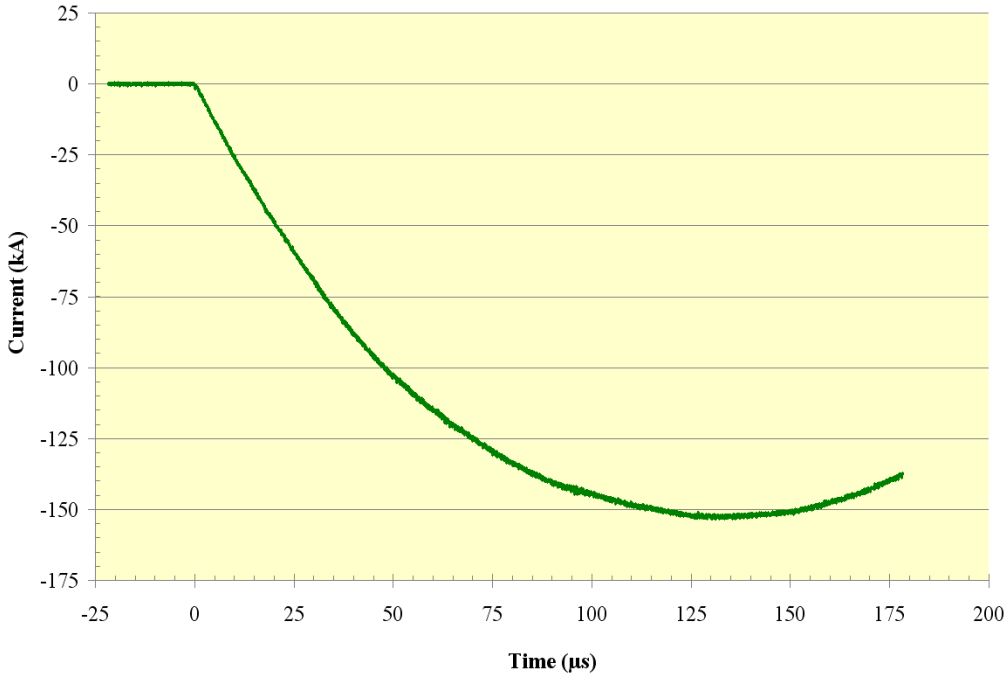


Figure 83. Bias current waveform from test #4, 3 Mar 2008

As can be seen, the peak current that was attained was 152 kA, and it occurred approximately 132.5 µs after the start of current. This result differs substantially from the estimates mentioned in Section 4.1.2, which were a peak current of 390 kA with a quarter-cycle rise time of 81 µs. However, this waveform still shows improvement over the previous Bias bank parameters, which were a peak current of approximately 106 kA with a quarter-cycle rise time of 201 µs for a charge voltage of 4 kV (Section 3.5.2).

This result shows that the inductance of the Bias bank bus work and other circuit elements is more substantial than was anticipated. As the isolation inductance was decreased, the inductance of the rest of the circuit became more dominant and was then the limiting factor for the bank-current-rise time and peak value. If greater currents are still required from the Bias bank, other

areas of the bank circuit can be examined to determine where inductance might be further reduced.

The Bias bank had one capacitor fail in its west module as the FRC formation tests were just beginning. Thus, for the majority of the Phase II tests the Bias bank had a capacitance of 29 x 170 μF = 4.93 mF. No appreciable effect was seen in the Bias current amplitude or rise time, however.

The Main bank and Crowbar switch were tested next with a charge voltage of ±25 kV in the first Main bank test that had been performed since doubling up the trigger cables on each of the four Crowbar rail gaps, as described at the end of Section 3.5.1. On this first test all four of the Crowbar switch rail gaps conducted.

Figure 84 shows the recorded current waveforms from each of the Crowbar rail gap Rogowski coils and from Theta Rogowski #2.

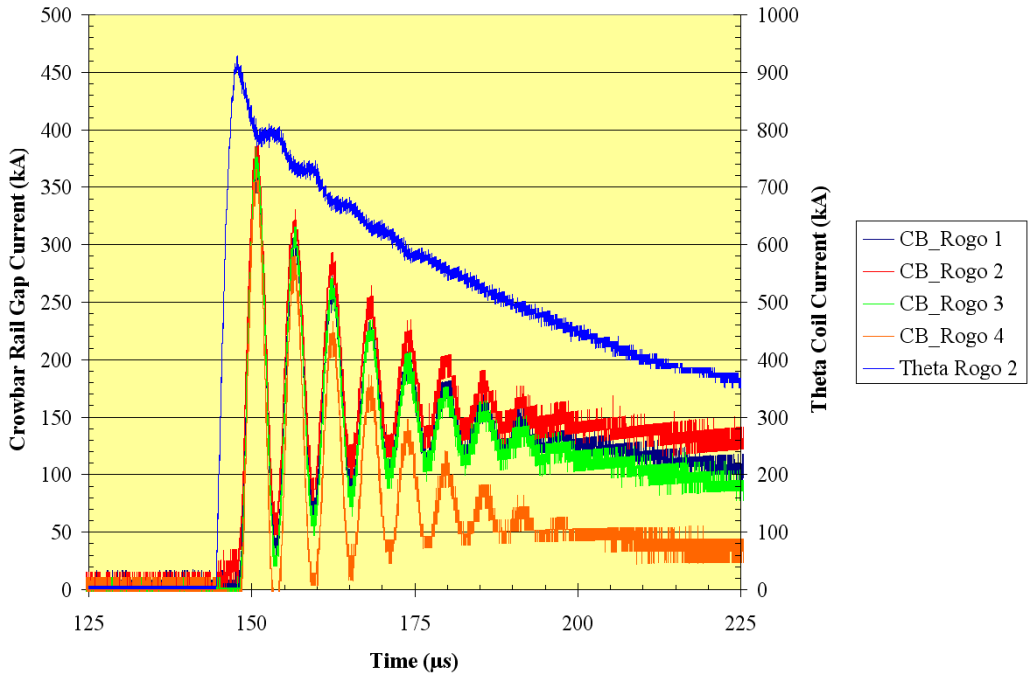


Figure 84. Theta coil and Crowbar rail gap current waveforms from test #9, 3 Mar 2008

As can be seen, the decaying Theta coil current waveform was observed to have very little modulation on it with all four of the Crowbar rail gaps conducting. Remarkably, the Crowbar switch continued to perform very well on subsequent shots, and, in fact, except for one instance in which the Main-to-Crowbar delay time was inadvertently changed from 3.3 μs to 4.3 μs the

Crowbar switch continued to operate with all four rail-gap switches conducting throughout the duration of the Phase II static FRC formation tests.

The Upper and Lower Cusp banks were the last banks to be tested, and these were, of course, the very first tests to be performed with these two banks, as they had just been brought on-line in the FRCHX experiment. Figure 85 shows the current waveforms recorded for these two banks during a test in which they were each charged to 3 kV.

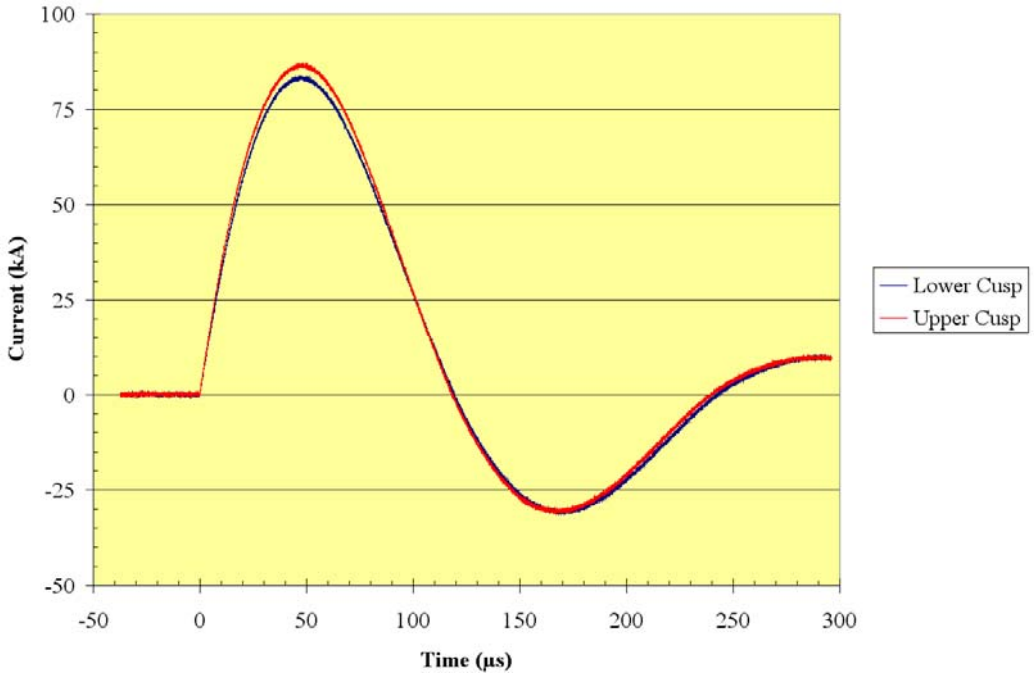


Figure 85. Upper and Lower Cusp current waveforms from test #7, 5 Mar 2008.

The two bank circuits are very nearly identical, as the waveforms follow each other very closely. A peak current of 87 kA was obtained for the Upper Cusp coil, and 83 kA was obtained for the Lower Cusp coil with the 3 kV charge voltage on both of them. The quarter-cycle rise times were 47.9 µs and 47.4 µs for the Upper and Lower Cusp, respectively.

After the banks were characterized individually and it was determined that they were working properly, plasma tests were finally started. Initially, the tests utilized just the PI, Bias, and Cusp banks to examine the properties of the formation-region plasma before the reverse field was applied. Finally, the Main bank was also included, and efforts to form FRCs began.

Figure 86 shows an overlay of several B-dot probe waveforms recorded during some of the first plasma (and vacuum) tests in which all five banks were used.

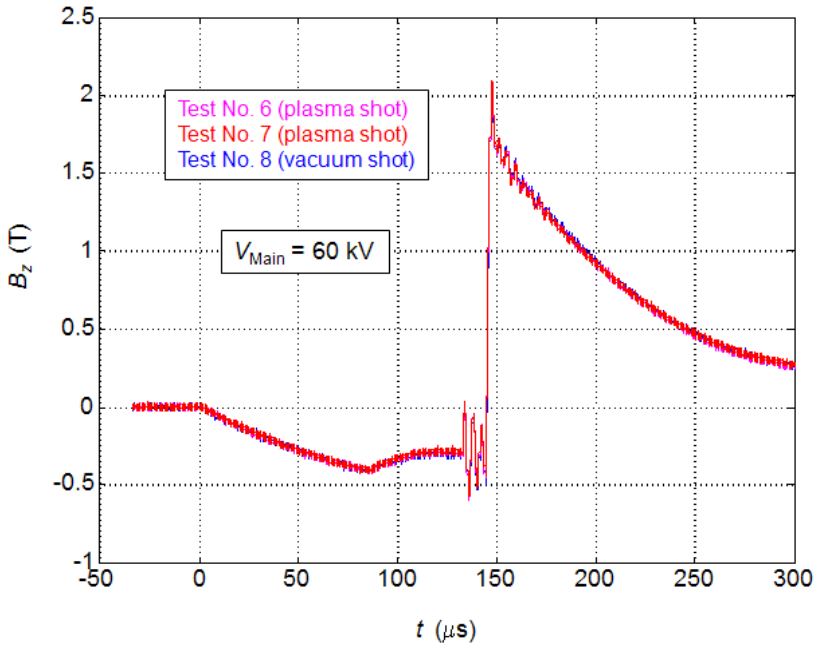


Figure 86. G-segment B-dot probe waveforms from three successive shots, 7 March 2008

The charge voltages for the banks during these tests were as follows: Bias = 5 kV, Lower Cusp = 3.8 kV, Upper Cusp = 3.6 kV, PI = 48 kV, and Main = ±30 kV. The Theta and Cusp coil current waveforms from Test #7 are shown in Figure 87 for comparison.

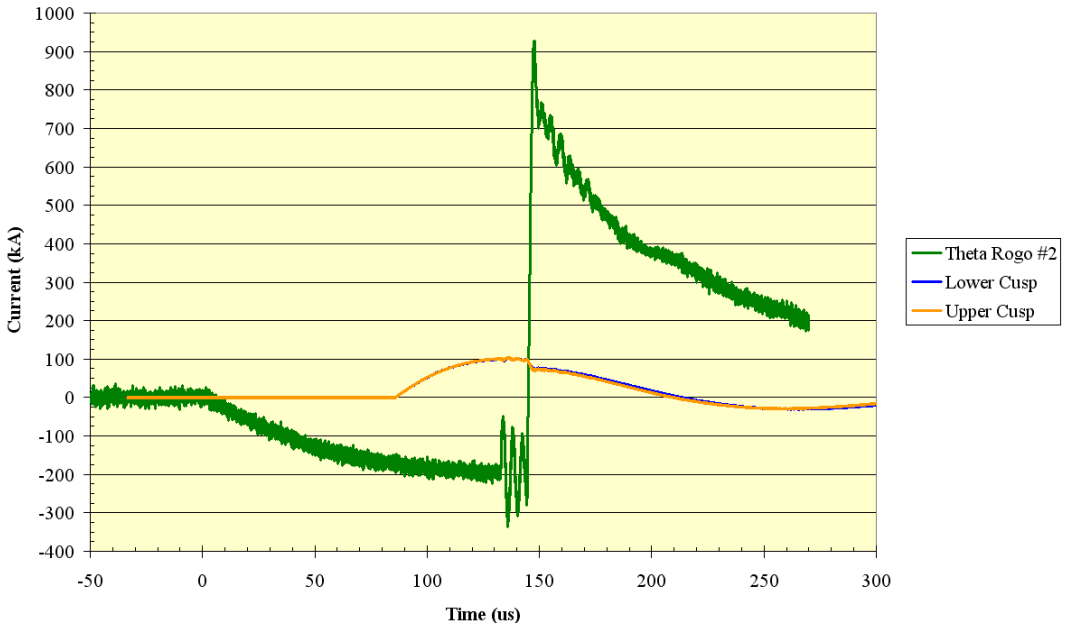


Figure 87. Theta and Cusp coil current waveforms from Test #7 in Figure 86

The distinct changes are clearly seen in the magnetic field profile that occur as each bank or set of banks is triggered. The Bias field is set up first at t = 0, and at t = 85 μs the Upper and Lower

Cusp fields are set up. The fast PI field is then initiated at t = 135 μs to breakdown of the static gas fill. Shortly thereafter the Main reverse field is applied, and 3.3 μs later it is crowbarred to lengthen its decay.

One immediately notes from the field measurement in Figure 86 that although the Cusp coils were at each end of the Theta coil, the Cusp fields penetrated into the Theta coil region and negated some of the applied Bias field. Thus, if it is desired to raise the Cusp fields, then the Bias field needed to be increased to compensate for the partial negation that would occur. Furthermore, varying either the Bias or the Cusp fields affected the degree of the field reversal provided by the PI bank. For the tests represented in Figure 86, moderate charge voltages were used for the Bias and Upper and Lower Cusp banks, and their 12 kV charging supplies could readily apply higher charge voltages to bring the currents up, but the PI bank was already being charged to the maximum voltage that its power supply could deliver, which was approximately 48 kV.

Several 100 kV (and greater) power supplies were available in-house at this time, though they all had a positive polarity. Thus, to address the charging problem with the PI bank, arrangements were made to send back one of these supplies to the manufacturer (Spellman) to have its polarity switched to negative. The capability would then exist to charge the PI bank to significantly higher voltages. The Spellman supply actually arrived back in-house during the summer of 2008, after the Phase II FRC formation tests had been completed, but it has since been set up in the experiment and will be used as soon as FRC translation tests begin in the next test effort.

4.6.3 Data from FRC Formation Tests

In March 2008 the first static FRC formation tests were performed since beginning the Phase II effort. FRC parameters that were being sought after included an excluded flux radius of approximately 2 cm, a length of 10–20 cm, a density of ~0.5 x 10^{17} ions/cc, an ion temperature of ~200 eV, and a lifetime of at least 15–20 μs. FRCs with these threshold parameters were deemed desirable for the compression-heating tests. Very early during the formation tests the excluded flux diagnostics began providing information that was highly suggestive that a 1.5- to 2.0-cm-radius FRC was being formed in the experiment. The lifetime of the FRC appeared to be somewhat shorter than expected, however, being at most ~6 μs.

Testing was put on hold in April to give time for NumerEx personnel to complete the final setup and alignment of the four-chord interferometer. When FRC formation experiments resumed

again in May, density data from the interferometer was then available and showed that plasma densities on the order of 10^{17} cm^{-3} were present at the same time that an excluded flux was being detected. The excluded flux and interferometer data together confirmed the presence of an FRC in these tests. However, FRC lifetimes remained rather short, still being at most 6 μs. Interestingly, lifetimes were observed to get even shorter at lower fill pressures, though it was expected that a lower fill pressure would lead to a lower-density FRC that would be longer lived. This observation led to the hypothesis that the FRCs were not remaining confined in the formation region but were escaping in one direction or the other. Analyses of the data recorded with the side-on fiber-optic translation and continuum array did not obviously support this hypothesis. The argument is the hypothesis that the FRCs are not remaining confined in the formation region, but were escaping one way or the other. In this section we discuss the results obtained with the excluded flux diagnostics, the four-chord interferometer, and the fiber-optic array.

4.6.3.1 Flux Loop and B-Dot Probe Excluded Flux Radius Measurements

In Figure 88, the magnetic field data from Figure 86 is expanded around the time that the PI and Main banks were triggered and presented again, along with the corresponding magnetic flux data observed with the G-segment flux loop. Data is from three tests, 7 March 2008. To get flux exclusion diagnostics to work, measures to reduce noise and improve signal precision included routing cables to avoid high-fringe magnetic fields, enclosing cables in conduit, and use of 12 bit instead of 8 bit transient digitizers.

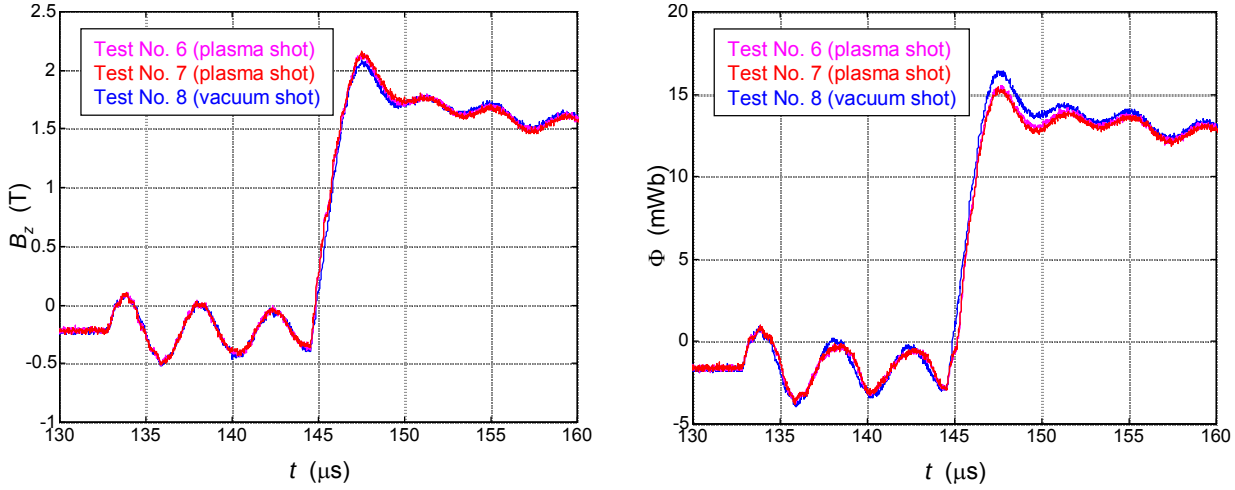


Figure 88. G-segment (a) B-dot probe and (b) flux loop waveforms

Small but noticeable differences are observed between the plasma and vacuum data in each plot shortly after the Main bank is triggered. Performing the usual analysis with this data to derive an excluded flux radius confirmed that such a radius existed at 1.5–1.75 cm and that it lasted for ~6 μs after the Main bank was triggered. Figure 89 shows plots of the excluded flux radius vs. time obtained with the test #6 and test #7 data shown in Figure 88, also 7 March 2008.

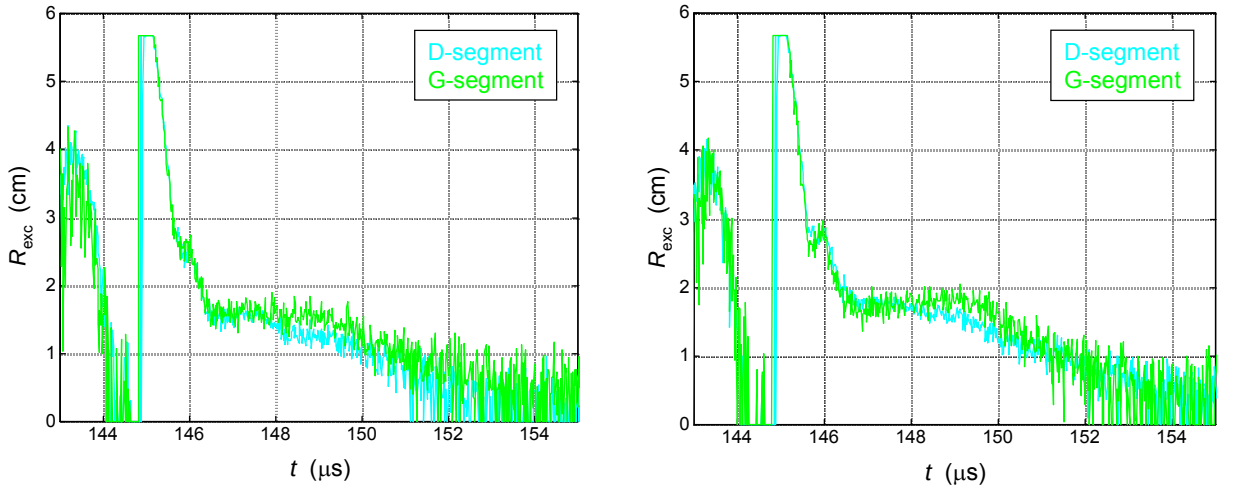


Figure 89. FRC excluded flux radius vs. time calculated, (a) Test #6; (b) Test #7

Waveforms obtained from a similar analysis using the D-segment B-dot probe and flux-loop data are also shown in these plots.

These excluded flux radii with these lifetimes were found to be fairly typical for the FRC formation tests that were performed during March and May. Test parameters primarily used during these tests included a pre-fill pressure of 50 mTorr; charge voltages for the Bias, Upper and Lower Cusp, and PI banks of 5 kV, 3.6–4.0 kV, 3.8–4.2 kV, and 48 kV, respectively; a delay from the PI bank trigger to the Main bank trigger of 12 μs; and a delay from the Main bank trigger to the Crowbar switch trigger of 3.3 μs.

The Main reverse field was varied, as might be expected, by adjusting the Main bank charge voltage; most tests were performed with a charge voltage of ± 30 kV, though a limited number of tests with ± 25 kV and ± 35 kV were also performed. There was little effect observed on the FRC lifetime or excluded flux radius when the Main bank voltage was varied, though.

Lower pre-fill pressures (10 and 20 mTorr) were also examined briefly, but, as was mentioned earlier, the lifetimes became even shorter, contrary to what was expected based upon results presented in the literature. This finding was what led to the hypothesis that the FRC was not decaying away but was simply leaving the formation region. Tests in which the delay between the PI and the Main bank triggering was to be varied were going to be performed next, but the D-segment flux loop signals began showing evidence of breakdown in the loop wire insulation (or possibly in the high voltage divider), so it was necessary to halt the testing. The nature of this problem is discussed further in Section 4.6.4.

Recent papers raised the possibility that FRC stability and lifetime could be improved by translating it (Ryutov 2004) and (Guo 2005). More specifically, Ryutov had observed analytically, and Guo experimentally, that the presence of a very weak toroidal field in the FRC had a stabilizing effect on the FRC, even under conditions in which rotational instabilities normally develop. In the ideal case, the FRC has no toroidal magnetic field, only a poloidal magnetic field, but they argue it is this quality that makes the FRC more sensitive to external magnetic field perturbations, which may then trigger the onset of instabilities. Because the translation scheme employed at FRCHX (and at FRX-L) introduces a small amount of toroidal field into the FRC—a "by-product" of having the conical bore in the Theta coil—it was suggested that the mere process of translating it could lead to the longer FRC lifetimes that were being sought. As a result, it was further decided not only to halt tests to correct the flux-loop problem, and the Theta coil current-joint problem that was uncovered in the process, but also to push forward our efforts to begin FRC translation tests. (See Section 4.6.4.) Doing so could lead

to greater improvements in FRC parameters than could be obtained with the present static formation setup.

4.6.3.2 Plasma Densities Measured with the Four-Chord Interferometer

The first static FRC formation tests in which the four-chord interferometer was operational were conducted at the beginning of May 2008. The performance of the interferometer system during these tests was extremely good, with significant improvements (reductions) being observed in acoustic and RF noise when compared to the eight-chord system fielded on FRX-L. More specifically, system vibration due to the magnetic impulse during each shot was observed to be very small on the FRCHX system and fully correctable with linear background subtraction. RF trigger noise was also not observed on any of the signal channels.

Unfortunately, once the interferometer was moved into place around the FRCHX vacuum stand, it was discovered that one of the support rods running through the Cusp and Theta coil assembly was blocking the path of the fourth chord. Moving the rod would have been very time-consuming, so it was decided that for the moment the path of the fourth chord would simply be redirected. Doing so resulted in a change in the chord's impact parameter, with the outcome being that the chord then intercepted some of the plasma in the tube during tests. Ideally, this chord should pass through the tube with its path completely outside of the plasma, and then it is possible to use the information acquired from it during tests to quantify and then subtract the effects of the radiation heating of the quartz tube on the other three chords. Such a correction is important, because this heating results in a non-negligible phase shift.

Despite the inability to correct for the effects of the radiation heating in the quartz tube during these tests, it was still possible to obtain a line-integrated density along each chord and a qualitative radial density profile for the FRC plasma. Figure 90 shows the raw phase-shift information from each chord recorded during one of the test shots and the line-integrated density determined from this information.

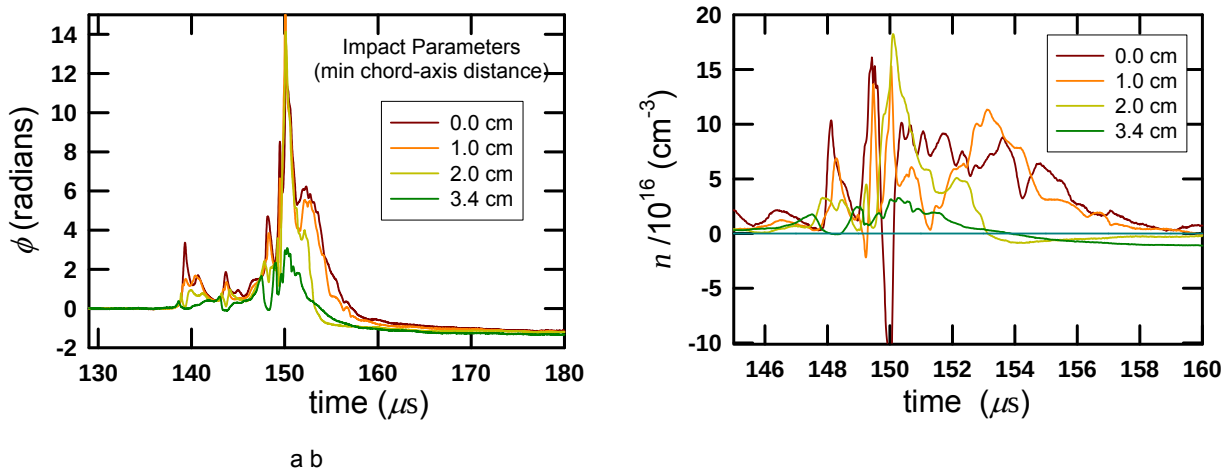


Figure 90. Interferometer data: (a) phase shift as a function of time; (b) corresponding line-integrated density

This test was test #4, 8 May 2008. The parameters for this test shot were the same as those from which the data shown in Figure 86–Figure 89 was obtained: a deuterium pre-fill pressure of 50 mTorr was used and charge voltages for the Bias, Upper and Lower Cusp, PI, and Main banks were 5 kV, 3.6 kV, 3.8 kV, 48 kV, and ±30 kV, respectively.

The interferometer chords were passed through the quartz tube between E and F segments of the Theta coil—in the middle of the formation region. Evidence of the phase shift caused by the tube heating is seen from the difference in the baselines on the left and right sides of the plot in Figure 90a, as well as from the negative densities observed on the r = 0.0 and 1.0 cm waveforms in Figure 90b. Despite the need for the phase-shift correction, one can still infer from Figure 90b that a peak density on the order of ~10^{17} cm^{-3} was achieved during this test. At the r = 0.0 cm impact parameter the density remained fairly flat at close to this value over a lifetime of ~6 μs. These results, together with the excluded flux radius data from this test, provide strong evidence that an FRC plasma was formed. Once FRC translation tests begin, it will be possible to perform an accurate Abel inversion to determine the quantitative density profile, because the position of the interfering support rod will have been moved by that time and the path of the fourth interferometer chord will have been cleared.

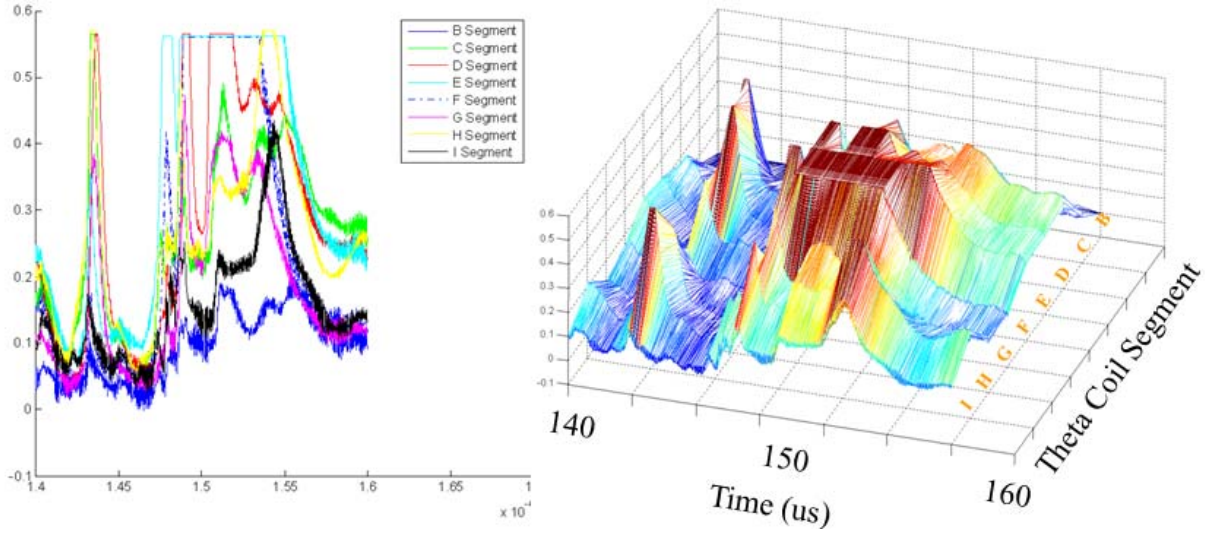
4.6.3.3 Plasma Profile and Behavior Observed with the Side-On Fiber-optic Array

Analysis of the interferometer and excluded flux data recorded during these FRC formation tests showed that FRC density and excluded flux radius were very close to the desired values but that lifetime was exceptionally short (~6 μs). It was therefore suggested that the FRCs were not truly

being confined to the formation region, but that they were escaping through one of the ends of the Theta coil, thereby making it appear to the formation region diagnostics that the FRCs were very short-lived. The data recorded with the side-on fiber-optic array was examined in greater detail to address this possibility.

As described in Section 4.3.3, the side-on fiber-optic array is comprised of 12 100/140 µm clad multimode fibers that were placed in the B-dot probe ports of eight of the Theta coil segments (Figure 56). The other ends of the fibers were routed to the remote data acquisition enclosure where they were connected to either photodiode (eight of the fibers) or PMT (four of the fibers) receiver channels. As the Theta coil segments containing the four PMT fiber-optic channels also had fibers in them that were connected to photodiode receiver channels, only the data set recorded with the photodiode channels is considered at this time.

Figure 91 shows an X-Y plot as well as a 3D surface plot of the photodiode fiber-optic channel data recorded during the same shot in which the data in Figure 90 was recorded, test #4, 8 May 2008.



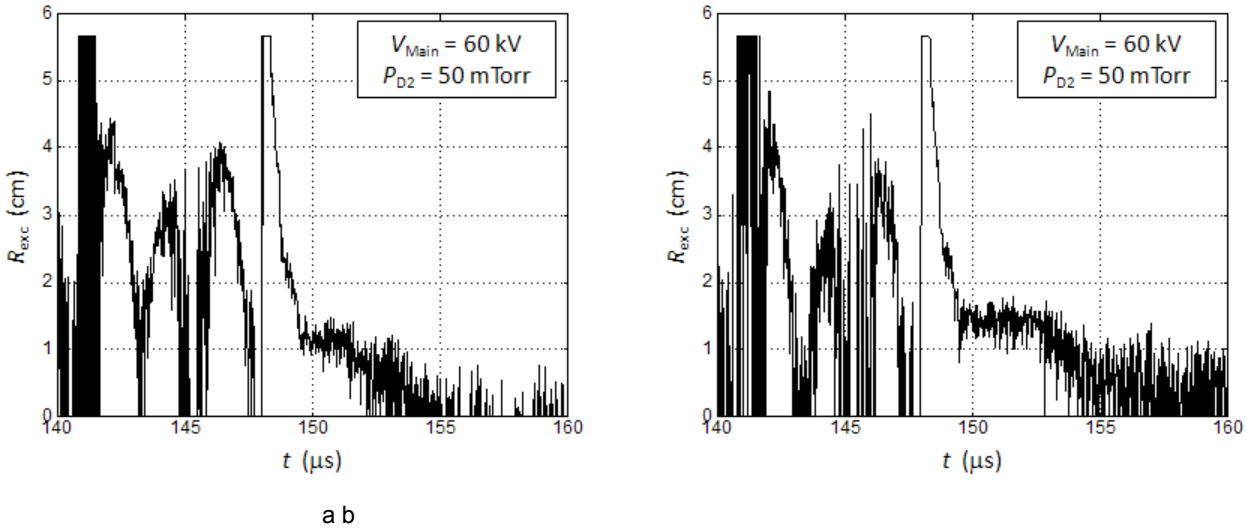
a b

Figure 91. Side-on fiber-optic-array data: (a) signal intensity vs. time; (b) surface plot

Though a number of the waveforms was clipped, the primary feature to look for is whether or not some of the signals decreased to zero while others, particularly those at either end of the Theta coil, persisted for a longer period of time or trailed off in a sequential fashion. What is observed, however, is that there was no particular grouping of channels that had signals that persisted for

any length of time. Rather, all eight channels began falling off rapidly at t = 154 – 156 μs, and by t = 160 μs, all the channels reached a local minimum. Though channels C, D, and E did maintain a slightly higher intensity than the others at this late time, the channel at H segment did, as well, and H segment was not adjacent to the other three. Furthermore, the signals from B and I, which were the two end segments, fell off to lower levels than did the signals from many of the inner segments.

The excluded flux radii calculated for this test #4 shot are shown for comparison in Figure 92; see the density data in Figure 90.

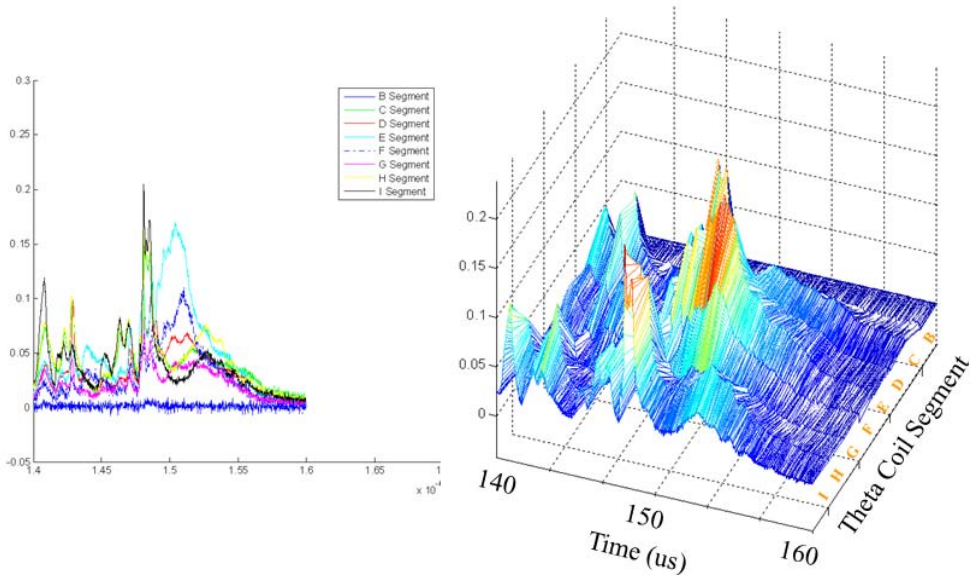


a b

Figure 92. Excluded flux radius vs. time calculated at (a) Theta coil segment D; (b) Theta coil segment G

The density for the r=0 impact parameter (Figure 90b) trailed off over a similar time frame (154 – 158 μs) as the light intensity in Figure 91, while the excluded flux radii measured at segments D and G fell off even sooner, over the span from t = 152 μs to t = 155 μs.

Figure 93 shows side-on fiber-optic-array data from another shot with essentially the same bank-charge parameters but with a 10-mTorr pre-fill. Data is from test #6, 14 May 2008.



a b

Figure 93. Side-on fiber-optic-array data: (a) signal intensity vs. time; (b) surface plot

Following the late-time signal peaks, which occurred between t = 150 – 153 μs depending on the channel, the fiber-optic-array data from this shot exhibited very similar properties as the data in Figure 91: the light intensities on all channels began falling off rapidly together, and by 160 μs the signal levels had all reached approximately the same baseline.

Therefore, the fiber-optic array data suggested only slightly longer FRC lifetime near one end of formation region, but not at either extreme end. This does not clearly support the escaping FRC hypothesis. In future such experiments, for which FRC escape will be intentional, it is planned to include field exclusion, interferometry, and fiber-optic probe diagnostics away from as well as in the formation region. As suggested at the end of Section 4.6.3.1, personnel anticipate that the FRC properties will improve once the FRC can be formed and then immediately translated out of the formation region. In addition to the assertions of this claim other researchers published in the literature, more recent translation tests at FRX-L would also appear to support this prediction.

4.6.3.4 Results Obtained with the UNR End-On Photography and Fiber-Probe Package

Most of the hardware for the UNR gated end-on photography and fiber-probe package had been set up by the time UNR personnel had to leave, and SAIC personnel were able to complete the remaining setup tasks and performed the alignment of the optics. Because of the time required to assemble a special trigger-receiver circuit for the CCD camera, however, the camera system was

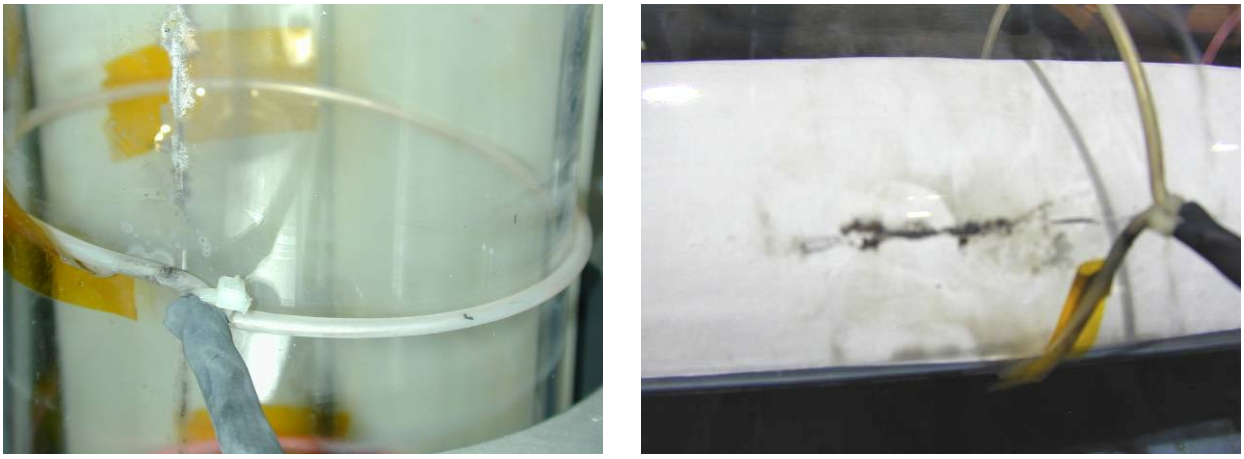
not able to be fielded during any of the static FRC formation tests, though it was otherwise ready for use.

The end-on fiber-optic probe appeared to detect only background light during tests. Given the fact that the FRCs appeared typically to have an excluded flux radius that was closer to 1.5–1.75 cm instead of 2 cm, the viewing position of the fiber probe should likely have been moved closer to the axis, to perhaps a radius of 1.9–2.0 cm instead of 2.5 cm. (See Section 4.3.4.) However, the interferometry data did not suggest that there were any rotational instabilities to be detected, and furthermore the available time also did not permit the fiber probe to be moved before the static formation tests had concluded.

4.6.4 Problems with Theta Coil Current Joints

Efforts to optimize the FRC parameters and/or track its motion were cut short when what appeared to be a breakdown was detected in one of the flux-loop signals (Section 4.6.3.1). Such breakdowns have often preceded the structural failure of the quartz tube on FRX-L; the breakdown most commonly occurs where the twisted flux-loop wires come up to the quartz tube and then separate to wrap around the tube in each direction. The voltage stresses are highest at this location, and if the wire insulation begins to break down regularly, the breakdown arc eventually creates a shock sufficiently large to crack the tube.

After the last static FRC formation test, the quartz tube was viewed from between the Theta coil segments and from the open port at the top of the vertical stand, and discolorations were observed on the surface of the quartz tube at not just one but approximately each of the locations where the twisted flux-loop wires came up to the tube. As the Theta coil was gradually disassembled, though, more discoloration and evidence of arcing was seen on the quartz tube than would have been caused by just a breakdown between the flux-loop wires. In addition, sputtered aluminum was observed in numerous places on the surface of the tube (Figure 94).



a b

Figure 94. (a) and (b) Images of the sputtered aluminum and arc marks on quartz tube

Placing a paper towel inside the tube readily highlighted the long line of arc marks and sputtered material that was present on the surface of the tube (Figure 94b). It thus became apparent that a second problem existed: metal was being sputtered onto the tube from the inside edges of the current joints on the Theta coil segments (Figure 95).

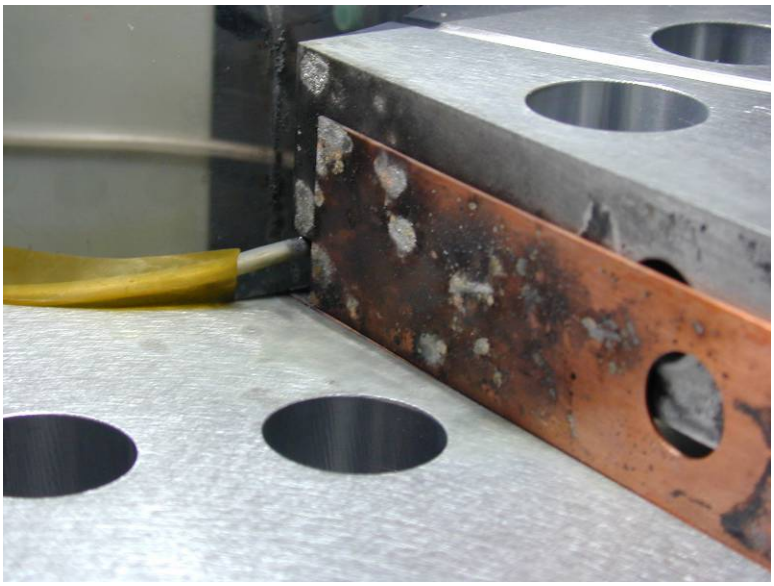


Figure 95. Current joint on topmost (J) segment of Theta coil showing extensive arcing

The arc marks, sputtered aluminum, and other discolorations being observed on the quartz tube near where the flux-loop wires came together were thus a coincidence of the fact that the segment-current joints were also located near these same areas.

The segments forming the passive mirrors at the upper and lower ends of the Theta coil showed the greatest evidence of arcing at their current joints. That the greatest arcing was here was not surprising, because the outer segments carried a greater fraction of the total current than the inner ones. Furthermore, it became apparent in retrospect that the locations of the clamping bolts on each segment were rather far away from the inner current joints. Given that the mirror segments also had a smaller inner radius than the other segments of the Theta coil, the compressive force of the bolts then needed to act over an even greater distance. It now seemed likely that the breakdown observed in the D segment flux loop was initiated by the D segment current joint arcing next to it over a period of time. Fortunately, this problem with the current joints was discovered at this time rather than during the middle of translation tests or when preparing for a compression-heating test; it was easier to begin devising an improvement for the current joint.

As stated at the end of Section 4.6.3.1, it was this problem with the Theta coil segment-current joints, together with the need to replace the D segment flux loop and the discussions regarding the possibility of improving the FRC lifetime by beginning to translate them, that led to the decision to bring the static formation tests to an end. Our efforts then shifted toward making preparations for starting FRC translation tests as soon as possible.

5.0 PREPARATIONS FOR TRANSLATION-ONLY AND FOLLOW-ON COMPRESSION HEATING TESTS

The work summarized thus far was largely concentrated on the assembly of systems and diagnostics pertaining to the FRC formation region of FRCHX and on the performance of FRC formation tests. The end goal for FRCHX has been, as its name implies, the performance of FRC compression-heating experiments. In support of this goal, the computer-based control system, the remote data acquisition enclosure, and even the vertical vacuum and field-coil stand and vacuum system itself were designed to be able to support FRC translation-only tests. These are to follow the Phase II static FRC formation tests, as well as the FRC compression-heating tests that follow the translation-only tests. Little, if any, additional work on these systems will be required before beginning these follow-on tests. All the diagnostics developed and fielded for observing FRC formation can also be fielded in the FRC translation region between the Theta coil and the solid liner.

In regard to the FRCHX systems or components that are specific to FRC translation or compression, a large portion of the design work for these items was actually performed in parallel with the FRC formation work. For example, as hardware designs were being finalized and constructed during the first part of the FRCHX Phase II effort, the Guide/Mirror coil bank was being assembled and linked up to the control system with the other banks. The basic designs for the translation and capture regions were also established at this time, based upon the formation-region hardware to which this new hardware had to connect.

The two most concentrated design efforts, which were somewhat interrelated, were those pertaining to the Guide and Mirror coils and to the electrodes, return conductor, and other hardware associated with the solid liner. The initial Guide and Mirror coil design concept was developed by LANL's Robin Gribble. AFRL personnel then used the results from that design to begin developing designs for the solid liner-return conductor and the upper and lower liner electrodes. COMSOL calculations by AFRL personnel were used to help guide this design effort and also to adjust the positions of field coils around the liner to improve radiography coverage of the liner. NumerEx personnel, in turn, used the COMSOL field calculations to establish their initial Mach 2 models of the entire FRC formation, translation, and capture process, while LANL's Tom Intrator took Mr. Gribble's design concept and the COMSOL field calculations and created hardware designs for a coil set that would produce this calculated magnetic field profile.

After the completion of the Phase II static formation tests, all SAIC's work was then concentrated upon implementing these coil and other hardware designs to prepare for FRC translation tests. First, however, the Theta coil current joints were redesigned and implemented so that assembly of the conical Theta coil could proceed. Next, even as the assembly of the Guide and Mirror coils began, design concepts for mounting them on the vertical stand were finalized, and hardware was fabricated to facilitate this mounting. A cable header and bus work for the Guide and Mirror coils were also designed and fabricated to allow the YK-198 cables coming from the bank to be connected to the coils and for all the coils to be interconnected.

In August 2008, when the design and assembly work for the upcoming FRCHX translation tests was nearing its climax, the FRCHX work moved over to the new HERA contract, under Task Order 2. This change was made largely because the ceiling had been reached on this task order.

Thus, the period over which technical work was performed under this task order is, in reality, from July 2006 through August 2008.

Section 5.1 discusses the new FRCHX systems that are specific to FRC translation and that have been developed and/or assembled while the Phase II effort for FRCHX was also in progress. Section 5.2 lists some of the changes or additional work performed on the existing FRCHX systems following the Phase II tests to prepare for translation tests. The redesign of the Theta coil current joints is described here, because this effort was necessary before advancing to the FRC translation-only tests. Overviews of the setting up of the new PI bank power supply and the fabrication of some additional diagnostic components are also included. Section 5.3 outlines the status of the solid liner hardware designs and describes how the Shiva portion of FRCHX is to be integrated together with the FRC formation and translation portions of the experiment.

5.1 New Systems for FRC Translation Tests

The primary goal for the FRC translation-only tests is to characterize the entire FRC formation, translation, and capture scheme to ensure that suitable FRCs are indeed captured reliably by the magnetic mirrors above and below the liner region. In light of previous discussions regarding an expected improvement in FRC parameters with translation, through the introduction of a small amount of toroidal field into the FRC, efforts will be made during the translation-only tests to somewhat re-characterize the FRCs that are formed. It is particularly important to determine if the FRC lifetime is, in fact, extended, because it is imperative that the FRC have a long enough lifetime following capture to allow it to be compressed by the solid liner.

The translation-only test setup is intended to be very similar to the final setup that will be used during the compression-heating tests. Though not available yet, it is desired to eventually have a mock-up of the liner and its related hardware in place in the translation-only test setup, so that all field and plasma boundary effects will be as close as possible to those of the “real” experimental setup. The mock-up of the liner would differ from the actual liner only in that the radius of the mock-up would be smaller to mimic the compression of the liner, which should already be underway when the FRC enters it.

Initially, however, an extended quartz tube is simply being used for the test setup, along with a stainless steel pipe that has been placed around it in the translation and capture regions to act as a flux-excluding boundary for the FRC. The magnetic mirrors at each end of the liner region

should still be able to catch the FRC, though some bank-trigger timings may have to be changed because the field diffusion will not be exactly the same. The use of the transparent tube in the liner capture region has the advantage, however, of allowing unlimited access to the plasma for interferometry and excluded flux measurements, and we will therefore be able to characterize it better as it is captured.

The two new items that are needed to carry out the proposed FRC translation-only tests, which were not operational during the static FRC formation tests, are the Guide/Mirror bank and the Guide and Mirror coil assembly.

5.1.1 Guide/Mirror Bank

Like the Cusp bank modules (Section 4.1.1), the modules that make up the Guide/Mirror bank were fabricated by LANL personnel at the FRX-L facility using capacitors, ignitrons, and support frames that had been on hand from the FRX-C experiment. A total of six modules were fabricated for the FRCHX Guide/Mirror bank, but unlike the modules that comprise the Cusp banks, the Guide/Mirror bank modules were each given four 500 μF capacitors, for a total capacitance of 2 mF each. Thus, the full bank has 12 mF of capacitance with a maximum rated voltage of 10 kV. The bank was designed to have such a high energy so that it could drive the Guide and Mirror magnetic fields long enough to allow them to diffuse uniformly through the solid liner and the other structure surrounding it.

LANL personnel completed the six Guide/Mirror bank modules and transported them from the FRX-L facility to AFRL's Building 322 in May 2007. Figure 96 shows the six bank modules after they had just been unloaded into the Building 322 high bay.



Figure 96. T2-mF Guide/Mirror bank modules, in high bay

As can be seen, ignitron switches were already integrated onto each module, as was the case with the Cusp bank modules.

A few months after the arrival of the bank modules, SAIC and Voss Scientific personnel began the work of assembling them into the present Guide/Mirror bank configuration. Figure 97 shows a photo of the bank after the modules had been stacked two-high to conserve floor space in their designated place just east of Bias bank.



Figure 97. Guide/Mirror bank modules, stacked two-high

Isolation inductors, each having an inductance of ~25 μH, were wound and used to connect the hot bus plates of adjacent modules together. These inductors were intended to allow the modules to be charged from a common power supply and yet supply a reasonable measure of isolation between them when their respective ignitrons are triggered. More specifically, the inductors should prevent the neighbors of a given module from trying to discharge through its ignitron instead of their own, as the inductance of the isolation inductors was chosen to be approximately 15–16 times larger than the downstream inductance of each module. This scheme is identical to that employed with the two Bias bank modules, though there was more space available for setting up such an inductor between the Bias bank modules. (As a result, a larger inductor, having an inductance of approximately 74 μH, was able to be employed there.)

After the Guide/Mirror bank was largely set up, three in-house-built ignitron-trigger generators, like the one used with the Bias bank, were mounted to the sides of the bank, and 1:1 isolation

transformers, each with two secondaries, were wound to enable each trigger generator to drive two ignitrons. Figure 98 shows the generators, with isolation transformers in yellow.



Figure 98. Two Guide/Mirror ignitron-trigger generators, with 1:1 isolation transformers

Two resistor stands to facilitate the charging and dumping of the bank, similar to those already set up for the PI, Bias, Upper, and Lower Cusp banks were also assembled for the Guide/Mirror bank. Figure 99 shows these stands after they were moved into place between the Bias bank and the Crowbar and PI bank MTGs.

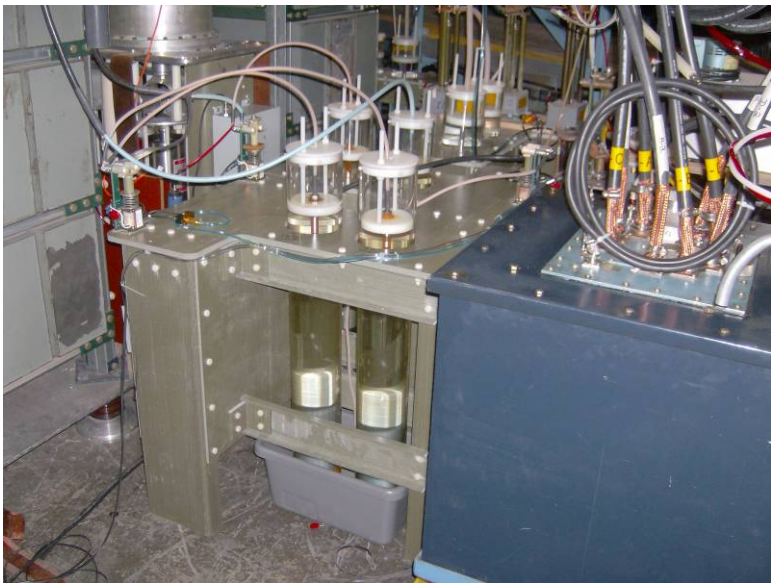


Figure 99. Two resistor stands for Guide/Mirror bank placed side by side

The reason that two resistor stands—each containing two 33-in. (83.8-cm) long, 4.5-in. (11.4-cm) diameter copper sulfate solution resistors—were used instead of just one was because of the large capacitance and total energy storage of the Guide/Mirror bank (600 kJ). By using two stands, the number of resistors was doubled, and it was possible to configure them in such a way that three of the four were in the dump circuit. This arrangement gave the resistor stands the capability of handling all the bank energy should the bank be fully charged when it was dumped. (Referring to the circuit diagram in Figure 3, the two additional resistors were connected in parallel and placed in the leg with the dump switch.)

As discussed in Section 4.1.2, one of the 12 kV, 5 A Peter Dahl power supplies that arrived in-house in June 2007 was set up to charge the Guide/Mirror bank. This supply was set up on the same stand on which the Bias bank power supply was placed. When the assembly work on both the Guide/Mirror bank and the power-supply stand was completed, the power-supply stand was moved into place adjacent to the bank (Figure 41), and personnel then began working on making all the cable connections between the Guide/Mirror power supply, the resistor stands, and the bank itself. Power cords for the three Guide/Mirror ignitron-trigger units were also run at this time. As with the Bias bank and the two Cusp banks, the final step in preparing the bank charging system was to change a pair of jumper connections on the phase controller and then set the phase-controller-current limit such that its line current was within 80 ~ 90 % of the current rating for the breaker on the power supply.

Once the bank and its power supply were set up, SAIC and Voss Scientific personnel began preparing the transmission-line cables to run from the bank to their respective coils. As with the Upper and Lower Cusp coil transmission-line cables, these cables were measured for the maximum run to the center of the Shiva bank, cut to length, and terminated at each end by soldering brass lugs (1/4 – 20 cap screws) onto them.

Before actually charging and firing the Guide/Mirror bank into its field-coil load, SAIC personnel stepped the LabVIEW control program through the charging and firing and sequences for the bank, observing each of the Ross relays and Jennings switches as they opened and closed and the other system components as they were activated, to verify that all the bank components were operating properly and at their proper times. The first actual charging and firing tests with the bank were not performed until the fall of 2008, after the FRCHX work had transitioned over to HERA Task Order 2.

5.1.2 Guide and Mirror Coil Design

With the Guide/Mirror bank, its power supply, and its transmission-line cables ready for operation, the last major fabrication and assembly effort that was required before FRC translation tests could begin was the fabrication and assembly of the Guide and Mirror coils. Designs for the coils and the spools on which they would be wound were finalized by LANL's Tom Intrator at the end of fall 2007. SAIC personnel then prepared mechanical drawings of the spool parts so that they could be fabricated by an outside machine shop, while fabrication of the coils themselves was carried out by SAIC personnel in-house.

Based upon the final LANL design, a total of 10 individual coils was needed to make up the Guide and Mirror coil assembly, and these could be grouped into four sub-sets: the Guide coils for the translation region, the lower mirror coils (Mirror 1) for the mirror at the base of the liner, a set of counter-pulsed coils (Mirror 2) just below the upper mirror that slightly depressed the field in the middle of the liner, and the primary upper mirror coils (Mirror 3) that generated the upper mirror field. Figure 100 shows this coil assembly around the solid liner, and Table 2 lists the notable coil parameters for each sub-set of coils.

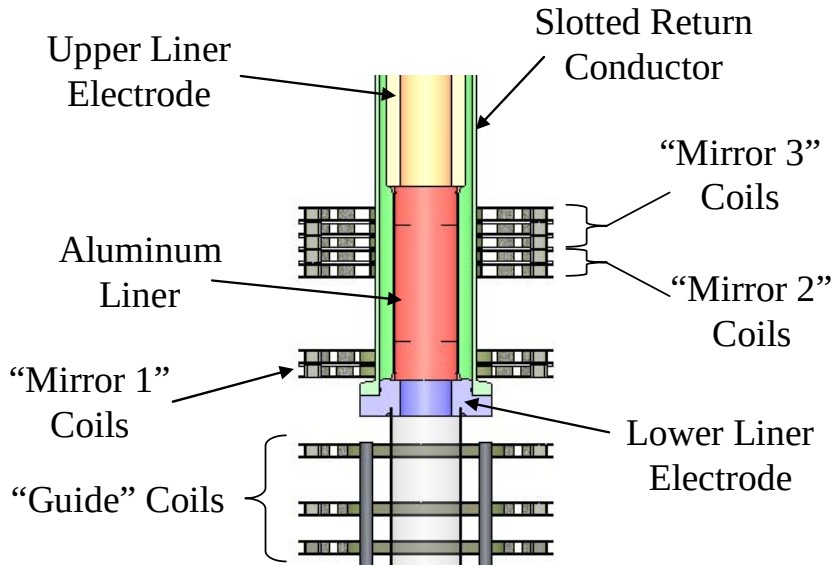
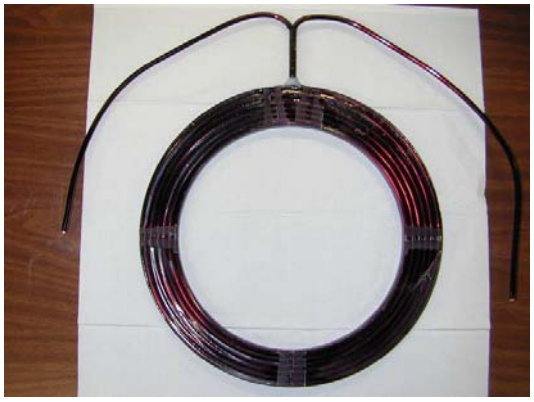


Figure 100. Guide and Mirror coil assembly around solid liner

Table 2. Guide and Mirror Coil Parameters

Name of Coil Sub-Set	Inner Radius of Windings	Number of Winding Layers in Coil	Number of Windings per Layer	Number of Coils in Sub-Set
Mirror 3	8.66 cm	2	12	3
Mirror 2	8.53 cm	2	5	2
Mirror 1	10.13 cm	2	6	2
Guide 12.14	cm	2	6	3

Before beginning fabrication, SAIC personnel first developed a methodology for winding and potting the coils. With 10 coils to be made, among which there were four different sub-sets with each having different inner radii and numbers of turns, the fabrication methodology needed to be accurate and repeatable, yet also fast and efficient with materials. Soon the following approach was decided upon: Each coil would be wound in a close-fitting polyethylene form and then potted in that form. Four different forms would therefore be needed, one for each type of coil. After curing, the coil would be removed from the form and placed within a pre-assembled G-10 spool and cast again. This procedure was felt to be among the simplest that would also allow very robust coils to be formed. Figure 101a shows the first coil to be wound and cast in one of the forms; Figure 101b shows several of the coils after they were subsequently cast in their G-10 spools.





a b

Figure 101. (a) First mirror coil; (b) several coils in G-10 spools

The range in the inner radii of the coils are also illustrated in Figure 101b, as the Mirror 2 coils, which have the smallest bore radius, are seen in the foreground, while one of the Guide coils, which have the largest bore radius, is shown in the background.

After being cast in the G-10 spools, the final step in the fabrication process was to solder or braze current contact tabs onto the wire leads of each of the coils. This task was left until two or more of the coils were ready for current tabs, as at that point the bus work between the coils was used to help align the tabs. Figure 102 illustrates both the simple bus-work design used for joining the coils that were separated axially as well as the cable header that would allow the transmission-line cables to be connected to the coil set.

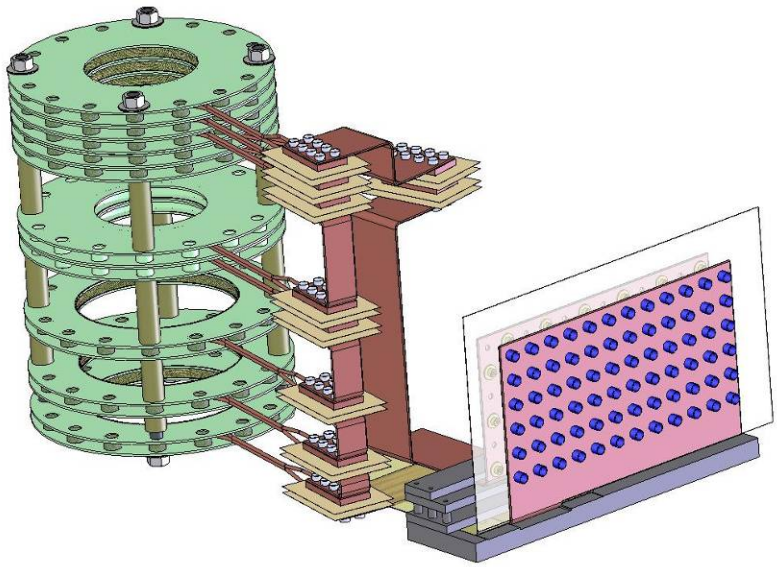


Figure 102. Guide/Mirror coil assembly and cable header and other bus work designed for it

The concept for the cable header design was taken from the Upper and Lower Cusp coil cable headers (Figure 37), as the Guide/Mirror bank had a similar maximum charge voltage (10 kV) and had the same type of transmission-line cables (YK-198). As such, the Guide and Mirror coil cable header and all the bus plates were fabricated from 0.125-in. (3.18-cm) copper plate. To enable the ground braids of the YK-198 cables to be clamped to the ground plate of the cable header, stubs of 0.500-in. (12.7-cm) copper tubing were soldered onto it. In addition, several sheets of 5-mil (127-μm) Mylar were placed between the hot and ground plates of the cable header for high-voltage insulation, and the transition connections between the header and the top and bottom Guide and Mirror coils were also painted with a red electrically insulating paint.

SAIC machinists fabricated the connecting bus work for the Guide and Mirror coils, while other SAIC personnel prepared detailed drawings of the cable header parts so that an outside vendor could fabricate them. Fabrication of the header was completed by the beginning of August 2008

(Figure 103). After delivery to Building 322, SAIC machinists soldered the 0.500-in. copper tubing stubs onto the header ground plate.

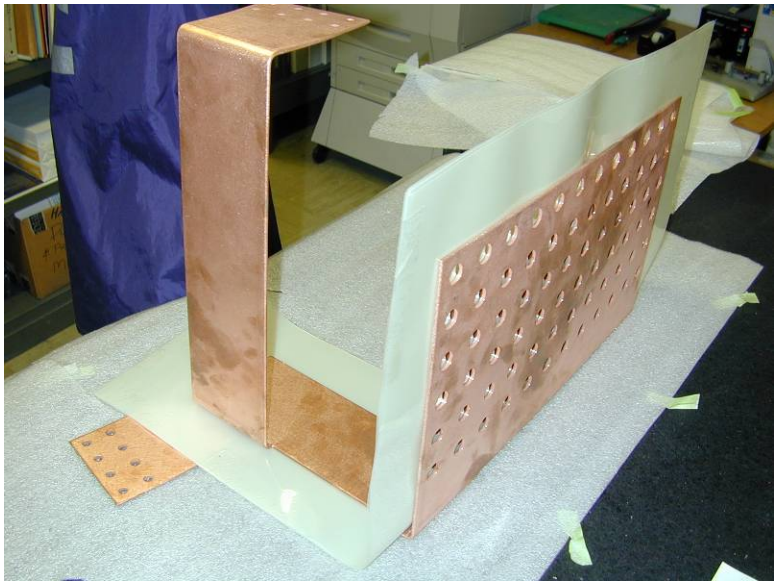


Figure 103. Guide/Mirror coil cable header along with Mylar pack prepared for it

In the middle of August 2008 the FRCHX work transitioned from this task order to HERA Task Order 2. Fabrication of the remaining Mirror coils, putting together the complete Guide and Mirror coil assembly, and the initial testing and characterization of the Guide and Mirror coils all took place under that task order.

5.2 Modifications and Additions to Existing FRCHX Systems

5.2.1 Improved Current Joints for Conical Theta Coil

After the discovery of the sputtering and arcing at the inner Theta coil segment-current joints, (Section 4.6.4), SAIC personnel spent the next couple of days considering how the segments could be easily modified to increase the compression at their inner current joints, as doing so would thereby decrease the probability of future arcing occurring at these locations. Figure 94 and Figure 95 show the effects on the quartz tube and the flux loops and the extent of the damage at the J segment (topmost segment) current joint that the arcing caused. This arcing is problematic for long periods of operation in which it is desired to conduct parameter scans of FRC formation and translation. If not addressed, the arcing would at best require that the Theta coil be rebuilt and refurbished after every 25 or 30 shots had been performed with the Main bank; at worst, the arcing would eventually lead to other failures in flux loops and possibly a failure of the quartz tube during a shot.

The inside surface of the coil segment is essentially where all the current flows, and in the unmodified segment design this part of the current joint between the segment halves was unfortunately the furthest away from the compression bolts at the outside edges of the segments. As was noted in Section 4.6.4, the arcing was particularly significant on the passive mirror segments at each end of the Theta coil (Figure 95), where coil current was naturally the highest and the segment inner radii were the smallest. After their review and consideration of the problem for several days, SAIC personnel developed a threefold approach to address the arcing problem.

First, the copper gasket placed between the halves of each coil segment was redesigned to have a current "nib" on it that would allow for more compression of the copper and result in formation of a better current joint between the two halves as the bolts running through them were tightened down (Figure 104).



Figure 104. Copper gasket, designed for improved current-joint contact

To have such a current nib, practical considerations required that the overall thickness of the copper gasket be increased. The original thickness was 0.032 in. (0.81 mm), and the new thickness was chosen to be twice that. Increasing the copper gasket thickness required that the current joint surfaces on each of the coil segment halves be skim cut by a similar amount—0.014 in. (0.36 mm) was chosen for each segment half, thereby allowing for 0.004 in. (0.10 mm) of compression in the copper. Skim cutting the current-joint surfaces had the additional benefit of

removing the pitting from those segments that had been used in the cylindrical Theta coil configuration.

A second and related means of addressing the arcing problem involved annealing these new copper gaskets once they had been fabricated. It is believed that the original copper gaskets had not been annealed. With the current nib present on the new gaskets the process of annealing them would make the copper even more compressible so that the material on the current nibs would better press into the edges of the coil segments. The annealing was performed in a vacuum oven that had recently been set up in Building 909 by SAIC for work related to AFRL's flux compression generator test program.

It was noted that the bolts used to compress the two segment halves together were located towards the outer radius of each segment, while the current flowing in each segment was predominantly located near the segment's inner radius. Thus, the compressive forces holding each segment together were not concentrated in the area where they would particularly benefit the current joint. (The locations of the two bolts in the coil segments were actually chosen to accommodate the possible addition of multi-pole field coils that would be run through the Theta coil to apply their fields in the FRC formation region.) A careful review of the coil segment geometry showed that it was possible to add a third, shorter bolt closer to the inner bore of some of the Theta coil segments—those having inner radii ranging from 5.90 to 6.99 cm (Figure 105).

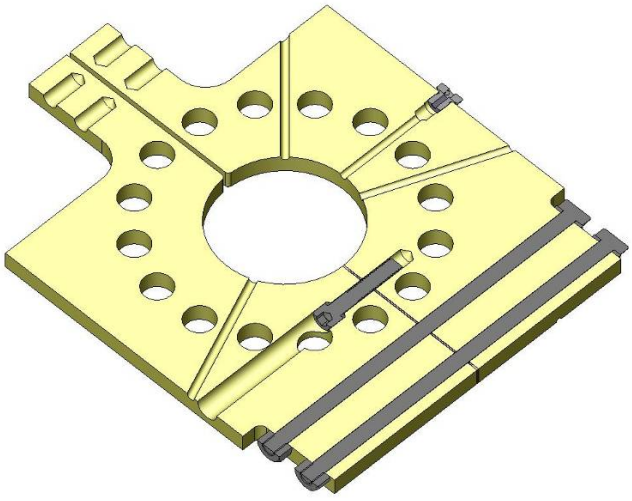


Figure 105. Theta coil segment, showing location for adding a third bolt

Thus, the third approach to addressing the arcing problem was to add a third bolt to these smaller-bore coil segments. As shown in Figure 106, the copper gaskets for these particular segments then also had to have a third hole placed in them.

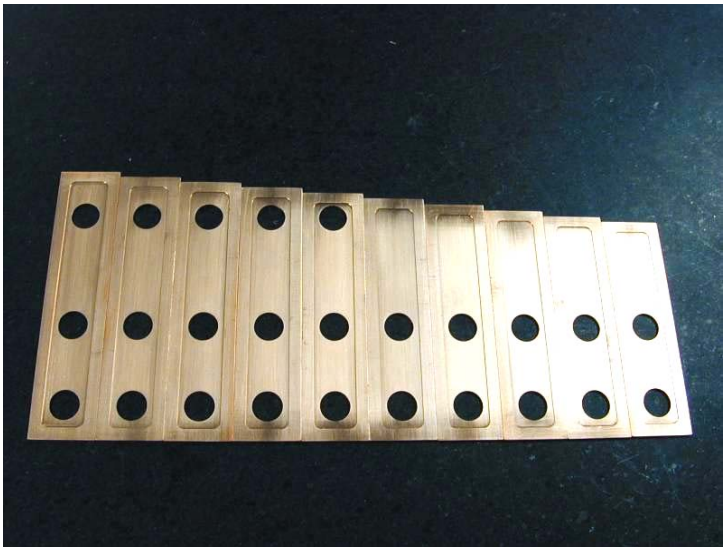
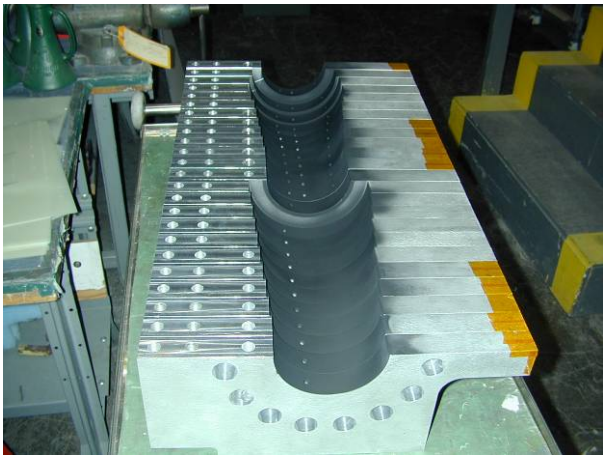
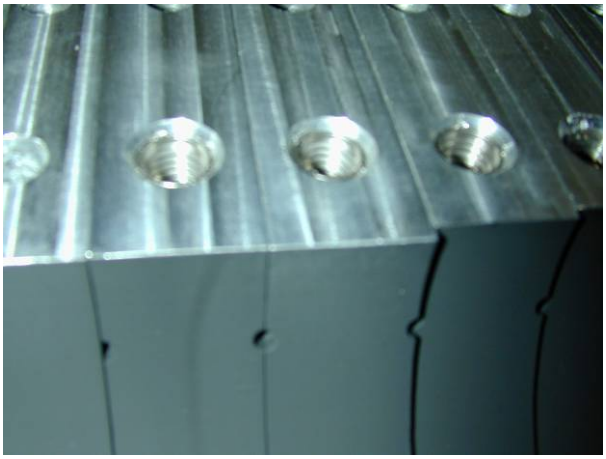


Figure 106. New Theta coil copper gaskets spread out side by side

The third hole in the copper gaskets was the determining factor for the largest-bore coil segment that could have the third bolt. Once the hole for this bolt began to cut into the current nib it was determined that the third bolt could no longer be added. Figure 107 shows the Theta coil segments (included those that would be used for the Cusp coils) after they had been skim cut and had the inner bolt holes added.





a b

Figure 107. (a) Modified Cusp and Theta coil segments; (b) close-up view of tapped holes added to several coil-segment halves

5.2.2 Higher-Voltage Power Supply for the PI Bank

In Section 4.6.2 we noted that the previous power supply used to charge the PI bank (a Maxwell Technologies CCS power supply with a negative polarity) had a maximum output voltage of only a 50 kV, though it had an appreciable 160 mA output current. With losses in charge cables and resistors this resulted in a maximum charge voltage for the bank was just above 48 kV. During a number of the static FRC formation tests performed in March and May 2008 it would have been advantageous to vary directly—by changing the PI bank charge voltage—the amplitude at which the PI magnetic field initially crossed the zero magnetic field baseline during the PI process. Such a change in the relative PI magnetic field could be achieved by reducing both the Bias and Upper and Lower Cusp fields, but making this change in this manner was somewhat cumbersome. It also had the negative result of decreasing the Bias field in the plasma, which could reduce the amount of trapped flux in the FRC.

A number of Spellman power supplies became available during the summer of 2007 when another project ended. While all these supplies had a positive polarity output, a conversation with personnel at Spellman revealed that it was possible to send the supplies back to the factory to have the polarity reversed. A 100 kV, 60 mA supply was therefore chosen for this modification, as the supply voltage was sufficient to charge the PI bank to its maximum charge voltage, and the current was large enough to perform the charging in only 3.5 s, thereby lessening the likelihood of breakdown occurring somewhere at such high voltages. It should be noted that it is unlikely that we will charge the bank much above 70 kV because of concerns about breakdown in air. Figure 108 shows the Spellman power supply after it arrived back in-house, was moved into place, and then set up for charging the PI bank.

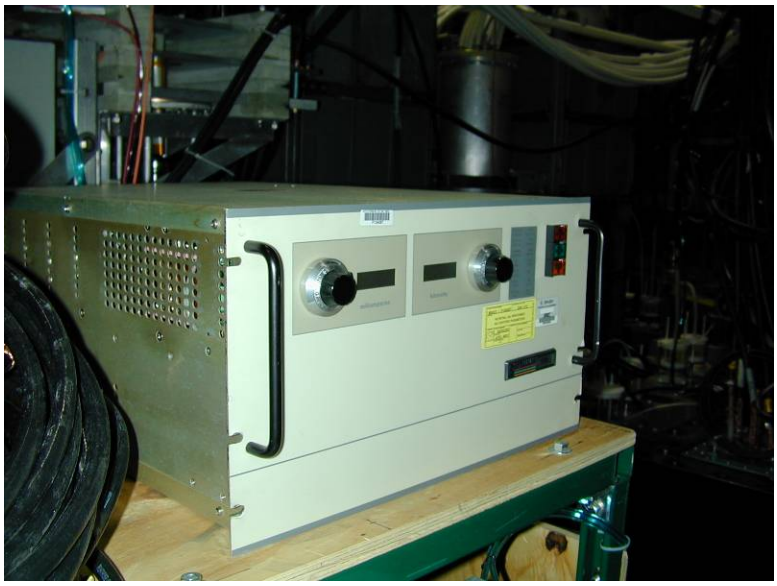


Figure 108. 100 kV, 60 mA, negative polarity Spellman power supply

5.2.3 Further Diagnostic Development

Following the completion of the Phase II static FRC formation tests, some additional diagnostic work was started with the goal of providing greater measurement capabilities when FRC translation tests began. This work included efforts at fabricating at least 24 channels of high-speed active integrators to be used with the magnetic diagnostics and 12–16 channels of high-speed amplifiers to boost the signal levels form the side-on fiber-optic translation and continuum array. SAIC personnel took the lead on this effort.

In parallel, NumerEx personnel began development work on a fiber-probe concept to be used with the four-chord interferometer. (The single-chord interferometer would have been included for consideration, as well, but it was returned to LANL to be fielded again on FRX-L.) The application of these interferometer fiber probes essentially involves injecting each of the chordal beams into an optical fiber. These fibers are then placed at locations external to the quartz tube where it is desired to probe the plasma inside, either all at one axial location or possibly at a variety of axial locations. Receiving fibers placed on the other side of the quartz tube then collect the light from the chordal beams and take it back to the interferometer-optics table. Such an interferometer setup is attractive for many reasons, but especially because it will allow interferometry to be fielded during the compression-heating experiments without risking damage to any of the expensive optical components on the interferometer-optics table. All these

diagnostic efforts were still in progress when the FRCHX work transitioned to HERA Task Order 2.

5.3 Integrated FRC Formation, Translation, and Compression Systems

In parallel with the Phase I and Phase II experimental efforts on FRCHX, AFRL, LANL, SAIC, NumerEx, and Varitec personnel also worked steadily toward developing designs for the solid liner hardware needed for FRC compression-heating tests and other structural hardware needed to integrate the solid liner into the FRC formation and translation segments of the experiment. SAIC personnel, with guidance and input from AFRL and LANL, focused first on the design of the liner electrodes and other current-feed hardware. To avoid possible problems with the mirror field above the liner compromising the magnetic insulation in the Shiva vacuum current-feed plates, a design was adopted that utilized the solid dielectric current feed from the earlier NTLX experiments on Shiva Star. With this design, only one vacuum region (along the bore of the liner and the quartz tube that passed down through the translation and formation regions) was needed. The solid liner wall then became the vacuum-air boundary. Figure 109 shows an early FRCHX conceptual layout in which the formation and translation sections of the experiment were joined directly to a solid liner that utilized the solid dielectric current feed.

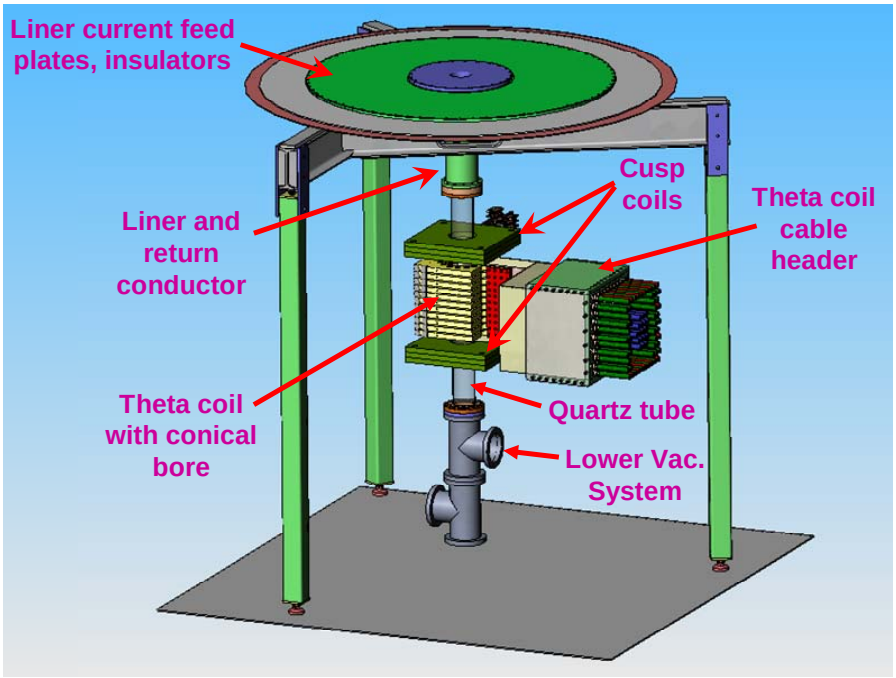


Figure 109. Layout for FRCHX formation and translation sections with solid liner

Note that the Guide and Mirror coils are not shown to allow viewing of the liner and return-conductor region. Though very attractive for its simplicity and because it mitigated the potential problem with the vacuum-current feed magnetic insulation, this approach has also carried with it some risk. Namely, since the original deformable-contact liner tests were performed with the vacuum current feed, this new scheme has required some notable changes to be made in how the liner is seated on its electrodes (also to allow it to maintain a vacuum seal) and in how the electrical insulation is maintained between the source and return-current paths in the vicinity of the liner's location.

While these issues were being discussed, AFRL, Varitec, and NumerEx personnel were incorporating the new hardware designs that SAIC personnel were developing into numerical models to calculate the diffusion of the Guide and Mirror fields through the liner, the proposed return conductor, and other proposed nearby structures. One concern that was raised initially in this process was would the Guide and Mirror fields pre-compress or otherwise deform the liner as these fields began diffusing through it, which was later determined not to be the case. A second and more basic issue that personnel set out to address in these analyses was that of determining whether or not the placement of the individual Guide and Mirror coils, as prescribed in the original LANL design, would still provide the appropriate field profile when all the magnetic diffusion effects were taken into account. Codes such as COMSOL Multiphysics were used to evaluate the diffusion times and their effects on the Guide and Mirror field profiles.

The initial analyses showed that the primary difficulty with the new hardware designs was the considerable time required for the magnetic field to diffuse through all these new structures around the liner. It quickly became apparent that these new conductors needed to be tailored both in physical shape and, in some cases, choice of material so that the field would diffuse much more quickly through them to fill the liner and translation region bore.

The choice of stainless steel for the upper and lower electrodes and at other locations that would not interfere with radiography helped to reduce the diffusion time, because stainless steel is not as good of a conductor as aluminum. Next, axially and/or radially thinning the liner electrodes reduced the diffusion time further. Putting slots in the return conductor, which still needed to be fabricated from aluminum for the benefit of radiography, had the benefit of making it effectively transparent to the upper and lower mirror fields. Lastly, the positions of some of the field coils were adjusted slightly, with respect to the original LANL configuration. These changes were

made not only to tailor the axial field further but also to allow for improved radiography access to the liner. After implementing all these changes in the COMSOL models, acceptable field profiles were obtained again in the translation and liner regions with appropriately sized mirror fields at the top and bottom of the liner.

NumerEx personnel then performed Mach 2 calculations using these field profiles determined in COMSOL to observe how the fields would be compressed inside the liner when the liner implosion started. The COMSOL field profiles were also included in NumerEx's integrated FRC formation, translation, and compression Mach 2 simulations to ascertain whether or not the FRC would be captured in the magnetic mirror in the liner region, and, if so, what its final density and temperature might be after compression.

As with the diagnostic work and the Guide and Mirror coil fabrication efforts, the final details of the electrodes, return conductor, and other liner-related hardware designs were still being resolved when the FRCHX work transitioned to HERA Task Order 2. In addition, subsequent tests performed with both the Guide and Mirror coils and with the liner hardware led to further COMSOL and Mach 2 simulations, which in turn led to additional hardware changes.

6.0 PRESENTATIONS

During the course of this task order, SAIC personnel had the opportunity to travel to two conferences and give presentations on the work being performed on FRCHX. We participated in the 2007 Innovative Confinement Concepts Workshop, February 12–14 in College Park, Maryland. With AFRL and LANL personnel, SAIC gave a poster presentation describing the progress over the previous year on the FRC formation and translation portions of FRCHX. The presentation was similar in format to the poster given at the 2006 Innovative Confinement Concepts Workshop; however, a number of new slides were added, detailing the progress with the hardware assembly and presenting some of the experimental data from the Phase I FRC formation tests.

SAIC and NumerEx personnel also attended the 2007 IEEE International Pulsed Power and Plasma Science Conference, June 18–22 in Albuquerque. There, SAIC personnel again had the opportunity to give a poster presentation describing the recent progress that had been made with FRCHX. Because this conference was shortly after the 2007 Innovative Confinement Concepts

Workshop, the poster presentation was somewhat similar. We included new slides describing the tests with the Crowbar Auxiliary bank and some of the solid liner hardware design work.

7.0 CONCLUSIONS

The purpose of this task order was to perform much of the ongoing effort to demonstrate MTF in a laboratory environment. The FRCHX is the principal system of this effort, and this report has described the advances made toward this goal under Task Order 16 of the DETAR contract. SAIC and our subcontractors have performed this work under the guidance of AFRL personnel and in collaboration with scientists from LANL, UNM, and UNR.

The two completed phases of the FRCHX development work have led to better operation of the FRC formation pulsed power systems; a suite of diagnostics capable of fully characterizing FRCs; the establishment of a self-contained, remote, shielded data acquisition enclosure to record the data from these diagnostics; the development of an extremely reliable computer-based control system for the experiment; and the formation of the first FRCs to be characterized on the experiment. Through Phase I, in particular, a solution was finally found for the problem of unreliable Crowbar rail gap conduction that had affected the operation of the FRCHX Main bank since pulsed power tests had started with this bank and that had plagued the FRX-L experiment for many years. This solution suggested by AFRL, though not fully tested until the Phase II experiments began, involved simply doubling the number of trigger cables to each Crowbar rail gap to double the current (charge) in each trigger pulse.

Several improvements to the Bias bank were also implemented during or shortly after the Phase I tests to increase peak current and then to decrease rise time. These improvements included incorporating a second spare module into the bank that had already been set aside for this purpose and redesigning the isolation inductors. If additional reductions in rise time are necessary, further changes to the circuit will be implemented, such as rearranging the placement of the Bias bank cables in the Theta coil cable header to lower the header inductance for the bank circuit or redesigning the bank bus work to make it lower inductance.

Also, though it did not appear from the excluded flux data obtained during Phase I FRC formation tests that there was ever any evidence of FRC formation, these tests prompted NumerEx personnel to perform a number of important Mach 2 simulations with the experimental setup. The results from these simulations showed that the absence of FRC formation (or at best

very minimal FRC formation) was likely due to the Cusp fields not yet being present on either side of the formation region. When the Cusp fields were in place, the simulations indicated that the magnetic reconnection during FRC formation occurred much more efficiently and much more rapidly, resulting in larger FRCs being formed.

It was these findings that can perhaps be attributed to the immediate successes obtained in the Phase II static FRC formation tests begun in the spring of 2008, because the performance of any tests was held back until the last of the preparations for the Upper and Lower Cusp banks were completed and these banks were completely operational. Indeed, once the FRC formation tests had begun, the excluded flux diagnostics began to show very early on that a 1.5–2.0-cm-radius FRC was being formed in the experiment. The lifetime of the FRC appeared to be somewhat shorter than expected, however, being at most ~6 μs. Once the interferometer was operational, the density data obtained with it showed that plasma densities on the order of 10^{17} cm^{-3} were present at the same time that an excluded flux was being detected. The excluded flux and interferometer data together thus confirmed the presence of an FRC in these tests. FRC lifetimes remained rather short during the course of the tests, however, not exceeding 6 μs.

The side-on fiber-optic-array data did not appear to support the newer hypothesis that the FRC only appeared to be short-lived because it was leaving the formation region; rather, this data seemed to support the original notion that the FRC was just decaying away within the formation region. However, as suggested in Section 4.6.3.1, personnel are anticipating that the FRC properties—and in particular, lifetimes—will improve once the FRC can be formed and then immediately translated out of the formation region. We base this optimism upon the work of D. D. Ryutov (2004) and Guo (2005), who asserted that the presence of a very weak toroidal field in an FRC had a stabilizing effect on the FRC. Such a weak toroidal field will be introduced naturally into the FRCHX FRCs through the use of the conical Theta coil to be employed when translation tests begin. Recent FRC translation tests at FRX-L, which also utilize the same type of conical Theta coil, appear to support these claims.

The FRCHX work has thus been moving forward with preparations for FRC translation tests. Before the technical work under DETAR Task Order 16 ended, the assembly of the Guide/Mirror bank was completed; the transmission-line cables for the bank had been fabricated, the design and much of the assembly work for the Guide and Mirror coils was done, the problem with the Theta coil segment current joints was addressed and several steps to mitigate this

problem taken, and assembly of the conical-bore Theta coil had begun. Designs for the liner electrodes, the return conductor, and other hardware mating the liner portion of the experiment to the formation and translation segments were largely completed, though many of the details were still being resolved. Figure 110 shows a diagram approximately illustrating the state of the integrated hardware design as of Aug 2008.

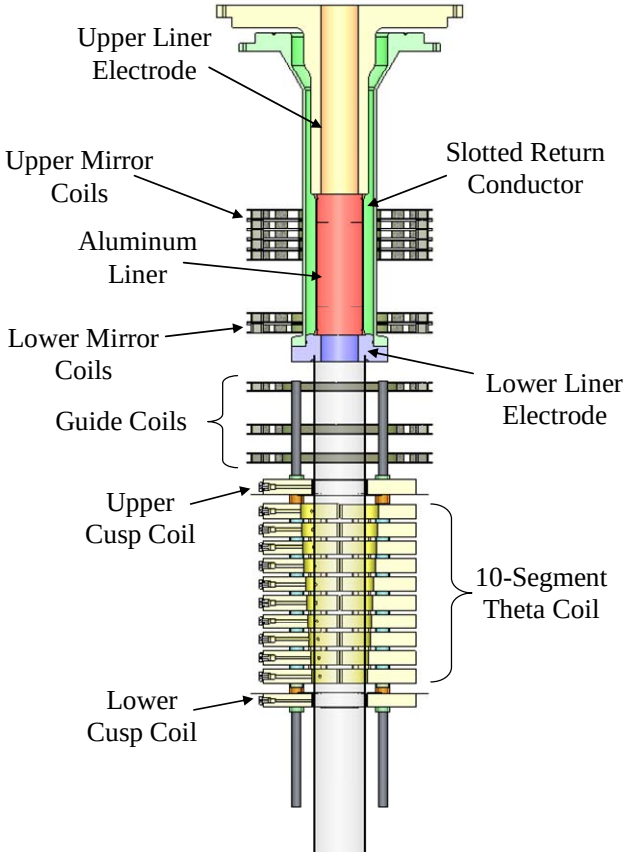


Figure 110. FRCHX formation, translation, and liner-compression regions

The design and fabrication tasks performed during the June 1–August 31, 2008 quarter of Task Order 16 enabled a fairly smooth transition of the FRCHX work over to HERA Task Order 2. Plans for FRCHX tests, which had been established as this transition was taking place and would therefore now be carried out under the new HERA task order, involved performing a series of translation-only tests again to characterize and now also optimize the FRC formation parameters before attempts were made at performing the first FRC compression-heating test.

8.0 RECOMMENDATIONS

Recommendations for future work on FRCHX, and on the magnetized target fusion work in general, can be broken up into near-term, mid-term, and long-term efforts. Near-term efforts include simply performing the FRC translation-only tests to characterize the FRCs that will be formed now that the system has been reconfigured. As these tests are performed various parameters will be scanned in an attempt to optimize lifetime; densities and excluded flux radii were of appropriate values during the Phase II static formation tests, and so the main task should be to improve the FRC lifetime.

After significantly longer FRC lifetimes have been obtained (15–20 μs vs. 6 μs), the FRCHX vacuum and field-coil stand should be reconfigured to mate with the solid liner hardware assembled in the Shiva center section. A small number of additional translation-only tests should be performed to verify that the FRC properties have not changed, and then the first FRC compression-heating test can be performed.

Mid-term recommended efforts include optimizing the FRC compression-heating experiments to maximize the neutron yield. These optimization efforts may include simply compressing FRCs with varying densities and/or temperatures to determine the resulting changes in neutron yield, or it may involve such things as modifying the profile of the imploding liner. As part of this effort, more detailed characterization studies should be performed in translation-only tests, with an increased number of diagnostics such as VUV spectroscopy and visible spectroscopy to understand better the physical processes occurring in the FRC plasmas. A particular emphasis might be placed in such studies on understanding the processes (instabilities, losses) occurring towards the end of the FRC lifetime, and with such understanding further increases in lifetime could perhaps be obtained.

The primary long-term recommendation would be to begin a study of possible reactor scenarios for magnetized target fusion. Of course, the degrees of success with each of the FRC compression-heating tests will greatly determine the feasibility of an MTF-based reactor and the appropriateness of considering such a reactor scheme. However, assuming that the tests are successful and show promising neutron yields, a study that is a step beyond the mere design-concept level for an FRC reactor should be pursued.

9.0 REFERENCES

Grabowski 2006a — T. Grabowski and C. M. Gilman, “Magnetized Target Fusion—Field Reversed Configuration Formation and Injection (MTF-FRC),” 1 January 2006–31 March 2006

Grabowski 2006b — T. Grabowski and C. M. Gilman, “Magnetized Target Fusion—Field Reversed Configuration Formation and Injection (MTF-FRC),” 1 April 2006–30 June 2006

Grabowski 2006c — T. Grabowski, *Directed Energy HPM, PP, and PPS Efforts: Magnetized Target Fusion—Field Reversed Configuration,* AFRL-DE-PS-TR-2006-1086, 31 July 2006

Guo 2005 — H. Y. Guo, et al, “Observations of Improved Stability and Confinement in a Highly Self-Organized Spherical-Torus-Like Field-Reversed Configuration,” *Phys. Rev. Lett.* **95**, pp. 175001-1 to 4, 2005

Ryutov 2004 — D. D. Ryutov, et al, “Magnetic field perturbations in closed-field-line systems with zero toroidal magnetic field,” *Phys. Plasmas* **11**, pp. 2318-2321, 2004

Tuszewski 1981 — M Tuszewski, *Phys Fluids* **24**, pp. 2126-2127, (1981)

Tuszewski 1988 — M. Tuszewski, “Field Reversed Configurations,” *Nucl. Fusion* **28**, pp. 2033-2092, 1988

Um 1994 — E. Um, “Diamagnetic loop diagnostic system for the TRAP experiment,*”* Masters Thesis, Aeronautics and Astronautics, University of Washington, June 1994

APPENDIX A. QUICK FIELD CALCULATIONS OF THETA COIL MAGNETIC FIELD PROFILE

Parameter Summary

The inner two coil segments have an inner radius r_i = 6.66 cm, and the outer two segments have an inner radius r_i = 6.16 cm. Each segment has a width of 8.26 cm, and the overall length of the Theta coil is 36 cm. A current of 375 kA is assumed in each segment (1.5 MA total current).

The inner two segments have an inner radius that is 0.5 cm larger than the inner radius of the outer two segments. This geometry should create somewhat of a mirror effect on each end to help contain the FRC formed within.

Quick Field Results

Figure A1 shows the geometry model that was set up in Quick Field. The bottom edge of the model region (green region) is the central axis for the coils.

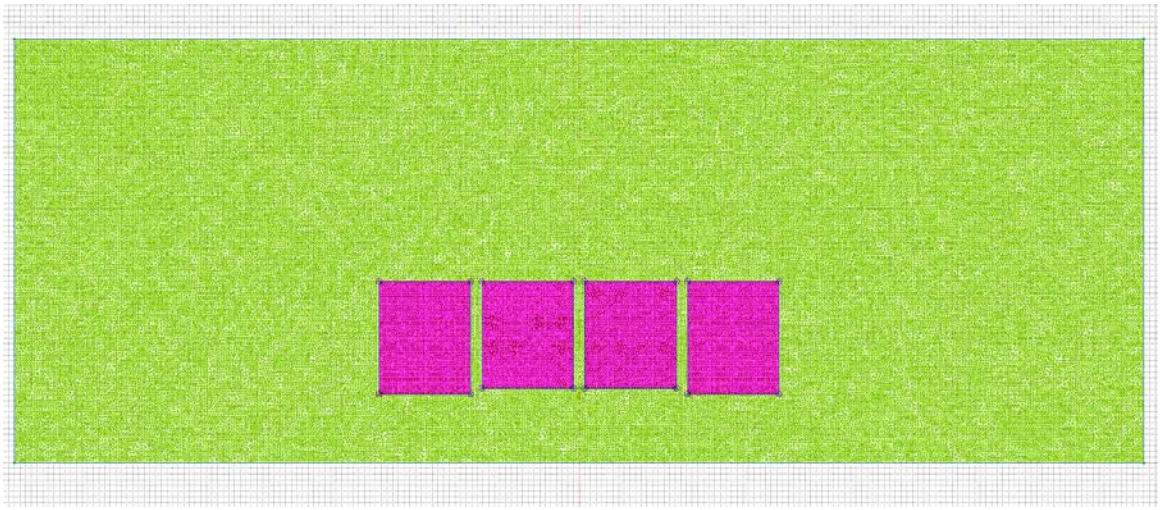


Figure A1. Geometry model in Quick Field

For the geometry shown in Figure A1, the distribution of the current density that was then calculated for the right half of the Theta coil is shown in Figure A2.

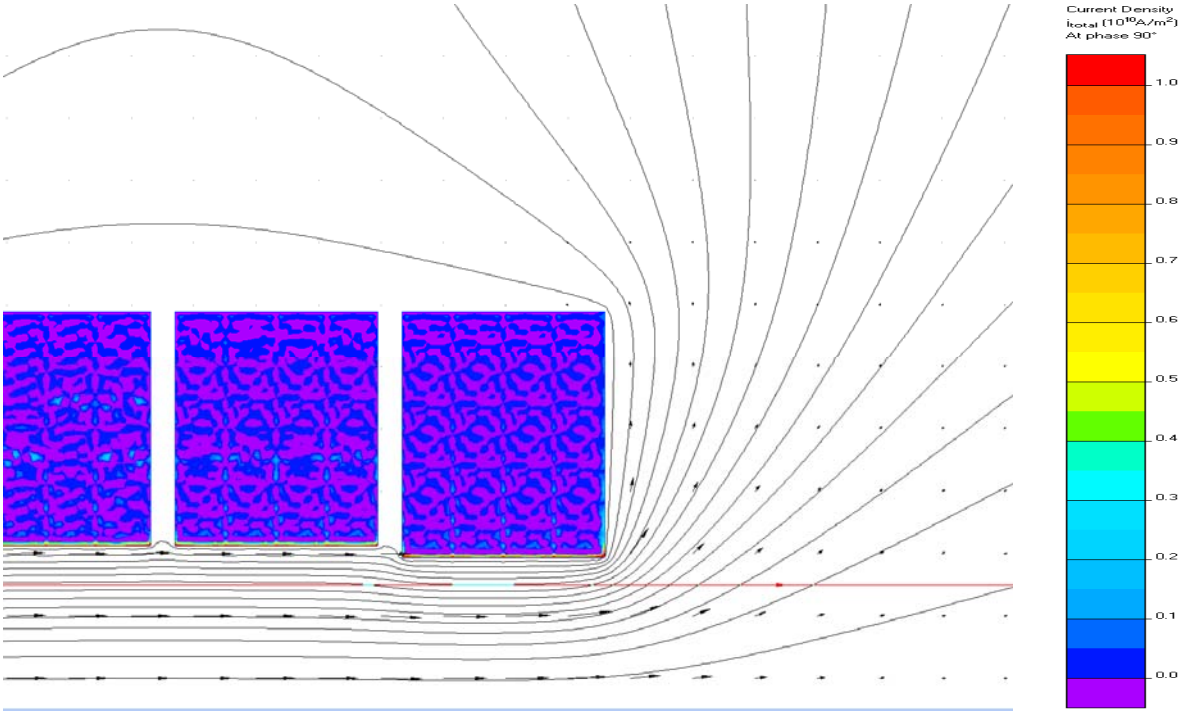


Figure A2. Calculated current density in field-coil segments

The left half is, of course, a mirror image of the right half. The colors of the contour plot show the value of the current density, while the lines and vectors show the magnetic field lines associated with the current and the direction of the magnetic field.

Figure A3 shows the calculated magnetic flux density around the right half of the Theta coil.

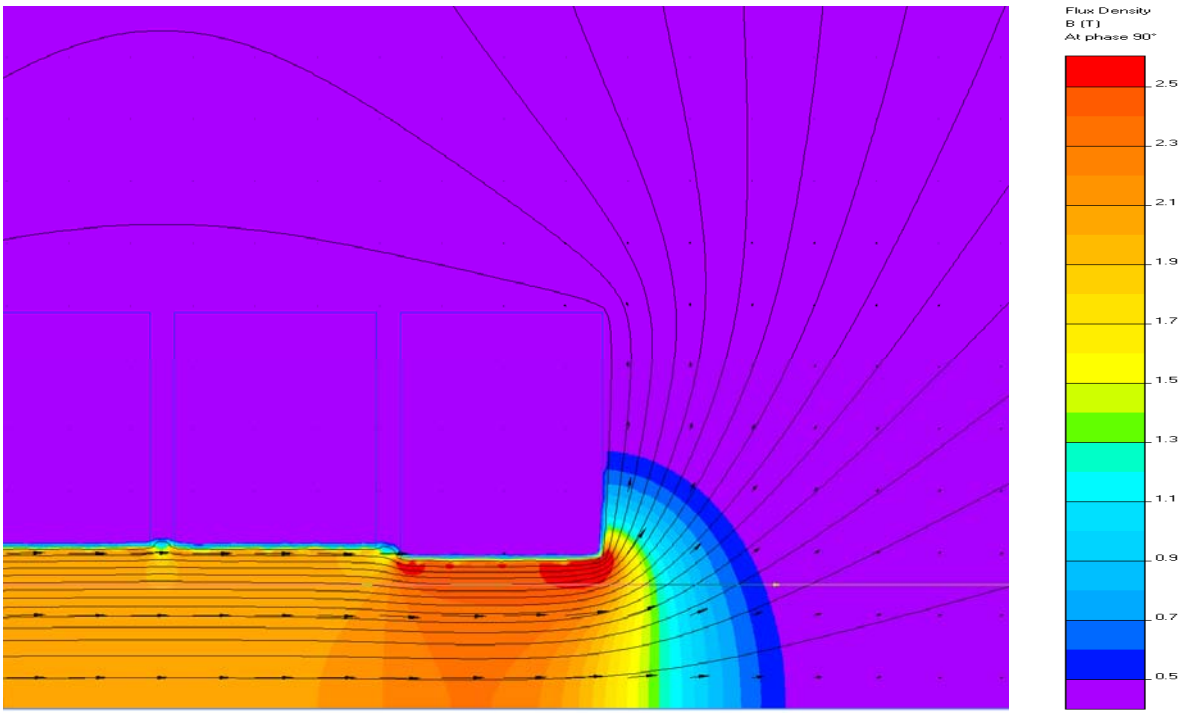


Figure A3. Magnetic flux density around field-coil segments

Here, the lines and vectors again indicate the magnetic field lines associated with the current and the direction of the magnetic field, but the colors of the contour plot now show the value of the magnetic flux density.

Figures Figure A4 through Figure A6 show 2D plots of the magnetic flux density along three different straight-line contours drawn parallel to the axis of the Theta coil. (See for example the contour at r = 2.3 cm shown in Figure A3.) From these plots, the variations in flux density are observed to be more gradual closer to the axis, but more abrupt and of larger amplitude near the inner surfaces of the coil segments.

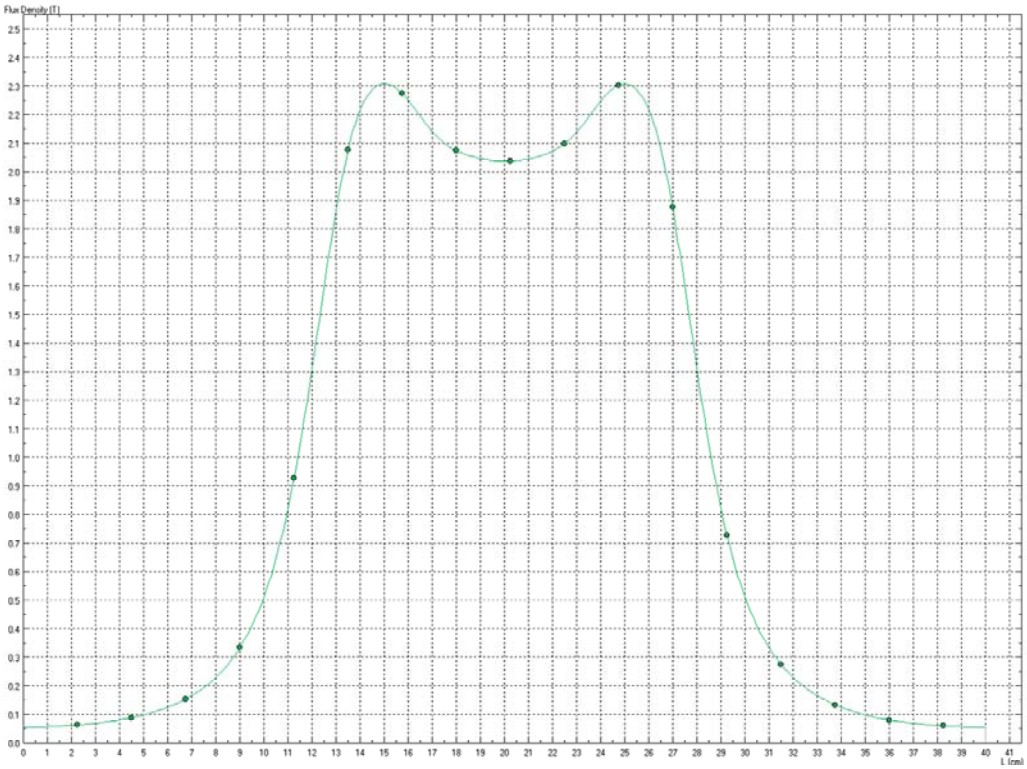


Figure A4. Magnetic flux density at r = 0 cm (on axis) vs. axial position

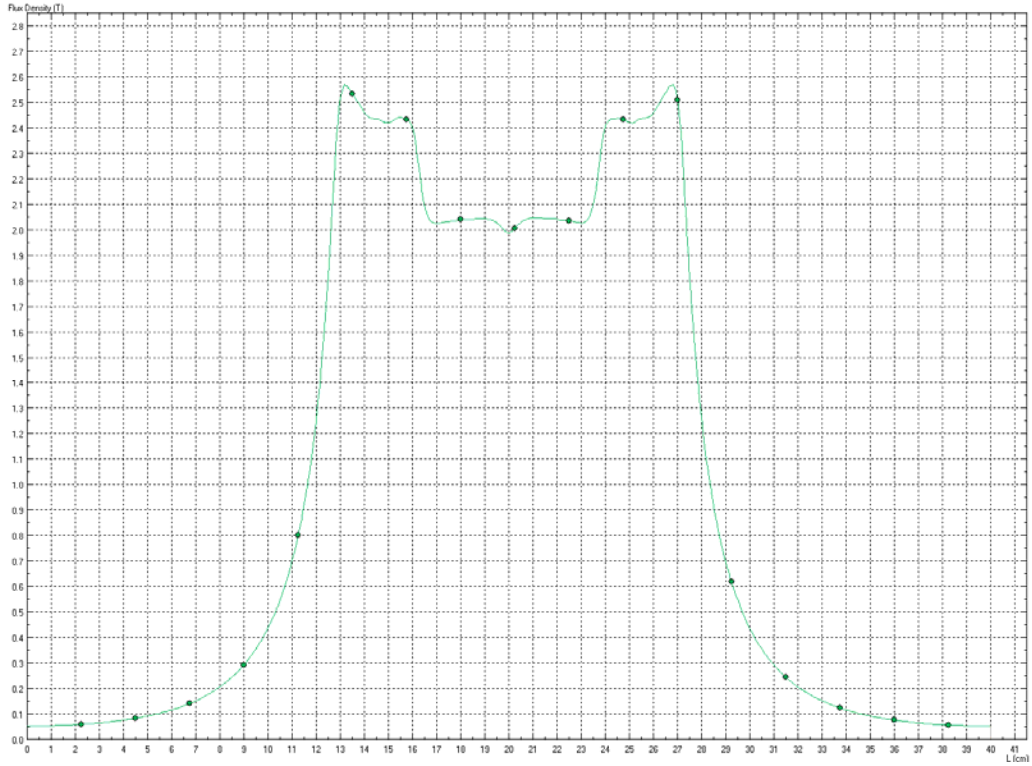


Figure A5. Magnetic flux density at r = 2.0 cm vs. axial position

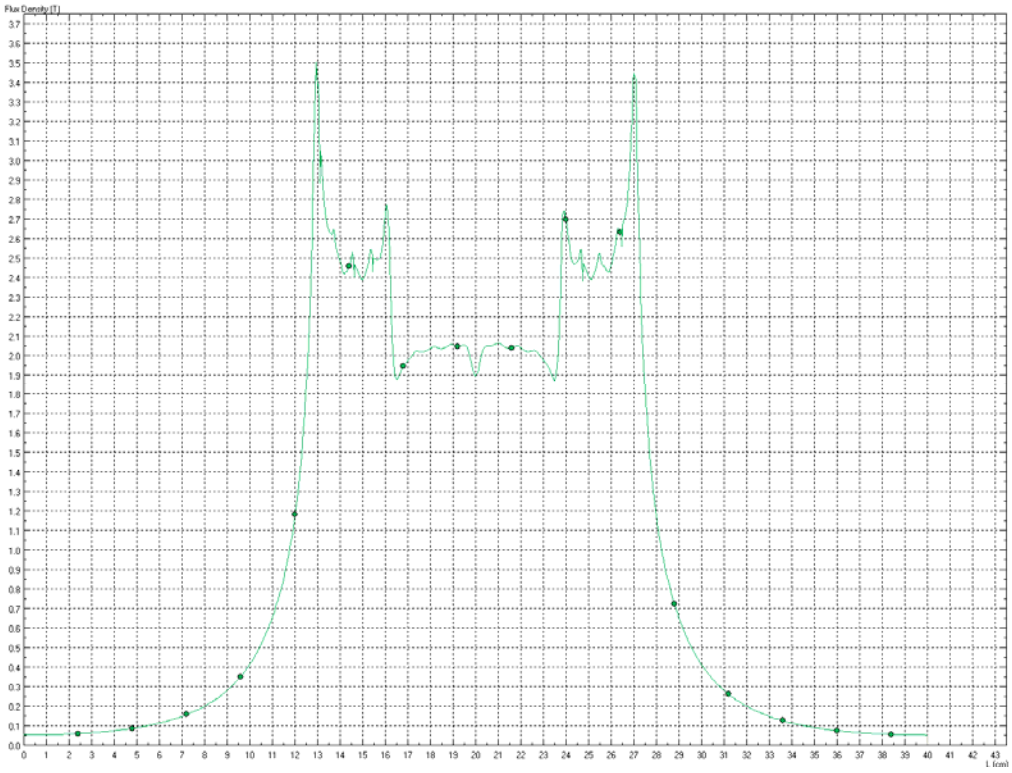


Figure A6. Magnetic flux density at r = 2.3 cm vs. axial position

THIS PAGE INTENTIONALLY LEFT BLANK

APPENDIX B. A BRIEF SUMMARY OF THE PERFORMANCE OF THE MTF CROWBAR SWITCH

This memo attempts to compile the data obtained during the initial Main bank and Crowbar switch system tests, performed in the fall of 2006, together with the data obtained from a review that SAIC personnel performed shortly thereafter of prior Crowbar switch tests. The data includes the experimental results and other notable features of the Main bank, Crowbar switch, and/or triggering-system configuration. Thus, the initial portion of this memo provides an overview of the results obtained during the characterization tests performed with the original Crowbar switch in the spring of 2001. We follow this discussion with an analysis of the difficulties encountered shortly thereafter with both Crowbar switches at FRX-L and then a summary of the recent test results. This memo concludes by listing several possible solutions that were brought up for addressing the Crowbar switch-triggering problem in light of data presented here.

1. First Design of Crowbar Switch

Characterization Tests at AFRL

A short series of characterization tests were performed with the first Crowbar switch at AFRL during May and June 2001. The test setup is as shown in

Figure B1. Here, the frame of the lower section of the bank module is grounded, as is the Crowbar trigger generator, and the load is floating.

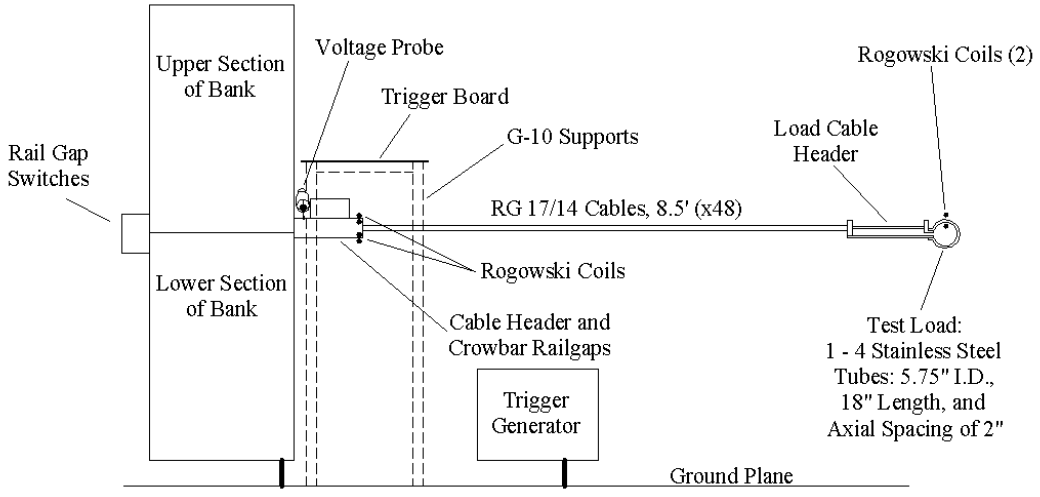


Figure B1. Test setup for crowbar switch

Table B1 summarizes data from the May–June, 2001 test shots performed at AFRL.

Table B1. Summary of Key Parameters from Characterization Tests, First Crowbar Switch

Shot #	Module Voltage (kV)	Crowbar Delay (us)	Main Bank T0 (us)	Crowbar T0 (us)	Actual Delay (us)	T_{Actual} - $T_{Delay\ Gen.}$ (us)	Comments
1	30	----	1.180	----			10 nH Load; $T_{1/4}$ ~ 2.23 us.
2	30	----	1.180	----			
3	40	----	1.176	----			
4	40	----	1.180	----			
5	40	----	1.160	----			
6	50	----	1.176	----			
7	50	----	1.160	----			
8	40	1.7	1.168	3.064	1.896	0.196	
9	40	1.7	1.152	3.032	1.880	0.180	
10	40	1.7	1.140	3.050	1.910	0.210	
11	40	1.5	1.160	2.832	1.672	0.172	
12	40	1.3	1.164	2.452	1.288	-0.012	
13	40	1.9	1.160	3.244	2.084	0.184	
14	50	----	1.166	----			
15	60	----	1.156	----			
16	60	----	1.160	----			
17	70	----	1.160	----			
18	70	----	1.150	----			
19	80	----	1.148	----			
20	80	----	1.155	----			
21	60	1.5	----	----			Scopes not armed.
22	60	1.5	1.150	3.010	1.860	0.360	
23	60	1.3	1.155	2.640	1.485	0.185	
24	60	1.7	1.155	3.030	1.875	0.175	
25	60	1.9	1.140	3.250	2.110	0.210	
26	60	2.1	1.150	----			Crowbar did not fire!
27	40	2.0	1.160	3.390	2.230	0.230	40 nH Load; $T_{1/4}$ ~ 2.85 us.
28	50	1.8	1.160	3.220	2.060	0.260	
29	60	1.8	1.120	3.100	1.980	0.180	
30	60	2.0	1.140	3.400	2.260	0.260	
31	80	2.0	1.140	3.390	2.250	0.250	
32	80	1.8	1.140	3.150	2.010	0.210	
33	80	1.8	1.125	3.290	2.165	0.365	
34	60	1.8	1.150	3.200	2.050	0.250	
35	70	1.8	1.160				Sensitivity on CB Rogowski too high, signal clipped.
36	70	1.8	1.140	3.220	2.080	0.280	
37	80	1.8	1.140	3.200	2.060	0.260	
38	80	2.2	1.150	3.860	2.710	0.510	
39	80	2.6	1.150	4.170	3.020	0.420	
40	80	3.0	1.160	4.740	3.580	0.580	

A total of 40 test shots were performed; these included 15 ring-over shots for Rogowski coil calibration and overall circuit characterization and 25 shots with the Crowbar switch being triggered. Jitter for the Crowbar switch (defined here as the additional time delay between the delay generator setting and the start of current through the Crowbar switch) tended to be 200 ~ 300 ns. The exception is the last three shots in which the Crowbar was triggered close to the load current maximum/Crowbar voltage minimum. Here the jitter was 400 ~ 500 ns. Only once (Shot

26) did the Crowbar switch fail to conduct. The trigger time was again very close to the load current maximum for this shot.

Figure B2 illustrates the effect on the load current waveform as Crowbar trigger time was varied, namely that there is a growth in the oscillations on the load-current waveform as the trigger time is moved closer to the time of the current peak.

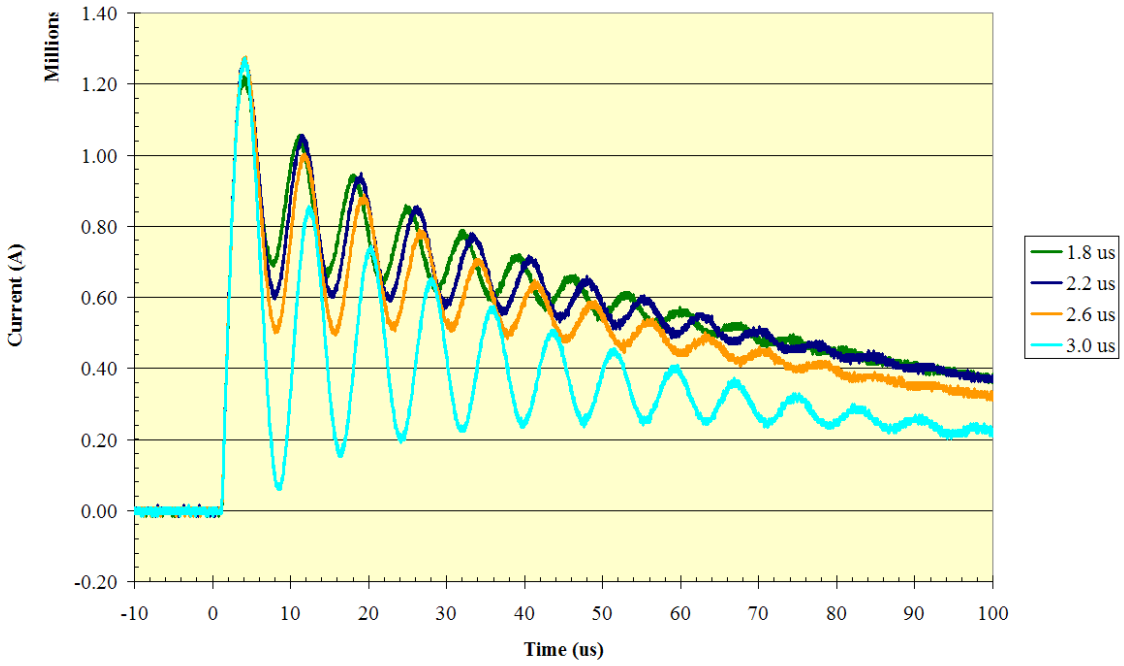


Figure B2. Overlay of load-current waveforms from shots 37, 38, 39 and 40

The respective Main-to-Crowbar trigger delays are as indicated in the legend. A probable explanation for this trend is that as the crowbar switch is triggered closer to the time of the current peak, multi-channeling in the rail gaps is poorer due to there being a lower voltage across the rails at this time. The inductance of the crowbar switch thus becomes larger and as a result the oscillation amplitude grows.

Performance of the Crowbar Switch at LANL's FRX-L Facility

Tests with the Crowbar switch immediately after installation on the FRX-L Main bank revealed a number of problems. Initially it was observed that the modulation was considerably worse on FRX-L than it was during tests at AFRL for early trigger times. Part of the problem was because the net Theta coil inductance was discovered to be only ~21 nH due to the position of the flux-excluder plates with respect to the Theta coil and not the anticipated 36 nH. However, even when accounting for the lower load inductance, the modulation was observed to be excessive.

Interestingly, when the trigger times were moved closer to the Theta coil current maximum the modulation then decreased and switch performance seemed to be better, counter to what was observed at AFRL.

As was done with the AFRL data shown in Table B1, a closer look at the FRX-L data was taken to determine when the actual start of current flow through the Crowbar switch was vs. the start of the Main bank current flow. Often larger-than-normal delays between the two were found. Table B2 provides a summary of these observed delays for several FRX-L shots along with the intended delays based upon the delay-generator settings.

Table B2. Main-to-Crowbar Delay Times from Selected FRX-L shots, First Crowbar Switch Design

Shot #	Delay Generator Dial Delay (us)	Trig. Mon. Delay (us)	Rogowski Delay (us)	Rogowski Delay - Delay Generator (us)
1299	2.5	2.55	3.147	0.647
1300	2.38	2.42	3.26	0.880
1302	2.29	2.32	3.414	1.124
1303			3.421	
1306	2.2	2.24	3.509	1.309
1308	2.1	2.16	3.139	1.039
1310	1.9	2	9.29	7.390
1311	1.9	2	9.034	7.134
1313	1.8	1.88	14.119	12.319
1314	1.6	1.68	9.4	7.800
1315	0.6	0.68	1.087	0.487
1316	1.1	1.2	8.882	7.782
1318	0.8	0.92	1.111	0.311
1319	0.9	1.02	1.149	0.249
1320	0.9	1.02	1.218	0.318
1321	1	1.1	1.486	0.486

It should be noted that with the lower load inductance the quarter-cycle rise-time of the current on FRX-L was slightly shorter than at AFRL, being 2.65 μs, approximately. Though in a few cases, the 200 ~ 300 ns delays typical of AFRL tests were found again, in general the delay was several hundred ns or even μs. Figure B3 and Figure B4 display this same data in graphical form; comparison of the trigger monitor data and the delay generator settings in Figure B3 would suggest that the trigger pulse is arriving when it should, but the rail-gap switches are just not conducting.

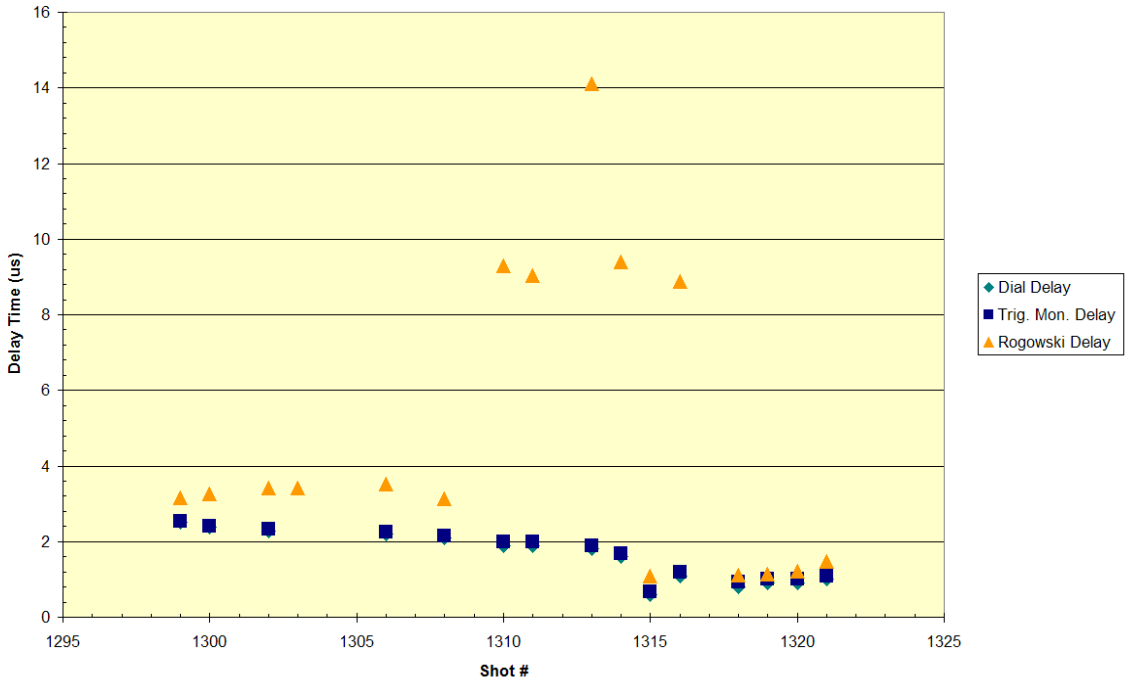


Figure B3. Delay data presented in Table B2 vs. shot number

In Figure B4 we see that there was a particularly problematic region for delays ranging between 1 and 2 μs.

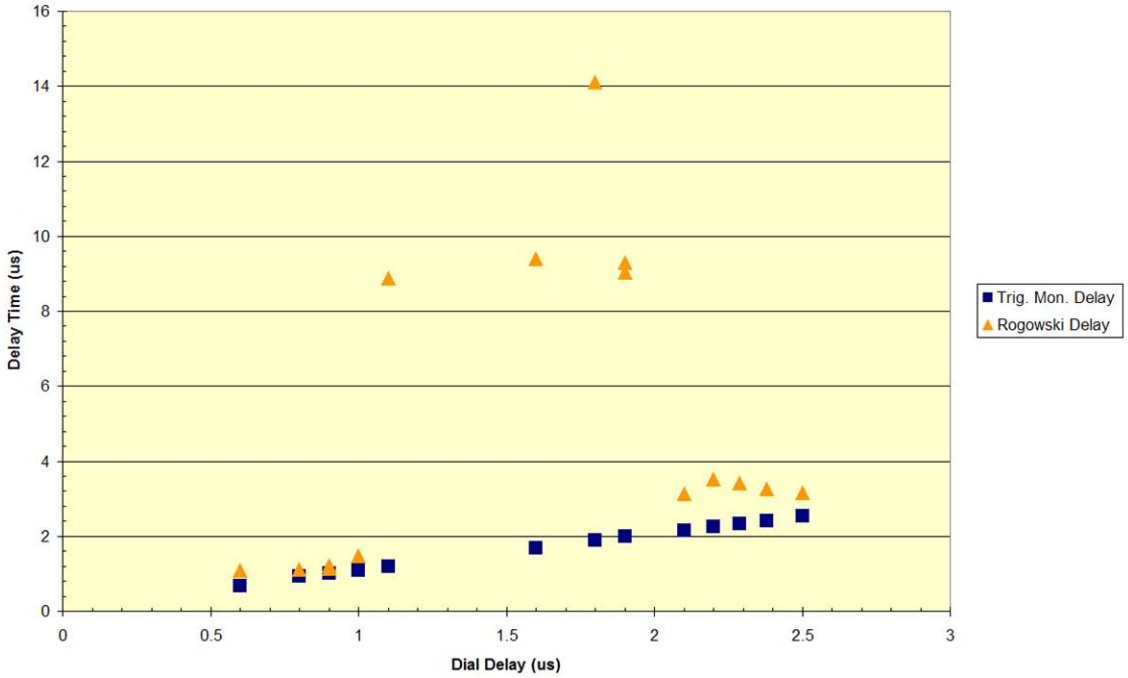


Figure B4. Trigger monitor and Rogowski coil delay data from Table B2 vs. intended delay set by the delay generator ("Dial Delay")

For delay-generator settings in this range, considerable discrepancies are found between the time between trigger monitor pulses and the time between the current start times, as determined by the Rogowski coil signals. Test shots began to include the use of open shutter photos, and these photos revealed that as the delay time was decreased from the time of Theta coil current maximum toward the range of 1 or 2 μs from the start of Main bank current, one or more of the four rail-gap switches that comprise the Crowbar switch would stop conducting. The reason for this action is not clear.

Figure B5 and Figure B7 show plots of the Theta coil current and the Crowbar switch voltage for a later test series that again looked at varying Main bank-to-Crowbar switch-trigger delays. Figure B5 illustrates the extreme nature of the modulation.

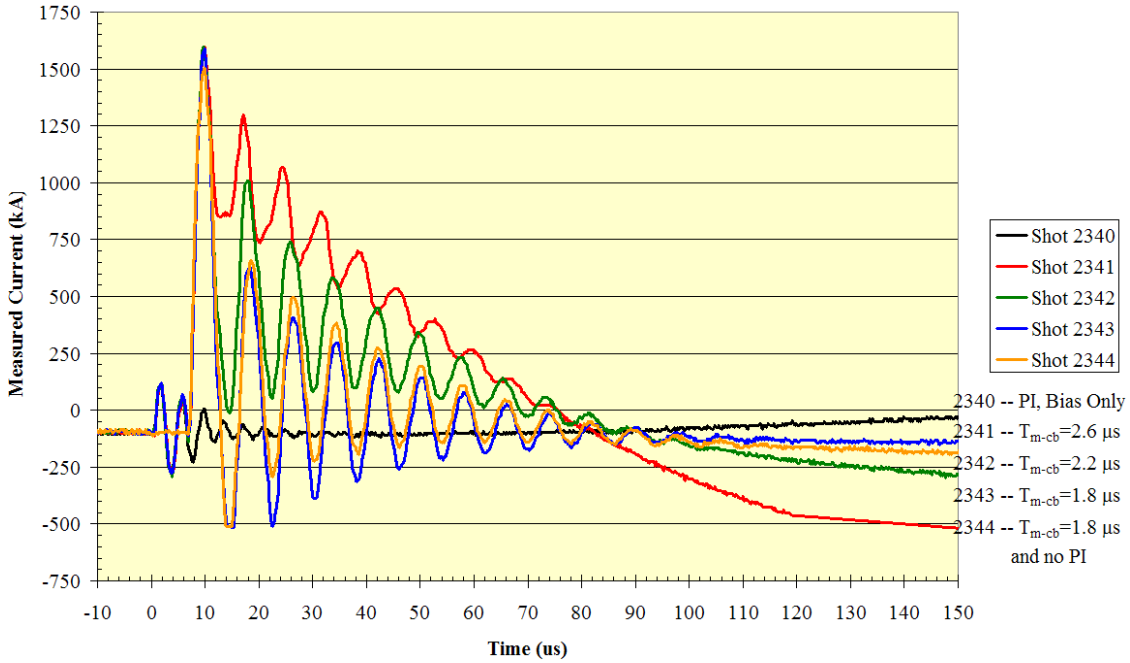


Figure B5. Overlay of several FRX-L Theta coil current waveforms from several shots with varying Main bank-to-crowbar triggering delays

Figure B6 shows one shot without the Main bank, #2340. When compared with Figure B1, the overlay also shows how the trend of modulation growth with respect to trigger delay was opposite that observed at AFRL; that is, the crowbar triggering becomes worse and the current modulation increases as the delay time is decreased. The voltage waveforms in Figure B7 show how the closure of the Crowbar switch, indicated by the sudden drop in voltage, moved later in time though the actual trigger time was moved earlier. These are the same shots considered in Figure B5.

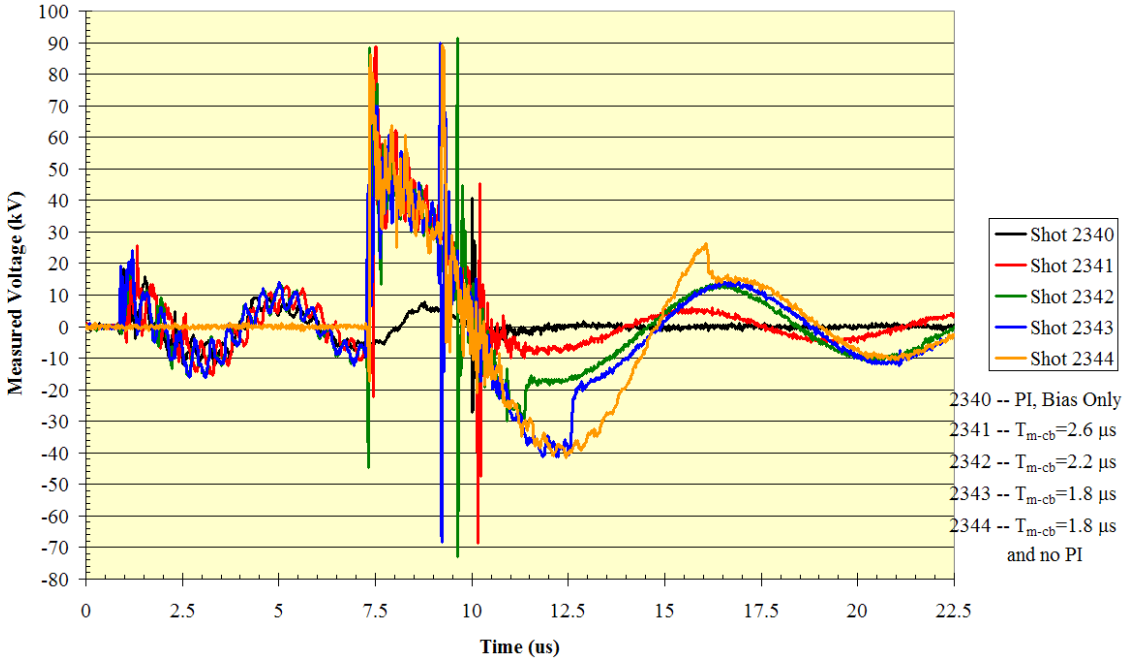


Figure B7. Voltage across the Crowbar switch vs. time

2. Second Crowbar Switch Design

Initial Tests at FRX-L

To address the severe modulation on the Crowbarred Theta coil current waveform on FRX-L, the Crowbar switch was eventually redesigned. The new design virtually eliminated all shared volume (coupling) between the two current loops formed when the Crowbar switch is fired, and after beginning tests with the new switch the resulting Theta coil current was indeed much improved. However, triggering problems with the discrete rail-gap switches in the Crowbar switch persisted. The new Crowbar switch design incorporated into it the ability to monitor currents in the individual rail gap switches, and two memos that were prepared in September 2005 take a look at some of this data in an effort to characterize these triggering problems and address a solution. We include these memos.

Copy of Crowbar Data Analysis Memo Prepared 8 Sept 2005

Figure B8 shows the delay (y-axis) between the start of the Main bank current (measured from the Theta coil Rogowski) and the start of current in each Crowbar switch rail gap (measured from the corresponding Crowbar Rogowski) for a number of recent shots (Shot # on x-axis).

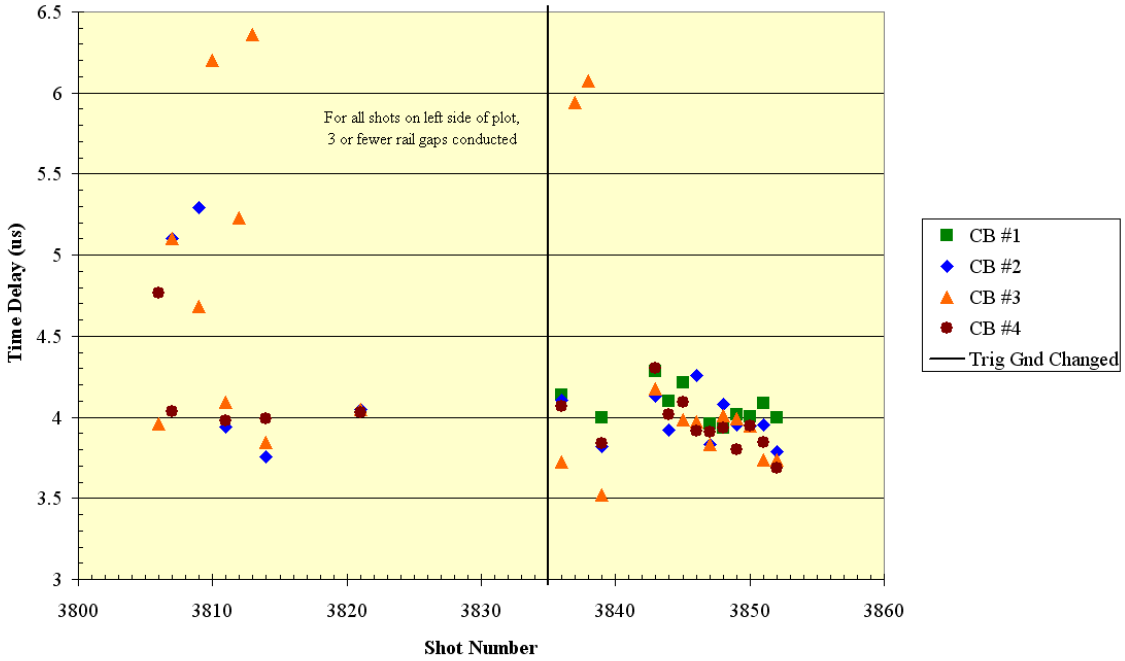


Figure B8. Delay between start of Main bank current and start of current in Crowbar rail gaps

Somewhat erratic current start times were observed right before the change in the crowbar trigger circuit grounding. Such erratic behavior does not appear to have been always the case, though. Figure B9 adds a few data points from a shot taken quite some time ago.

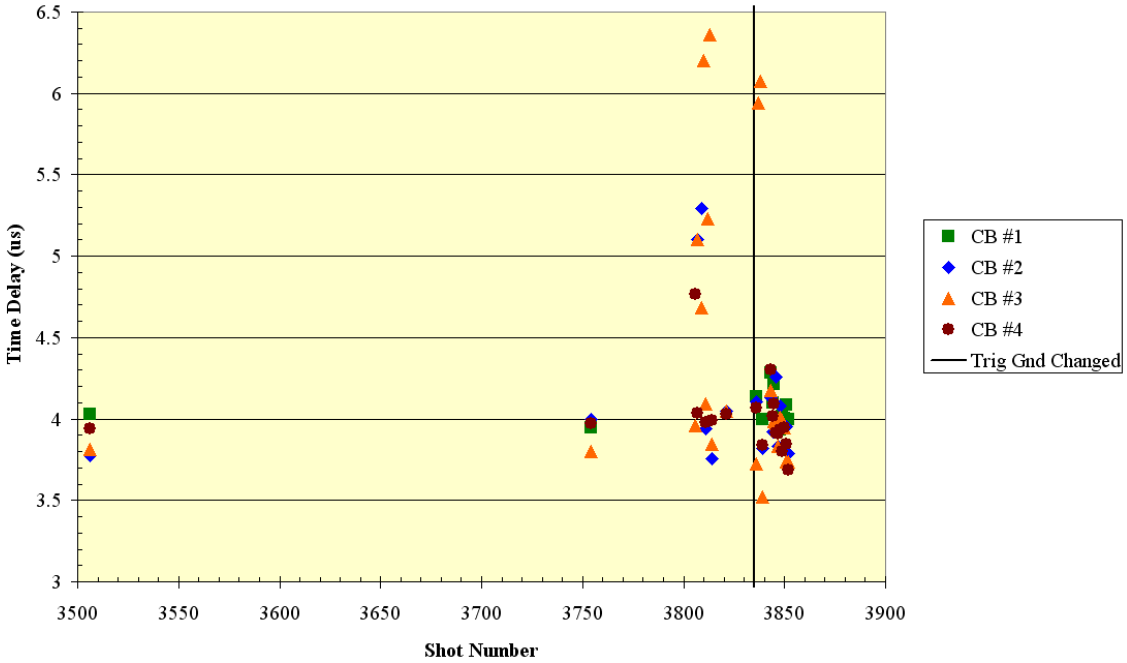


Figure B9. Data to Figure B8, shown again along with earlier data points

The delays for this particular shot are quite similar to those from the recent shots. This plot also provides a comparison of the switch behavior before (Shot 3506) and after (Shot 3754) the electrode spacing in the inner two rail gaps was decreased.

Figure B10 shows only data from the 2-Sept-05 and 7-Sept-05 shots, following the change in the Crowbar trigger-circuit grounding. Data starts with the shots performed with the floating Crowbar trigger-ground scheme.

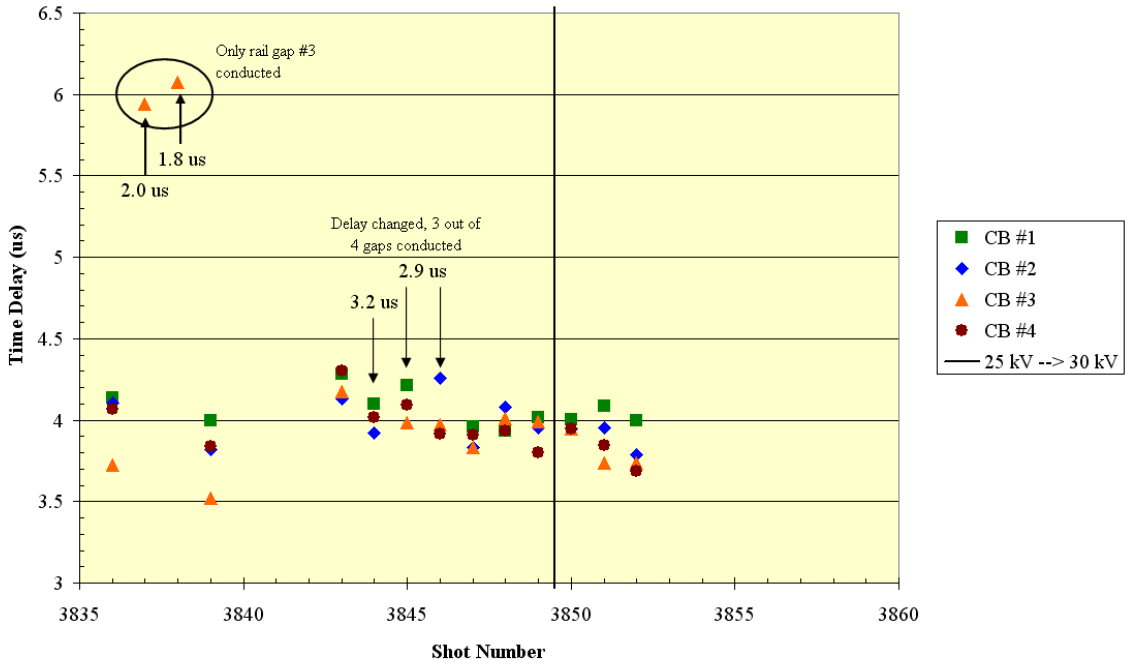


Figure B10. Enlarged view of data in Figure B8

As already observed, with the Crowbar trigger-delay generator set to 3 μs all four rail gaps conduct reliably, though with a delay from Main bank start closer to 4 μs. When the delay generator setting is changed, either increased or decreased, one or more of the Crowbar rail gaps fails to conduct.

Table B3 shows the tabulated data used to generate these last three plots.

Table B3. Tabulated Data for Plots Shown in Figure B8 through Figure B10

(All times are in microseconds)

Main Bank Vcharge	Delay Gen Setting	Shot Number	Main to CB #1	Main to CB #2	Main to CB #3	Main to CB #4	
25	3	3506	4.026	3.772	3.814	3.941	Uniform gapping in all 4 CB rail gaps
25	3	3754	3.948	3.998	3.799	3.973	Rail gaps 2 & 3 gapped narrower; old triggering scheme
30	3	3806			3.96	4.763	
30	3.2	3807		5.102	5.102	4.035	
30	3.2	3809		5.294	4.683		
30	4	3810			6.204		
30	3	3811		3.942	4.091	3.979	
25	1.8	3812			5.227		
25	2.3	3813			6.359		
25	3	3814		3.759	3.842	3.988	
35	3	3821		4.05	4.05	4.03	
25	3	3836	4.14	4.103	3.724	4.067	New triggering scheme for CB switch; blocking caps from trigger cable braid sti
25	2	3837			5.941		both sides of CB switch.
25	1.8	3838			6.075		
25	3	3839	3.997	3.817	3.518	3.837	
25	3	3843	4.282	4.131	4.174	4.304	Blocking caps from trigger cable braid to "hot" side of CB removed
25	3.2	3844	4.098	3.921		4.019	
25	2.9	3845	4.211		3.986	4.09	
25	2.9	3846		4.26	3.97	3.917	
25	3	3847	3.958	3.83	3.83	3.907	
25	3	3848	3.935	4.082	4.009	3.935	
25	3	3849	4.014	3.95	3.993	3.799	
30	3	3850	4.002	3.946	3.946	3.946	
30	3	3851	4.084	3.95	3.737	3.844	
30	3	3852	3.998	3.788	3.736	3.683	

There are no obvious conclusions to draw from these data at this time, except that personnel should continue performing experiments with a gradually increasing Main bank charge voltage and continue to closely monitor the actual time that Crowbar current begins to flow in each rail gap.

Copy of Crowbar Data Analysis Memo Prepared on 21 Sept 2005:

Background

- Problems with crowbar rail gap #2 or #3 consistently not conducting led to re-gapping both these gaps slightly narrower than gap #1 and #4 (± ~45 kV vs. ± 50 kV) back in May 05 → results were fairly successful immediately after this change.
- Problems still persisted with random gaps not conducting intermittently.
- In Aug 05 problems became more consistent; the gap not conducting was random, but it was more consistent that only three gaps would conduct.
- Crowbar trigger system was isolated from other trigger systems and other FRX-L systems and allowed to float electrically during a shot –
    - No immediate change in crowbar behavior observed.
    - If crowbar trigger system is left grounded, Main bank trigger can sometimes cause crowbar trigger unit to fire, though.

- The four crowbar rail gaps seemed to want to be triggered at a delay from Main bank trigger of 3.0 μs; when triggering any amount earlier or later only three rail gaps would conduct.

- Examination of actual delay between start of current from Main bank and start of current through crowbar rail gaps showed an additional ~1+ μs (total delay was 4 μs or greater).
  - Such an extended delay between triggering and start of conduction could be from
    1. Gas pressure being too high
    2. Voltage across switch being too low
    3. Improper biasing on trigger electrode
    4. Trigger pulse not sufficient in amplitude, energy, and/or dV/dt
- Considering item 2, gap spacing of crowbar rail gaps was decreased further to ± 40 kV spacing during week of 12 Sept 05; same gapping chosen for all four gaps as a starting point.
- The bias resistances for the crowbar rail-gap-trigger terminals were checked again at this time:
  - CB#1 upper = 1.64 kΩ, CB#1 lower = 1.54 kΩ
  - CB#2 upper = 1.56 kΩ, CB#2 lower = 1.46 kΩ
  - CB#3 upper = 1.60 kΩ, CB#3 lower = 1.52 kΩ
  - CB#4 upper = 1.80 kΩ, CB#4 lower = 1.48 kΩ

    The largest deviation is for rail gap #4, where the actual bias appears to be 55-45 (as opposed to 50-50), but this particular rail gap has actually been one of the least problematic ones.
- Conversation with Mr. Hinkley from LANL that same week pointed out several of the same issues (1 through 4) that we were already considering; it was noted that the 15% SF_6/85% Ar mixture was chosen because it had similar breakdown thresholds as air.
- Conversation with Mr. Gribble from LANL that same week generated the idea of actually using air in the rail gaps. Mr. Gribble suggested that though multi-channeling might be less, turn-on time for the switches should be faster. From his experience, inductance increase from lower multi-channeling was not terribly severe. He implied higher pressure

(and shorter gap spacing, for a given voltage) would help to improve turn-on time, as well.

Description of Tests from 19 Sept 05

- Tests (three w/ Main bank) were conducted with SF_6/Ar mix in crowbar rail-gap switches. Again, gap spacing set for ± 40 kV.

Results:

1. Crowbar rail gap # 3 consistently did not conduct
2. Delay times between triggering and current flow in the other three rail gaps were about 1 μs, same as before.

Comments:

It looks like the problem from back in May has returned, where one of the inner two gaps has trouble being triggered → we likely need to return to a non-uniform gap spacing, decreasing the spacing slightly on gap #2 and gap #3 or increasing the spacing slightly on gap #1 and #4.

Description of Tests from 20 Sept 05

- Tests (13 w/ Main bank) were conducted with compressed air in crowbar rail-gap switches. Again, gap spacing set for ± 40 kV.

Results:

Table B4. Results from FRX-L Crowbar Switch Tests Using Compressed Air in Rail Gaps

Shot Num.	Main Bank Vcharge (+/- kV)	Rail Gap Pressure (psi)	Delay Gen Setting (μs)	Measured Delay from Trig Monitors (μs)	Main to CB #1 (μs)	Main to CB #2 (μs)	Main to CB #3 (μs)	Main to CB #4 (μs)	
3870	25	20	3	3.039	4.204			4.705	
3871	25	18	3	3.017	4.711			3.930	
3872	25	16	3	3.052	4.437			4.463	
3873	25	12	3	0.532	0.750	0.691	0.573	0.810	Crowbar seems to have been triggered early by Main bank trigger.
3874	25	12	3	3.035	3.765			4.392	
3875	25	9	3	3.012	4.011	5.643		4.654	
3876	25	9	2.5	2.535	5.635	5.127	9.190	5.105	
3877	25	9	2	2.076	5.020	5.111	6.424	5.038	
3878	30	13	2	2.021	4.917		5.463	5.167	
3879	30	11	2	1.968	5.015	5.087	5.395	4.422	
3880	30	11	1.8	1.847	4.830	4.427		4.533	
3881	30	11	1.8	1.883	5.763		4.789	4.349	CB voltmeter placed on rail gap #1 trigger terminal (at connection to bias resistors)
3882	30	11	3	3.074	3.973			4.430	

1. Pressures for best operation with air were close to those for operation with SF_6/Ar, as might be inferred from Mr. Hinkley's comment about the gasses.
2. Faster turn-on, which Mr. Gribble suggested we might be able to obtain, was not observed; rather, the same excessive delay times of 1 to even 2 μs were still observed between triggering and start of conduction. The only time a "quick turn-on" was observed was for Shot 3873, during which we suspect that the Main bank trigger caused the crowbar trigger to fire very early. Perhaps an improved turn-on time with air over SF_6/Ar might be achieved with smaller gap spacings and/or higher voltages.
3. Overall performance of the rail gaps was poorer, which might be expected, because multi-channeling is expected to be poorer in air (see Mr. Gribble's comment above).
4. For shots 3881 and 3882 the crowbar voltage monitor was connected to the trigger terminal of crowbar rail gap #1, and a "bias" voltage approximately ¼ that of the total voltage applied across the crowbar was observed. After a review of past notes, it was discovered that the resistance of the volt monitor resistor is 588 Ω. When placed in parallel with the 1.54 kΩ of the lower part of the bias network, a resistance of 425.5 Ω is obtained. In series with the upper bias resistance of 1.64 kΩ, a voltage division of 0.26 is obtained, thereby explaining why we observed only ¼ of the Main bank on the trigger terminal of rail gap #1. With this information, these results actually verify, then, that the biasing of the crowbar trigger terminals seems to be correct.

Comments:

The fact that only gap #2 and/or gap #3 were the ones that failed to turn on again suggests that we should return to a non-uniform gap spacing for the inner two vs. the outer two gaps.

The persistent long turn-on times from trigger to start of conduction would suggest that even with the changes we have made

1. Gas pressure is still too high (for the voltages at which we are triggering),
2. Voltage across the switch is still too low (for this gap spacing and pressure),
3. The trigger pulse not sufficient in amplitude, energy, and/or dV/dt, or
4. There is some other physics issue we have not considered.

Our last tests would seem to have verified proper biasing of the trigger rails.

Tests with AFRL's Compression-Heating Experiment (CHX) Main Bank and Crowbar Switch

As was the case with the testing of the first Crowbar switch at AFRL, the completion of AFRL's CHX Main bank and Crowbar switch allowed a short series of tests to be performed with the second Crowbar switch design that are focused specifically on the Crowbar switch itself. These tests also have the advantage of having a much simpler experimental setup; as was the case with the original tests, there has been only the Main bank, the Crowbar switch, and the test load, so there are no possibilities of other hardware interfering with or affecting the performance of the switch. The quarter-cycle rise-time for the current with this new setup is 3.3 μs.

Unfortunately, the behavior of the CHX Crowbar switch has been remarkably similar to the FRX-L Crowbar switch. When all four rail gaps conduct, the load-current waveform has very low modulation (Figure B11), and the overall shape is quite similar to waveforms obtained from circuit calculations that were performed when designing the switch. Figure B11 shows shot 13.

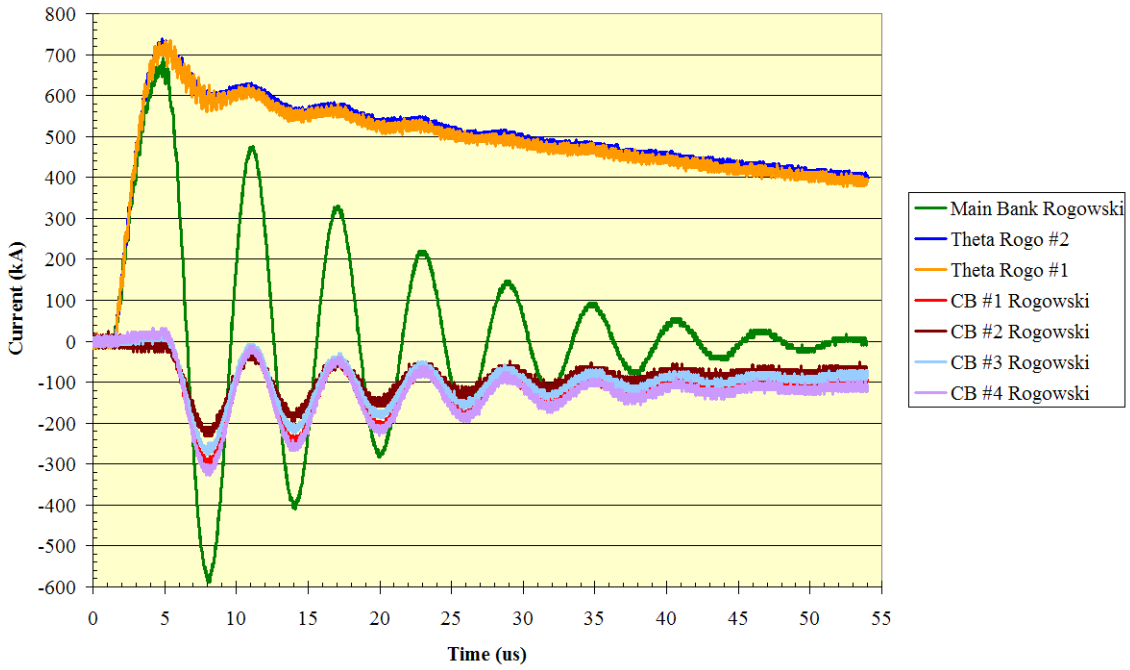


Figure B11. Current waveforms obtained from Main bank, Theta coil, and Crowbar rail-gap Rogowski coils

However, as can be seen from the tabulated data in Table B5 and Table B6 and the accompanying plot of the number of rail gaps conducting vs. delay generator setting in Figure B12, there is often a problem with triggering the rail gaps in the Crowbar switch and getting them to conduct.

Table B5. Charge Voltage and Crowbar Delay Data from Recent FRCHX Main Bank and Crowbar Tests

Shot #	Shot Date	LabVIEW ID	*Target* Module Voltage (kV)	P.S. Set Point (kV)	*Final* Comp. Voltage (kV)	DG 535 Crowbar Delay (us)	Comments
1	8/17/2006	t02.dat	40	±20	36.5	2.0	CB 40168 pre-triggered; only CB#4 conducted. Many data channels had problems.
2	8/22/2006	t02.dat	40	±20	38.1	2.0	CB 40168 pre-triggered again; this time only CB#2 conducted.
3		t03.dat	40	±20	37.9	----	HV on CB 40168 turned off. 40168 Sync Out still showed pre-triggering. Main bank Rogo signal had problems.
4		t04.dat	40	±20	38.2	----	HV on CB 40168 turned off. 40168 Sync Out still showed pre-triggering. Replaced integrator on Main Rogo; signal good now.
5	9/11/2006	t01.dat	40	±20	35.9	2.0	HV on CB 40168 turned off; checking to see if CB 40168 still pre-triggers ==> pre-triggering problem is now gone!
6		t02.dat	40	±20	32.9	2.0	No CB rail-gaps conducted; pressure in CB was a bit high.
7		t03.dat	40	±21	37.9	2.0	CB #2 and CB #3 conducted.
8		*not recorded*	40	±21	36.1	3.0	No CB rail-gaps conducted.
9		t05.dat	50	±25	42.6	3.0	No CB rail-gaps conducted, but pressure would have been a bit high for the charge voltage the P.S. decided to stop at.
10	9/12/2006	t01.dat	50	±27	52.6	3.0	Only CB #1 conducted.
11		t02.dat	50	±27	52.4	3.0	CB #2, #3, and #4 conducted.
12		t03.dat	50	±27	49.4	3.0	CB #2 and CB #4 conducted.
13		t04.dat	50	±27	47.3	3.3	**All four CB rail gaps conducted!**
14		t05.dat	50	±27.5	48.8	3.3	CB #1, #2, and #4 conducted.
15		t06.dat	50	±28.5	49.9	2.7	CB #2 and CB #3 conducted.
16		t07.dat	50	±28.5	46.5	3.6	CB #1, #2, and #3 conducted.
17	10/11/2006	t01.dat	50	±27	53.2	3.0	***Polarity of Main bank NEG now, CB trigger POS polarity.*** Only CB #3 conducted.
18		t02.dat	50	±27	52.8	3.3	Forgot to turn on CB trigger HV.
19		t03.dat	50	±27	52.7	3.3	CB #1 and CB #4 conducted.
20		t04.dat	50	±27	52.6	3.3	Only CB #1 conducted.
21	10/17/2006	t01.dat	50	±27	53	2.7	***40168 replaced, original Crowbar MTG used, isolated ground added between Main bank and Crowbar trigger system.*** CB #2 and CB #4 conducted.
22		t02.dat	50	±27	53.1	2.7	Only CB #3 conducted.
23		t03.dat	50	±27	53	3.0	CB #1, #2, and #4 conducted.
24		t04.dat	50	±27	53.2	3.0	Only CB #1 conducted.
25		t05.dat	50	±27	53.3	3.3	All four CB rail gaps conducted, but CB #2 triggered early with the Main bank.
26		t06.dat	50	±27	53.7	3.3	All four CB rail gaps conducted, but CB #3 triggered early with the Main bank.

Table B6. Crowbar Current Start Times and Measured Delays from Start of Main Bank Current for tests in Table B5

Shot #	Shot Date	Times Between Start of Current Signals: Rail Gap 1 - Theta Rogo (us)	Rail Gap 2 - Theta Rogo (us)	Rail Gap 3 - Theta Rogo (us)	Rail Gap 4 - Theta Rogo (us)	Measured - Delay Gen for Rail Gap 1 (us)	Measured - Delay Gen for Rail Gap 2 (us)	Measured - Delay Gen for Rail Gap 3 (us)	Measured - Delay Gen for Rail Gap 4 (us)	DG 535 Crowbar Delay (us)	Number of Conducting Rail Gaps
1	8/17/2006				0.904				**-1.096**	2.0	1
2	8/22/2006		0.616				**-1.384**			2.0	1
3											
4											
5	9/11/2006										
6										2.0	0
7			6.506	6.490			4.506	4.490		2.0	2
8										3.0	0
9										3.0	0
10	9/12/2006	5.140				2.140				3.0	1
11			5.660	5.896	5.876		2.660	2.896	2.876	3.0	3
12			6.176		5.900		3.176		2.900	3.0	2
13		3.540	3.776	3.740	3.564	**0.240**	**0.476**	**0.440**	**0.264**	3.3	4
14		3.560	4.224		3.532	**0.260**	**0.924**		**0.232**	3.3	3
15			5.918	5.938			3.218	3.238		2.7	2
16		3.872	3.828	3.796		**0.272**	**0.228**	**0.196**		3.6	3
17	10/11/2006			5.316				2.316		3.0	1
18											
19		4.856			3.632	1.556			**0.332**	3.3	2
20		4.402				1.102				3.3	1
21	10/17/2006		4.960		4.941		2.260		2.241	2.7	2
22				4.636				1.936		2.7	1
23		6.132	5.680		5.560	3.132	2.680		2.560	3.0	3
24		5.140				2.140				3.0	1
25		3.420	0.060	3.352	3.384	**0.120**	**-3.240**	**0.052**	**0.084**	3.3	4
26		3.348	3.364	0.100	3.376	**0.048**	**0.064**	**-3.200**	**0.076**	3.3	4

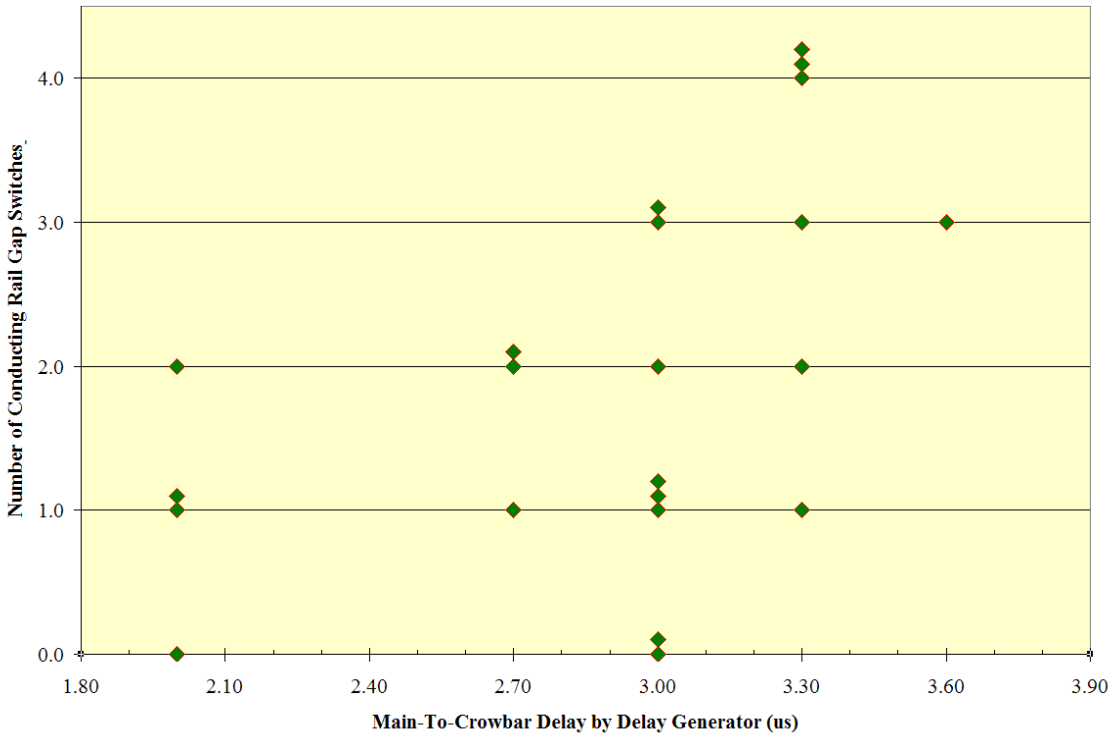


Figure B12. Number of rail gaps conducting in Crowbar switch vs. Main-to-Crowbar trigger delay

The peak of the Main bank current is at approximately 3.3 μs. In Table B6 the delay values shown in green are comparable to the jitters observed with the first Crowbar switch. Delay values that are negative are shown in red in the table and indicate a pre-fire of that particular rail-gap switch.

Data analysis is still in progress, but as Table B6 shows, the time difference between triggering the Crowbar rail gaps and when conduction starts is often rather excessive, like the FRX-L data in Table B2 and unlike the previous AFRL data in Table B1. Several variations in the setup, such as grounding and bank polarity have been tried as indicated, but unfortunately there is still difficulty in triggering Crowbar rail gaps, as is the case with FRX-L. Figure B12 shows a plot of this time different data (i.e., the rail-gap jitter) Figure B13.

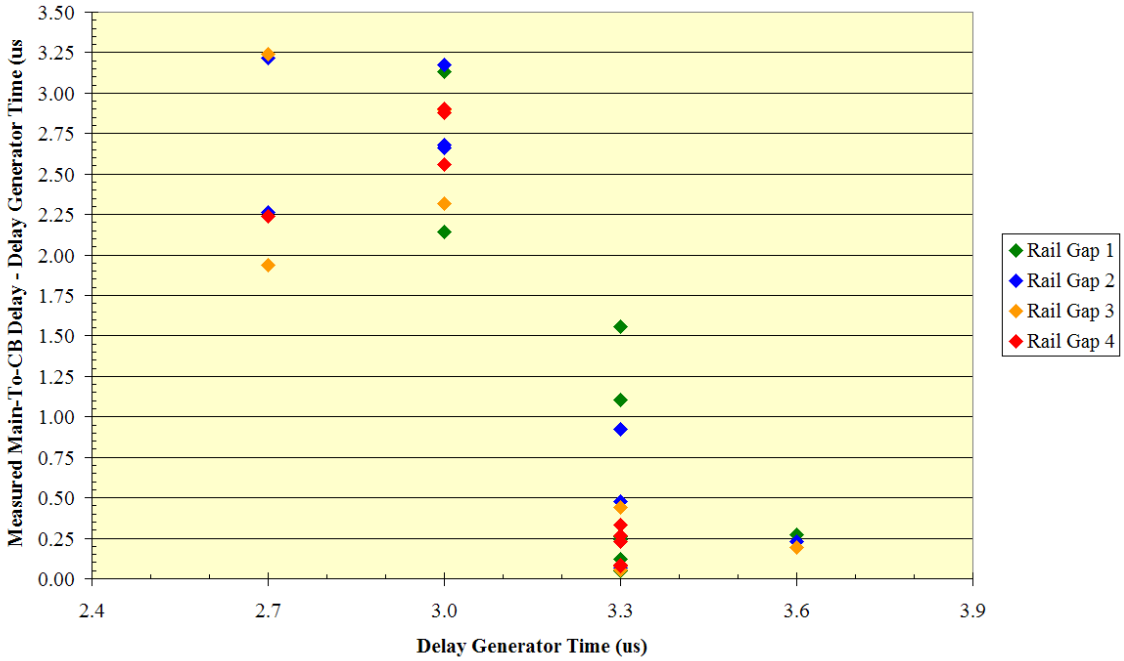


Figure B13. Delay between Crowbar rail-gap trigger and start of conduction vs. desired Main-to-Crowbar delay

The jitter drops around the load current maximum. In fact, the 3.3-μs-delay shots and the one 3.6-μs-delay shot have the lowest jitters associated with them, and it is also within this range of delays that a greater number of the rail-gap switches tend to conduct, as is indicated by the data in Figure B12. Note that only one shot has been performed to date with a 3.6 μs delay.

3. Path Forward For the Crowbar Switch

On 24 October 2006 AFRL and SAIC personnel met to discuss the performance of the Crowbar switch to date and the best approach to addressing the continuing problems with its triggering. Five possible scenarios were brought up, the last two of which are somewhat related. These scenarios include:

1. Instead of pressurizing the existing rail-gap switches pull a vacuum on them. Replace the knife-edge trigger electrodes with multiple trigatron-like trigger electrodes that are embedded in the ground-side rail electrode.
2. Continue to use the rail-gap switches as pressurized switches but replace the knife-edge trigger electrodes with plasma injectors to trigger the switch.
3. Completely replace the quad set of rail gaps with an array of det switches.

4. Make no changes and continue to operate under the assumption that the existing Crowbar setup will have enough “good” shots at the 3.3 ~ 3.6 μs delays to allow usable data to be obtained.
5. Shift focus immediately to FRC translation experiments, bypassing any static formation experiments, because once the FRC leaves the formation region (which will likely be very close to Theta coil current maximum) it does not matter how the Crowbar switch performs.

At the end of the meeting it was tentatively decided to pursue the first scenario, which essentially entails turning the rail-gap switches into vacuum switches. However, before any modifications are made to the FRCHX Crowbar switch, it was suggested to perform some preliminary tests with a single spare rail-gap switch to determine how difficult it will be to evacuate the switch and to set up the trigatron-like trigger electrodes in one of the rail electrodes. Some hi-pot tests will also be performed on the evacuated switch to determine what gap spacing is necessary to hold off an 80 ~ 100 kV potential placed between the rail electrodes. If these modifications prove to be fairly straightforward, the Crowbar rail-gap switches will then be modified in a similar manner.

THIS PAGE INTENTIONALLY LEFT BLANK

APPENDIX C. POTENTIAL SOLUTIONS TO ADDRESS THE FRCHX AND FRX-L CROWBAR SWITCH TRIGGERING PROBLEM

This document reviews three of the most promising ideas that have been proposed for solving the triggering problems experienced with the FRX-L and FRCHX Main bank Crowbar switches. Figure C1 shows an end-on view of the Crowbar switch design.

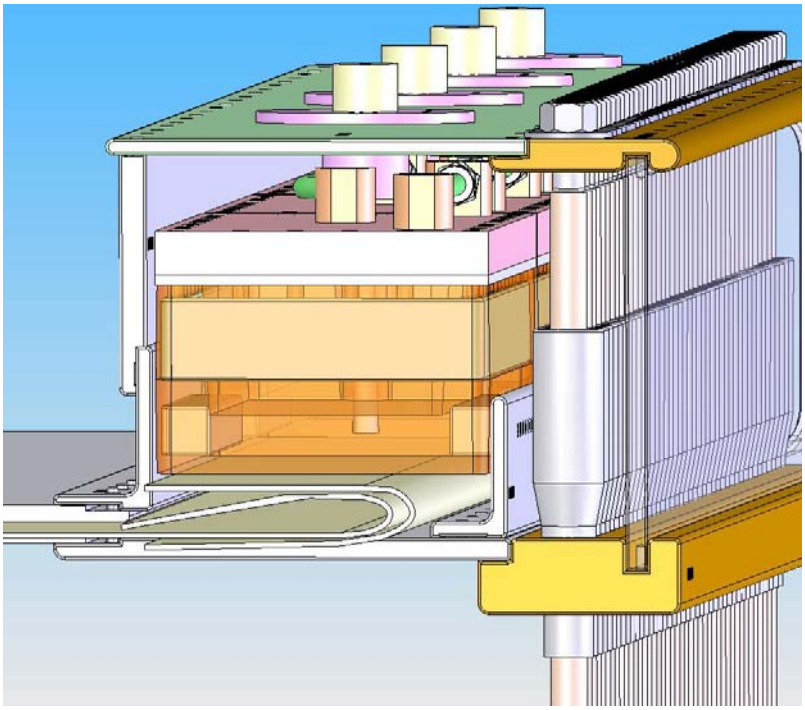


Figure C1. Basic Crowbar switch design

The bus work shown here is like that on FRCHX; the FRX-L Crowbar switch bus work was slotted to attempt to provide a small measure of inductive isolation between the individual rail gaps.

1. RESISTIVE ISOLATION OF SINGLE RAIL-GAP SWITCHES

For FRCHX implementing this concept would require splitting the bus work feeding current to the Crowbar switch, as was done for FRX-L, and inserting Franklin (or similar) resistors (Figure C2) in the current paths of the individual rail-gap switches. The Franklin resistors are low-resistance (60 mΩ) and high energy (100 kJ).



Figure C2. Franklin resistors that are commonly used in-house

This idea is the simplest approach conceptually; however, as apparent from the Crowbar design drawing in Figure C1, significant hardware changes would be needed. The slotted bus work would have to be fabricated for the FRCHX Main bank, and unlike FRX-L the parallel bus plates extending from the Main bank to the Crowbar switch are integral with the Main bank. These plates would have to be removed from the bank and modified (Figure C3).



Figure C3. Integral nature of FRCHX Main bank and Crowbar switch bus work

The resistive isolation scheme could possibly be implemented a little more readily on FRX-L, though some additional hardware would still be required to bolt the resistors to the bus work. Because these particular Franklin resistors are somewhat long (16 in.), they would likely have to be mounted vertically between the Crowbar switch and the FRX-L Main bank. Even so, the Crowbar switch may still have to be moved a little further out from the Main bank to make room for the resistors (Figure C4), which would require still more hardware to be fabricated.

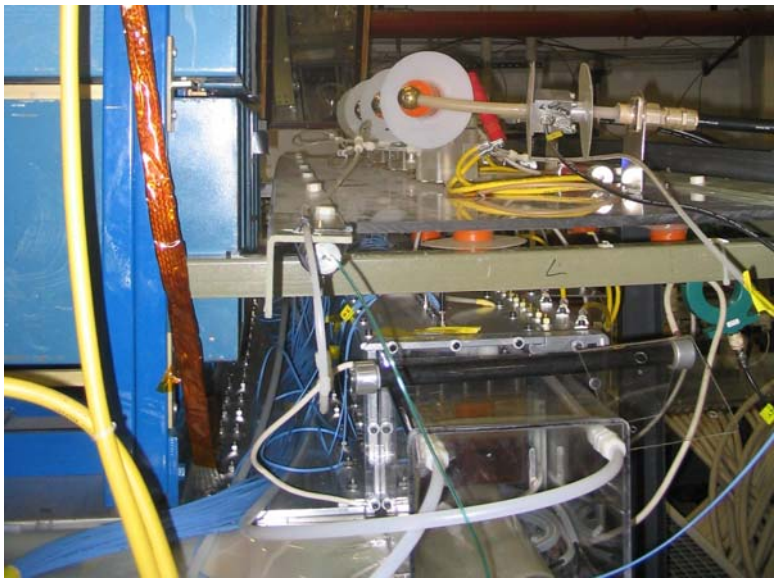


Figure C4. FRX-L Crowbar switch showing its close proximity to Main bank

2. CONVERSION OF RAIL GAPS TO VACUUM SWITCHES

The conversion of the pressurized rail-gap switches into vacuum switches is a somewhat more involved approach conceptually than the resistive isolation scheme. However, a preliminary design suggests that the only components that would need to be modified are found inside the switch (Figure C5).

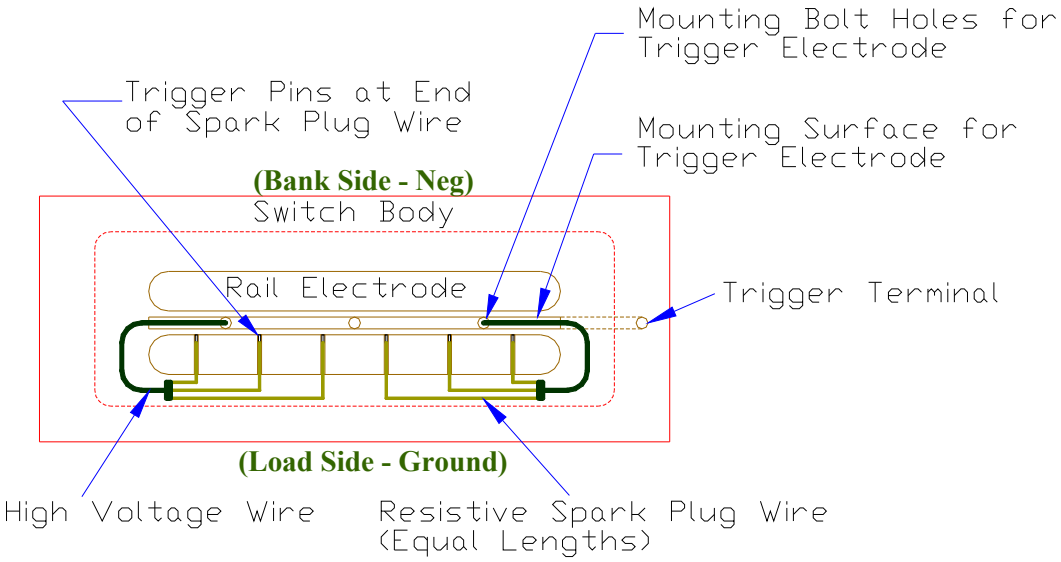


Figure C5. Vacuum rail-gap switch concept

The knife-edge trigger rail would be removed, and holes (perhaps 3 ~ 6) would need to be bored into each of the ground-side rails so that trigger pins could be inserted. Connections to the trigger pins, as well as resistive isolation between the pins, could be realized using the same resistive high-voltage spark-plug wire that is currently used for biasing the Crowbar trigger rails. These pins would receive their trigger pulse from low-profile connections made to the mounting bar on which the trigger rail had been resting in the switch body, and essentially the same external trigger-circuit setup that is currently used to trigger the pressurized rail-gap switches could be used for triggering the vacuum rail-gap switches.

To evacuate each of the rail-gap switches, a dry scroll (oil-free) mechanical pump could be used, as mTorr pressures would be sufficient for the vacuum switch voltage hold-off and operation. Furthermore, through the use of a blank-off flange with two ½-in. Swagelok fittings welded into it, the same 0.5-in. polyethylene tubing that is currently used to pressurize the switches could be used for evacuating them. Some bench-top tests would have to be performed to determine an appropriate rail-electrode spacing for the switches to hold off the full Main bank voltage in vacuum, as well as an appropriate depth to set the trigger pins within the ground-side rails to achieve reliable triggering.

In addition to the bench-top tests, a little design work may be needed to develop the insulated connection between the single high-voltage wire on each side of the rail gap and the three resistive spark-plug wires that fan out to each of the trigger pins on that side. An additional

downside to this approach is that there could likely be greater wear to the switch electrodes with vacuum operation when compared to the present pressurized-switch configuration. Greater wear would require more frequent maintenance periods for the Crowbar rail gaps.

3. AUXILIARY CAPACITOR BANK TO APPLY VOLTAGE ACROSS RAIL GAPS

Setting up an auxiliary capacitor bank to apply voltage across the Crowbar switch could perhaps be less involved than the conversion of the pressurized rail-gap switches to vacuum switches. With this concept no actual changes are needed to the present Crowbar switch, its bus work, or its triggering system. An additional capacitor bank with its own triggering system and charging system must be set up, however.

An appropriate bank is already on hand in storage at AFRL. This bank is the "mock PI bank" that was used during the initial Crowbar switch characterization tests at AFRL in 2001 to evaluate whether or not the PI bank at FRX-L could potentially cause the FRX-L Main bank to pre-fire (Figure C6).



a b

Figure C6. Mock PI bank side (a) and top (b) views

The bank can be configured to use either two or four 6-μF, 60-kV Shiva-style capacitors, and it has a Physics International T-508 spark-gap switch with a Maxwell 40295 (100 kV) trigger generator integrated into it. As part of the setup for the 2001 tests, four RG 17/14 transmission line cables were attached to the spark-gap switch to connect the bank to the Main Bank-Crowbar switch test load that was being used (Figure C6b). These cables are still attached to the bank. To attach this bank across the FRCHX Crowbar switch with our present setup, four of the RG 17/14 transmission-line cables connected to the Crowbar cable header can be removed and replaced

with the four RG 17/14 cables attached to the Auxiliary bank. As one might imagine, the bank cables should probably be distributed across the Crowbar cable header so that each of the four cables is in close proximity to one of the Crowbar rail gaps.

The only item still required to make the bank operational is a power supply. The polarity of the bank should be the same as that of the Main bank, which also happens to be the same as the PI bank. Thus, it seems feasible to use the same power supply (a -50 kV, 8 kJ/s Maxwell CCS power supply) to charge the Auxiliary bank that is currently being used to charge the PI bank. A separate set of Jennings switches, protection diodes for the power supply, and charge-and-dump resistors would be all that is required. Circuit simulations will be performed to obtain an estimate of the required charge voltage for the bank for it to be effective in helping the Crowbar switch to trigger, but if possible we will attempt to apply the same charge voltage to the Auxiliary bank that is applied to the PI bank. This choice will eliminate the need for allocating additional control system channels for the Auxiliary bank, with the exception of a channel to monitor charge voltage.

With a trigger unit and spark-gap switch already integrated into the bank setup, and a power supply identified to charge it, all that is needed to implement the Auxiliary bank concept for the Crowbar is to pull this bank out of storage, clean it up, and move it into position near the FRCHX Main bank. In parallel, the charge-and-dump resistor stand can be set up for the bank and a charge cable and fiber-optic cable for triggering can be run to the location selected for the bank.

4. CONCLUSIONS

Because much of the required hardware is already available at AFRL and because of the simplicity of the manner in which it can be integrated into the Main bank-Crowbar switch setup, the Auxiliary bank concept to improve Crowbar triggering appears to be the most straightforward to implement. Because the rail gaps are still pressurized, this approach does not have some of the drawbacks of the vacuum-switch concept, either. This path will, therefore, be the one that is pursued. Circuit simulations should still be performed (and in fact are presently being set up) to estimate the interaction of this bank with the Main bank and Crowbar switch, to ascertain whether or not this bank can indeed be effective in assisting the Crowbar switch to trigger (conduct), and to determine if the Main bank discharge might adversely affect the Auxiliary bank in some way. However, the application of this bank does mean that a third bank

must be moved when the FRCHX formation and translation hardware is moved under the Shiva bank.

For FRX-L the Auxiliary bank concept would also likely be the most promising concept to implement. There would be the burden of assembling such a bank and triggering system, however, unless an appropriate bank can also be found in storage there. However, there will not be the added complication of having to move the bank at various times to set up for compression-heating tests. Simulation results, as well as subsequent Crowbar test results from AFRL and translation test results at FRX-L, can hopefully guide in making the decision regarding whether or not to set up an Auxiliary bank for the FRX-L Crowbar switch.

THIS PAGE INTENTIONALLY LEFT BLANK

APPENDIX D. ANALYSIS OF THE POTENTIAL BENEFITS OF THE PROPOSED CROWBAR AUXILIARY BANK

To evaluate the potential benefits of introducing an additional bank to apply voltage across the Crowbar switch during triggering, a circuit model was first developed to simulate the existing set of three FRCHX banks. This circuit model is shown in Figure D1, and the values for the various elements were derived from analysis of the data from shots 33, 51, and 67.

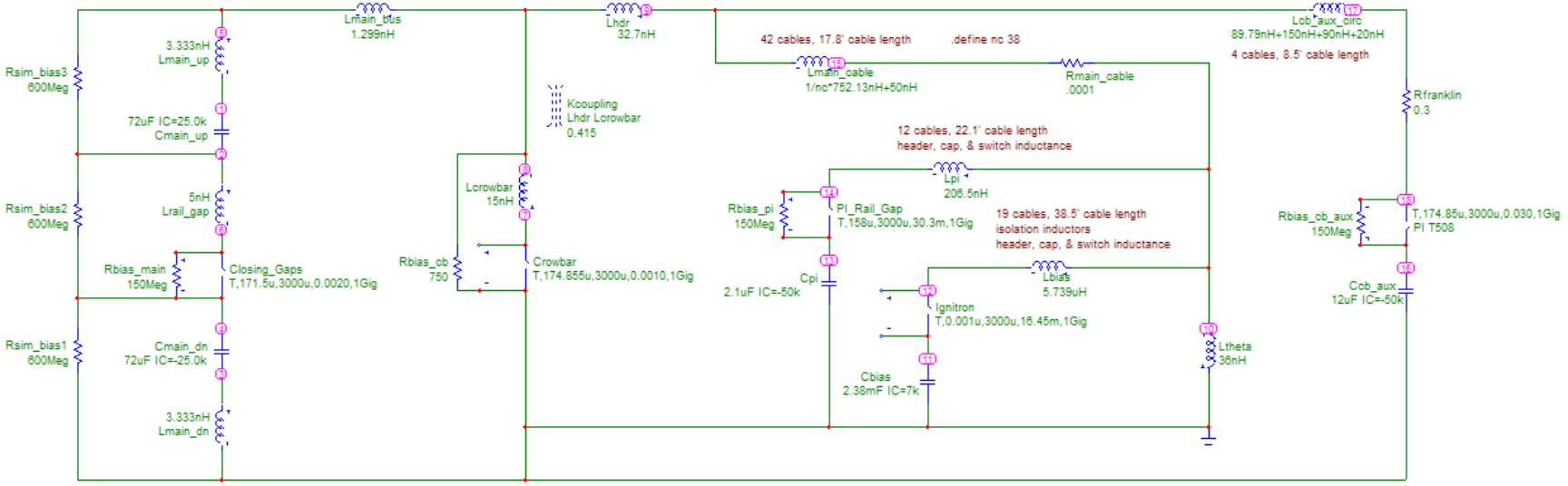


Figure D1. Bias, PI, Main, and Auxiliary (right) banks and Main bank Crowbar switch

Timing for switch closures in the model were determined as follows: the Bias bank switch closes at t = 0 and the PI bank switch closes at t = 158 μs, as is done in experiments; the Main bank switch was chosen to close 13.5 μs after PI switch closure, which corresponds to slightly more than 3 PI periods (4.4 μs/period); the Crowbar switch closes 3.355 μs after Main bank switch closure, approximately the peak of the Main bank current waveform; and the new Auxiliary bank switch was chosen to close at 3.35 μs after Main bank switch closure, just before the Crowbar switch closure.

Figure D2 shows waveforms calculated for a PI- and Bias-only shot.

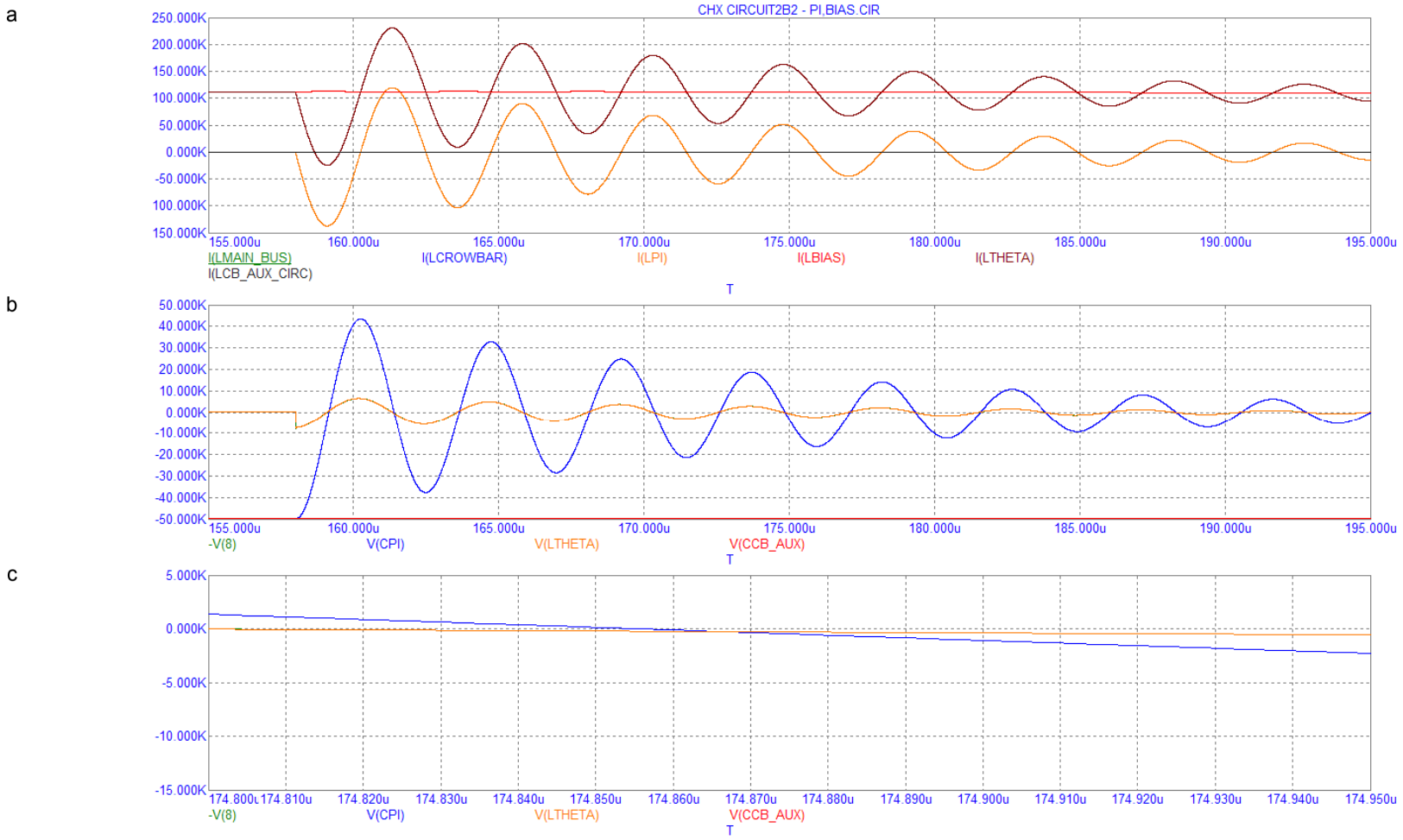


Figure D2. Current and voltage waveforms—only PI and Bias banks were triggered

Figure D2a shows the current waveforms from the Main bank (I(LMAIN_BUS), the Crowbar switch (I(LCROWBAR), the PI bank (I(LPI)), the Bias bank (I(LBIAS)), the Theta coil (I(LTHETA)), and the Auxiliary bank (I(LCB_AUX_CIRC)). Figure D2b and Figure D2c show the voltage waveforms from the Main bank (-V(8)), the PI bank (V(CPI)), the Theta coil (V(LTHETA)), and the Auxiliary bank (V(CCB_AUX)); the difference between these two graphs is that Figure D2c shows a close-up view around the time of Auxiliary bank and Crowbar triggering. As can be seen from Figure D2c, the voltage is essentially zero at the Main bank (across the Crowbar switch) at the particular time chosen here for triggering the Crowbar.

Figure D3 shows waveforms calculated for a shot with the PI, Bias, and Main banks, not the Crowbar switch.

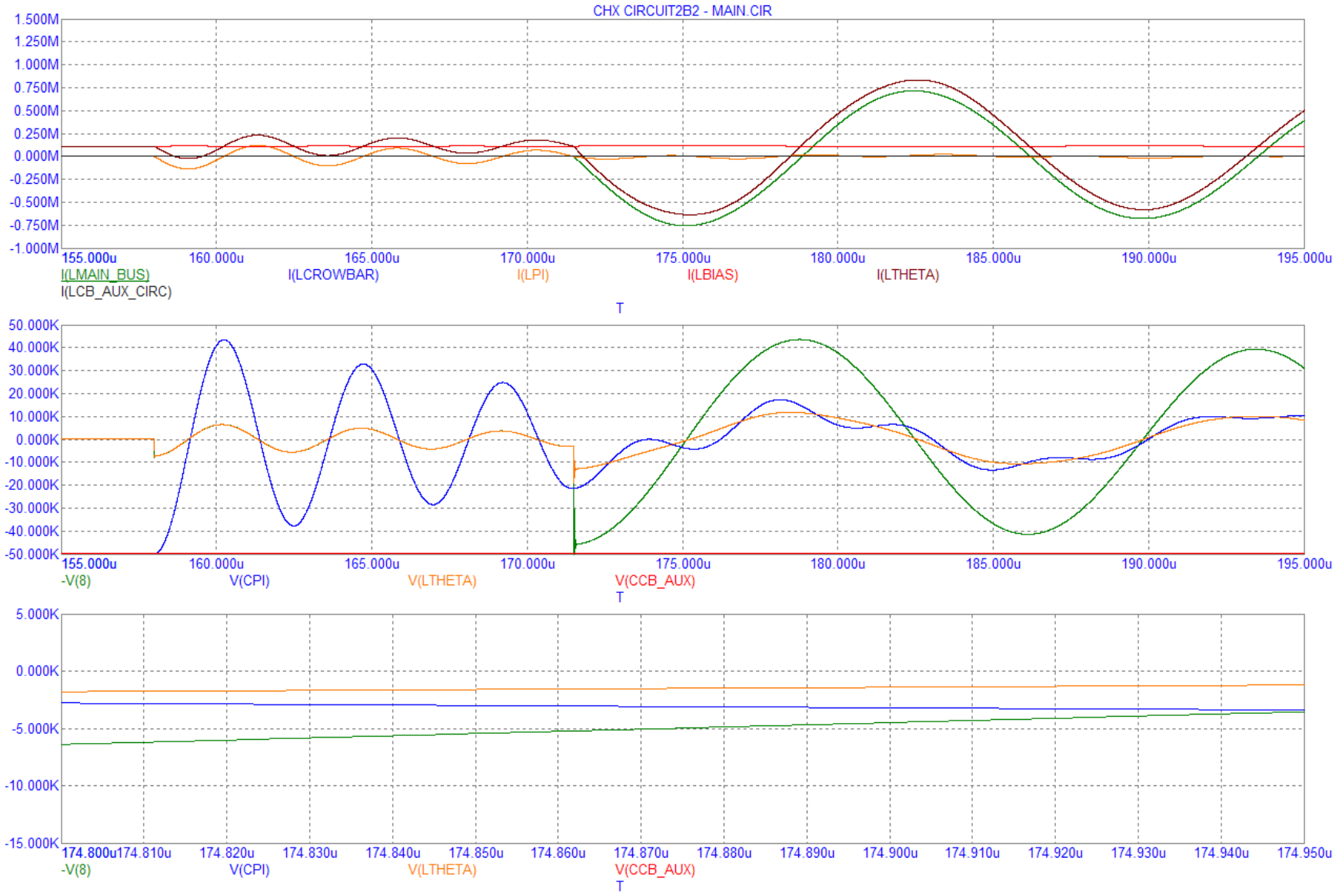


Figure D3. Second set of current and voltage waveforms—Bias, PI, and Main banks all triggered

The Crowbar switch was not triggered to show that there is some residual voltage across the Crowbar switch at this time (~5.4 kV).

Figure D4 shows the corresponding set of waveforms for a shot in which all three banks are triggered with the Crowbar switch.

a

b

c

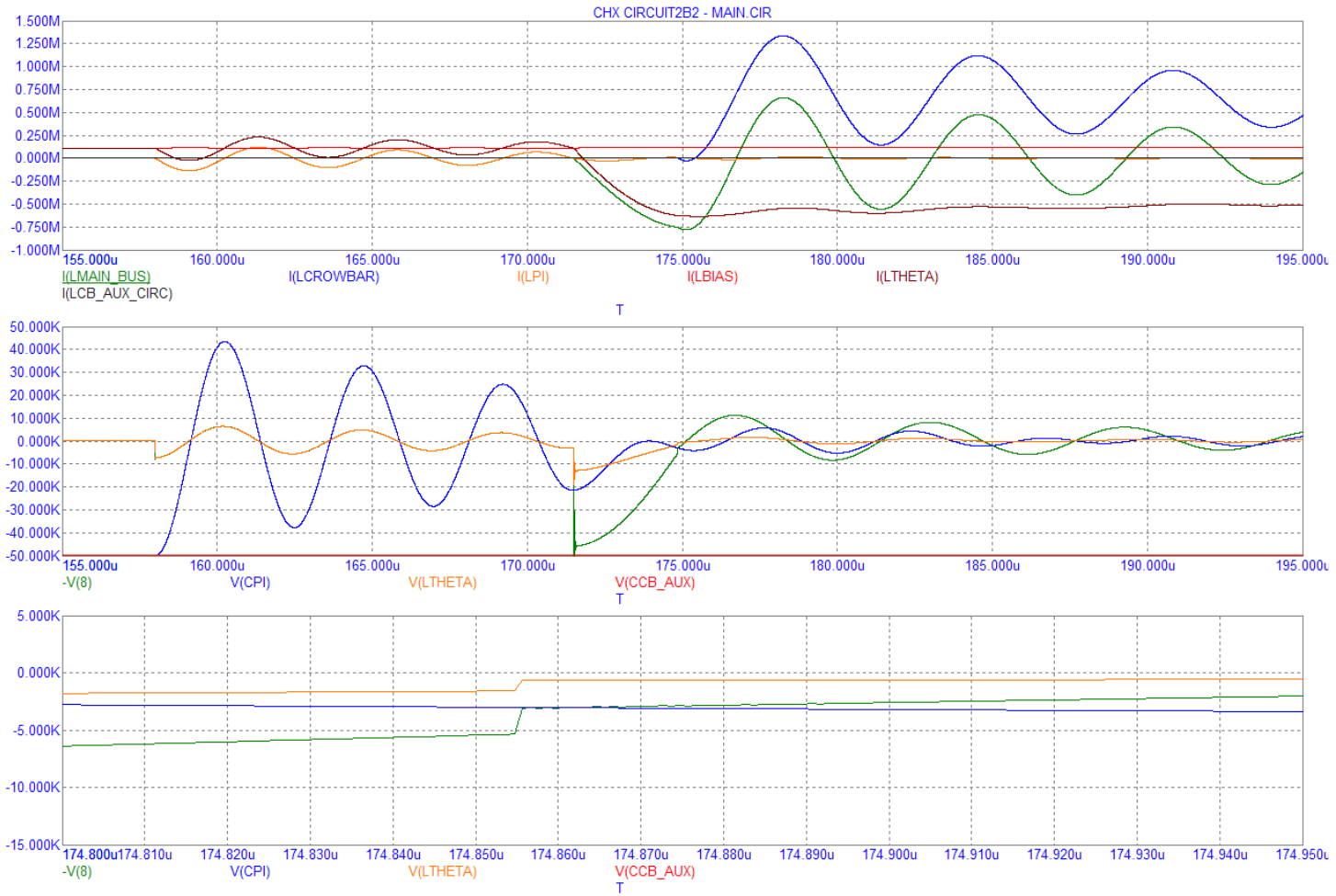
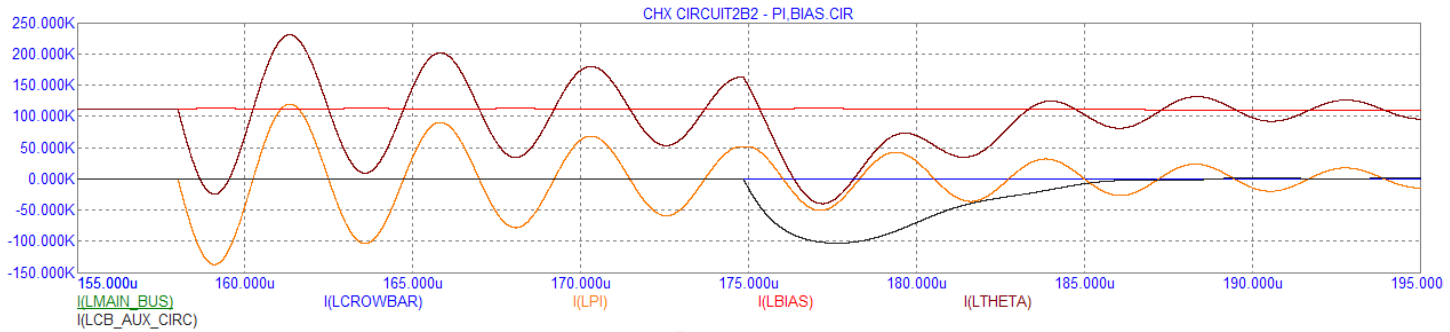


Figure D4. Third set of current and voltage waveforms—all three banks and Crowbar switch triggered

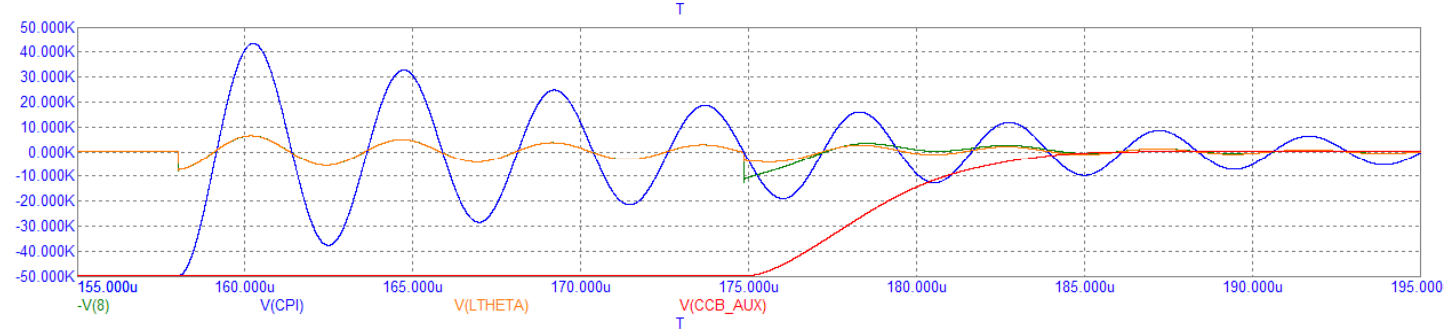
As can be seen from Figure D4c, according to the model the voltage at the switch drops immediately from 5.4 kV to 3.1 kV once the Crowbar is triggered. The model is not refined enough to show any inductances or capacitances between the individual rail gaps in the Crowbar switch or to allow us to place any extreme confidence in the possibility that the magnitudes of the voltages shown here are indicative of what is really occurring in the experiment. However, one can readily see how a single rail-gap switch in the Crowbar can remove voltage from the neighboring rail gaps if it begins conducting significantly earlier than they do.

With Figure D5 we begin looking at the effects of the Auxiliary bank.

a



b



c

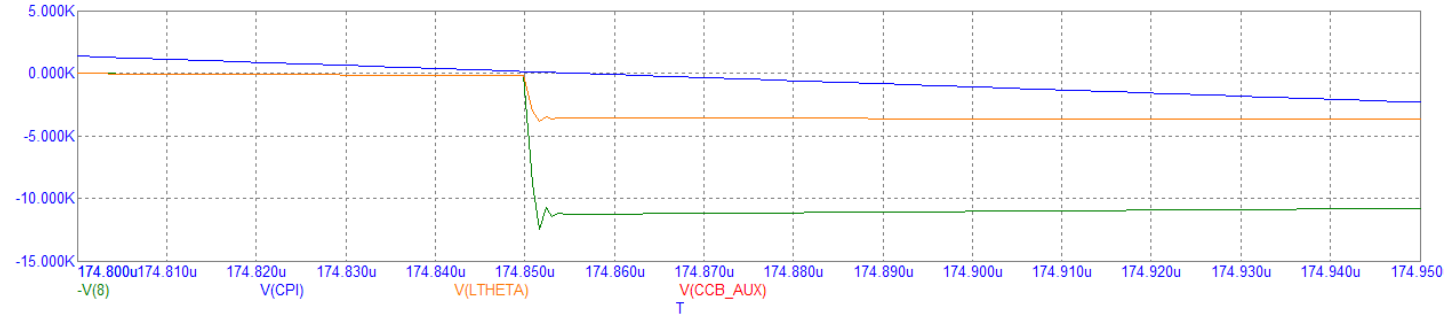


Figure D5. Current and voltage waveforms—Auxiliary bank triggered following PI and Bias banks

For this case the Auxiliary bank is triggered at its appropriate time following the triggering of PI and Bias banks, though the Main bank and Crowbar switch were not triggered to provide a baseline for Auxiliary bank's effects on the circuit. Once the Auxiliary bank is triggered, it raises the voltage across the Crowbar switch from approximately 0 V to ~12.5 kV. Figure D5a and Figure D5b show that the 0.3 Ω series resistance in the Auxiliary bank circuit is effective in damping any oscillations in the Auxiliary bank circuit. While some perturbation in the Theta coil current is observed, its magnitude is comparable that of the PI bank.

When the Main bank is triggered (Figure D6), any effects that the Auxiliary bank may have had on the Theta coil current waveform are quickly "washed out," and the Theta coil current waveforms with (Figure D6) and without (Figure D4) the Auxiliary bank are fairly indistinguishable.

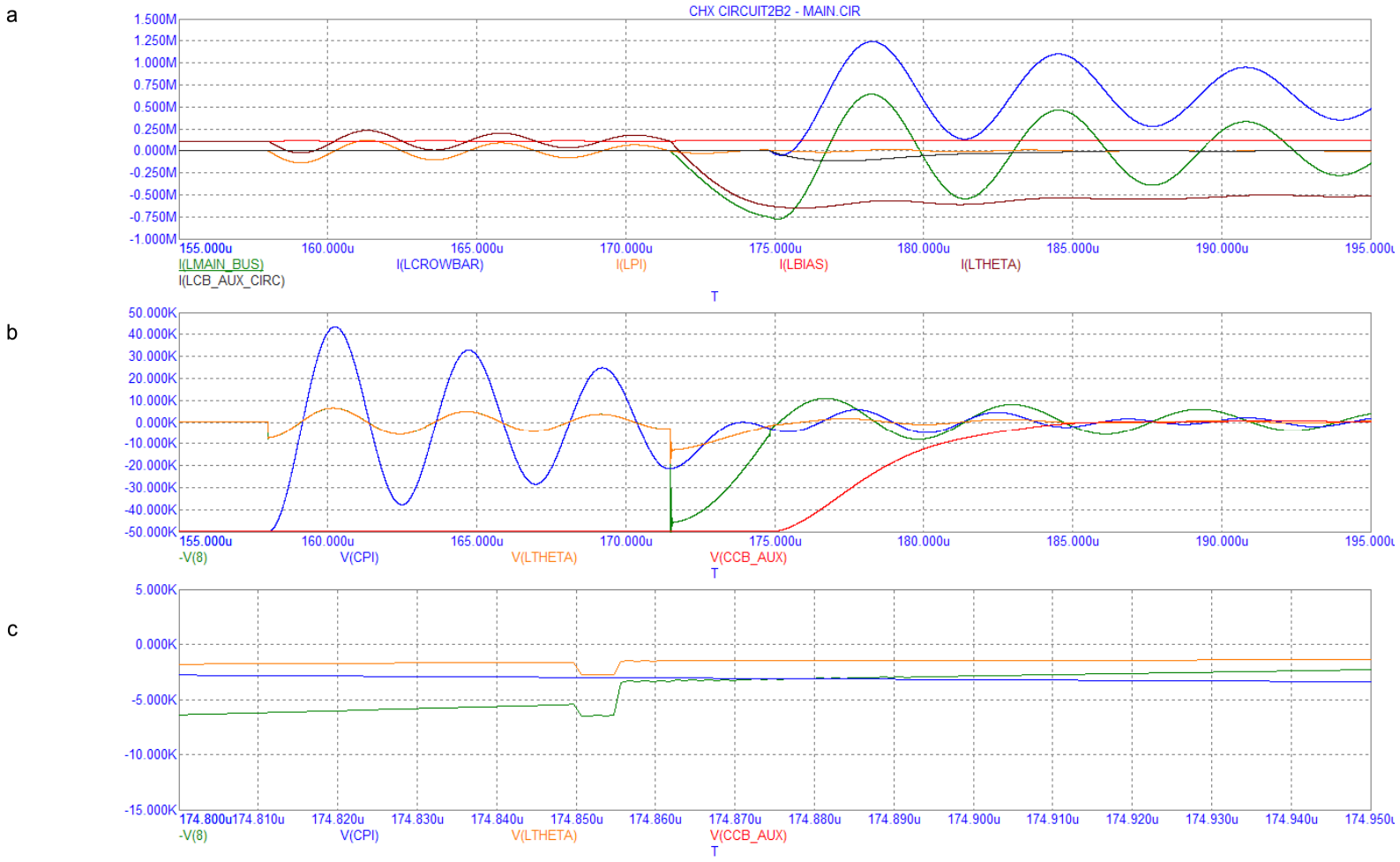


Figure D6. Current and voltage waveforms—Auxiliary bank triggered at its appropriate time, and all other banks also triggered

The apparent voltage that was added across the Crowbar switch is also somewhat washed out by the Main bank, as is evidenced by Figure D6c. There is still some advantage provided by the Auxiliary bank, however, as the Crowbar voltage before triggering the Auxiliary bank is 5.5 kV. After the bank is triggered there is a modest rise to 6.5 kV, and then, as before, the Crowbar voltage collapses to ~3.5 kV after the Crowbar switch is triggered.

A reduction in inductance in the Auxiliary bank circuit, with respect to what is indicated in Figure D1, would allow a greater voltage to be impressed upon the Main bank and Crowbar switch, although it may be that even the net gain of 1 kV may be sufficient to aid in closing all four rail gaps when they are triggered. This approach of using an Auxiliary bank remains the simplest and fastest to implement, and so we will proceed with preparing the Auxiliary bank for testing. Modifications to the bank can be pursued if tests prove to be promising and yet suggest that some changes are needed.

THIS PAGE INTENTIONALLY LEFT BLANK

LIST OF ABBREVIATIONS

AC Alternati	ng Current
AFRL	Air Force Research Laboratory
CCD Char	ge-Coupled Device
cFP Comp	act Field Point
FRC field-rev	ersed configuration
FRCHX	FRC Compression Heating eXperiment
FRX	Field Reversed eXperiment
FRX-C	Field-Reversed theta pinch eXperiment, version C
FRX-L	Field Reversed eXperiment-Liner
HDPE hig	h-density polyethylene
ICCD	Intensified Charge-Coupled Device
KAFB	Kirtland Air Force Base
LANL	Los Alamos National Laboratory
LED	light emitting diode
MCP Micro-Ch	annel Plate
MTF	magnetized target fusion
MTG	Master Trigger Generator
ND neutra	l density
PI Pre-Ioniz	ation
PMT photom	ultiplier tube
RF Radi	o Frequency
SAIC	Science Applications International Corporation
TTL transistor-trans	istor logic
UNM	University of New Mexico
UNR	University of Nevada, Reno
UPS	uninterruptible power supply
UV	Universal Voltronics
v-to-f	voltage to frequency

DISTRIBUTION LIST

DTIC/OCP
8725 John J. Kingman Rd, Suite 0944
Ft. Belvoir, VA 22060-6218 1 cy

AFRL/RVIL
Kirtland AFB, NM 87117-5776 2 cys

Official Record Copy
AFRL/RDHP
Attn: Dr. James H. Degnan 1 cy